The Fate and Transport of Carbon-Based Nanomaterials in the Environment

By

Riccarda Thelma MacDonald

Bachelor of Science with Honours in Chemistry (University of the Western Cape)

Bachelor of Science, Chemical Science (University of the Western Cape)

A mini-thesis submitted in fulfilment of the requirements of the degree of Magister of Scientiae in Nanoscience in the Department of Chemistry, Faculty of Natural Science, University of the Western Cape.

Supervisor: Prof. Leslie Petrik (University of the Western Cape)

December 2020

Abstract

The interest in carbon-based nanomaterials, such as carbon-nanodots and graphene, has grown exponentially because these materials have unique properties and applications in the medical, electronic, clean energy and several other fields for biochemical sensing, energy conversion, photocatalysis, optoelectronics, etc. Carbon dots were discovered in 2004, yet very little research has been done on the colloidal stability thereof. Nanomaterials such as carbon dots will inescapably make their way to natural waters with an unknown environmental fate. Therefore, it is of great importance to understand the behaviour of carbon dots under the influence of certain environmental conditions such as pH, ionic strength, and in the presence of natural organic matter.

In this study, plain/unfunctionalised carbon dots were synthesised from glycerol and sodium dihydrogen phosphate in a domestic microwave, and amino-functionalised or amine-capped carbon dots were synthesised through hydrothermal synthesis in a silicon oil bath from citric acid (as the carbon source) and branched polyethylenimine. The influence of synthesis conditions, such as the heating power/temperature, heating time (or reaction time), and molar ratios of precursors, on the colloidal stability of the materials were studied to determine ideal or adequate synthesis conditions. Synthesised carbon dots were characterised by analytical techniques such as ultraviolet-visible spectroscopy to obtain qualitative information, i.e., compound identification; and Dynamic Light Scattering and Laser Doppler Velocimetry to determine the hydrodynamic size, surface charge, and particle distribution of carbon dots and amine-capped carbon dots. Furthermore, the synthesised materials were subjected to a variety of environmental conditions including pH, ionic strength, and the presence of natural organic matter. Carbon dots showed greater stability at higher power levels and longer reaction/heating times, while amine-capped carbon dots were more stable when prepared at 170 °C. An increase in the molar quantity of the carbon source (i.e., Gly and CA) aided in the process of carbonisation of hydrocarbons into the graphitic structure of carbon dots and amine-capped carbon dots. Carbon dots displayed greater stability in water suspensions of a circumneutral pH, whereas amine-capped carbon dots showed higher stability in water suspensions of a basic nature (pH 9). The presence of divalent cations greater influenced characteristics of the materials than monovalent cations; plain carbon dots displayed negatively charged surfaces throughout all ionic strength studies, whereas amine-capped carbon dots presented more positive surfaces. With the increase in ionic strength, the surfaces of both carbon dots and amine-capped carbon dots became more positive due to compression of their electrical double

layer. In the presence of natural organic matter, amine-capped carbon dots showed greater stability than carbon dots as evidenced by their surface charges which remained fairly stable.

The findings of this study provide a detailed description on the aggregation behaviour of both unfunctionalised and functionalised carbon dots with a thorough investigation into several particle characteristics under the applied environmental conditions. The findings of this study branching on pre-existing information on the topic speaks to its novelty.

Keywords: carbon dots, hydrothermal synthesis, microwave-synthesis, toxicity

Declaration

I declare that "The Fate and Transport of Carbon-Based Nanomaterials in the Environment" is my own work, that it has not been submitted for any degree or examination in any other university, and that all the resources I have used or quoted have been indicated and acknowledged by complete references.

Riccarda Thelma MacDonald December 2020

Signature: ……

Acknowledgements

My efforts in completing this degree would have been nothing, if at all existent, without my rock, my saviour, my ultimate guide, and my light—My Heavenly Father, God Almighty. As we strive to understand all that He has created and already know, there is one thing that will always be true: God is the only entity whose existence is within Himself. Therefore, there is no other that deserves more praise than Him. So, I would love to thank God for being who He is and for making me all that He wants me to be.

For it is written, *'For everything, absolutely everything, above and below, visible and invisible… everything got started in him and finds its purpose in him.'* – Colossians 1:16 (MSG)

I would not have been able to reach the end of this beautifully chaotic road without the help, motivation, and inspiration of a few very important people. There are not enough words to describe how immensely thankful I am to have been under the supervision and guidance of such an incredible leader and renowned professor in science as my supervisor, Professor Leslie Petrik. She has completely fulfilled her role in providing guidance and support throughout this journey. What I have learnt from her goes far beyond the laboratory and I would therefore like to thank her for shaping me into a better researcher. To the Environmental Nano Science (ENS) family, a group of remarkable researchers who are excellent in their respective fields—all working hard to save our environment: thank you for making our time together so memorable, filled with laughter and joy. There are a few who deserve a special thank you—Emmanuel Ameh, George Michael Ndilowe, Jean-Luc Mukaba Muvumbu, and Cosmas Uche—thank you for all your support. To Mrs Vanessa Kellerman, Mrs Ilse Wells, Mr Rallston Richards and Mr Denzil Bent—thank you for everything that you have done for all of us in the ENS group.

I will always be grateful to Professor Leslie Petrik for the opportunities she made possible for me. During my masters, I have been fortunate to participate in the International Student Practice as part of the South Africa-Joint Institute for Nuclear Research (SA-JINR) bilateral at the Joint Institute of Nuclear Research in Dubna, Russia. Attending the student practice was very beneficial to my research and I have gained much knowledge at the Frank Laboratory of Neutron Physics (FLNP) from the professors, doctors, PhD students, all the other staff members and the other students who participated in the practice. Special thanks to Professor Marina Frontasyeva, Dr Wael Badawy, Dr Inga, and Dr Yury Kochnev. I have also been privileged to spend nine weeks at the University of Missouri, in Columbia Missouri, as part of the University of Missouri South African Education Program (UMSAEP). It was such a

blessing to visit Prof. Maria Fidalgo de Cortalezzi and her research team and I am extremely grateful for the kindness and wisdom that this team have imparted unto me. Special thanks to Mohamed Bayati, Mohammed Numaan, Zahra Salahshoor, Sally Qasim, and Abbas Kadhem for creating such an inspiring and supportive environment during my stay.

The National Nanoscience Postgraduate Teaching and Training Platform is greatly acknowledged for the financial assistance to complete this study. To Mrs Valencia Jamalie and Mrs Chyril Abrahams, thank you for always being available to assist with any queries and for your kind and caring hearts to all.

Lastly, but definitely not the least, I would love to thank my incredibly supportive family, my father Richard, my mother Thelma and my brother Alexander, and my partner Jesse Harmse, for their unconditional love and encouragement. No matter how my day went, I always looked forward to that daily phone call to brighten up my day and put the wind back into my sails. The truth of the matter is that a ship needs the sea and wind to sail and as I am setting bold sail into the future with a burning passion for Chemistry, filled with potential and a desire to live and excel, I believe that this journey was one worth taking!

"I was taught that the way of progress was neither swift nor easy."

– **Marie Curie**

Table of Contents

List of Figures

List of Tables

List of Abbreviations

a-CDs	amine-capped or amino-functionalised carbon dots
AFM	atomic force microscope/y
BPEI	branched polyethylenimine
$CaCl_2$	calcium chloride
C-dots/CDs	(plain/unfunctionalised) carbon dots
CNTs	carbon nanotubes
CA	citric acid
DLS	dynamic light scattering
EDL	electrical double layer
EM	electromagnetic
EMR	electromagnetic radiation
ENMs	engineered nanomaterials
ENPs	engineered nanoparticles
ELSA	ethical, legal and social aspects
GMO	genetically modified organism
Gly	glycerol
HA	humic acid
HCl	hydrochloric acid
D_h	hydrodynamic diameter
IC	integrated circuit
IS	ionic strength
LDV	laser doppler velocimetry
MW	molecular weight

MWCNT	multi-walled carbon nanotube
NM	nanomaterial
NP	nanoparticle
NOM	natural organic matter
HNO_3	nitric acid
n( )	number of moles of
PL	photoluminescence
PAA	polyacrylic acid
PDI	polydispersity index
PEG	polyethylene glycol
PEI	polyethylenimine
PPEI-EI	polypropionylethyleneimine-co-ethyleneimine
QD	quantum dot
QY	quantum yield
STM	scanning tunneling microscope
Si	silicon
SWCNT	single-walled carbon nanotube
NaCl	sodium chloride
NaH_2PO_4	sodium dihydrogen phosphate
NaOH	sodium hydroxide
H_2SO_4	sulfuric acid
TiO_2	titanium dioxide
UV-Vis	ultraviolet-visible
ZP	zeta potential

List of Publications

1. MacDonald, R. T. and Petrik, L. The effect of synthesis parameters on the characteristics of unfunctionalised carbon dots and amine-capped carbon dots.
   Manuscript in preparation
2. MacDonald, R. T. and Petrik, L. The effect of environmental conditions—pH, ionic strength, and natural organic matter—on the colloidal stability of unfunctionalised carbon dots and amine-capped carbon dots – A study on the Fate and Transport of carbon dots.
   Manuscript in preparation
3. MacDonald, R. T., Bayati, M., Fidalgo de Cortalezzi, M. and Petrik, L. The Effect of pH and Ionic Strength on The Adsorption of Sulphamethazine onto Laser-Induced Graphene.
   Manuscript in preparation

Chapter 1 – Introduction

1. Introduction

This chapter serves as a general introduction to this study. The first section covers background information; starting with a short description of nanotechnology, how to go about managing the risks associated with it, and a short introductory piece on carbon dots (C-dots or CDs). A statement of the problem, a description of the research aim, objectives, questions pertaining to the study, as well as an overview of the research approach, then follows. The scope, delimitations of the study as well as the thesis structure are also outlined later in this chapter.

1.1. Background

"The Inquisitive Man" is a fable, written by Ivan Andreevich Krylov, a Russian poet and fabulist in 1814 (Ralston 1883). It is about a man who goes to a museum and notices all kinds of tiny things but fails to notice the presence of an elephant. Is humankind just like Krylov's Inquisitive Man, who didn't notice the elephant in the museum? In this case the elephant would be nanotechnology, that has grown quite fast in the last few years, with great promise in many applications but with little ethical and toxicity regulation.

"The principles of physics, as far as I can see, do not speak against the possibility of maneuvering things atom by atom. It is not an attempt to violate any laws; it is something, in principle, that can be done; but in practice, it has not been done because we are too big." Those are the words of the father of nanotechnology, renowned Nobel Prize winner Richard Feynman, from his visionary speech at the California Institute of Technology (CalTech) on December 29, 1959 (Feynman 1960). Who would have thought that words, that once were perceived as pure science fiction, would form the foundation on which many years of remarkable scientific research and progress would rest?

The *United States National Nanotechnology Initiative* stated that over a decade later Professor Norio Taniguchi coined the term nanotechnology in his studies on ultraprecision machining (United States National Nanotechnology Initiative n.d.). Nanotechnology is a rapidly evolving field showing great promise for application in many disciplines, therefore there seems to be no one definition that fully explains it. Some describe it as the engineering of matter at the nanoscale in order to achieve unique properties and functions related to size—with a safe conclusion that the properties of materials can be size-dependent. Others say that it is the study of phenomena and manipulation of materials. Nevertheless, it involves the four main processes,

namely design, characterisation, production and application. Over the years, the main focus of scientists and engineers is to find various ways of synthesising materials at the nanoscale in an effort of taking advantage of their enhanced properties, which include greater chemical reactivity, larger strength, lighter weight and increased control of the light spectrum (Khan *et al* 2019).

A general consensus exists among researchers and scientists regarding the classification of nanomaterials (NMs) in that there are three main categories. The first category belongs to naturally-occurring nanoparticles (NPs) that are sized in the nano-range and found in nature; examples of such particles include particles born in forest fires, volcanic eruptions, and salt particles produced by oceanic waves. The second category is made up of unwanted by-products produced by the industrial sector, such as particles produced from welding and diesel exhaust (Ellenbecker and Tsai 2011). The third category consists of engineered nanoparticles (ENPs) that are intentionally-made nanoparticles which can range from carbon black to nanospheres utilised in drug delivery, and could have a variety of shapes, i.e., spherical particles such as CDs or quantum dots (QDs), cylindrical particles such as carbon nanotubes (CNTs), nano-clay that are plate-like, or irregularly-shaped particles such as nano-alumina (Ellenbecker and Tsai 2011).

Concerns regarding the release of engineered nanomaterials (ENMs) into the environment have increased as the interest in new properties of materials have amplified due to the nanoscale dimensions of NMs (Wang *et al* 2014b). The use of engineered nanoparticles (ENPs) (such as nanocomposites, metals, metal oxides, biological NMs, nanoceramics, and the main interest of this study: carbon-based NMs) in an industrial setting have grown all the more frequent (Ellenbecker and Tsai 2011). However, the rate at which these materials are produced is much faster than the rate at which safety studies are performed. Therefore, the safety of NMs is questionable and of great concern.

1.1.1. The safety of nanomaterials

In the past, the scientific community has been presented with several other emerging technologies with a promise of being revolutionary and having an enormous potential for commercialisation; the most note-worthy in 2013 was probably the genetic engineering of foodstuffs. Genetically modified organisms (GMOs) were expected to advance the food and medical industries and bring profit but due to a number of problems, they were not received positively by the consumers and ended up being banned or strongly regulated in several

countries (Bawa and Anilakumar 2013). According to Filipponi and Sutherland, several questions, of an ethical nature, were raised such as 'who' would profit from these products, and what are the possible consequences of these organisms on the long-term health of humans, as well as the life cycle of animals and plants. The GMO case serves as a clear example of an emerging technology that did not go through a careful Ethical, legal and social aspects (ELSA) analysis (Filipponi and Sutherland 2012). It is necessary to consider the 'bigger picture' and think about the effect of NMs on the environment and not just remain focused on the progression of nanotechnology and science itself. Although there are numerous benefits to nanotechnology (with some of those benefits yet to be discovered), it is a science that is rapidly growing, which makes it extremely necessary to think about what the ultimate fate of these materials would be.

As the number of consumer products containing NMs has grown exponentially each year, and due to the fact that they have a size comparable to biomolecules, such as proteins and DNA, the question of the safety thereof becomes rather vital. Biological behaviours at the cellular, subcellular and protein levels have been expected to be affected by NMs for quite some time now as some of these NMs make their way through the body and, due to their small size, could penetrate cell membranes and set up camp in mitochondria (Wang *et al* 2014b). The question remains: does the possibility exist for NMs to trigger a toxic effect by interacting with biomolecules in an adverse manner? Seeing as NMs are designed to pass through cell membranes in order to target infected cells and serve as drug agent delivery systems in nanomedicine, the possibility exists for NMs to pass barriers of protection in cells (Filipponi and Sutherland 2012). Another question would be one in which toxicity extends to ecotoxicity: What would the outcome be when materials containing NPs ultimately find their way to landfills and degrade? Will they be dispersed? What would the dosage be? Could this be harmful to ecosystems? Nevertheless, research progress has been made in the last few years on the toxicological properties of NMs. The relevance of these results to humans is not clear, since testing is mainly being conducted on animals or in vitro, and the consistency is also questionable seeing as testing methods vary from one lab to another. This makes the comparison of results quite difficult. Therefore, it is necessary to discuss the process in which the risk of these materials could be managed.

In 2014, a research group reported on the bibliometric analysis regarding the risk of ENMs which have increased from just one article and three authors in 1999 to 256 articles and 1473 authors in 2012 (Wang *et al* 2014b). The interest in risk assessment was rather low from 1999

to 2005 as the total number of articles reported on by Wang's team were below 10. In 2006 the interest grew larger as about 30 articles were published on the risk of ENMs which increased to the aforementioned 256 publication outputs by about 1473 authors in the year 2012. It should be noted that the bibliometric analysis performed by this team involved a keyword search on a large number of NMs as well as topics such as nanotoxicity, health effect and environmental behaviour (Wang *et al* 2014b).

Furthermore, Wang and co-workers also ranked countries according to their contribution i.t.o. publications on risks of ENMs, in which the United States of America (USA) ranked first with 373 publications that translates into 41.9 % of publications during 1999 to 2012. China followed with 132 publications which is a 14.8 % contribution from their side; the UK ranked 3rd with 9.1 % (82 publications) and Italy, Germany, Switzerland and Japan followed with 6.1 %, 5.9 %, 5.4 %, and 5.3 %, respectively. Funding has a great impact on projects and determines whether all the objectives of a study can be met or even if studies on those particular topics could be performed. Therefore, it should be noted that some countries might not have produced as many—if any—articles as others, due to funding limitations. Wang and co-workers also looked at the funding agencies and the top three were: 1) The National Science Foundation in the USA, 2) the National Natural Science Foundation of China and 3) the US Environmental Protection Agency Science (Wang *et al* 2014b). Another important factor to look at is the subject categories, and the top three categories regarding the risks of ENMs were Environmental sciences, Toxicology and Nanoscience & Nanotechnology that contributed 285 (15 %), 270 (14.2 %) and 222 (11.7 %), respectively. Several conclusions have been made such as, when dealing with ENPs, surface area serves a greater role than mass; and common behaviours have also been identified. Although there is an agreement that some progress has been made in the evaluation of the toxic effects of NMs, much research still needs to be done.

1.1.2. Managing the risk of nanomaterials

Before the development of a risk management framework, it is important to know the real risk of nanotechnology. At the moment, the term 'nanotechnology' is seen as an umbrella term that covers a large variety of materials, applications and instrumentations—therefore, there is a need to classify nanotechnology applications and NMs. When it comes to risk, it is necessary to identify what the real safety concerns of NMs are and identify the key safety needs in specific areas of applications. This will provide a coordinated framework of toxicological assessment of NMs for all institutions (Filipponi and Sutherland 2012).

In assessing the risks associated with ENMs, several topics are of critical importance to explore and examine, such as gaining an understanding on their reactivity, persistency, mobility or transportive nature, and their behaviour in the environment. Studies have been focused greatly on the agglomeration behaviour of ENMs as it is closely associated with the cytotoxicity thereof and could provide insights into migration (Wang *et al* 2014b). Due to the small size of NMs, ENMs could undergo agglomeration rapidly after synthesis which is attributed to their high mobility allowed by Brownian motion (Ellenbecker and Tsai 2011).

1.2. Carbon dots

Carbon dots (CDs) are small carbon NPs with sizes smaller than 10 nanometres and include a variety of unique properties including their water solubility, chemical inertness, good photostability, low cytotoxicity, and excellent biocompatibility (Baker and Baker 2010, Bayati *et al* 2018, Zhang *et al* 2017, Deng *et al* 2014). These materials with rich oxygen-containing groups on their surfaces find application in a wide range of fields such as bioimaging, photocatalysis, bio-sensing, targeted drug delivery, energy conversion/storage devices, optoelectronic devices, etc. (Ray *et al* 2009, Wang and Hu 2014, Zhang *et al* 2017, Deng *et al* 2014). The purification of single-walled carbon nanotubes (SWCNTs) through preparative electrophoresis in 2004 (Xu *et al* 2004) marks the origin of these remarkably small NMs, which then later made another appearance via laser ablation of graphite powder and cement in 2006 (Sun *et al* 2006, Wang and Hu 2014). Due to their inexpensive nature and fascinating properties, CDs have found their rightful place as a nanocarbon family member. Its mother-material 'carbon' is commonly known for its black appearance and was generally considered to have low solubility in water and weak fluorescence. However, CDs have caught much attention for their good solubility and strong luminescence, and are sometimes called carbon nanolights (Baker and Baker 2010, Wang and Hu 2014). It is not just its extraordinary luminescent nature that draws attention but, compared to traditional semiconductor quantum dots and organic dyes, photoluminescent carbon-based dots have gained superiority in terms of strong chemical inertness, high resistance to photobleaching and facile modification (Baker and Baker 2010). Whereas, semiconductor QDs such as CdSe pose cytotoxic and environmental threats due to Cd^{2+} or Se^{2-} ion release; and if the core or core/shell material is less protected, faster appearance of cell viability interferences may be observed (Wang *et al* 2014a, Michalet *et al* 2005, Zhao *et al* 2008).

The application of a material in the biological field generally requires biological properties, such as low toxicity and good biocompatibility. CDs seem to be entrusted with these properties

and opened the door to potential applications in bioimaging, biosensors and biomolecule/drug delivery. These materials have not only made headlines in the biological field but also in optronics, catalysis and sensors due to their outstanding electronic properties as electron donors and acceptors to produce chemiluminescence and electrochemical luminescence (Wang and Hu 2014, Bayati *et al* 2018). However, with all these benefits there seem to be some disadvantages when it comes to the fate and transport of these materials in the environment.

1.3. Problem statement

The interest in carbon-based NMs, such as CDs, has grown exponentially because of their unique properties and applications in the medical, electronic, clean energy and several other fields. CDs have also generated interest because of their water solubility, chemical inertness, low toxicity, ease of functionalisation and resistance to photobleaching (Baker and Baker 2010). Although there are numerous benefits to the development of nanotechnology and the rapid growth thereof, it is necessary to pay attention to possible risks to human health and the environment along with other public concerns about social and ethical issues. CDs have been discovered in 2004 by Scrivens and co-workers through purification of single-walled carbon nanotubes (SWCNTs) by electrophoresis (Xu *et al* 2004), yet very little research has been done on the toxic effects thereof. These NMs will inescapably make their way to natural waters with an unknown environmental fate (Baker and Baker 2010, Bayati *et al* 2018). Therefore, it is of great importance to observe and understand the behaviour of these NMs in the environment.

1.4. Research aim and objectives

The aim of this study was to synthesise and examine the behaviour of unfunctionalised CDs and amine-capped CDs (a-CDs) and to determine the fate and transport of these materials through the investigation of their colloidal stability in the environment by placing them under certain environmental influences, such as varying pH levels, alternating ionic strength (IS) of monovalent and divalent cations, and the presence of natural organic matter (NOM).

The objectives include:

- Optimisation of synthesis conditions for CDs,
- Optimisation of synthesis conditions for a-CDs,
- Investigation of the influence of pH on the colloidal stability of CDs and a-CDs,
- Investigation of the influence of ionic strength (IS) or salinity, by the use of monovalent (NaCl) and divalent ($CaCl_2$) salts on the colloidal stability of CDs and a-CDs, and

- Investigation of the influence of the presence of NOM on the colloidal stability of CDs and a-CDs.

1.5. Research questions

1) How is the colloidal stability of CDs and a-CDs affected by changes in their synthesis conditions?
2) How is the colloidal stability of plain CDs and a-CDs affected by changes in environmental conditions, such as variation in pH, IS (introduced by monovalent and divalent cations from NaCl and $CaCl_2$, respectively), and the presence of NOM, i.e., humic acid (HA)?
    (a) Does a purification process such as centrifugation influence the size of the synthesised materials by reverting the process of aggregation?
    (b) How is the hydrodynamic diameter of CDs and a-CDs affected by the above-mentioned environmental influences?
    (c) How is the surface charge of CDs and a-CDs affected by the above-mentioned environmental influences?
    (d) How is the size distribution of CDs and a-CDs affected by the above-mentioned environmental influences?
3) Does the amine-functionality of a-CDs provide improved stability over unfunctionalised CDs?

1.6. Research approach

In the last decade, there has been a number of methods for the preparation of CDs. These methods can by classified into "Top-down" and "Bottom-up" approaches. There are three problems found with the production of CDs: (a) during carbonisation, carbonaceous aggregation could occur but could be prevented by the use of electrochemical synthesis, confined pyrolysis or solution chemistry methods, (b) problems with size and uniformity could occur, which could be optimised by post-treatment, such as gel electrophoresis, centrifugation, and dialysis, and (c) there are surface properties that are critical for solubility and designated applications, which can be tuned during preparation or post-treatment.

The focus of this study has been on the effect of synthesis parameters and environmental conditions on the colloidal stability of the materials under study. Firstly, optimisation procedures for the synthesis of CDs and a-CDs were performed in order to investigate the effect of synthesis conditions on the colloidal stability of the aforementioned materials, and to determine optimal or adequate synthesis conditions. Secondly, CDs and a-CDs were

synthesised. Thirdly, the effects of pH, IS and the presence of NOM on the colloidal stability of CDs and a-CDs, were tested.

Several methods exist for the synthesis of CDs, such as chemical ablation, electrochemical carbonisation, laser ablation, microwave irradiation and hydrothermal/solvothermal treatment (Ray *et al* 2009, Baker and Baker 2010, Wang and Hu 2014). Chemical ablation is the most accessible; a variety of sources could be used but it requires harsh conditions, involves drastic processes, multiple steps, and poor control over size. Electrochemical carbonisation has the advantages of controllable size and nanostructure, stability, and is a one-step process, yet few/small molecule precursors are required. In laser ablation, surface states are tuneable; the process is rapid and effective but low quantum yields are achieved, modification is necessary and control over size is poor. Furthermore, hydrothermal/solvothermal treatment is a cost-effective, eco-friendly, non-toxic method but control over size is poor. Microwave irradiation also has the disadvantage of poor size control but is a rapid, scalable, cost-effective, eco-friendly method (Wang and Hu 2014). Therefore, this method was used for this study.

Surface modification is a method which possesses a lot of power to tune the surface properties of materials for certain applications. A number of methods exist for the functionalisation of C-dot surfaces through surface chemistry or interactions, such as coordination, covalent bonding, π–π interactions, and sol–gel technology. The surfaces of CDs are rich in oxygen-containing groups, which provides many binding sites for covalent bonding (Bayati *et al* 2018). A common method of enhancing the photoluminescence (PL) of CDs is surface passivation via covalent bonding of amine-containing agents (Baker and Baker 2010, Bayati *et al* 2018, Wang and Hu 2014, Zhang *et al* 2017), which is done within this study. Two types of CDs were used for this study, obtained from thermal treatment of organic molecules and surface functionalisation, to compare CDs of different surface chemistries. The synthesis of the plain/unfunctionalised CDs was carried out using a modified version of the method initially performed by Wang and co-workers (Wang *et al* 2011a). The process involves microwave irradiation—a rapid, cost-effective method. In this process, a carbon source i.e., glycerol (Gly) and sodium dihydrogen phosphate (NaH_2PO_4) are used as precursors. The synthesis of a-CDs was initially performed by Zheng et al. in 2014, in which a carbon source (i.e., citric acid, CA) and branched polyethylenimine (BPEI) were used as precursors (Zheng *et al* 2014). According to Zang et al., PEI with its unique proton sponge mechanism, beneficial for endosomal escape in cells, is rated as the fastest growing, most well-researched and greatest potential non-viral gene delivery vector (Zhang *et al* 2017). A silicone oil bath was used to heat the solution

mixture and the resulting solutions were then dialysed against ultrapure water through a dialysis membrane to obtain a purified product.

Furthermore, three conditions were under investigation for this study: pH, IS, and the presence of NOM. The colloidal behaviour of the synthesised materials was investigated at pH levels 1–13 and the effect of IS was tested by the presence of monovalent (Na^+) and divalent (Ca^{2+}) cations. Also, the influence of the presence of NOM was studied over the HA concentration range from 20 to 200 mg/L. The effects of these applied environmental conditions could be used to map aggregation behaviour of CDs and a-CDs. Figure 1 below is a schematic of the experimental procedure performed on CDs and a-CDs.

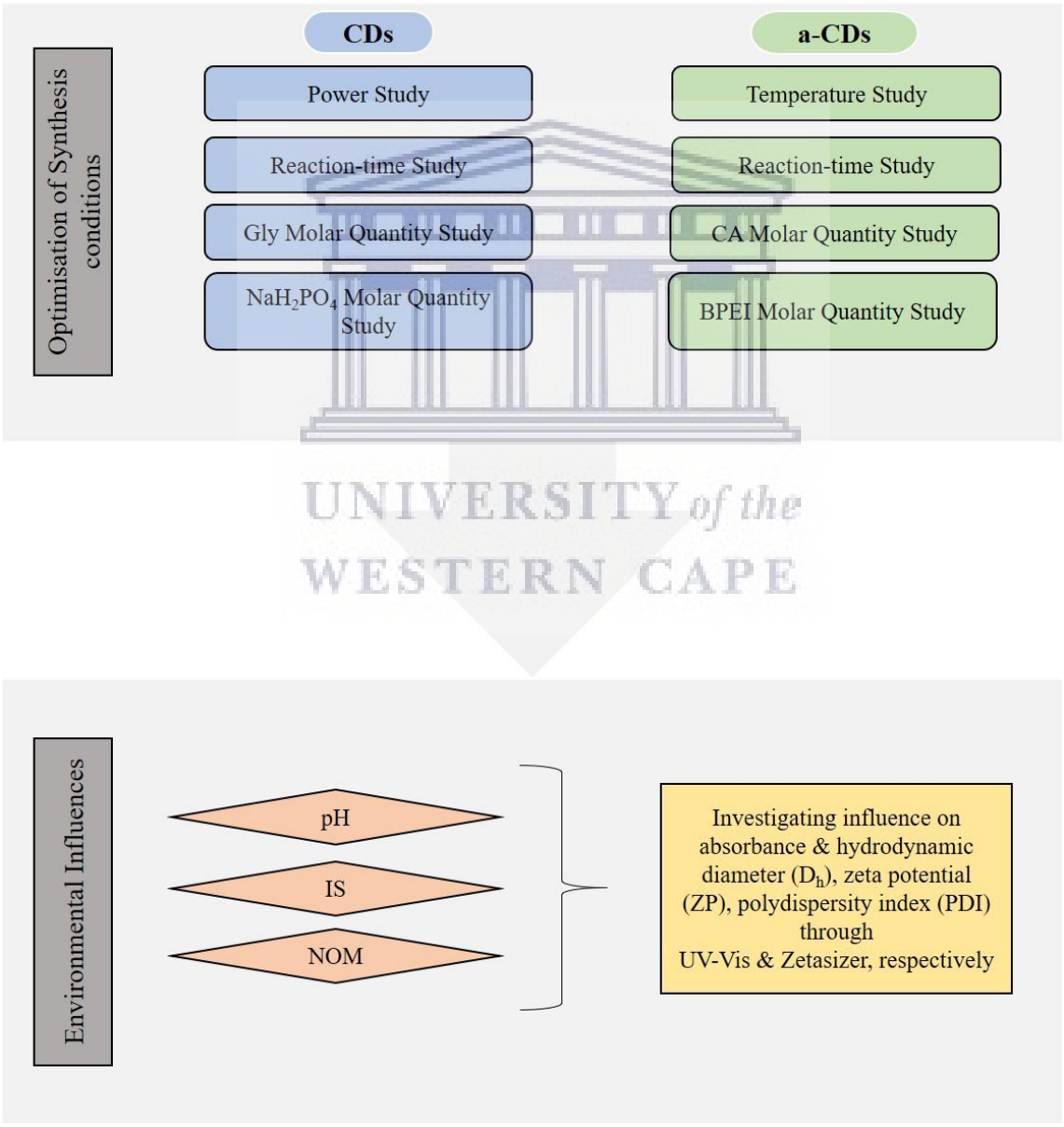

Figure 1. Schematic illustration of flow of experiments for optimisation, synthesis, and testing of various parameters on the colloidal stability of CDs and a-CDs.

The characterisation techniques used in this study, for analysis and testing of CDs and a-CDs are described below:

- Ultraviolet-visible (UV-Vis) spectroscopy was used in order to obtain the absorption spectra for synthesised materials, with scanning range of 200–600 nm for CDs and a-CDs. From the absorbance spectrum, the information obtained includes: a) particle size values, b) size distribution of NPs, c) visualisation of the degree of particle aggregation, and d) information regarding the electronic structure, chemical identity, and sample-induced electron phase shift.
- Zeta potential (ZP) and hydrodynamic size measurements were carried out to investigate the colloidal stability of CDs and a-CDs. Hydrodynamic diameter, surface charge, degree of polydispersity, and size distribution were measured under a wide range of solution compositions, including various pH levels, monovalent and divalent electrolytes (NaCl and $CaCl_2$ respectively), and the presence of NOM.

1.7. Scope and delimitations of the study

Thus far toxicity research on carbon-based nanomaterials has been mainly focused on CNTs and fullerenes (Ray *et al* 2009), as well as other NMs such as metal or metal-oxide NPs (e.g. ultrafine titanium dioxide, TiO_2), which makes this study quite relevant, as the toxicity of CDs has not fully been investigated. Some forms of CNTs have shown pulmonary toxicity in a number of studies. This, of course, depends on the surface properties, length, and method of production of the CNTs. For example, titanium dioxide, when inhaled in large doses, has also been reported to cause inflammation in the lungs (Filipponi and Sutherland 2012). According to a previous study, the effect of electrolyte concentrations on the aggregation behaviour of fullerene NPs has been investigated. Furthermore, previous studies have been focussed on determination, migration, and transformation of ENMs, as well as their interaction with other polluting molecules (Nowack and Bucheli 2007, Hassellöv *et al* 2008, Chen and Elimelech 2006). Therefore, the study on the fate and transport of carbon-based NMs, such as CDs and a-CDs, is vital in further understanding their behaviour under environmentally relevant conditions. This study provides important information on the aggregation behaviour of CDs and a-CDs and focuses on the effect of synthesis parameters and environmental conditions on the colloidal stability of the materials under study.

1.8. Thesis outline

The thesis is divided into two parts: part A is focused on studies performed on CDs and a-CDs under synthesis conditions, and part B concerns the investigation of the influence of several environmental conditions on the colloidal stability of CDs and a-CDs. Furthermore, the thesis is divided into six chapters. An outline of the chapters within the thesis is provided below:

Chapter 1 – Introduction

This chapter serves as a general introduction and describes the aim and objectives of this study. The problem is identified, and the significance of the research work is explained thoroughly. The safety of NMs is discussed and a brief description on CDs is laid out within this chapter. Furthermore, research questions, research approach, as well as scope and delimitations pertaining to this study are also included in this chapter.

Chapter 2 – Literature Review

This chapter provides an overview of the literature by taking a look at the work that has already been done on the fate and transport of carbon-based NMs. It starts off with a short history of nanotechnology such as Feynman's speech, miniaturised electronics, and advanced materials. To understand the foundation of this study, a closer look will be taken at what makes nanotechnology special before discussing the safety of NMs and other important subjects such as ELSA and risk management. Fundamental nano-effects are also under discussion in this chapter, namely what happens at the nanoscale, and unique material properties such as surface properties, the importance of surface atoms, surface energy, and electronic and optical properties. The review then goes into a rather detailed description of CDs, its fabrication, properties, and applications. Then, the significance of colloid science is discussed which includes technological and biological significance of colloidal dispersions, behaviour of colloidal dispersions such as Brownian motion and diffusion, colloidal stability, particle size and shape, and particle coagulation. Lastly, background information is provided on the analytical techniques utilised within this study.

Chapter 3 – Research Design and Methodology

The research design and methodology are outlined within this chapter. It consists of several sections such as a statement of the materials and chemical reagents used within this study as well as a list of equipment. Also, detailed descriptions on the optimisation of the synthesis parameters, the synthesis of CDs and a-CDs under optimum conditions, and the investigation

of the influence of environmentally relevant conditions on the colloidal stability of CDs and a-CDs, are discussed. Furthermore, two characterisation methods have been used, including UV-Vis, to understand the electrochemical nature of the materials under study, and zeta potential and hydrodynamic properties have been determined in the investigation of the influence of pH, IS and dissolved NOM on the colloidal stability of CDs and a-CDs.

Chapter 4 – Studies on Unfunctionalised Carbon Dots and Amine-Capped Carbon Dots

In this chapter, the results on the influences of synthesis parameters of CDs and a-CDs are discussed which includes information on (a) the % yield, (b) the colour of the product, (c) the mass of dialysis bags throughout dialysis, (d) the interaction of light with the synthesised materials through UV-Vis, and (e) the average hydrodynamic diameter (D_h), polydispersity index (PDI) and surface charge (i.e., zeta potential, ZP) of the synthesised materials.

Chapter 5 – Environmental Influences on Colloidal Stability of Unfunctionalised Carbon Dots and Amine-Capped Carbon Dots

This chapter provides comparative results on the influence of environmental conditions such as pH, IS and the presence of NOM on the colloidal stability of CDs and a-CDs. It consists of discussions on the effect of the above-mentioned parameters on the hydrodynamic diameter, surface charge, polydispersity index, and size distribution of CDs and a-CDs.

Chapter 6 – Conclusions and Recommendations

This chapter entails a final discussion and summaries on the main findings of this study as well as recommendations for future research on this study.

Chapter 2 – Literature Review

2. Introduction

This chapter delves deeper into the literature on which this research rests. It consists of background information regarding the work that has already been done on carbon-based nanomaterials, the safety of these nanomaterials, and highlights the reasoning behind the choice to work with the materials within this study. Briefly, the history of nanotechnology will be discussed which includes parts of Richard Feynman's speech, miniaturisation of electronics and advanced materials. Thereafter, the safety of nanomaterials and important subjects, such as Ethical, legal and social aspects (ELSA), nanomaterials in consumer products, cytotoxicity as well as ecotoxicity, will be discussed. Moreover, detailed descriptions on carbon-based nanomaterials will be explored, such as graphene, carbon-nanotubes and carbon nanodots. Furthermore, fabrication methods of carbon-based nanomaterials as well as the colloidal behaviour thereof is touched on. Lastly, information regarding the characterisation techniques pertinent to this study rounds off this chapter.

2.1. Nanoscience & nanotechnologies

2.1.1. History of nanotechnology

The first discussions regarding the manipulation of materials at the nanoscale date far back to the '50s when Richard Feynman posed a rather interesting question (Feynman 1960): *"Why cannot we write the entire 24 volumes of the Encyclopedia Britannica on the head of a pin?"* Later in 1974, Norio Taniguchi, a professor of Tokyo University of Science, first coined the term *nanotechnology* for manufacturing materials with dimensions in the nanometre-range (Loos 2015, Leon *et al* 2019, Mohan Bhagyaraj and Oluwafemi 2018, Bayda *et al* 2020). In 1981 the first instrument, known as the scanning tunneling microscope (STM), to image atomic-sized materials, was invented by Gert Binnig and Heinrich Rohrer (Binnig *et al* 1982, Binnig and Rohrer 1986). In 1985 Robert F. Curl Jr., Sir Harold W. Kroto and Richard E. Smalley discovered a new allotrope of carbon: the Buckyball (NobelPrize.org n.d., Science History Institute 2017)—a fitting name as it resembles a football. This molecule is made up of 60 carbon atoms (C_{60})—one C-atom found at each corner of the twenty hexagons and twelve pentagons—fused together in a ring structure (the geometrical shape of truncated icosahedron) bearing similarity to a cage (Tofighy and Mohammadi 2019). Back in 1970, Eiji Osawa of Toyohashi University of Technology predicted that C_{60} exists, and because of his prediction researchers were able to develop discrete methods of synthesis and characterisation for this

material. This new allotrope of carbon was officially named Buckminsterfullerene in honour of Buckminster Fuller, a well-known architect best known for his geodesic dome design (Filipponi and Sutherland 2012).

In the past, the idea of moving atoms individually sounded absurd, yet today specialised equipment has been developed for that particular purpose, such as the STM and Atomic Force Microscope (AFM). These two tools of analysis have enabled the development of nanotechnologies and revolutionised the imaging (with atomic resolution) and manipulation of surfaces at the nanoscale (Bayda *et al* 2020, Binnig and Rohrer 1986).

Metal colloids (metal nanoparticles, NPs, dispersed in a medium) have been shown to possess optical properties related to surface plasmons. In 1857, at the Royal Society of London, Michael Faraday presented a lecture in which he displayed a purple-coloured slide and made the statement that it consisted of *"gold reduced in exceedingly fine particles, which becoming diffused, produce a ruby-red fluid … the various preparations of gold, whether ruby, green, violet or blue … consist of that substance in a metallic divided state"* (Edwards and Thomas 2007, Faraday 1857). He went on to describe the process in which a gold colloid could change to blue in colour when in the presence of salt. Several artefacts containing metal colloids share these noteworthy colour effects. The Lycurgus cup (an ancient Roman dichroic glass that represents King Lycurgus being pulled into the underworld by Ambrosia) dates back to the fifth century and appears green when subjected to a light stimulus from the outside (Freestone *et al* 2008, Loos 2015, Edwards and Thomas 2007, Leon *et al* 2019). But when illuminated from the inside it appears ruby-red with the King appearing purple. The reason behind the coloured glass was only discovered in 1990, when a detailed SEM analysis was performed. Embedded in the glass, nano-sized particles of silver (66.2 %), gold (31.2 %) and copper (2.6 %), of up to 100 nm in size, were found and the absorption and scattering of light by these NPs gave way to different colours (Loos 2015). The beautifully stained-glass windows still seen today in several churches, which encompass a composite of glass and nano-sized metal particles, serve as another example. Glass is mixed with nanogold powder to produce the ruby-red colour, and gold NPs are mixed with tin dioxide to give rise to the purple hue (Filipponi and Sutherland 2012). Another example, dating back to the 20th century, was the Mie theory created by Gustav Mie: a description of the relationship of colloid-sized metals and the optical properties of solutions which contain them by a mathematical treatment of light scattering (Filipponi and Sutherland 2012).

2.1.1.1. Miniaturised electronics

Over the years, nanotechnology has aided in the evolution of electronics; its biggest focus being miniaturisation, allowing for faster and more compact devices. An example of this advancement can be seen in the semiconductor industry in which nanotech is utilised for the assembly of smaller integrated circuits (ICs). The transistor forms the core of the IC and every chip consists of numerous transistors acting like gates for the flow of electrons. In 1965 an IC chip was populated by 30 transistors, which increased to 2000 in 1971 (Hazari 2017, Loos 2015). In 2013, this figure skyrocketed to approximately 40 million! In 1965 Gordon E. Moore (co-founder of Intel Corporation) gave rise to Moore's Law which effectively suggests that electronic devices double in speed and capability about every 18 months (Loos 2015). For the past four decades his prediction has proved correct as the pace at which the data density of computer chips' growth increased exponentially at his predicted rate. Since then, the electronic industry has been driven by Moore's Law. Every year tech companies produce newer, faster, smarter and better gadgets (Hazari 2017).

According to Hazari, transistors are the fundamental unit necessary for driving every electronic gadget being used. The smaller they get, the faster they become and the less electricity is consumed during operation (Hazari 2017). Over the years, as the demand for miniaturisation increased, the dimensions of the transistor have been reduced significantly. In the year 2002, the dimensions of the transistor finally reached the nanoscale, with a single transistor of only 90 nm (Filipponi and Sutherland 2012). The important question of the 21st century became: how small can transistors be? In 2017, companies such as Intel mass-produced transistors of size only 14 nm in diameter, made of silicon, the second most abundant material on Earth. These transistors are about 70 silicon atoms wide, with an atom of silicon being about 0.2 nm in size. Has the smallest limit for a transistor's size been reached? An alternative was suggested by Hazari, in which light replaces electrical signals for the operation of a transistor—so instead of electrons moving from one end to another, photons would be moved in its place (Hazari 2017).

2.1.1.2. Advanced materials

Many NMs have been produced unintentionally and had gone uncharacterised for several years before the proper tools to discover them had been invented. History includes many examples of processes in which NMs are unknowingly formed. Anodising, a process first patented in the early 1930s, is one of the most significant processes utilised in industry for protecting

aluminium from corrosion in which the surface of aluminium is coated with a thin oxide layer (Filipponi and Sutherland 2012). At the time, it was unknown to the inventors that the protective layer was in actual fact a NM—an anodic layer consisting of closely packed hexagonal channels, approximately 10 to 250 nm in diameter. Other examples of unintentionally-made NMs include: NPs found within the rubber of car tyres, titanium dioxide within some modern-day sunscreens, and synthetic molecules in certain drugs (Mohajerani *et al* 2019).

2.1.2. Defining nanoscience & nanotechnology

Nanoscience is a rapidly evolving and interdisciplinary science that cuts across all vertical sciences and engineering, and could be defined as the study of fundamental principles of matter in the nanoscale (1–100 nm) (Mohan Bhagyaraj and Oluwafemi 2018, Leon *et al* 2019, Bayda *et al* 2020). Therefore, there does not seem to be any one definition that completely explains it. Nanotechnology is the application of nanoscience into practical (or technological) devices which involves the manipulation, control and integration of atoms and molecules in order to give rise to systems, materials, components and devices at the nanoscale (Bayda *et al* 2020). It could be seen as determined engineering of matter at or within the nanoscale for the achievement of properties and functions that relate to size. Science at the nanoscale has also been described as the study of phenomena and manipulation of materials (Mohan Bhagyaraj and Oluwafemi 2018). It involves the four main processes: design, characterisation, production and application. Today's scientists and engineers are determined to find various ways of synthesising materials at the nanoscale in order to take advantage of their enhanced properties such as higher strength, lighter weight, increased control of the light spectrum, and greater chemical reactivity. In theory, all materials could be improved with nanomaterials but in reality, the 'cost versus added benefit' relationship determines which industrial sectors will benefit the most from nanotechnologies (Filipponi and Sutherland 2012).

The prefix 'nano-' specifically means a measure of 10^{-9} units. A nanometre is a unit of length equivalent to one billionth of a metre. Even though the nanoscale ranges from 1 to 100 nm, the definition allows for some nanomaterials to fall outside the boundaries, which shows that the upper and lower boundaries are approximate (ISO/TS 80004-1:2015 2015). 1 nm is set as the lower limit in order to distinguish single and small groups of atoms and individual molecules from nanomaterials. And even though the upper limit of the nanoscale is 100 nm, there are materials above this limit which could still be classified as nanomaterials.

When the nanoscale is reached, classical (or Newtonian) physics can no longer be used to describe the behaviour of particles within these dimensions; at this scale quantum mechanical principles apply. Therefore, the properties of materials are size-dependent in this scale; a nanomaterial would have very different properties from its bulk counterpart. These properties can be: chemical, mechanical, magnetic, optical, electric, etc. (Loos 2015).

A nanomaterial is described, in principle, as a material of which a single unit is sized (in at least one dimension) between 1 and 1000 nm, but is usually between 1–100 nm (Ellenbecker and Tsai 2011). Nanomaterials are developed to exhibit novel characteristics compared to their bulk counterparts, such as size, shape, morphology, and chemical composition, as well as increased strength, chemical reactivity and conductivity. A well-known definition for a nanomaterial defined by the International Organization for Standardization (ISO/TS 80004-1:2015 2015) is that it is a *"material with any external dimension in the nanoscale (size range from approximately 1 – 100 nm) or having internal structure or surface structure in the nanoscale"*. There are different types of nanomaterials and they are defined by the quantum confinement effect.

Quantum mechanics is defined as a scientific model that was developed in order to describe the motion and energy of atoms and electrons. The process of synthesising NMs from their bulk counterparts essentially involves the process of quantum confinement. Quantum confinement could be described as the restriction in the motion of a particle in one or more dimensions by a potential well (Arivazhagan 2014). The particle behaves as if it were free when the confining dimension is large compared to the wavelength of the particle. The particle's energy is indirectly related to the confining dimension; there is an increase in energy with a decrease in the confining dimension. In nanomaterials, the electrons are confined in space rather than free to move in the bulk of the material. The degree of that confinement determines the shape of the material; a nanosphere (quantum dot/nanocrystal) is confined in all three dimensions and is known as a zero-dimensional (0D) material; a nanorod (quantum wire/nanowire) is confined in two dimensions, which makes it a one-dimensional (1D) material; a quantum well (or superlattice) is confined in one dimension and is known as a two-dimensional (2D) material; and lastly a bulk material is not confined in any dimension, has all dimensions free and is therefore known as a three-dimensional (3D) material (Arivazhagan 2014).

2.1.3. The uniqueness of nanoscience

The most noteworthy significance of nanomaterials would be the fact that they are so small, meaning that nanomaterials can assume very different properties from their bulk counterparts. This is where their novelty lies—the ability to create materials with more enhanced properties. Several properties are improved such as chemical reactivity or magnetic, mechanical, electrical, optical properties, etc. (Loos 2015). In addition, several new effects arise when moving from a bulk material to its nano-counterpart. For example, silver in its bulk form is non-toxic but silver nanoparticles have the ability of killing viruses upon contact (Galdiero *et al* 2011). A metal could become a semiconductor or insulator at the nanoscale because of the change in bandgap. The second significant property of nanomaterials would be that they could be manufactured by a process known as "bottom-up synthesis" in which they are fabricated atom by atom, carrying information in the building blocks of the material for them to self-assemble in formation of the final product (Baker and Baker 2010, Wang and Hu 2014). Lastly, due to their small size, nanomaterials have a larger surface-to-volume ratio than their bulk counterparts, meaning that NMs have a larger number of surface-atoms which allows for enhanced processes—those that occur at the surface of a material, such as catalysis and detection (Gao *et al* 2009, Song *et al* 2017b).

2.1.3.1. The importance of surface atoms

As previously mentioned, nanomaterials are known for their very large surface area as well as their large surface-to-bulk ratio. This is due to the fact that there are more atoms present on the surface of these materials than in their core. There are several properties that depend on the nature of the surface such as chemical reactivity, catalytic reactivity, electrical resistivity, gas storage and adhesion (Biener *et al* 2009, Loos 2015). This is what makes NMs so attractive. The shape of the material plays a defining role in the magnitude of the surface area.

It has already been established that atoms and molecules existing at the surface or at an interface have different properties, such as lower stability and higher surface energy, compared to those found within the core of a material. A fundamental chemical principle is that 'systems of high energy will strive to attain a state of lower energy, by whatever means possible'. As such, NMs will attempt to undertake any and every method or route in order reduce their high surface energy. This could be achieved by agglomeration in order to effectively reduce the surface area and in turn reduce the surface energy, which is easily achieved due to the fact that surface energy is an additive quantity (Filipponi and Sutherland 2012).

2.1.4. The safety of nanotechnology

2.1.4.1. Nanotechnology in consumer products

Over the last few years there has been a rapid rise in the amount of consumer products containing some form of nanomaterial. A nanotechnology consumer product inventory was compiled in 2006 by Woodrow Wilson International Center for Scholars (WWICS) in the Project on emerging nanotechnology. Their intention was to collect, archive and share information regarding consumer products claimed by their manufacturers as nano. In March 2006, approximately 200 products were noted on their list after which this number doubled in the year 2007. The inventory list grew even longer and by August 2010 it consisted of more than 1100 products that claimed to have some form of nanotechnology incorporated in them (Ellenbecker and Tsai 2011). It should however be noted that the number of nano-characteristics that could be incorporated in a consumer product could stretch from nanocoatings to the incorporation of a nanomaterial itself and could also just mean that the product was manufactured with the aid of nanotechnology, and hence might not contain any nanomaterials itself (Filipponi and Sutherland 2012). The most common type of nanomaterial, claimed to be found in the above-mentioned consumables, is silver which is followed by carbon, zinc, silica, titanium and gold. The pace of emerging nanotech far exceeds that of studies on their toxicity, which is a matter that is quite alarming. The question becomes: if all these products do have some form of nanotechnology enhancing them, were there any sorts of toxic regulation on the nanomaterials found in them before these products hit the shelves and before they were rolled out to consumers?

2.1.4.2. Ethical, legal & safety aspects

Looking at the ethical, legal and safety aspects (ELSA) of technology means looking at the bigger picture; with all the progress of science and innovation there will ultimately be implications when it comes to the environment and living organisms. The main objective of ELSA is to critically evaluate the impact of science and technology on society. According to Filipponi and Sutherland, there are several factors to consider when ethics comes into play such as privacy and justice (Hullmann 2008, European Defence Agency 2019). There is no argument that nanotechnology is changing the world around us, as it is being utilised in just about every field of science. However, with all these advancements in technology, there are many concerns regarding the disadvantages that accompany it. Several things to consider surfaced with the growth of nanotechnology such as identifying its benefactors, deciding on the extremities, the invasion of privacy, and the furthering of economic and social divide. With the important role

that nanotechnology already plays in modern medical diagnostics and treatment technologies, we also need to consider any abilities and advantages that are inhumane in nature (Hullmann 2008).

2.1.4.3. Nano-pollution and engineered nanoparticles

Nanopollution is a term which has found its dwelling in a number of workplaces; this includes aeroplane and motor vehicle exhaust emission nanoparticles, nanoparticles produced from the erosion of man-made materials (such as tyres), and also those produced by natural erosion and volcanic activity (Filipponi and Sutherland 2012). Humankind has already been, and definitely still is, exposed to nanopollution in many ways and to different extents, with some effective protective measures being taken for workers exposed to ultrafine particles in the workplace, i.e., through filters, textiles, and gloves (Filipponi and Sutherland 2012, Mohajerani *et al* 2019). To this day, the effects of engineered nanoparticles (ENPs) and nanopollution on living organisms and the environment are still under study. It is no secret that ENMs could be hazardous to the environment as well as human health (Biswas and Sarkar 2019, Pramanik and Maity 2013, Ellenbecker and Tsai 2011). Therefore, the question of ecotoxicity is raised in which the toxic nature of nanomaterials in the environment is brought to light. Would these materials pose any threat to ecosystems or would they degrade? How would the colloidal stability of these material be affected by environmental conditions? Would they be dispersed or would they agglomerate? The size of these nanomaterials is the reason for their possible toxic nature, because they are on a similar scale to that of biomolecules such as DNA and proteins (Soutter 2019). Therefore, there is no telling how these materials would interact and whether their interaction would be adverse or not, which also brings about the issue of cytotoxicity.

2.1.4.4. Cytotoxicity, bioimaging and surface modification

Cytotoxicity is greatly important when it comes to biological applications of any material. Due to their small size, nanomaterials could breach dermal barriers, pass through the membranes of cells, migrate via neural pathways, penetrate regions for gas exchange within the lungs and then migrate to other parts of the body (Ellenbecker and Tsai 2011). In the medical field, nanomaterials are designed to pass through the membranes of cells, and are seen as a solution for targeted drug delivery (Zhang *et al* 2017). For example, researchers have previously synthesised hyaluronate and polyethylenimine (PEI) functionalised CDs (HP-CDs) for tumor targeting and gene delivery as these materials exhibited superior dispersibility in water and

good biocompatibility (Zhang *et al* 2017). The idea behind these drug delivery systems is that drugs containing nanomaterials would only be delivered to infected cells.

According to Wang et al., the toxicity of CNTs has been examined in numerous previous papers that showed that there might be significant health effects related to exposure to CNTs such as granulomatous pneumonia, oxidative stress, decrease in pulmonary function, and cardiac tissue inflammation. Oxidative stress, caused by high levels of reactive oxygen species (ROS), could cause major damage to cells through peroxidising lipids such as inflammation, interference with gene functions and signalling, and alteration of proteins and DNA. Therefore, it is seen as the most common way for ENMs to induce toxicity (Wang *et al* 2014b). Due to the fact that the size of CNTs are two orders smaller than asbestos and that they have a morphology comparable to asbestos, they have been proven to pose a greater threat of mesothelioma (a fatal cancer) following the installation of CNTs into the peritoneum of mice in recent studies (Ellenbecker and Tsai 2011). Another study, done on hairless mice, investigated the effects of exposure to titanium dioxide (TiO_2) nanoparticles. Evidently, these particles passed through the skin, after dermal exposure of about 60 days, and caused diverse pathological lesions in many vital organs (Wang *et al* 2014b).

Over the past few years substantial progress has been made in the use of carbon quantum dots (CQDs) in bioprobes (Wang and Hu 2014). These ENPs have shown great stability but when functionalised, their biocompatibility becomes questionable. According to Wang and Hu, several cytotoxic experiments were performed on plain CQDs and their passivated forms; one such experiment being the fabrication of CQDs from the arc-discharge of graphite rods followed by a 12-hour nitric acid (HNO_3) reflux (Wang and Hu 2014). In that study, the authors have reported that raw CQDs seemed to have no toxic effects on cells up to a concentration of 0.4 $mg.mL^{-1}$. Further studies on CQDs produced by numerous fabrication methods seem to arrive at the same conclusion: that CQDs show negligible cytotoxic behaviour at concentrations essential for fluorescence bioimaging (Wang and Hu 2014). In other studies, CQDs, produced via microwave irradiation, were introduced into C6 glioma cells and displayed low cytotoxic levels, meaning that their use in bioimaging could be possible.

Photoluminescence (PL) is an essential property that materials, utilised in bioimaging, need to possess. The PL of a nanomaterial can be tuned by surface modification, electron/energy transfer and numerous capping strategies and the characteristics of CDs have been proven to be tuneable by a) the choice of precursors during synthesis, b) surface passivation, and c)

functionalisation (Wang and Hu 2014). Surface passivation allows for the tunability of certain properties and in the case of CDs, it has previously been used to tune their fluorescence intensity by means of amine-containing agents which makes them suitable for desired applications such as bioimaging. Previous studies have shown that surface passivation of CDs can be achieved through covalent bonding (due to the oxygen-rich surface of CDs) (Yang *et al* 2012a, Yin *et al* 2013), coordination (Zhao *et al* 2011), sol-gel technology (Mao *et al* 2012) and π-π interactions (Li *et al* 2011). Previous papers have focused on the pyrolysis of citric acid in fabrication of CDs of high PL. In these studies, various amine molecules had been used and the findings were that primary amine molecules yielded CDs with enhanced PL properties due to their dual use as nitrogen-doping precursors as well as surface passivating agents. A rather large increase in quantum yield (QY) of 30.2 % had been observed as the nitrogen content increased due to surface passivation (Wang and Hu 2014). The overall conclusion was that these CDs displayed properties that would be highly compatible with biological molecules and thus meant that the biomedical industry could benefit greatly from it (Wang and Hu 2014).

In order to alter PL properties of PL materials, a technique known as doping is used. Nitrogen (Manioudakis *et al* 2019, Bhattacharyya *et al* 2017, Song *et al* 2017a, Pang *et al* 2017, Zheng *et al* 2020), sulphur (Song *et al* 2017a, Pang *et al* 2017) and phosphorus (Kandasamy 2019, Song *et al* 2017b) are amongst the most common elements used to tune or adjust properties of CDs and are introduced by means of doping. An introduction of nitrogen-containing groups via doping induces an upward shift of the Fermi level as well as the electrons of the conduction band, and hence, also enhances the emission of CDs (Ayala *et al* 2010). Previous studies have shown that only C-N bonding really leads to the enhancement of PL emission of CDs (Wang and Hu 2014). There have also been very successful co-doping studies which involved CDs doped with both phosphorus and nitrogen, as well as CDs co-doped with sulphur and nitrogen. The resultant phosphorus- and nitrogen- co-doped CDs displayed increased photoluminescent properties and high electrocatalytic activity, whereas the CDs co-doped with sulphur and nitrogen (Song *et al* 2017a, Pang *et al* 2017) exhibited exceptional solubility and biocompatibility as sulphur provided a variety of bonding configurations.

In previous studies, CQD-surfaces were passivated with a number of functional groups such as polyethylene glycol (PEG), polypropionylethyleneimine-co-ethyleneimine (PPEI-EI), polyethylenimine (PEI), branched polyethylenimine (BPEI), and polyacrylic acid (PAA) in order to profile their cytotoxicity levels (Wang and Hu 2014). The introduction of PEG functional groups to the surface of CQDs proved to be nontoxic to cells at considerably higher

concentrations than required for applications such as cell imaging. Moreover, in a study where mice were injected with PEG_{1500N}-functionalised CQDs, there were no noteworthy in vivo toxic effects (Wang and Hu 2014). Furthermore, CQDs functionalised with PPEI-EI groups typically displayed no toxic effects when subjected to cells under a higher concentration than that for imaging purposes. In the studies done with PEI-functionalised CQDs subjected to HT-29 cells, their cytotoxicity was also practically non-existent at fairly high concentrations. Due to the presence of a higher number of EI units in PEI, PEI-passivated CQDs turned out to be more cytotoxic with their concentration thresholds being fairly lower than that of PPEI-EI-passivated CQDs. However, the cytotoxic effects of PAA-passivated CQDs on cells at moderately low concentrations (of about 50 $\mu g.mL^{-1}$) proved to be more alarming (Wang and Hu 2014).

It has long been established that the risk of any material depends on the route of exposure and the dosage of that exposure. As previously mentioned, ENMs could possibly be inhaled or cross dermal barriers and exposure to ENMs could happen during manufacturing and product incorporation (known as occupational exposures) or during product use and product disposal, i.e., environmental exposures (Ellenbecker and Tsai 2011). Usually, the toxic nature of a substance increases as the time of exposure increases, which was the case with the PAA-functionalised CQDs. Its toxicity level increased as the time of exposure to cells was increased from 4 to 24 h (Wang *et al* 2011c). The overall findings indicated that molecules of a low cytotoxic nature could still be suitable for applications in biosensors and for imaging purposes; some examples include functional groups such as PEG and PPEI-EI. Functional groups such as BPEI and PAA showed higher cytotoxicity in vivo but could still be utilised given that their concentrations are kept low enough (Wang *et al* 2011b). In the case of titanium dioxide (TiO_2), reports have stated that exposure to high doses thereof caused inflammation in lungs (Choi *et al* 2014). It is safe to say that if these materials were to be introduced to humans, animals or the environment in doses larger than what is reported to be safe, then they could pose a threat.

Toxicity studies go far beyond just the materials under investigation. It has been discovered that the choice of reference materials, dispersion medium, and route of synthesis could heavily influence the degree of toxicity the material could possess (Filipponi and Sutherland 2012). Since the discovery of fullerenes, research has been focussed on carbon-based NMs and metal or metal-oxide NPs such as ultrafine TiO_2. Scientists have performed several toxicity studies on CNTs and have found that some forms thereof led to pulmonary toxicity. The toxic nature of CNTs were then traced back to the presence of iron in its manufacturing process (depending on its surface properties and length) which gave rise to the reactive oxygen species 8, meaning

that the CNTs itself did not contribute to the cytotoxicity and the removal of iron then led to a decrease in the production of oxidant in the material and in turn reduced the cytotoxic levels thereof. Another important factor to consider is the medium of dispersion of the NMs when toxicity studies are underway. Reports on fullerenes have mentioned that fullerenes are well dispersed when in calf serum but fail to be dispersed in water (Filipponi and Sutherland 2012). Dispersity of NMs thus greatly depend on the medium they are dispersed in. In water suspensions CDs are well known for their colloidal stability at low ionic strength (IS) as well as their PL stability under those conditions. However, the stability of the PL of CDs is generally expected to decline under conditions such as aggregation (Bayati *et al* 2018).

Aggregation, as previously mentioned, is one of the ways in which materials regain stability by lowering their surface energy. To map the aggregation of materials and to understand their colloidal behaviour, colloid science is used. Apart from all the valuable contributions of colloid science to the biological, engineering, medical and agricultural industries, colloid science also has an important role to play in reducing the harmful effects of the development of nanotechnology. According to Hunter, several pollution problems exist due to the presence of unwanted colloidal materials, and their removal from the environment requires the application of colloid chemical techniques. For removal, concentration and possible recovery of industrial products from air and water, the use of certain properties of adsorption of colloids is required (Hunter 1987). Therefore, colloid science is of importance in order to understand and map the behaviour of carbon nanodots in the environment.

2.2. Carbon-based nanomaterials

Having already discussed CNTs and fullerenes and their cytotoxic effects, the natural progression of conversation leads to other carbon-based nanomaterials such as graphene and carbon-nanodots.

2.2.1. Graphene

Graphene is made up of monolayers of carbon atoms arranged in a honeycomb network, and is a two-dimensional material which could be seen as the parent of all graphitic carbon forms (Li and Kaner 2008). Originally, in 2004, graphene was isolated from graphite by two Nobel Prize winners in Physics, Andre Geim and Konstantin Novoselov from the University of Manchester, by repetitively peeling apart shavings of graphite until one-atom thick pieces were produced (Filipponi and Sutherland 2012). To keep the graphene sheets separated is vital but rather challenging. Bulk graphene sheets—if left unprotected—will spontaneously undergo

agglomeration and restack to form graphite (Li and Kaner 2008). According to Li and Kaner, unusual electronic properties surfaced from the confinement of electrons in two dimensions when physicists were finally able to isolate graphene sheets from mechanically cleaved graphite (Li and Kaner 2008). Graphene is said to be "*a giant aromatic macromolecule that conducts both electricity and heat well in two dimensions*". Individual graphene sheets possess a specific surface area significantly larger than that of activated carbon utilised in water purification and their mechanical strength is 200 times stronger than steel and comparable to that of CNTs (Filipponi and Sutherland 2012, Li and Kaner 2008). According to Bayati, graphene, in many ways, enhances the properties of materials by producing higher mobility and mechanical stability due to its high surface area (Bayati *et al* 2020).

Chemical functionalisation or the use of dispersants is usually required for the prevention of agglomeration. The surface of graphite oxide is highly rich in oxygen-containing groups such as carboxyl and hydroxyl groups providing an increased number of reactive sites for surface functionalisation (Li and Kaner 2008). When the surface of graphite oxide is functionalised with suitable organic groups it allows for effective separation of graphene sheets during synthesis. Stability of graphene sheets could also be achieved through the control of colloid chemistry by electrostatic repulsion. Chemical conversion of graphene oxide to graphene yields residual oxygen-containing groups on the graphene surfaces and results in negatively charged surfaces when dispersed in water (Li and Kaner 2008).

Graphene-based materials have been under study for quite some time. In the mid-1800s, strong oxidising agents such as potassium chlorate ($KClO_3$) and nitric acid (HNO_3) were used for graphene synthesis. Whereas in 1958 the experimental procedure for the fabrication of graphene oxide nanomaterials originated with the production of graphitic oxide by a process still known today as Hummers' method (Bayati *et al* 2020). Although these experimental procedures produced the desired materials, several undesired materials were also produced such as toxic gases (namely NO_2, ClO_2 and N_2O_4) and other dangerous chemicals such as sulfuric acid, sodium nitrate and potassium permanganate. Some research teams bettered fabrication routes by eliminating the production of some hazardous materials but in turn required larger quantities of the reagents in a modified version of Hummers' method, in which they successfully managed to eliminate $NaNO_3$ but in turn needed more $KMnO_4$ (Bayati *et al* 2020).

2.2.2. Carbon dots

Carbon dots (CDs) form part of a class of quasi-spherical, photoluminescent (PL) carbon nanoparticles and are rapidly emerging with their growing applications in various fields (Baker and Baker 2010, Bayati *et al* 2018, Zhang *et al* 2017). CDs can easily be fabricated by many inexpensive approaches, ranging from simple candle burning (Liu *et al* 2007) to in situ dehydration reactions (Peng and Travas-Sejdic 2009) to laser ablation methods (Baker and Baker 2010, Zhao *et al* 2008). Studies have shown that carbon dots are biocompatible, have low toxicity, and distinctive PL properties and could possibly be used for a number of applications, such as bioimaging, biological labelling, anticounterfeiting, information encryption, and information storage (Ray *et al* 2009, Qu *et al* 2012). According to Baker and Baker, their excellent water solubility could be owed to their carboxylic acid-rich surface, making them suitable for further functionalisation with a variety of species including biological, polymeric, organic, and inorganic species (Baker and Baker 2010). With their successful utilisation in biomedicine, optoelectronics, catalysis and chemical sensors, their application in the environment is rather promising (Ray *et al* 2009, Deng *et al* 2014, Wang and Hu 2014). Furthermore, what makes CDs even more attractive is the fact that they might be suitable to replace the toxic metal-based quantum dots (QDs) previously found to pose biological and environmental hazards (Michalet *et al* 2005, Ray *et al* 2009, Baker and Baker 2010, Sun *et al* 2006).

2.2.2.1. Fabrication methods

Over the years, many studies have been done on CDs and three main complications were found with their fabrication processes: (a) agglomeration during carbonisation, (b) size management and consistency, and (c) vital surface properties pertaining to solubility (Wang and Hu 2014). There are several post-treatment solutions in order to control the size of these nanoparticles, such as gel electrophoresis (a rather difficult task) (Liu *et al* 2007, Ray *et al* 2009) and purification methods such as centrifugation and dialysis. Furthermore, the aggregation problem could possibly be avoided or alleviated by an electrochemical synthesis route, using solution chemistry methods or confining pyrolysis (Wang and Hu 2014).

CDs can be fabricated through a number of ways which could be classified into two categories, namely top-down, formed from a larger carbon structure, or bottom-up, in which CDs are produced from molecular precursors (Baker and Baker 2010, Zhang *et al* 2017). Top down methods include arc-discharge (Xu *et al* 2004), laser ablation, and electrochemical oxidation; whereas bottom up approaches include thermal, or microwave-assisted methods. Some of the

experimental approaches for the fabrication of CDs via either bottom-up or top-down approaches are outlined below which is followed by detailed information on purification procedures.

A. Top-down methods

- ***Arc-discharge***

As previously mentioned, the first method in which CDs were produced was through an arc-discharge method performed by Xu et al. in which SWCNTs were purified or separated from other arc soot species through electrophoresis in agarose gel and glass bead matrices (Xu *et al* 2004). To the surprise of the researchers, the suspension separated into three classes of NMs: long nanotubes, slow moving tubular material, and a fast-moving band of highly fluorescent material (later known as CDs or carbon nanodots, CNDs) (Baker and Baker 2010, Xu *et al* 2004).

- ***Laser ablation***

Numerous studies have made use of laser ablation for the fabrication of CDs. One of these studies was performed by Sun et al. in which a carbon substance was subjected to laser irradiation at 900 °C in the presence of water vapour and a carrier gas such as argon at 75 kPa (Sun *et al* 2006). CDs of high luminescence were fabricated after a 12-hour reflux in nitric acid (HNO_3) with the addition of simple organic molecules such as diamine-terminated oligomeric poly(ethylene glycol) (PEG_{1500N}), and poly(propionylethyleneimine-co-ethyleneimine) (PPEI-EI) (Baker and Baker 2010, Sun *et al* 2006, Wang and Hu 2014). According to literature, another research group, Hu et al., synthesised fluorescent CDs through a one-step process of subjecting a carbon powders (i.e., graphite powders) to an organic solvent and then irradiating the mixture with a laser for 2 hours as illustrated in Figure 2 below (Baker and Baker 2010, Hu *et al* 2009, Wang and Hu 2014). The choice of organic solvent determines the state of ligands on the surfaces and, in turn, allows tuneable fluorescence emission of the CDs produced (Hu *et al* 2009, Wang and Hu 2014).

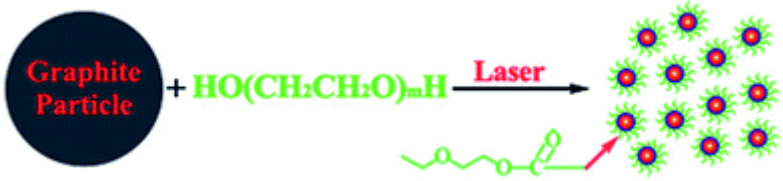

Figure 2. One-step synthesis of CQDs through laser irradiation (Hu et al 2009).

- ***Chemical oxidation/ablation***

In chemical ablation, organic molecules are carbonised by strong oxidising acids in the production of carbonaceous substances that in turn could further be reduced in size through controlled oxidation into small sheets (Peng and Travas-Sejdic 2009, Shen *et al* 2013, Wang and Hu 2014, Ray *et al* 2009). However, this approach involves rather harsh experimental conditions and, in some studies, yielded lower PL intensities with increasing pH levels (Shen *et al* 2013). One of these studies, performed by Peng and Travas-Sejdic, reported on the fabrication of luminescent CDs by dehydration of carbohydrates with concentrated sulfuric acid (H_2SO_4). The intermediate carbonaceous material was then treated with nitric acid (HNO_3) producing individual CDs which then underwent surface passivation to yield amine-functionalised CDs (Peng and Travas-Sejdic 2009). They found that the emission wavelength was tuneable by the choice of starting material and the duration of nitric acid treatment (Peng and Travas-Sejdic 2009, Wang and Hu 2014). In another study performed by Shen et al., pH-sensitive multicolour photoluminescent carbon nanoparticles (CNPs) were fabricated by carbonisation of a cationic branched polyelectrolyte of large molecular weight, with the possibility of being utilised in cell metabolisation monitoring as proton sensors and HeLa cell (Henrietta Lacks strain of cancer cells) imaging (Shen *et al* 2013, Wang and Hu 2014).

- ***Electrochemical oxidation***

The process of electrochemical carbonisation is another top-down approach of synthesising CDs from their bulk counterparts, i.e., carbon materials. The use of this synthesis method is rather rare and very few studies have made use thereof. This synthesis technique was first employed by Zhou et al. in the synthesis of CDs, in their study of growing multiwalled carbon nanotubes (MWCNTs) through chemical vapor deposition (CVD) from scrolled graphene layers on carbon paper to serve as the working electrode in an electrochemical cell; with a platinum (Pt) wire and $Ag/AgClO_4$ as counter and reference electrodes, respectively (Baker and Baker 2010, Zhou *et al* 2007). This cell was embedded in a degassed acetonitrile electrolyte solution of 0.1 M tetrabutylammonium perchlorate ($TBA^+ClO_4^-$). CDs were recovered through exfoliation from the MWCNTs after electrochemical cycling between −2.0 and +2.0 V at a scan rate of 0.5 $V.s^{-1}$ which caused intercalation of TBA cations into gaps of CNTs (Zhou *et al* 2007). Furthermore, Zhao et al. reported on the synthesis of carbon nanocrystals (CNCs) through electrooxidation of graphite in an aqueous solution with convenient separation; in which a graphite column electrode underwent oxidation at 3 V against a saturated calomel electrode (SCE) with a Pt wire as counter electrode immersed in 0.1 M NaH_2PO_4 electrolyte

(Baker and Baker 2010, Zhao *et al* 2008). In another study, performed by Deng et al., researchers employed alcohols of low molecular weight that were carbonised under ambient conditions through electrochemical oxidation (Deng *et al* 2014). The use of several alcohols showed that these NPs have universal application. In the study, two platinum (Pt) sheets formed the working and auxiliary electrodes, whereas a calomel electrode was used as the reference electrode. They found that the size and graphitisation degrees increased with an increase in potential across the electrodes and that various molecular alcohols of low molecular mass could be used to prepare CDs of low toxicity to human cancer cells (Deng *et al* 2014, Wang and Hu 2014).

B. Bottom-up methods

- ***Microwave irradiation***

Several studies have made use of microwave irradiation for the production of CDs which has been found to be a time-effective method of low cost (Gong *et al* 2014, He *et al* 2015, Jaiswal *et al* 2012, Li *et al* 2012, Liu *et al* 2015, 2011b, 2016, López *et al* 2015, Mitra *et al* 2012, Wang *et al* 2014a, Zhu *et al* 2009, Baker and Baker 2010, Georgakilas *et al* 2015, Wang and Hu 2014). Zhu et al. produced fluorescent CDs from poly(ethylene glycol) (PEG-200) and saccharide (i.e., glucose, fructose) in a 500 W microwave over 2-10 minutes (Zhu *et al* 2009). Liu et al. reported on a one-step microwave-assisted pyrolysis method of synthesising photoluminescent CDs from glycerol and 4,7,10-trioxa-1,13-tridecanediamine (TTDDA) (Liu *et al* 2011a). Furthermore, green luminescent CQDs have been synthesised within one minute of irradiation in a microwave and involved a reaction between a carbon source (i.e., sucrose) and a reaction media such as diethylene glycol (DEG) (Wang and Hu 2014).

- ***Hydrothermal/solvothermal treatment***

Hydrothermal carbonisation is an environmentally friendly technique used for the low-cost synthesis of carbon-based materials from a variety of reagent materials. This presumably nontoxic method usually involves an organic precursor, such as citric acid, chitosan, banana juice or glucose, that is sealed in a hydrothermal reactor and heated to a high temperature (Wang and Hu 2014). Luminescent CDs produced via this method have also been reported on by several research teams who fabricated CDs of good photostability, seemingly low toxicity with potential application in bioimaging. Another interesting precursor of the above-mentioned list is chitosan, which underwent carbonisation at 180°C for 12 hours in the production of fluorescent amine-capped CDs as performed by Yang et al. in only one step (Yang *et al* 2012b, Wang and Hu 2014). Furthermore, in 2017, Zhang et al. fabricated hyaluronate and

polyethylenimine (PEI) functionalised CDs (HP-CDs) through hydrothermal reaction (at 180 °C in a Teflon-lined stainless steel autoclave) of hyaluronic acid and PEI, for tumour targeted and gene delivery (Zhang *et al* 2017).

The above-mentioned synthetic routes used for the preparation of CQDs all have their advantages and disadvantages. Chemical ablation is the most accessible method in which a variety of sources could be used. However, it requires harsh conditions, drastic processes, multiple steps, and provides poor control over size. Electrochemical carbonisation, on the other hand, is a stable, one-step process which provides better control over size and nanostructure; however, it has the disadvantage of producing CDs of mixed sizes, and further separation through filtration or chromatography is required (Deng *et al* 2014). *Furthermore, laser ablation is an effective, rapid process that allows tunability over surface states, however it has a low quantum yield, provides poor control over size and requires modification. Moreover, hydrothermal/solvothermal treatment is a cost-effective, eco-friendly, and non-toxic method but it provides poor control over size* (Wang and Hu 2014). *Lastly, even though microwave irradiation provides poor control over size, it is a rapid, scalable, cost-effective, and eco-friendly method, and therefore has been utilised in this study.*

2.2.2.2. Purification procedures

According to Robert J. Hunter, both centrifugation and dialysis are methods of successive dilution in which particles are brought into contact with a large volume of liquid and are allowed to reach equilibrium (Hunter 1987). A separation process then follows which is repeated with the introduction of a new sample of liquid known as the wash liquid. The process of separating a colloid from a liquid always depends on the size difference between the impurities and colloid particles. The difficult task of separating the colloid from a liquid can be accomplished by sedimentation, in which gravitational separation or centrifugation could be undergone, or by the process of dialysis in which a semipermeable membrane is used (Hunter 1987).

In sedimentation, large or heavy particles sediment under gravity, provided their densities are significantly greater than that of the liquid. Aggregation could serve to speed up the process of sedimentation as particles lump together to form large aggregates or floccules (Hunter 1987). The problem with sedimentation procedures is proper separation of small particles of low density from the solvent. Dialysis, first employed by the Scottish chemist Thomas Graham

(often referred to as the “Father of Dialysis”) in 1861, proves to be a better choice for the separation of small molecules and ions from colloidal material (Cameron 2012, Hunter 1987).

Dialysis is a diffusive process which relies on the difference in concentration across a semipermeable membrane. The membrane is selected to be impermeable to the colloid intended to be retained but permeable to unwanted smaller materials such as impurities. Ions and small molecules migrate through the pores of the membrane from an environment of a high concentration to an environment of low concentration, effectively reducing the concentration of these small molecules within the sample (Hunter 1987). This process continues until an equilibrium is reached. The difference in chemical potential on either side of the membrane is the driving force for any species across the membrane. In dialysis, a membrane bag, in which the colloidal material is retained, is bathed in a wash liquid. According to Hunter, the dialysis bag, produced by the dissolution and reprecipitation of cellulose, is rather flexible and has the desired pore size for the elimination of impurities (Hunter 1987).

2.3. Characterisation techniques

Analysis of the structural characteristics of carbon-based nanomaterials involves investigating their physical and chemical properties. In order to describe the colloidal behaviour of the synthesised materials, the characterisation techniques pertinent to this study are described. These techniques were used in order to analyse material properties and to obtain information vital to understanding the behaviour of the materials under study such as size, surface properties, and size distribution. The properties of carbon-based nanomaterials are affected greatly by their size and morphology. The techniques used for analysis of the carbon-based nanomaterials are outlined below.

2.3.1. Spectroscopy

Electromagnetic radiation (EMR) could be seen as an electromagnetic (EM) wave that travels at the speed of light. It could also be considered as pockets of energy or photons and this brings in the topic of Heisenberg's uncertainty principle as the simultaneous measurement of both the particle-like and wave-like properties of a photon is impossible (Willard *et al* 1988). The wave-like properties of EMR come from electric and magnetic fields that oscillate transversely perpendicular to one another (Wayne and Wayne 1996). Light has several intrinsic properties, such as refraction, reflection, diffraction, propagation, polarization and interference, that are all accounted for by the wave theory (Wayne and Wayne 1996). But other concepts such as black-body radiation (BBR) and the photoelectric effect can only be understood if light is seen to behave as particles or considered as consisting of a stream of photons with fixed energies that is dependent on the wavelength or frequency of radiation (Wayne and Wayne 1996). Understanding the interaction of radiation with matter and interpreting the chemical changes that accompanies it, requires a mindset that relies on the assumption that radiation should be treated as behaving as particles of quantised energy (Wayne and Wayne 1996).

The EM spectrum is made up of a broad range of radiations that extends from low to high frequency or energy, and from short to long wavelengths (Willard *et al* 1988). Cosmic rays have the shortest wavelength (10^{-9} nm) but the highest energy, whereas radio waves have much longer wavelengths (up to 1000 km) and exhibit low energy (Willard *et al* 1988). In between these two extremes lie the rest of the spectrum which includes gamma rays, X-rays, ultraviolet (UV) rays, visible light, infrared (IR) rays, and microwaves, in increasing wavelength and decreasing frequency (Willard *et al* 1988). Each of the types of radiations mentioned above are used in different methods of analysis in order to study their interaction with matter and obtain a vast pool of knowledge on materials (Willard *et al* 1988).

Spectroscopy is the study of the interaction of EMR whether absorbed, emitted or scattered by atoms, molecules or other species of chemical nature. All of the above-mentioned radiation types move with the speed of light but their wavelength, frequency, physical and chemical effects with matter differ due to the changes in photon energies (Willard *et al* 1988). There are several changes that occur with the interaction of these radiations with matter. Due to their high energies, gamma rays are able to affect the nucleus of an atom and X-rays have the ability to eject inner electrons from a substance. Whereas radiation absorbed from the UV or visible regions leads to rotational-vibrational variations by inducing fluctuations in the energy of valence electrons (Willard *et al* 1988). Furthermore, when radiation of the IR region is absorbed, there are changes in energy states such as rotational and rotational-vibrational. Moreover, microwaves have the ability to change the electron spin states of electrons of substances that possess unpaired electrons, when subjected to a magnetic field (Willard *et al* 1988). Lastly, due to the very low energy of photons in the radio-wave region of the spectrum, their interaction with matter in a magnetic field affects the nuclear spin states of materials (Willard *et al* 1988).

2.3.1.1. Absorption

Quantum theory states that the existence of atoms can only be within discrete potential energy levels and an atom's energy is dependent on its electronic configuration. As valence electrons move between energy levels, absorption or emission of energy to and from energy states occur and the change in potential energy is related to the frequency of radiation (Wayne and Wayne 1996, Willard *et al* 1988). A spectrum of absorption or emission consists of certain frequencies that correspond to each energy transition that occurs. Radiation interacting with matter results in the excitation of electrons as it absorbs the radiation and then moves from the lowest, unexcited, electronic state (i.e., the ground state) to an excited state for approximately 10^{-9} seconds (Wayne and Wayne 1996). Thereafter, the electron loses all or a fraction of the energy that it absorbed either by collisions or through the emission of a photon. The energy that is absorbed or emitted by electrons can thus be studied through characterisation techniques such as ultraviolet-visible (UV-Vis) spectroscopy and photoluminescence (PL) spectroscopy (Willard *et al* 1988). Electronic excitation occurs when there is a transition between the energy states of a species that has just been subjected to radiation from the UV or visible region of the EMR spectrum as the energy introduced is of the right magnitude (Willard *et al* 1988). Whereas, when matter absorbs IR radiation, which is of lower energy than that of UV and visible light, it does not introduce enough energy for an excitation to occur but only enough

energy is absorbed by the species to allow transitions between rotational and vibrational states as these molecular rotational and vibrational energy levels are in close proximity to one another (Wayne and Wayne 1996).

Ultraviolet-visible spectroscopy

Ultraviolet-visible (UV-Vis) spectroscopy involves the study of the interaction of EMR from the near UV to near IR, from 180 to 1100 nm, with matter (Rouessac and Rouessac 2000). This domain of the EM spectrum consists of three subdivisions, namely near UV (185–400 nm), visible (400–700 nm), and some portion of the near IR (700–1100 nm) (Rouessac and Rouessac 2000). Information obtained from this technique can be either quantitative or qualitative and is not so much structural as it is on unsaturation sites of molecules (Rouessac and Rouessac 2000, Willard *et al* 1988). Qualitative information obtained from this technique refers to the identification of compounds through specific wavelengths at which their molecular species absorb radiation of the EM spectrum and inadvertently possess the required amount of energy to promote molecules (or electrons thereof) to an excited state (UV-1800 Series 2008, Willard *et al* 1988). Quantitative information obtained through this analysis technique involves information such as the concentration of the species under study which can be obtained through calculations and the use of the Beer-Lambert law (Willard *et al* 1988).

Light impinging on a sample can be transmitted, refracted, reflected, scattered or absorbed (Rouessac and Rouessac 2000). When a photon of EM energy from the UV/Visible range is absorbed by matter, or rather interacts with the valence electrons of a molecule thereof, there are a number of transitions that could occur within the same molecule that modifies the electronic, rotational, and vibrational energies (E_{elec}, E_{rot} and E_{vib}, respectively) and ultimately affects the total mechanical energy of that molecule (Rouessac and Rouessac 2000, Willard *et al* 1988):

$$\Delta E_{tot} = \Delta E_{rot} + \Delta E_{vib} + \Delta E_{elec}$$

When the absorption process reaches completion, the excited species can return to a relaxed state either by emitting the absorbed photons or through non-radiative transitions (Rouessac and Rouessac 2000). A spectrophotometer is used in order to measure the amount of light, or the intensity thereof, absorbed or transmitted by an absorbing species over a certain wavelength-range. The results are displayed in the form of a graph or spectrum, also known as charge transfer spectra, so called due to alterations in the polarity of chemical bonds that occur with the above-mentioned transitions, characterised by their respective wavelengths (Rouessac

and Rouessac 2000). Absorbance is plotted as a function of wavelength which is expressed in nanometres (nm) (Rouessac and Rouessac 2000). Sigma (σ), pi (π) and non-bonding (n) electrons are the ones involved in transitions of bonds formed between light elements (such as H, C, N and O) of organic compounds (Rouessac and Rouessac 2000).

The number of photons per unit time is dependent on the power of the beam of radiation in the sense that they are proportional to one another, meaning that as the power of the beam is increased, so does the number of photons (Willard *et al* 1988). The rate of absorption therefore is influenced by the number of photons and in turn also the number of collisions (Willard *et al* 1988). Also, the rate at which photons collide with molecules of the absorbing species is proportional to the rate at which photons are lost (Wayne and Wayne 1996). If there is an increase in the number of photons that collide with the molecules of the material under study, there is an increase in the rate of absorption by the absorbing atoms or molecules (Willard *et al* 1988). The concentration of absorbing species also affects the rate of absorption and is directly related to it, meaning that as the concentration is increased so does the number of collisions and that leads to an increased rate of absorption (Willard *et al* 1988).

One might ponder on the method through which molecules absorb light—a chromophore is the fragment (or chemical group) of a molecule responsible for absorption of light at a specific frequency and the generation of colour (Rouessac and Rouessac 2000). It is therefore known as the site where electronic transitions occur when the energy difference between two molecular orbitals (MOs) matches that of a specific wavelength of radiation and an electron can be promoted from the ground state to the excited state (Rouessac and Rouessac 2000). Resonance in organic substances fuels electronic transitions when there are chromophore groups, such as C=C, C=N, N=O, or C=S, present (Delahay 1957). As conjugation within a molecule increases with the number of carbons present, electron delocalisation also increases, meaning that the energy difference between the ground state and excited state decreases and ultimately leads to a bathochromic shift in the absorption band toward longer wavelengths and a higher intensity (Delahay 1957, Rouessac and Rouessac 2000). It is important to note that the absorbance of a compound is influenced by the type of solvent used as well as variations in pH level (i.e., the alkalinity or acidity) and gives rise to a rise or fall in the absorbance maximum of the compound (Rouessac and Rouessac 2000). Hence, absorbance bands could be shifted toward longer wavelengths through a bathochromic shift or its intensity could be increased or decreased through either a hyperchromic or hypochromic effect, respectively (UV-1800 Series 2008).

As mentioned above, the transitions that result in the absorption of EM radiation in this region of the spectrum are transitions between electronic energy levels—generally, from the highest occupied molecular orbital (HOMO) to the lowest unoccupied molecular orbital (LUMO). The specific frequencies at which light is absorbed are affected by the structure and environment of the chromophore (light absorbing species). Excited electrons return to the ground state by vibrational transitions through smaller energy increments and the energy absorbed ultimately appears as heat in solution. A plasmon resonance absorption, that allows for the intense coloured solutions, is characteristic to metal NPs such as gold and silver. Electrons that are confined at the surface of a particle oscillate collectively at a certain frequency and give rise to the absorption band—commonly known as surface plasmon resonance frequency. This effect occurs for particles of diameter up to about 50 nm and scales with particle volume (Filipponi and Sutherland 2012).

The wavelength, λ, (i.e., the distance from crest to crest of either the electrical or magnetic constituent of the EM wave) and frequency, υ, (the amount of waves passing a static point in a unit of time) are related by the equation: $c = \upsilon \times \lambda$, where c is the speed of light (expressed in $m.s^{-1}$), υ is frequency (expressed in Hertz, Hz), and λ is the wavelength (expressed in m) (UV-1800 Series 2008, Wayne and Wayne 1996, Willard *et al* 1988). The energy (E) of a photon is related to the frequency, υ, and wavelength, λ, by Planck's constant, (h, 6.62×10^{-34} J.s) and the speed of light, (c, 3.00×10^{8} $m.s^{-1}$) and can be expressed by $E = h\upsilon = hc/\lambda$ (Wayne and Wayne 1996, Willard *et al* 1988). The electric vector or component of EMR interacts with electrons bound to a substance and hence allows the propagation of radiation through matter at velocities lower than that of the speed of light; the frequency of radiation remains the same but the velocity is expected to decrease (Willard *et al* 1988).

Photometry as well as colorimetry rests on the works of Johann Heinrich Lambert, a French mathematician, and August Beer, a German physicist, whose work relates to one another through the Beer-Lambert law (Willard *et al* 1988, Rouessac and Rouessac 2000). This law describes the linear relationship between the absorbance and the concentration of the absorbing species, and it is as follows:

$$A = \varepsilon lC$$

where A is the absorbance (possessing no units); l is the thickness of solution; C is the molar concentration; and ε is the molar absorption coefficient ($1\ mol^{-1}cm^{-1}$) at a given wavelength. There are a number of factors influencing the molar absorptivity, or the degree to which a

solution attenuates light in terms of its concentration, such as the wavelength, the nature of the solvent, and the temperature (Rouessac and Rouessac 2000). It should be noted that contaminants or turbidities in the solution will scatter radiation along with changes in refractive indexes on surfaces of the absorbing molecules (Willard *et al* 1988). Figure 3 below illustrates the process of absorption through Beer's law:

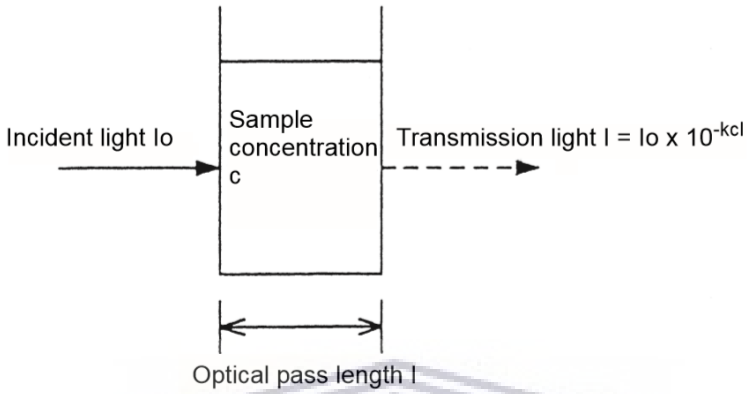

Figure 3. Illustration of the Beer-Lambert law.

Beer-Lambert's law can be applied when conditions such as the following are met: the nature of the light should be monochromatic, the concentration has to be weak, the solution should be homogeneous and should not fluoresce; the solute need not undergo photochemical reactions nor interact with molecules of the solvent (Rouessac and Rouessac 2000).

Components of a spectrophotometer

Illustrated below in Figure 4 are the key components of a spectrophotometer which consists of the following: a source of radiation (which is required to provide a beam of photons to interact with the sample), a monochromator (to discern between radiation frequencies which is achieved by the use of filters, gratings or prisms), a photoelectric detector (needed to convert the data obtained from transmitted radiation into an electrical signal) and a readout device or digital display (Rouessac and Rouessac 2000, Willard *et al* 1988).

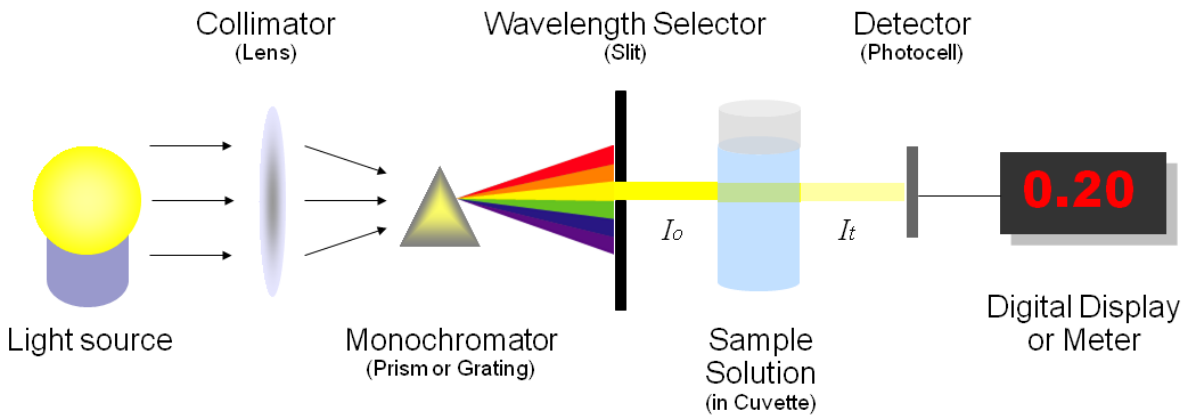

Figure 4. A representation of the basic structure of spectrophotometers.

A radiation source should be able to uphold its radiation intensity for the duration of each measurement and is expected to provide adequate energy over the wavelength region of interest (Willard *et al* 1988). For the UV/Vis region of the spectrum two radiation sources are used: an incandescent lamp for the visible region and a medium/low pressure hydrogen or deuterium arc lamp of approximately 0.2–0.5 torr for the UV range, under low voltage conditions (Willard *et al* 1988, Rouessac and Rouessac 2000). The incandescent lamp consists of a tungsten wire filament enveloped in a glass bulb (replete with inert gas or under vacuum) which is heated to incandescence (Willard *et al* 1988). This filament is coiled to increase its efficiency, luminance and effectiveness of radiation emission (Willard *et al* 1988). The deuterium arc lamp consists of two electrodes separated by a metallic screen with a 1 mm-diameter mechanical aperture in a deuterium atmosphere (Rouessac and Rouessac 2000). The deuterium arc lamp is so called due to the presence of an arc formed by a discharge current at the aperture, constricting the discharge to a narrow path (Willard *et al* 1988). The stability of radiation sources depends on the transformers used, these should be of a voltage that is kept constant, and the use of electronic voltage regulators (Willard *et al* 1988). There are also mirrors and lenses present in a spectrophotometer that are essential for the collection and direction of radiation to the entrance slit of the monochromator (Willard *et al* 1988).

The second pivotal part of a spectrophotometer is a wavelength selector (such as a filter or a monochromator) which is needed for the segregation of radiation bands in a desired, narrow, and discrete band of wavelengths (Willard *et al* 1988). A monochromator containing a metal piece with a narrow slit, described by Delahay as *"the heart of a spectrophotometer"*, is used rather than a filter because filters transmit bands that are too wide (Delahay 1957). The typical components of a monochromator include: (a) an entrance slit through which radiation traverses

in a narrow path from the radiation source (Rouessac and Rouessac 2000); (b) a collimator which is a lens that focuses the radiation from the entrance slit into a straight beam of parallel rays; (c) a grating or prism to disperse incoming parallel rays; (d) a second collimator (identical or similar to the first) which intercepts the discretised or dispersed beam to recreate images of the entrance slit onto the exit slit; and (e) an exit slit for selection of the desired wavelengths by obstructing radiation falling out of the desired spectral band region (Rouessac and Rouessac 2000, Willard *et al* 1988). The slit width of the exit slit can be adjusted to influence the luminous flux emanating from it; an unduly wide slit width, however, could lead to deviations from Beer's law, whereas an extremely narrow slit leads to weaker energy release and possibly lower analytical sensitivity (Willard *et al* 1988). Factors such as (a) resolving power or resolution (which greatly depends on the slit width of the monochromator and the dispersion of wavelengths by a grating or a prism), (b) radiation-gathering power (known as the ability of the collimator to collect radiation), and (c) radiation-output purity (which depends on the amount of radiation scattered) influences a monochromator's performance (Willard *et al* 1988). The more capable a collimator is in capturing radiation, the slower the speed of the spectrometer (Willard *et al* 1988).

The third part of a spectrophotometer is the detector that measures the intensity of light at a certain wavelength and converts it into an electrical signal (Delahay 1957, Rouessac and Rouessac 2000). There are two types of detectors used in a spectrophotometer, namely photomultiplier tubes and photodiode arrays (Rouessac and Rouessac 2000). The photodiode array of a detector is a multichannel device and can therefore perform detection simultaneously, whereas a photomultiplier tube is a single channel device that finds it challenging to compare two light intensities (that, from the reference and the sample) in a precise manner (Rouessac and Rouessac 2000). Therefore, the use of photodiodes leads to outstanding dynamic range, sensitivity, and linearity as each diode is connected to a capacitor (Rouessac and Rouessac 2000).

The power supply of a source can be either modulated of pulsed with the assistance of a feedback loop (Rouessac and Rouessac 2000). In the case of modulation, the voltage system can be altered to follow one of three functions, i.e., a sine, ramp or square, but is limited to the lamp operating conditions. Whereas the pulsing mode allows the achievement of greater optical output through higher lamp operating conditions at a fixed low current with a brief increase during a pulse. However, both of these modes of operation lead to a decrease in lamp life (Willard *et al* 1988).

Changes in electronic levels

As previously described, shifts in electronic orbitals occur when atoms or molecules are activated through the absorption of radiation and therefore go into an excited state when electrons possess enough energy to jump from one energy level (i.e.,, the ground state) to another of higher energy (i.e.,, the excited state). In addition, there also exists the possibility of changes in vibrational and rotational levels that require less energy than that of electronic (Delahay 1957). Electronic shifts due to radiation absorbed from the X-ray and ultraviolet ranges, to some extent, of the EMR spectrum being higher in energy because they occur closest to the nucleus and require typical discrete energies of about 100 kcal.mol^{-1} or more (Delahay 1957). Furthermore, electronic shifts incurred by absorption of UV-, visible-, or very near IR-radiation, occur in the outer orbitals of molecules (Willard *et al* 1988). A potential-energy curve is used to illustrate the effect of energy and interatomic distance on a molecule. When a diatomic molecule is activated by the absorption of radiation matching its required activation energy, its potential energy curve is shifted toward longer interatomic distances as bonds are weakened through activation (Delahay 1957). When the activated molecule is in a compressed state vibration occurs and this in turn results in a multitude of lines on the absorption spectrum because vibrational and rotational changes of molecules accompany their electronic transitions (Delahay 1957).

Changes in vibrational levels

Absorption bands produced by substances absorbing radiation in the near IR could be attributed to changes in vibrational levels which require much lower energies than that of electronic transitions and more energy than for rotational level changes and is typically between 1 to 20 kcal.mol^{-1} (Delahay 1957). There are a number of vibrational modes that could be observed for molecules of a complex nature and spectrums produced for vibrations that occur are convoluted by transitions occurring between rotational levels (Delahay 1957).

Changes in rotational levels

Transitions between rotational levels are much lower in energy than transitions that occur between electronic levels and vibrational levels, and are said to be lower than 1 to 2 kcal.mol^{-1} (Delahay 1957). These kinds of transitions that are only due to rotational energy changes are observed when radiation is absorbed from either the far IR or microwave ranges of the EMR spectrum (Delahay 1957).

2.3.2. Hydrodynamic properties

The hydrodynamic properties of colloidal suspensions are defined by the motion of fluids (i.e., the dispersion medium) and the forces that act on the kinetic units dispersed throughout the solvent (also known as the dispersive phase) (Hunter 1987). Properties such as viscosity, sedimentation, and particle size could be altered or modified for the achievement of desired characteristics for specific applications by varying the repulsive and attractive forces (Ravina 1993). In the case of pharmaceuticals or paint, it is desired to keep the particles discrete and prevent sedimentation by maximising the repulsive forces between particles in suspension (Ravina 1993). On the contrary, the opposite effect might be desired in processes such as filtration, i.e., the separation of colloids from the fluid, in which the repulsive forces are minimised or removed to allow agglomeration to occur in which particles are attracted to one another more strongly and form flocs (Ravina 1993).

Instruments that have the ability to measure properties or characteristics of particles suspended in a liquid medium, include the Zetasizer Nano range (Malvern Instruments Ltd. 2004). The zetasizer is able to measure three parameters, namely particle size, zeta potential (ZP), and molecular weight (MW), over a wide range of concentrations and has facilities to measure other vital properties such as concentration and pH (Malvern Instruments Ltd. 2004). Random molecular motion, as defined by Filipponi and Sutherland, involves the movement of molecules according to their kinetic energy, which at the macroscale is non-influential because it is a very small motion compared to the size of a material, whereas the same motion at the nanoscale has a significant effect on the behaviour of particles as they might be of the same scale as the size of particles. One such example is Brownian motion, which becomes very important at the nanoscale (Filipponi and Sutherland 2012). Particle size is determined by the Zetasizer through measurement of the Brownian motion of particles in colloidal suspension, which is achieved by Dynamic Light Scattering (DLS) through the illumination of particles with a laser, and measurement of intensity of fluctuation of scattered light (Malvern Instruments Ltd. 2004). On the other hand, Static Light Scattering (SLS) is the measurement technique used to determine the MW of a substance which in turn is crucial for other parameters such as density, flexibility and strength, all vital for work which involves polymer compounds (Malvern Instruments Ltd. 2004).

In 1827, Robert Brown, a botanist, observed the random motion of pollen in water and the term ‘Brownian motion’ was coined in his honour but the motion of dust particles was first described by a Roman poet, Lucretuis, 60 B.C. and later, in 1905, Albert Einstein explained that the

movement of the pollen was induced by the water molecules in the liquid (Helmenstine 2019). Therefore, Brownian motion is described as the random motion of particles in a fluid or gas induced by collisions with other fast-moving atoms or molecules in the dispersion medium (Gottlieb and Pfeiffer 1963, Helmenstine 2019, Malvern Instruments Ltd. 2004). The rate of Brownian motion can be influenced by several different factors such as temperature, number of particles (or concentration), particle size, and viscosity (Helmenstine 2019). The size of particles is determined by the speed of particles in random motion; large and small particles can be identified by their movement i.e., small particles move fast whereas large particles move slowly (Malvern Instruments Ltd. 2004).

2.3.2.1. Zeta potential and electrophoresis

A liquid has the ability to dissociate ionic compounds into negatively charged ions, i.e., anions and positively charged ions, i.e., cations; therefore, most dispersion mediums contain ions (Malvern Instruments Ltd. 2004). If a charged particle is introduced to a liquid there would be an attraction between the surface of the suspended particle and surrounding ions of opposite charge, meaning that a positively charged colloid would attract negatively charged ions in suspension and vice versa (Malvern Instruments Ltd. 2004). A diffuse layer is formed around each charged colloid and consists of neutralising ions, i.e., ions closest and strongly bound to the surface of the charged colloid and ions further away that are loosely bound due to a weaker attraction (Malvern Instruments Ltd. 2004, Ravina 1993). A slip plane is found within the diffuse layer which is a boundary that serves to separate particles moving with the liquid from those that remain stationary (Malvern Instruments Ltd. 2004). At the slip plane there is a potential, roughly proportional to the colloid's surface charge, between the surface of the colloid (or particle) and the dispersion medium that varies with distance from the colloid surface (Ravina 1993). This potential is known as the zeta potential (ZP) which is measured with a combination of electrophoresis and Laser Doppler Velocimetry (LDV) techniques (Malvern Instruments Ltd. 2004).

The basic working principle involves subjecting the colloidal suspension to an electrical field and measuring the velocity of a colloid or particle within the suspension (Malvern Instruments Ltd. 2004). From this, the ZP can be determined through known values of velocity, viscosity, dielectric constant, and electric field (Malvern Instruments Ltd. 2004). This complex ionic environment around a charged colloid is best visualised by the double layer model in which a series of steps occur around a negatively charged colloid (Ravina 1993). A layer of rigidly-attached counter-ions (cations) is formed around the surface of the colloid through attraction

that occurs between the negative colloid surface and the positive ions that surround it and is called the Stern layer (Ravina 1993). Approximate to the Stern layer is a diffuse layer, a densely charged atmosphere of counter ions formed from supplementary positive ions that are still attracted to the negative colloid but also repelled by the Stern layer and other positive ions attempting to approach the colloid (Ravina 1993). As the concentration of counter-ions (cations) decreases with increasing distance from the colloid surface, the concentration of co-ions (anions) gradually increases with the diminishing repulsive forces due to the dominant presence of cations until equilibrium is achieved (Ravina 1993). The double layer consists of the Stern layer and diffuse layer with thickness dependent on the nature of ions and their concentration (Ravina 1993). An illustration of the double layer is shown in Figure 5.

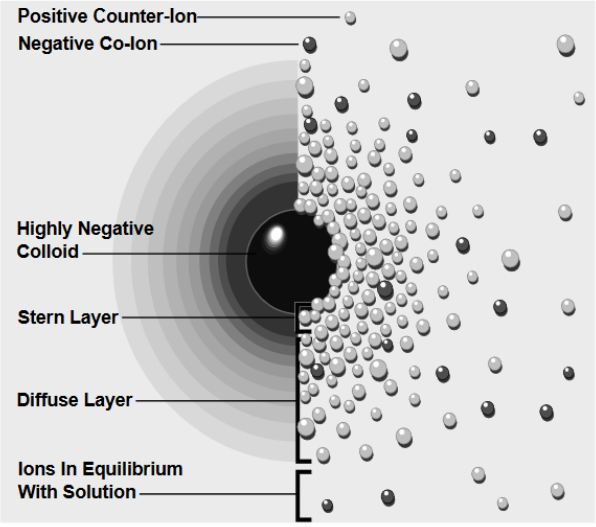

Figure 5. A representation of the double layer. An illustration of charge density surrounding the colloid (Ravina, 1993).

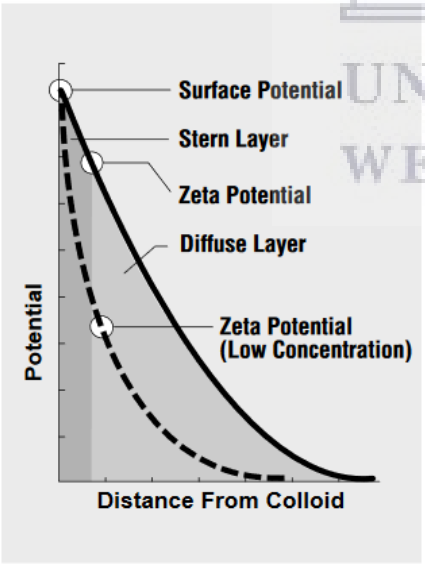

Figure 6. A representation of the relationship between zeta potential and surface potential with respect to the distance from the colloid (Ravina, 1993).

In the potential curve shown in Figure 6, the potential decreases as the distance from the surface of the colloid increases. In the Stern layer, the decrease in potential is rather linear in nature and exponentially decreases in the diffuse layer to ultimately approach zero at the imaginary boundary of the double layer (Ravina 1993). According to Verwey, the double layer is produced independently of external influence when the particles and the solution come into contact with one another and is accompanied by a decrease in the system's free energy. For two double layers to interact, there should be an increase in the free energy of the system that would lead to repulsion (Verwey 1947).

In electrophoresis, the mobility of a charged particle in a voltage field occurs at a fixed velocity and is proportional to the dielectric constant, the viscosity of the dispersion medium and the electrical potential at the slip plane (Ravina 1993).

The tendency of particles in the suspension to agglomerate (or flocculate) or not, is determined by the ZP and is useful in a number of industries such as ceramics for densely packed particles, waste water treatment in which agglomeration is sensitive to pH and chemical flocculants, and in the stable use of emulsions in the environment (Malvern Instruments Ltd. 2004). Modification in the dispersion medium through changes in pH or ionic species, or the adsorption of surface-active agents onto the colloid's surface, could alter the particle charge (Malvern Instruments Ltd. 2004). Particles or ions that carry a like-charge to that of the colloid causes mutual electrostatic repulsion between them and the suspended colloid, meaning that the suspended colloids will remain dispersed and discrete throughout the medium if the charge is large enough (Ravina 1993). On the contrary, the opposite effect occurs when the charge is reduced and particles are attracted to one another to the degree that they undergo agglomeration and alter the characteristics of the suspension (Ravina 1993).

In order to investigate the stability of colloidal CDs and a-CDs, ZP measurements were carried out. Surface charges were measured using the zeta analyser, a Malvern Zetasizer nano ZS90. The hydrodynamic properties of the synthesised materials were measured under a wide range of solution compositions, including a) monovalent and divalent electrolytes (NaCl and $CaCl_2$, respectively), b) pH levels ranging from 1 to 13 as adjusted by the addition of hydrochloric acid (HCl) (10 mmol/L) and sodium hydroxide (NaOH) (10 mmol/L) solutions, and c) the presence of NOM (Bayati *et al* 2018).

2.4. Summary

This review paved the way to the choices made regarding the study of the materials mentioned above. Carbon-based nanomaterials have been around for quite some time yet little research has been done on their colloidal behaviour in nature. The review perfectly points to the advantages in utilisation of carbon-based materials in various applications and literature has shown that there is a great need to study their possible toxic effects. If these materials make their way into the environment, it is necessary to understand their properties and vulnerability to environmental conditions simulated by the study of the effect or influence of pH, salinity and the presence of natural organic matter, hence the decision to test those parameters. In water suspensions CDs are well known for their colloidal stability at low ionic strength (IS) as well as their PL stability under those conditions (Bayati et al 2018). However, the stability of the photoluminescence of CDs is generally expected to decline under conditions such as aggregation.

Chapter 3 – Research Design and Methodology

3. Introduction

This chapter consists of a full description of the experimental and analytical procedures employed in this study. It reports on the chemical reagents and instrumentation used, and defines the synthesis routes for all materials pertinent to this study. Moreover, the optimisation procedures for the synthesis of CDs and a-CDs are described; and the investigation of the influence of pH, ionic strength, and the presence of natural organic matter on the colloidal stability of synthesised materials are presented. Lastly, the analytical characterisation techniques used in this experimental work are described in detail.

3.1. Materials and chemical reagents

A list of chemicals used throughout the experimental procedures of this study is provided in Table 1 below.

Table 1. List of chemical reagents used, along with the supplier-name and further specifications.

Name of chemical reagent	***Supplier***	***Purity***	***Specifications***
	Synthesis of plain CDs		
Glycerol ($C_3H_8O_3$)	Sigma-Aldrich, South Africa	≥ 99.5 %	ACS reagent MW: 92.09 g/mol Mp: 20 °C (lit.) Bp: 182 °C Density: 1.25 g/mL (lit.)
Sodium dihydrogen phosphate/Sodium phosphate monobasic (NaH_2PO_4/H_2NaO_4P)	Sigma-Aldrich, South Africa	≥ 99.0 %	ReagentPlus MW: 119.98 g/mol pH: 4.0–4.5 (25 °C, g/L in water)
	Synthesis of a-CDs		
Citric Acid ($C_6H_8O_7$)	Sigma-Aldrich, South Africa	≥ 99.5 %	ACS reagent MW: 192.12 g/mol Mp: 153–159 °C (lit.)
Branched polyethylenimine (BPEI)	Sigma-Aldrich, South Africa		Average MW ~ 800 Da Density: 1.050 g/mL (at 25 °C)

Dialysis		
Spectra/Por®6 Dialysis Membrane, Pre-wetted Regenerated Cellulose (RC) Tubing	SpectrumLabs (USA), G I C Scientific, Roodepoort, South Africa	MWCO: 1 kDa Nominal flat width: 45 mm Diameter: 29 mm Vol/Length: 6.4 mL/cm Length: 10m/33ft

The purchased chemical reagents were used as received. For the synthesis of CDs and a-CDs, deionised water was used for the preparation of standard solutions. Ultra-pure water, with a specific resistance of 18 MΩ*cm, was obtained from the Millipore Synergy water system and used for dialysis of CDs and a-CDs. Hydrochloric acid (HCl) and sodium hydroxide (NaOH), used for pH adjustments, along with a technical grade humic acid (HA), were purchased from Sigma-Aldrich, South Africa.

3.2. Equipment list

Equipment used for synthesis of CDs and a-CDs are listed in Table 2 below.

Table 2. List of equipment used throughout this study.

Equipment	***Use (s)***
Analytical balance	Weighing
Centrifuge	Purification of CDs and a-CDs
Domestic microwave	Microwave irradiation of organic molecules for synthesis of plain CDs
Silicone oil bath	Thermal treatment of organic molecules in production of a-CDs
Thermo-stated heater/stirrer plate	Mixing step, a-CDs synthesis
pH meter	pH measurements

3.3. Optimisation of synthesis conditions for plain CDs and amine-capped CDs

Several optimisation procedures were performed in search of the ideal or adequate synthesis conditions for CDs and a-CDs. For the synthesis of CDs, optimum heating-power, heating-time and molar quantities of precursors were determined. For the synthesis of a-CDs, optimal heating-temperature, heating-time and molar quantities of precursors were sought after. For these studies sturdy and rigid glassware was necessary, possessing high mechanical strength and the ability of withstanding very high temperatures. With that said, a Pyrex heavy duty Griffin beaker made of borosilicate glass was used throughout all microwave synthesis studies. Borosilicate glass is a hard glass consisting of approximately 7–13 wt% of boron oxide (B_2O_3) and about 70–80 wt% of silica (SiO_2) (Hasanuzzaman *et al* 2016) and has a working temperature of up to 230 °C (Lab Manager 2009).

3.3.1. Optimisation of synthesis power for synthesis of plain CDs

According to the settings available for the 900-W domestic microwave used, five power settings were chosen for the power optimisation study, namely: 10 % (90 W), 30 % (270 W), 50 % (450 W), 80 % (720 W) and 100 % (900 W). From this point onward these will be referred to as PowOpt_A1, PowOpt_A2, PowOpt_A3, PowOpt_A4, and PowOpt_A5, respectively. The plain/unfunctionalised CDs were synthesised according to the procedure described in Section 3.4, as illustrated in Figure 7 below, with the variation in synthesis power as mentioned above. The reaction time was kept constant at 20 minutes and the molar ratio of reagents (glycerol and sodium dihydrogen phosphate, NaH_2PO_4), was also kept constant in a 10:1 ratio.

Figure 7. Microwave-assisted method for synthesis of plain carbon dots: (a) mixing of reagent materials in a 250 mL Erlenmeyer (conical) flask, (b) placing of the reagent mixture into the microwave and heating thereof, (c) cooling of product to room temperature, and (d) storage of product after resuspension in DI water.

3.3.2. Optimisation of reaction time for synthesis of plain CDs

To determine the ideal heating time for effective synthesis of plain CDs, five different reaction times were analysed as CDs were prepared within the following reaction times: 5, 10, 15, 20, and 25 minutes. The plain CDs were synthesised according to the procedure described in Section 3.4 with variation in reaction/heating-duration as mentioned above. The heating power remained constant at 720 W and the molar ratio of reagents (glycerol and sodium dihydrogen phosphate, NaH_2PO_4) was also kept constant in a 10:1 ratio.

3.3.3. Molar quantity optimisation of 70 % w/w glycerol for synthesis of plain CDs

To determine the ideal molar quantity of 70 % w/w Gly for effective synthesis of plain CDs (as prepared according to the experimental steps described in Section 3.4), the following molar ratios of 70 % (w/w) Gly to 20 % NaH_2PO_4 were investigated, namely: 6:1, 8:1, 10:1, 12:1, and 14:1. These five samples were prepared with an increase in the number of moles of Gly, i.e., 0.14, 0.18, 0.23, 0.27, and 0.32 mol (molar calculations presented in Appendix E) and here forth will be referred to as G_Opt_A11, G_Opt_A12, G_Opt_A13, G_Opt_A14, and G_Opt_A15, respectively. The following parameters remained fixed: (a) the concentration of Gly at 70 % w/w or 7.6 $mol.L^{-1}$, (b) the concentration and molar quantity of NaH_2PO_4 at 20 % w/w and 5.1×10^{-3} mol, respectively, (c) the synthesis power at 720 W, and (d) the reaction time at 14 minutes as used in literature (Wang *et al* 2011a).

3.3.4. Molar quantity optimisation of sodium dihydrogen sulphate for synthesis of plain CDs

To determine the ideal molar quantity of 20 % w/w NaH_2PO_4 for effective synthesis of plain CDs (as prepared according to the experimental steps described in Section 3.4), the following molar ratios of 70 % (w/w) Gly to 20 % NaH_2PO_4 were investigated, namely: 10:0.5, 10:1, 10:2, 10:3, and 10:4. These five samples, of increasing number of moles of NaH_2PO_4, i.e., 2.6×10^{-3}, 5.1×10^{-3}, 1.02×10^{-2}, 1.53×10^{-2}, and 2.04×10^{-3} mol (molar calculations presented in Appendix F), will from this point forward be referred to as N_Opt_A16, N_Opt_A17, N_Opt_A18, N_Opt_A19, and N_Opt_A20, respectively. The following parameters remained fixed: (a) the concentration of NaH_2PO_4 at 20 % w/w = 1.7 $mol.L^{-1}$; (b) the concentration and molar quantity of Gly at 70 % w/w and 0.23 mol, respectively; (c) the synthesis power at 720 W; and (d) the reaction time at 14 minutes.

3.3.5. Optimisation of synthesis temperature for synthesis of a-CDs

To determine the ideal synthesis temperature for effective synthesis of a-CDs (as prepared according to the experimental steps described in Section 3.5), five different temperatures were analysed as a-CDs were prepared at the following temperatures: 130 °C, 150 °C, 170 °C, 190 °C and 210 °C, while several other parameters remained fixed, such as the molar quantities of reagents and the heating duration of the reaction at 2 hours.

3.3.6. Optimisation of reaction time for synthesis of a-CDs

To determine the ideal heating time for effective synthesis of a-CDs (as prepared according to the experimental steps described in Section 3.5), five different reaction times were analysed and samples were prepared within the following reaction times: 1, 1.5, 2, 2.5, and 3 hours. Other parameters remained fixed, such as the molar quantities of reagents and the synthesis temperature at 170 °C (lit.).

3.3.7. Molar quantity optimisation of citric acid for synthesis of a-CDs

To determine the ideal molar quantity of CA for effective synthesis of a-CDs (as prepared according to the experimental steps described in Section 3.5), the a-CDs were prepared with the following molar values of CA, namely: 7.8×10^{-3} mol (1.5 g), 9.4×10^{-3} mol (1.8 g), 1.1×10^{-2} mol (2.1 g), 1.2×10^{-2} mol (2.4 g), and 1.4×10^{-2} mol (2.7 g) (molar calculations presented in Appendix I). These will here forth be referred to as CA_Opt_B11, CA_Opt_B12, CA_Opt_B13, CA_Opt_B14, and CA_Opt_B15, respectively. The following parameters remained fixed: (a) the concentration of CA at 0.01 mol.L^{-1}, (b) the concentration (1.3 mol.L^{-1}) and molar quantity (1.3×10^{-2} mol) of BPEI, (c) the synthesis temperature at 170 °C, and (d) the reaction time of 2 hours (Bayati *et al* 2018, Zheng *et al* 2014).

3.3.8. Molar quantity optimisation of branched polyethylenimine for synthesis of a-CDs

To determine the ideal molar quantity of BPEI for effective synthesis of a-CDs (as prepared according to the experimental steps described in Section 3.5), the a-CDs were prepared with the following molar values of BPEI, namely: 7.9×10^{-3} mol (6 mL), 1.1×10^{-2} mol (8 mL), 1.3×10^{-2} mol (10 mL), 1.6×10^{-2} mol (12 mL), and 1.8×10^{-2} mol (14 mL) (molar calculations presented in Appendix J). From this point forward these will be referred to as BPEI_Opt_B16, BPEI_Opt_B17, BPEI_Opt_B18, BPEI_Opt_B19, and BPEI_Opt_B20, respectively. The following parameters remained fixed: (a) the concentration of BPEI (1.3 mol.L^{-1}), (b) the concentration (0.01 mol.L^{-1}) and molar quantity (1.1×10^{-2} mol) of CA, (c) the synthesis

temperature of 170 °C, and (d) the reaction time of 2 hours (Bayati *et al* 2018, Zheng *et al* 2014).

3.4. Synthesis of raw carbon-dots (CDs)

The synthesis of the plain CDs was carried out using a modified version of the method initially undergone by Wang et al. in 2011.

Step 1: Preparation of a 70 % (w/w) standard solution of glycerol

Firstly, 56 mL of glycerol was mixed with 100 mL of deionized water in order to prepare a 70 % (w/w) solution of glycerol (See Appendix A for volume calculation). The preparation of a 70 % (w/w) standard solution of glycerol is illustrated in Figure 8 below.

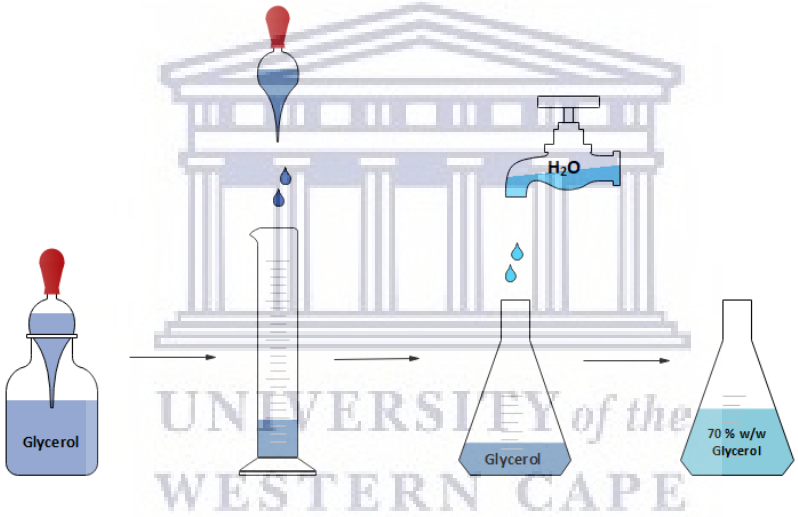

Figure 8. Preparation of a 70 % w/w solution of glycerol.

Step 2: Preparation of 20 % (w/w) standard solution of NaH_2PO_4

Firstly, 20 g of NaH_2PO_4 was weighed on an analytical balance. Then the solute was quantitatively transferred into a volumetric flask. Thereafter, the flask was filled up to its calibration mark with deionised water. Lastly, the solution mixture was shaken to ensure that the solute completely dissolved in the solvent. The preparation of a 20 % (w/w) standard solution of sodium dihydrogen phosphate is illustrated in Figure 9 below.

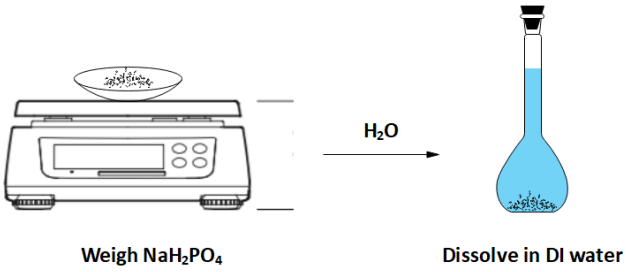

Figure 9. Preparation of a 20 % w/w sodium dihydrogen phosphate solution.

Step 3: Mixing and microwave irradiation

The prepared 70 % (w/w) glycerol solution and 20 % (w/w) solution of NaH_2PO_4 were mixed in a 10:1 volume ratio. Thereafter, the solution was heated in a domestic microwave at 720 W power for 14 minutes. The product was allowed to cool to room temperature and the resultant CDs were resuspended in water with continuous stirring until a homogeneous brown coloured suspension was obtained. The resultant solution of CDs was then dialysed against ultrapure water for 2 days with a pre-wetted RC tubing dialysis membrane in order to obtain a purified product. The water was replaced every 6 hours and the final product was centrifuged before characterisation. The synthesis procedure is illustrated in Figure 10 below.

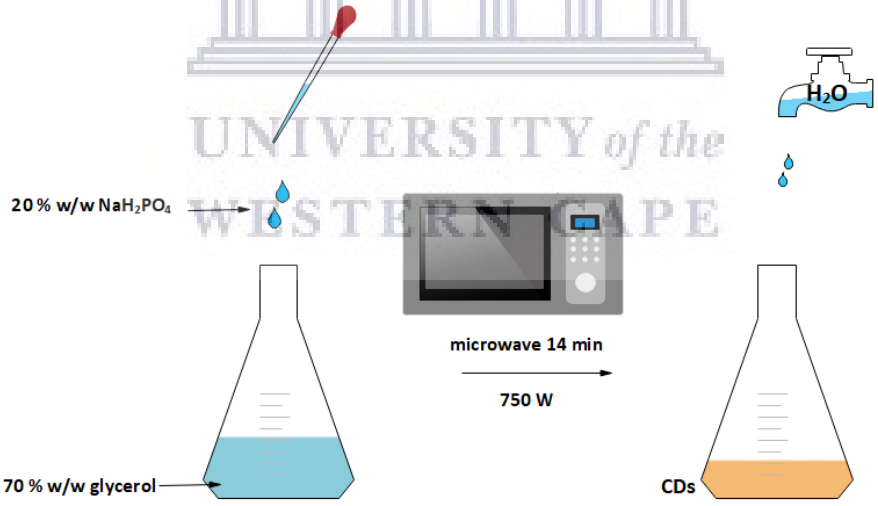

Figure 10. Microwave irradiation for plain CD synthesis.

3.5. Synthesis of amine-capped CDs

The a-CDs were fabricated by a method initially performed by Zheng et al. in 2014. Firstly, a 10 mmol stock solution of CA was prepared in which 0.048 g (see mass calculation of CA in Appendix B) of CA was weighed, quantitatively transferred into a 25-mL volumetric flask, dissolved and made up to the calibration mark with DI water. Secondly, 2.10 g of the 10 mmol

solution of CA was added to 10 mL of BPEI. Then, the prepared solution mixture was heated at 170 °C in a silicone oil bath for 2 hours. The product was allowed to cool to room temperature and deionised water was added. The resultant solution of a-CDs was dialysed against ultrapure water for 2 days with a pre-wetted RC tubing dialysis membrane in order to obtain a purified product. The water was replaced every 6 hours and the final product was centrifuged before analysis. The experimental procedure is illustrated in Figure 11 below:

Figure 11. The synthesis of amine-capped carbon dots: (a) transfer of reagent mixture (citric acid (CA) and branched polyethylenimine (BPEI)) into round bottom flask, (b) heating of reagent mixture in a silicone-oil bath with a reflux condenser, (c) cooling of the resultant amine-capped carbon dots (a-CDs) to room temperature, (d) resuspension of the a-CDs in deionised water, and (e) storage of sample.

The set-up for the thermal treatment of organic molecules, by means of a silicone oil bath, for synthesis of amine-capped CDs is illustrated in Figure 12 below:

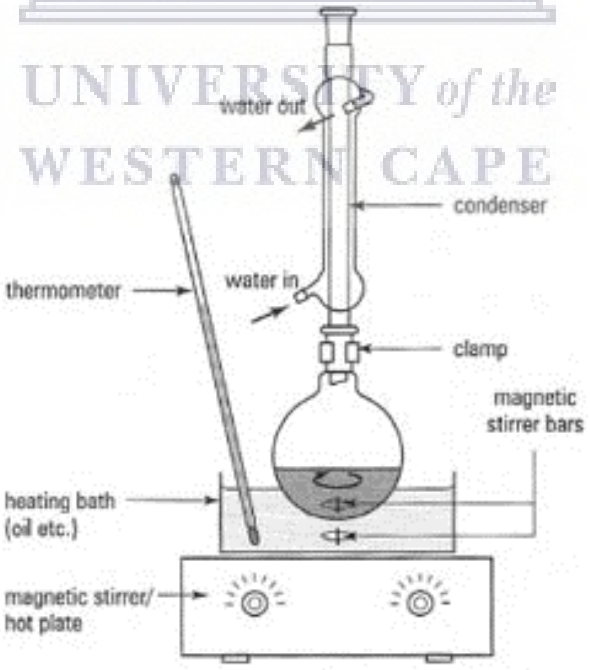

Figure 12. Silicone-oil bath set-up for a-CDs synthesis.

3.6. Dialysis

In this study, dialysis was used for the purification of the synthesised materials (CDs and a-CDs) by removal of small unwanted materials (impurities). The dialysis membrane has a molecular weight cut-off (MWCO) which describes the pore size of the membrane measured in angstrom (Å) units. It also describes the smallest average molecular mass of a molecule that would fail to diffuse through the dialysis membrane (Thermo Fisher Scientific); in this study the MWCO was 1 kD. Evidently, the smaller MWCO corresponded to a smaller pore size. The dialysis bag was weighed throughout the 2-day dialysis process until a constant mass (i.e., equilibrium) was reached. The dialysis equipment set-up is illustrated in Figure 13 below:

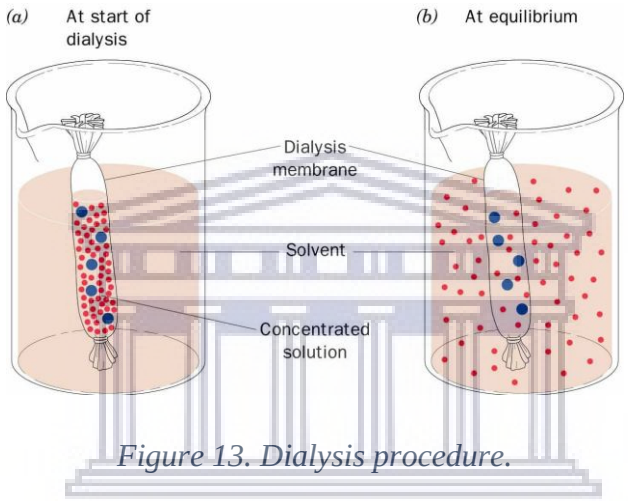

Figure 13. Dialysis procedure.

In preparation for the dialysis process, the samples were all suspended in ultrapure water with resistance of 18.2 MΩ.cm. The water-suspended samples were carefully pipetted into their respective dialysis bags according to its specifications, i.e., the volume that can safely be placed in the membrane was 6.4 mL/cm. The required volume of the wash liquid, i.e., ultrapure water, for dialysis was calculated according to the following requirements: for effective dilution, the volume of the solution for dialysis, V_2, (i.e., ultrapure water) should be significantly greater than the volume of the solution to be dialysed, V_1, (i.e., the water suspended sample); meaning that $V_2 >> V_1$. Hence, the following should be:

- $\frac{V_1}{V_1+V_2} << 1$,
- $\frac{V_2}{V_1+V_2} \approx 1$, and
- $\frac{V_1}{V_1+V_2} + \frac{V_2}{V_1+V_2} = 1$

When V_2 is 300 mL the process of dialysis would be much more effective than when V_2 is 200 mL, as it yields much better values for the 2nd requirement of $\frac{V_1}{V_1+V_2} << 1$ with its calculated values being much smaller than 1. Moreover, for the 3rd requirement of $\frac{V_2}{V_1+V_2} \approx 1$, the values produced by calculations when V_2 = 300 mL are much closer to 1 than those calculated when V_2 is 200 mL. For effective dialysis, 300 mL of ultrapure water was used throughout all studies as calculated according to the equations above (see calculations for all synthesis parameter studies in Appendix).

3.7. Investigation of the colloidal stability of CDs and a-CDs under environmental influences

Once the adequate synthesis conditions were determined according to the methods described in Section 3.4 and Section 3.5 for CDs and a-CDs, respectively, the influence of various conditions, i.e., changes in pH, salinity, and the presence of NOM, were tested. The effect of ranging pH levels, ionic strengths, and humic acid concentrations on the absorbance, hydrodynamic diameter, aggregation behaviour, surface charges, and size distribution of CDs and a-CDs were under investigation.

Firstly, seven pH levels were investigated, namely: 1, 3, 5, 7, 9, 11, and 13, which were adjusted using HCl or NaOH. All other parameters remained fixed, such as the IS of each reaction mixture for both plain/unfunctionalised and passivated/functionalised CDs; as well as the reaction power (900 W), heating time (20 minutes), molar quantity of Gly (0.23 mol), and molar quantity of NaH_2PO_4 (5.1×10^{-3} mol) for CDs (PowOpt_A5); and the temperature (170 °C), reaction time (2 h), molar quantity of CA (1.1×10^{-2} mol), and molar quantity of BPEI (1.3×10^{-2} mol) for a-CDs (TpOpt_B3). The CDs and a-CDs were analysed at above-mentioned pH-levels to obtain size measurements through Dynamic Light Scattering (DLS) and zeta potential measurements through Laser Doppler Velocimetry (LDV) using the Malvern Zetasizer nano ZS90, to (a) examine the behaviour of the particles in acidic and basic environments, (b) determine the dispersity of particles in those environments, and (c) to map the aggregation behaviour thereof through study of the hydrodynamic diameter of particles.

Secondly, the presence of monovalent (i.e., NaCl) and divalent (i.e., $CaCl_2$) cations, were investigated. Four salt concentrations were investigated, namely: 0.001, 0.01, 0.1, and 1 M (introduced by monovalent cations, Na^+ and divalent cations, Ca^{2+}), while several other parameters remained fixed, such as the pH of each reaction mixture for both unfunctionalised

CDs (pH 5) and amine-capped CDs (pH 9); as well as the reaction power (720 W), heating time (15 minutes), molar quantity of Gly (0.15 mol), and molar quantity of NaH_2PO_4 (3.4×10^{-3} mol) for CDs (RTOpt_A8); and for a-CDs (TpOpt_B3) the temperature (170 °C), reaction time (2 h), molar quantity of CA (1.1×10^{-2} mol), and molar quantity of BPEI (1.3×10^{-2} mol). Size, surface charge, and polydispersity index (PDI) measurements were performed through methods described above to (a) examine the behaviour of the particles in the presence monovalent and divalent cations introduced by two salts (i.e., NaCl and $CaCl_2$), (b) determine the dispersity of particles in those environments, and (c) to map the aggregation behaviour and stability of particles.

Lastly, the effect of the presence of NOM (i.e., HA) on the colloidal stability of CDs and a-CDs was investigated. Five concentrations of HA were examined for CDs and a-CDs: 20, 60, 100, 140 and 200 mg/L; while several other parameters remained fixed, such as the reaction power/temperature and time, concentration of precursors for CDs and a-CDs, as well as the pH of the reaction mixtures (all according to the fixed values mentioned above). Particle sizes and surface charges were obtained through methods described previously, to examine the behaviour of the particles in the presence of natural organic matter, i.e., HA.

These tests were performed in order to see whether water chemistry would alter the surface charge of the CDs and a-CDs and if the hydrodynamic size could be correlated to the possible changes, and furthermore, to investigate the influences of environmentally relevant conditions on the aggregation behaviour of the synthesised materials.

3.8. Characterisation techniques

Two techniques were used for analysis of the synthesised CDs and a-CDs. The influence of environmental conditions or water chemistry on the synthesised materials could be understood through application of these analysis techniques to provide vital information regarding the structure and characteristics of the materials. The characterisation techniques used were: ultraviolet-visible (UV-Vis) spectroscopy and zeta potential measurements.

3.8.1. Ultraviolet-visible spectroscopy

Ultraviolet-visible (UV-Vis) spectroscopy, carried out on a UV-Vis system, was used in order to obtain the absorption spectra for CDs and a-CDs, in examination of the effect of pH, salinity, and the presence of NOM on the hydrodynamic properties of the synthesised materials. In each case, the materials were placed in a cuvette of 1 cm path length, where ultra-pure distilled water was used as a blank because of its transparency in the region of interest in the determination of the baseline spectrum (Willard *et al* 1988). The spectra were recorded and treated with various computer algorithms (Rouessac and Rouessac 2000). Characterisation of CDs and a-CDs was performed in the scanning range of 200–800 nm. Both studies were performed at room temperature and were chosen in those specific ranges because they are above the ultraviolet cut-off (i.e., the absorbance wavelength at which the solvent approaches an absorbance of 1) of 191 nm for water (Willard *et al* 1988).

3.8.2. Zeta potential and hydrodynamic size

The colloidal stability of plain CDs and a-CDs were studied by a Malvern Zetasizer nano ZS90 model under varied conditions such as changes in pH (ranging from 1–13), salinity or IS (1, 0.1, 0.01, and 0.001 molar), introduced by monovalent and divalent cations from NaCl and $CaCl_2$, and in the presence of NOM. The hydrodynamic size and zeta potential of the synthesised materials were studied under the above-mentioned conditions through microelectrophoresis (Ravina 1993). Prior to analysis, the samples underwent centrifugation at 3300 rpm for 1 hour and dilution (200 µL of sample in 2 mL of solvent). A disposable polystyrene cuvette for size measurements (and an electrophoresis cell for zeta potential measurements) was filled with the sample material, loaded into the cell area, and analysed at logged measurement settings (Ravina 1993). The software used to control the measurement of the sample comprised of two basic measurement methods—either the use of a Standard Operating Procedure (SOP) (i.e., a template with pre-defined measurement settings) or a manual (essentially a once-off) measurement (Malvern Instruments Ltd. 2004). In the case of ZP measurements, an electric field is activated when the cell undergoes measurement, which

causes the particles in the sample to move at a rate proportional to that of their ZP in a direction indicated by their charge (Ravina 1993). A number of runs were performed for size measurements in order to filter data; the best data was used for final calculations—the more runs, the better the quality of the result. Whereas, in the case of ZP measurements, all individual runs are summed for the final result (Malvern Instruments Ltd. 2004).

3.9. Summary

This concludes the detailed report on the materials, methods, and analysis techniques used within this study. In summary, this study is divided in two parts in which a) the optimisation of synthesis parameters in search of ideal or adequate synthesis conditions for effective synthesis of CDs and a-CDs, and b) the investigation of the influence of pH, IS, and the presence of NOM on the colloidal stability of CDs and a-CDs, were undertaken. The following two chapters contain the results and discussions on the synthesised materials as produced according to the materials and methods described above.

Chapter 4 – Studies on Unfunctionalised Carbon Dots and Amine-Capped Carbon Dots

4. Introduction

The results presented in this chapter describe and explain optimisation procedures for both unmodified (plain) and modified (amine-capped) CDs in search of ideal or adequate synthesis conditions and in determining the effects of applied synthesis parameters on the colloidal stability of the materials under study. Furthermore, discussions on the influence of pH, ionic strength, and the presence of natural organic matter on the hydrodynamic properties of both CDs and a-CDs will be presented in chapter 5.

4.1. Optimisation of synthesis conditions for plain/unfunctionalised CDs

In this section, the results on the optimisation procedures for the synthesis parameters of plain or unfunctionalised CDs will be discussed. The aim was to determine the optimal synthesis conditions for unfunctionalised CDs prepared by the method described in Section 3.4 and to determine which applied parameter has the greatest influence on the colloidal stability of CDs. There were four main synthesis conditions under study, i.e., microwave power of synthesis, reaction duration, molar quantity of glycerol (Gly) and molar quantity of sodium dihydrogen phosphate (NaH_2PO_4).

4.1.1. Power optimisation for synthesis of carbon dots

In this section, the results on the effect of synthesis power on the colloidal stability of CDs are presented and the samples were prepared according to the experimental procedure described in Section 3.3.1. Five different power levels were analysed to determine the ideal power setting for effective synthesis of plain CDs. The synthesis power was varied as follows: 90, 270, 450, 720, and 900 W, while the molar ratio of glycerol (70 % w/w) to NaH_2PO_4 (20 % w/w) remained constant at 10:1 and the heating time of the reaction remained constant at 20 minutes. The aim was to investigate the effect of synthesis power on (a) the % yield (calculated in Table 25 in Appendix C), (b) the mass of dialysis bags throughout dialysis, (c) the interaction of light with the CDs through UV-Vis, and (d) the hydrodynamic diameter, polydispersity index and surface charge (i.e., zeta potential) of CDs. Figure 14 below presents the % yield of the five samples prepared at different power levels.

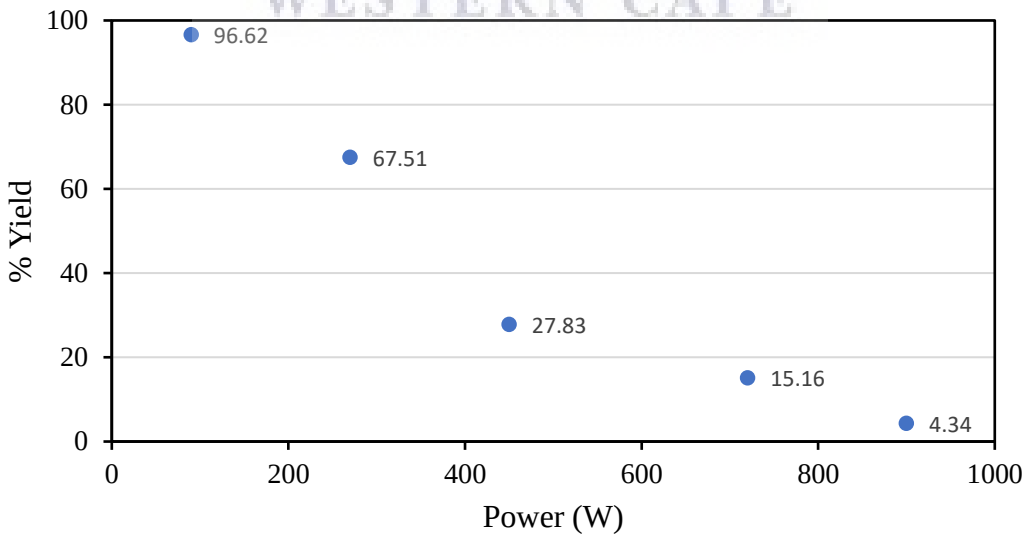

Figure 14. % Yield of plain CDs prepared in 20 minutes with a Gly:NaH_2PO_4 ratio of 10:1 for the power optimisation study.

According to the results in Figure 14 above, the % yield decreased with an increase in synthesis power from 96.62 % at 90 W to 4.34 % at 900 W. There is a negative correlation between the % yield and applied synthesis power. Typically, a high % yield is desired; however, due to the difficulty of drying the synthesised material, the results shown above are of the prepared samples before a drying procedure. With that said, the high % yields produced at low power levels could be due to the presence of unreacted reagent materials. This reaction is greatly dependent on heat and the lower power levels possibly do not provide sufficient amounts thereof for effective synthesis of CDs. In a previous study performed by Barman and Patra, quantum yields of graphene quantum dots (GQDs) were observed to decrease with an increase in size (Barman and Patra 2018), and this is evident in the shift of absorbance spectra (shown in Figure 18) due to increased conjugation (and size). In another study, a reduction in the % yield with an increase in microwave power was also reported; they have attributed the yield reduction to an increase in the burning energy in the fabrication of CDs which according to them would influence the loss of volatile materials leading to a decrease in the weight of the burned carbon (Sutanto *et al* 2020). From this it can be concluded that a similar effect occurred for this study in which the decrease in the % yield with an increase in synthesis power could be correlated to an increase in particle size or agglomeration.

The colour of a substance greatly depends on its interaction with light (Filipponi and Sutherland 2012) and in Figure 15 below, an increase in the colour intensity of synthesised CDs is noticeable from clear/transparent to dark brown in colour. According to literature, it is known that the formation of CDs is represented by the appearance of a brown colour (Zhu *et al* 2009, Ray *et al* 2009, Zhou *et al* 2007, Zhang *et al* 2017, Zhao *et al* 2008, Liu *et al* 2007, Deng *et al* 2014, Bayati *et al* 2018). Therefore, the formation of CDs was only noticeable in Figure 15 b-e. Typically, the rate of a reaction is accelerated with a raise in temperature as the particles that make up the solution move faster and increase the frequency of effective collisions between reacting particles (Bewick *et al* 2019). Therefore, the higher the power level, the higher the temperature of the solution, which allows for more effective collisions between reagent molecules.

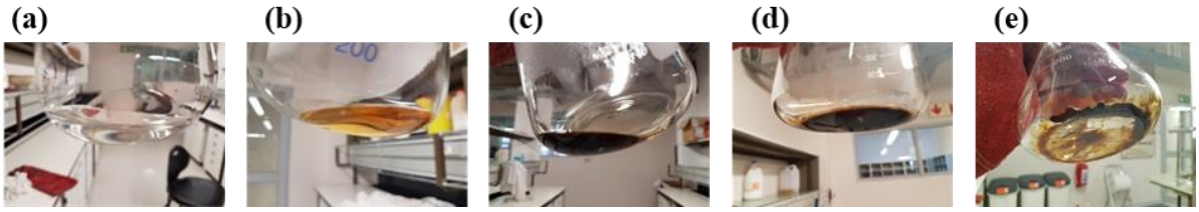

Figure 15. Synthesis power optimisation of plain carbon dots from the lowest to the highest power, namely (a) 90 W (10 %), (b) 270 W (30 %), (c) 450 W (50 %), (d) 720 W (80 %) and (e) 900 W (100 %).

4.1.1.1. Dialysis

In this section, data regarding the dialysis of the above-mentioned samples from the power optimisation study of CDs is presented. The samples underwent dialysis right after microwave irradiation (through a procedure described in Section 3.6) to ensure effective purification of CDs through the removal of unreacted reagent molecules and small molecular by-products from the solution mixture. The samples consisted of the freshly synthesised CDs, unreacted reagent molecules and molecular by-products of low molecular weight (Chen *et al* 2019), hence the importance of removing unwanted materials to yield a purified product. Shown in Figure 16 below are images of CDs before and after dialysis. It is noticeable that diffusion occurred from the higher concentrated solute within each dialysis bag to the surrounding solution of lower concentration evident by the colour difference of the wash liquid before and after dialysis, i.e., the surrounding liquid became less transparent and light brown in colour.

Figure 16. Dialysis of plain carbon dots for the power optimisation study, (a) before, and (b) after dialysis.

According to Hunter, dialysis is a purification method used to separate the colloidal material (i.e., CDs) from small ions and molecules through a membrane (which, in this case, has a molecular weight cut-off, MWCO, of 1 kD) (Hunter 1987). Due to a salt concentration difference between the inside and outside of the bag (or membrane), the CDs are retained on

the inside of the dialysis bag, while molecules and ions of molecular weight smaller than 1 kD can diffuse through the pores of the membrane into the surrounding liquid (i.e., the washing solution) of lower concentration.

It is essential to monitor the mass of each dialysis bag in order to determine whether dialysis was successful. This will be apparent in the stabilisation of the mass of the dialysis bag and pH of the wash liquid or bathing solution for each sample. Therefore, the mass of each dialysis bag was recorded after each wash liquid (i.e., ultrapure water) replacement. The data tabulated in Table 27 (see Appendix) and the graphic representation in Figure 17 below shows the monitored masses of dialysis bags for each sample after each consecutive dialysis period (i.e., directly before each replacement of bathing solution).

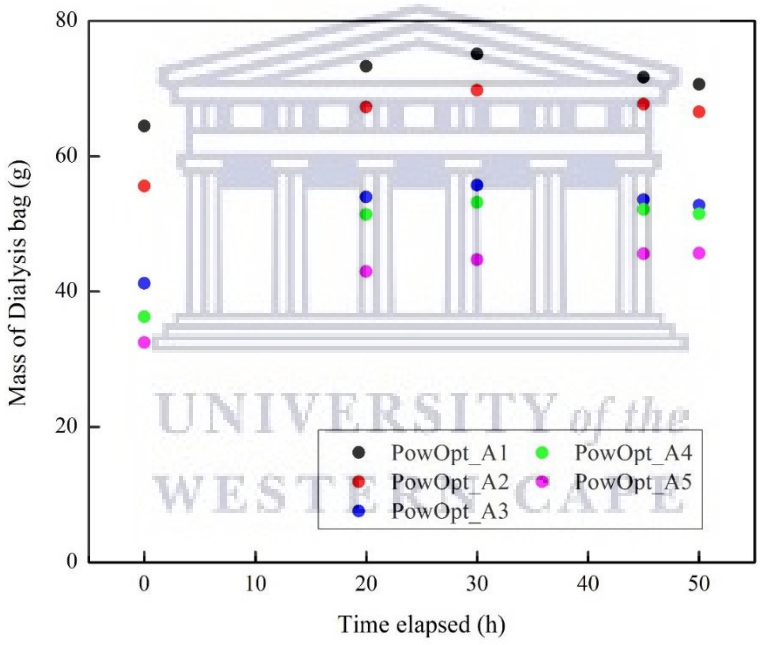

Figure 17. Dialysis of plain CDs in power optimisation study.

In Figure 17, there is a slight increase, initially, in the mass of each dialysis bag which could be due to the fact that each sample contains water because the plain CDs were resuspended in water before they were placed in their respective dialysis bags. According to Hunter, this means that the initial chemical potential at the surface of the membrane inside the bag was lower due to rapid diffusion of water into the bag through the membrane via a process called osmosis, causing a zone of low solute concentration (Hunter 1987). Proper diffusion only occurred when the osmotic pressure was built up high enough to oppose the osmotic flow. Therefore, the mass

of the dialysis bag for each sample initially increased and then gradually decreased due to retardation of the process of diffusion with the exception of PowOpt_A1. When comparing the mass graph of PowOpt_A1 with that of PowOpt_A5, it is clear that the mass of dialysis bag of the former follows an overall increasing trend, whereas that of the latter increases initially and then gradually decreases to eventually reach a somewhat constant mass. The reason behind this is that the power used for preparation of PowOpt_A1 was rather low and possibly too low for successful production of CDs, hence, sample PowOpt_A1 mainly consisted of unreacted reagent molecules and water, therefore, osmosis continued to occur into the dialysis bag leading to a constant increase in mass. However, the mass of each bag eventually reached a somewhat constant mass after the dialysis period.

See Appendix for dialysis results of reaction-time and molar quantity studies of Gly and NaH_2PO_4 of plain CDs; and that of temperature, reaction-time, and molar quantity studies of CA and BPEI for a-CDs.

4.1.1.2. Absorbance study through ultraviolet-visible spectroscopy

The absorbance of unfunctionalised CDs was analysed using UV-Vis spectroscopy (as described in Section 3.8.1) to qualitatively determine whether unfunctionalised CDs were produced and to understand the effect of synthesis power on the absorbance thereof. The five samples from the power optimisation study, i.e., PowOpt_A1 (90 W), PowOpt_A2 (270 W), PowOpt_A3 (450 W), PowOpt_A4 (720 W), and PowOpt_A5 (900 W), were studied. The absorbance data, i.e., the maximum absorption peaks of the above-mentioned samples with their respective absorbances, is tabulated in Table 3 below and the absorbance spectra are shown in Figure 18.

Table 3. The absorbance values of CDs synthesised in 20 minutes for the power optimisation study.

Sample code	***λ_{max} (nm)***	***Absorbance (A)***
PowOpt_A1 (90 W)	254	0.013
PowOpt_A2 (270 W)	232	0.048
PowOpt_A3 (450 W)	232	0.081
PowOpt_A4 (720 W)	262	0.286
PowOpt_A5 (900 W)	263	0.549

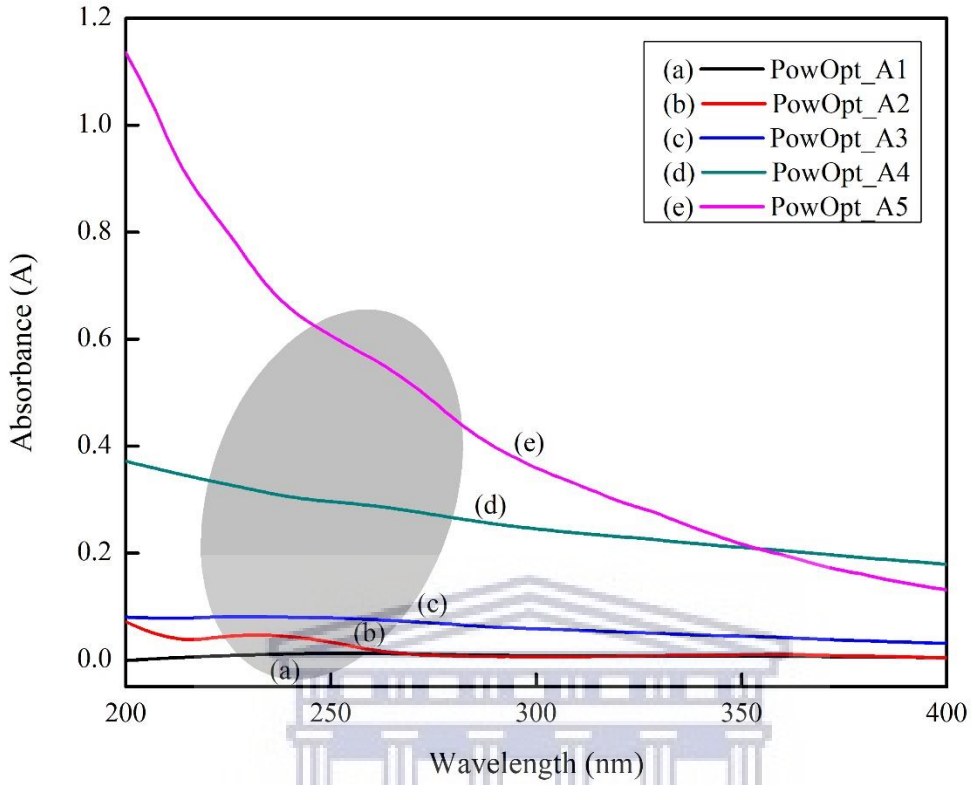

Figure 18. Ultraviolet-visible spectra for unfunctionalised carbon dots (CDs) synthesised within 20 minutes at varied power intensity levels of (a) 90 W (10 %), (b) 270 W (30 %), (c) 450 W (50 %), (d) 720 W (80 %) and (e) 900 W (100 %). The molar ratio of glycerol (70 % w/w) to NaH_2PO_4 (20 % w/w) remained constant at 10:1.

In Figure 18, the optical absorption peak is visible between 220 nm and 270 nm, which is in agreement with the peak observed for CDs in previous studies (Ismail *et al* 2020, Sutanto *et al* 2020, De and Karak 2013, Joseph and Anappara 2016, Zhou *et al* 2007). As the synthesis power was increased from 90 to 900 W, a hyperchromic effect (i.e., an increase in absorbance intensity) from 0.013 to 0.549 is observed in Figure 18 as tabulated in Table 3. According to the Beer-Lambert law, $A = \varepsilon lC$, there is a direct proportionality between absorbance and concentration, therefore the increase in absorbance is directly related to an increase in the concentration of CDs. Also, according to Ray et al., stronger absorbance is an indication of a decrease in particle size (Ray *et al* 2009). Furthermore, there is a bathochromic effect (i.e., a red shift) in the absorption band of CDs from 254 to 263 nm that occurred with an increase in power and according to Barman and Patra, a red shift in the absorption band of CDs is related to an increase in the size of the nanoparticles (Barman and Patra 2018). According to literature, CDs have a highly conjugated network, especially in their core, and this causes a decrease in

their band gap energy which leads to a displacement in the absorption spectrum towards longer wavelengths (Barman and Patra 2018, Rouessac and Rouessac 2000). Also, the alternating single and double bonds in conjugated systems lead to increased spatial delocalisation of electrons which also causes a decrease in band gap energy (Rouessac and Rouessac 2000). The wavelengths of light that are absorbed by a sample material is dependent on the energy levels of the substance and involves electronic transitions specific to chromophores and fluorophores, such as rotations and vibrations (Filipponi and Sutherland 2012). According to previous studies, most CDs have been reported to undergo n–π* transitions of the C=O bands and π–π* transitions of the conjugated C=C bands (Ismail *et al* 2020, Chen *et al* 2019), which is also observed in Figure 18 above. Typically the $n \rightarrow \pi^*$ transition is observed in molecules with a heteroatom connected to an unsaturated system and is usually due to a carbonyl band between 270 and 295 nm (Rouessac and Rouessac 2000).

A desired result would be the achievement of small sized CDs and maintenance of these size dimensions which directly relates to stability through the control over size. Quantum confinement results in smaller sizes of materials which gives rise to larger band gap energies that in turn cause a decrease in wavelength (i.e., a blue-shift). Therefore, as the size of a material is decreased to the nanoscale, quantum confinement occurs in which the motion of electrons is confined in one or more dimensions depending on the size and shape of a material. CDs are confined in all three dimensions and have a larger number of surface atoms in relation to core atoms, hence, atoms at an interface are more unstable due to their increased reactivity and greater surface energy. According to the fundamental chemical principle that 'systems of high energy will strive to attain a state of lower energy, by whatever means possible', nanomaterials would adopt any method possible to reduce their high surface energy and one of these methods is agglomeration (Filipponi and Sutherland 2012).

4.1.1.3. Hydrodynamic properties – Zetasizer

The above-mentioned unfunctionalised CDs, prepared according to the method described in Section 3.3.1, were characterised at various synthesis power levels to obtain size measurements through Dynamic Light Scattering (DLS) and zeta potential measurements through Laser Doppler Velocimetry (LDV) by the Malvern Zetasizer Nano ZS90, to determine the ideal synthesis power (see Section 3.8.2 for experimental procedure). When radiation interacts with matter scattering occurs, which is a physical process determined by cluster size, and the refractive index of both the cluster as well as the suspension medium (Filipponi and Sutherland 2012). The hydrodynamic properties of CDs were studied to understand the effect of the synthesis power on the average hydrodynamic diameter (D_h/Z-Ave), particle dispersity index (PDI), and zeta-potential (ZP) as tabulated in Table 4. The D_h, PDI, and ZP are plotted as functions of synthesis power in Figure 19 below.

Table 4. Results of the hydrodynamic diameter, particle dispersity, and zeta potential of unfunctionalised CDs synthesised in 20 minutes for the power optimisation study.

Sample code	***Z-Ave (nm)***	***PDI***	***ZP (mV)***
PowOpt_A1 (90 W)	869.1	0.935	−6.23
PowOpt_A2 (270 W)	1257	0.775	+2.83
PowOpt_A3 (450 W)	3687	0.703	+8.12
PowOpt_A4 (720 W)	2282	0.911	−8.86
PowOpt_A5 (900 W)	597.6	0.720	−17.0

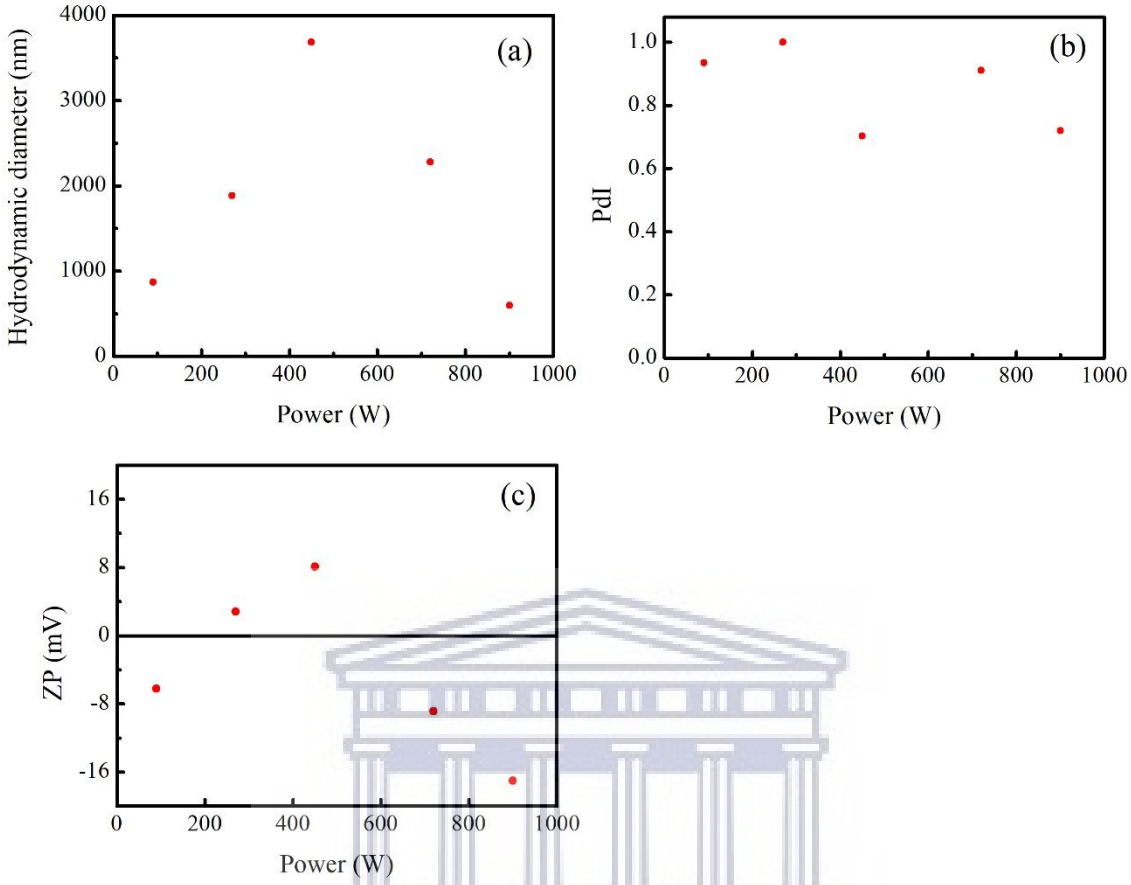

Figure 19. (a) Hydrodynamic diameter, (b) polydispersity index, and (c) zeta potential over a range of power levels (from 90 to 900 W) for synthesis of plain CDs (20 minutes; Gly:NaH_2PO_4 in a 10:1 ratio).

The first parameter under investigation was the hydrodynamic diameter. In Figure 19a, there was an initial increase in the hydrodynamic diameter of CDs from power level 90 W to 450 W, which was followed by a sharp decrease in diameter at 900 W, which shows that the diameter of CDs is sensitive to synthesis power. The smaller hydrodynamic diameters seen for the 90-W and 270-W samples could be attributed to the prevalence of unreacted reagent material due to the low conversion rate of reagent molecules into desired product at low power. The particles show greatest stability at the highest power of 900 W; as smaller sizes were reported which corresponded to the lowest zeta potential of −17 mV. According to Bayati et al., this less negative surface charge can be credited to the electrical double layer compression (Bayati *et al* 2018). As previously mentioned, CDs that are smaller and more stable (such as those found within the samples prepared at higher synthesis powers) would remain in suspension and could be transported to other ecosystems leading to further contamination. The samples prepared at

intermediate power levels underwent agglomeration to a larger extent and would typically be the particles that would sediment and affect organisms found on the floor of natural water bodies. According to Hunter, smaller particles undergo Brownian motion and constantly collide with other particles but remain discrete as their collisions result in non-permanent associations, whereas a colloidally unstable system undergoes collisions that result in permanent associations or the formation of aggregates (Hunter 1987). The very large sizes could be attributed to the occurrence of agglomeration and the formation of clusters of particles in order to obtain stability by lowering the high surface energy.

The second parameter under investigation was the polydispersity index (PDI) of CDs over the above-mentioned synthesis power levels (as displayed in Figure 19b). The PDI is a width parameter obtained by a Zetasizer which refers to the degree of dispersity of particles. It is displayed as a function of synthesis power and the lower the PDI, the more monodisperse and less polydisperse the particles are which translates to narrow size distributions. Overall, the PDIs of unfunctionalised CDs at varied synthesis powers displayed broad size distributions which means that the particles were generally polydisperse and no clear trend was observed. For CDs to be considered stable, monodispersity is desired; however, a change in the synthesis power-level did not provide control over the dispersity of particles and rendered CDs more polydisperse.

Another important parameter under investigation was the zeta potential (ZP) of CDs at various synthesis powers. The ZP was measured by a Zetasizer using Laser Doppler Velocimetry (LDV) which involves an electrophoresis experiment in which the velocity of particles (i.e., the electrophoretic mobility) is determined and the Henry equation is applied (Malvern Instruments Ltd. 2004). ZP is plotted as a function of synthesis power of CDs (Figure 19c). The ZP values were power-sensitive and they were most negative for smaller hydrodynamic sizes which occurred at higher power levels of 720 W and 900 W with values as low as −8.86 and −17 mV, respectively. Visibly, there is a direct relationship between the hydrodynamic size of CDs and their surface charge; the smaller the CDs are, the more negative the ZP (Bandi *et al* 2020). According to Verwey, when particles approach one another there will be an attraction between them and London-van der Waals potential will prevail for small double layer values and could lead to flocculation. On the other hand, if double layer potential values are large, the potential barrier is high and coagulation is prevented (Verwey 1947). Therefore, it could be possible that the large sizes recorded in Figure 19a are due to coagulation and that attractive forces prevailed, whereas, the opposite is true for smaller sizes recorded in which

coagulation could have been prevented by a high potential barrier, as might be the case for the 900 W sample. A greatly negative surface charge for CDs translating to great colloidal stability, achieved by particles of smaller sizes, is desired. Therefore, CDs produced at high power (i.e., 720 W and 900 W) with the most negative surface charges were more colloidally stable.

Particles or ions that carry a like-charge to that of the colloid causes mutual electrostatic repulsion between them and the suspended colloid; meaning that the suspended colloids will remain dispersed and discrete throughout the medium if the charge is large enough (Ravina 1993). On the contrary, the opposite effect occurs when the charge is reduced and particles are attracted to one another to the degree that they undergo agglomeration and alter the characteristics of the suspension (Ravina 1993).

Furthermore, the size distributions of CDs are shown over the above-mentioned range of power levels expressed in number (Figure 20) and intensity (Figure 21) as determined with a Malvern Zetasizer Nano ZS90 (Malvern Instruments Ltd. 2004). The objective was to examine the distribution of particles by determining the relative amounts (%) of particles found in each size range. This is essential in understanding physical and chemical properties of CDs synthesised at different power levels.

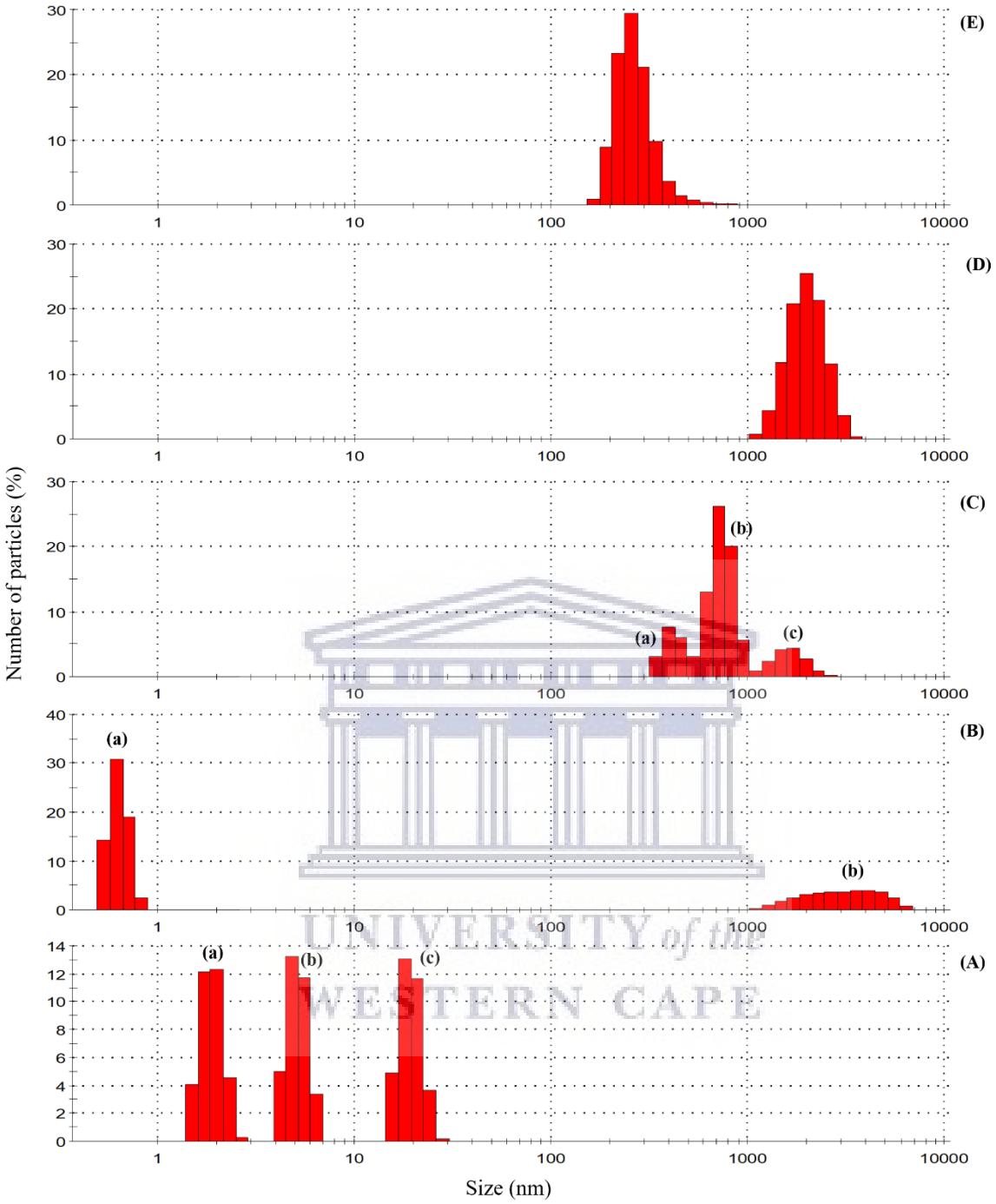

Figure 20. Particle size distribution of unfunctionalised CDs by Number for (A) PowOpt_A1 (90 W), (B) PowOpt_A2 (270 W), (C) PowOpt_A3 (450 W), (D) PowOpt_A4 (720 W), and (E) PowOpt_A5 (900 W) (20 minutes; Gly:NaH_2PO_4 in a 10:1 ratio).

The histograms in Figure 20 above give the percentage of particles in each size class (logarithmically spaced) based on the intensity of light scattered as a function of the particle size distribution of unfunctionalised CDs. In Figure 20(A), the size distribution for the lowest power level, PowOpt_A1 (90 W), is presented in which there are three clusters of particles of the following size classes, namely (a) 1.5 to 2.7 nm (33.3 % of particles) with a 12.3 %

maximum at 2.01 nm, (b) 4.2 to 6.5 nm (33.3 % of particles) with a 13.3 % maximum at 4.849 nm, and (c) 15.7 to 28.2 nm (33.4 % of particles) with a 13.1 % maximum at 18.17 nm. In Figure 20(B), the size distribution for PowOpt_A2 (270 W) is presented in which there are two clusters of particles of the following size classes, namely (a) 0.5 to 0.8 nm (66.7 % of particles) with a 30.9 % maximum at 0.6213 nm, and (b) 1106 to 6439 nm (33.3 % of particles) with a 3.9 % maximum at 4145 nm. In Figure 20(C), the size distribution for PowOpt_A3 (450 W) is presented in which there are three clusters of particles of the following size classes, namely (a) 342 to 531.2 nm (19.6 % of particles) with a 7.6 % maximum at 396.1 nm, (b) 615.1 to 955.4 nm (64.8 % of particles) with a 26.2 % maximum at 712.4 nm, and (c) 1106 to 2669 nm (15.6 % of particles) with a 4.3 % maximum at 1718 nm. In Figure 20(D) the size distribution for PowOpt_A4 (720 W) is presented in which there is one cluster of particles of the following size class from 1106 to 3580 nm with a 25.5 % maximum at 1990 nm. Lastly, in Figure 20(E) the size distribution for PowOpt_A5 (900 W) is presented in which there is one cluster of particles of the following size class from 164.2 to 966.4 nm with a 29.4 % maximum at 255 nm.

The majority of particles were of sizes greater than 100 nm (the upper limit for the nano-range), however, the majority of the particles for the sample prepared at 450 W and all particles of the 900-W sample were intermediate in size (above the upper limit of 100 nm for the nano-range and below the upper limit of 1000 nm for colloidal dispersions). Whereas, PowOpt_A2 (270 W) has a bimodal size distribution with about 66 % of its particles of very small sizes below 1 nm, which could be attributed to unreacted reagent molecules as this synthesis power was very low, while the rest of the particles were of sizes larger than 1000 nm showing some agglomeration. Lastly, all of the particles for the sample prepared at 720 W (PowOpt_A4) were larger than 1000 nm, which could indicate a large degree of agglomeration.

In Figure 21 below, the relative percentage of particles in each size class based on the intensity of light scattered is plotted as a function of the particle size distribution according to logarithmically spaced size classes, as obtained by the Malvern Zetasizer Nano ZS90.

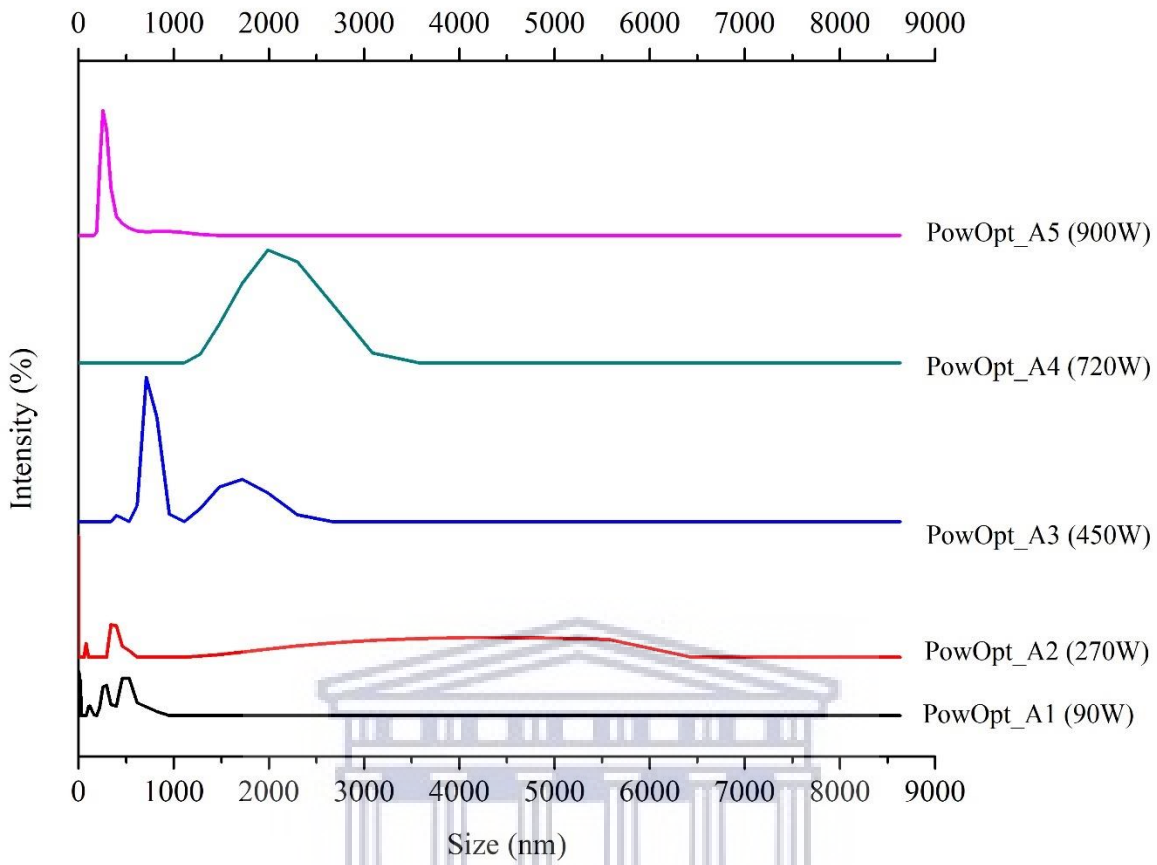

Figure 21. The particle size distribution by intensity of unfunctionalised CDs at varied synthesis powers.

In Figure 21, the size distributions of CDs are displayed over the above-mentioned range of power levels expressed by intensity. Notice that the samples prepared at 270, 450, and 720 W displayed a wider range of particles that stretches in size from 0–6500 nm, 500–2500 and 1000–4000 nm, respectively; whereas CDs prepared at 90 and 900 W have narrower size distributions, which corresponds to the low PDIs and less polydisperse samples. The 90 W sample produced the smallest particles of about 20 nm but it is not certain that this could be due to the formation of CDs or contamination because if we look at the 270-W sample there were definitely reagent materials present as evident by the very small particle sizes below 1 nm.

4.1.1.4. Summary

According to literature, an increase in the synthesis power of CDs significantly affects the burn-off percentage, band gap energy, absorption intensity, and emission intensity (Sutanto *et al* 2020). Even though there was not a very clear trend observed from varying power, CDs proved to be very sensitive to changes in synthesis power. As the synthesis power was increased from 90 to 900 W, several parameters were affected, such as (a) the % yield which decreased, (b) the colour of the suspension of CDs which intensified, (c) the absorbance that increased and λ_{max} which underwent a shift towards longer wavelengths (red-shift), (d) the hydrodynamic diameter was smallest at the lowest power of 90 W and the highest power of 900 W, (e) the ZP became more negative, and (f) the overall size distribution of particles was very wide for most particles in larger size classes. Agglomeration occurred to a large extent at intermediate power and could be due to the instability of the materials produced, or the time-elapse between fabrication and analysis. Furthermore, an increase in the dialysis period along with the introduction of another purification method such as centrifugation could yield better results. The 900-W sample had the highest absorbance, lowest ZP and the narrowest size distribution; however, the high power-setting proved to be an experimental fire hazard due to the fact that the sample caught fire on some attempts. Therefore, the 720-W sample was chosen as the most suitable synthesis power for the synthesis of CDs without the concern regarding safety as it has been successful in previous studies (Chen *et al* 2019, Liu *et al* 2016, Wang *et al* 2019, Xu *et al* 2015). In comparison, the samples prepared at 90, 270, and 450 W had very low absorbance and their power-levels were too low for the complete conversion of reagent materials to product.

4.1.2. Reaction-time optimisation of synthesis procedure of CDs

In this section the results on the effect of synthesis reaction time on the colloidal stability of unfunctionalised CDs is discussed; samples were prepared according to the experimental procedure described in Section 3.3.2. Five different reaction times were analysed in determining the ideal reaction time for effective synthesis of unfunctionalised CDs. CDs were prepared within the following reaction times: 5, 10, 15, 20, and 25 minutes, while several other parameters remained fixed, i.e., the molar ratio of glycerol (70 % w/w) to NaH_2PO_4 (20 % w/w) of 10:1 and the synthesis power of 720 W. The aim was to investigate the effect of synthesis reaction time on (a) the % yield (expressed in Table 28 in Appendix), (b) the interaction of light with the CDs through UV-Vis, (c) the hydrodynamic diameter, polydispersity index, and zeta potential. Figure 22 below presents the % yield (calculated in Table 28) of the five samples prepared at different reaction times.

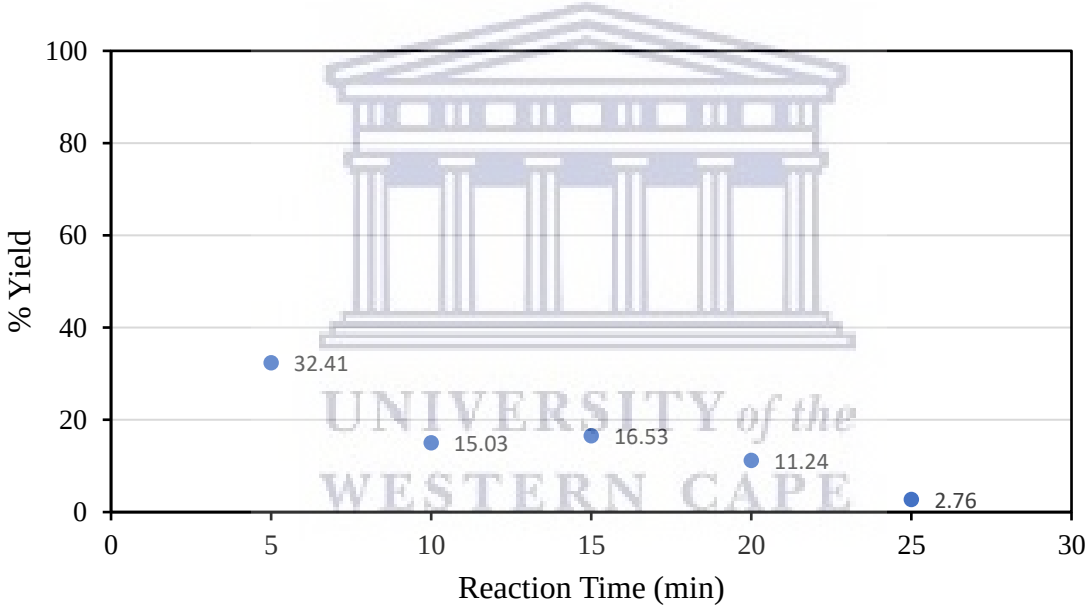

Figure 22. % Yield of plain CDs for the reaction-time optimisation study (10:1 ratio of Gly:NaH_2PO_4; 720 W).

According to the results in Figure 22 above, the % yield decreased from 32.41 % to 2.76 % with an increase in reaction time from 5 to 25 min. There is a negative correlation between the % yield and applied reaction time which is similar to the trend observed in the study of the effect of synthesis power (just at a smaller gradient) and is also in accordance with literature. However, the % yield values for the power study reached much higher values due to the lower synthesis powers in Figure 14. The values for the reaction time study are much lower because

the CDs were prepared at a higher power of 720 W, which means that a higher burn-off occurred and the overall conversion of reagents into desired product is much more effective.

In Figure 23 below, there is a gradual darkening in the brown colour of CDs as the reaction time was increased from 5 to 25 min which is in agreement with previous studies (Zhu *et al* 2009, Baker and Baker 2010, Wang *et al* 2011a). Notice how the texture of the samples vary by becoming more viscous the longer they remain in the microwave until it is completely burnt to the bottom of the flask. The higher power level of 720 W allows for a quicker increase in temperature, hence, the colour transformation from transparent to brown being visible from the lowest duration in the microwave of 5 minutes in Figure 23(a).

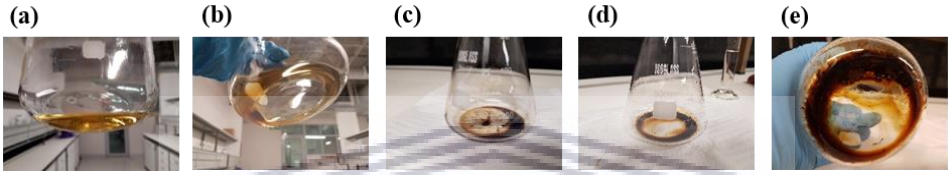

Figure 23. Reaction-time optimisation of CDs prepared at (a) RTOpt_A6 (5 min), (b) RTOpt_A7 (10 min), (c) RTOpt_A8 (15 min), (d) RTOpt_A9 (20 min), (e) RTOpt_A10 (25 min) (10:1 ratio of Gly:NaH_2PO_4; 720 W).

4.1.2.1. Absorbance study through ultraviolet-visible spectroscopy

The absorbance of unfunctionalised CDs was analysed using UV-Vis spectroscopy (as described in Section 3.8.1) to qualitatively determine whether unfunctionalised CDs were produced and to understand the effect of variation in the reaction time on the absorbance thereof. The five samples (of above) for the reaction-time optimisation study were examined. The absorbance data, i.e., the maximum absorption peaks of the above-mentioned samples with their respective absorbances are tabulated in Table 5 below and the absorbance spectra are shown in Figure 24.

Table 5. The absorbance values for the reaction-time optimisation study of CDs with their respective wavelengths (10:1 ratio of Gly:NaH_2PO_4; 720 W).

Sample code	***λ_{max} (nm)***	***Absorbance (A)***
RTOpt_A6 (5 min)	263	0.011
RTOpt_A7 (10 min)	260	0.149
RTOpt_A8 (15 min)	264	0.453
RTOpt_A9 (20 min)	265	1.044
RTOpt_A10 (25 min)	265	1.566

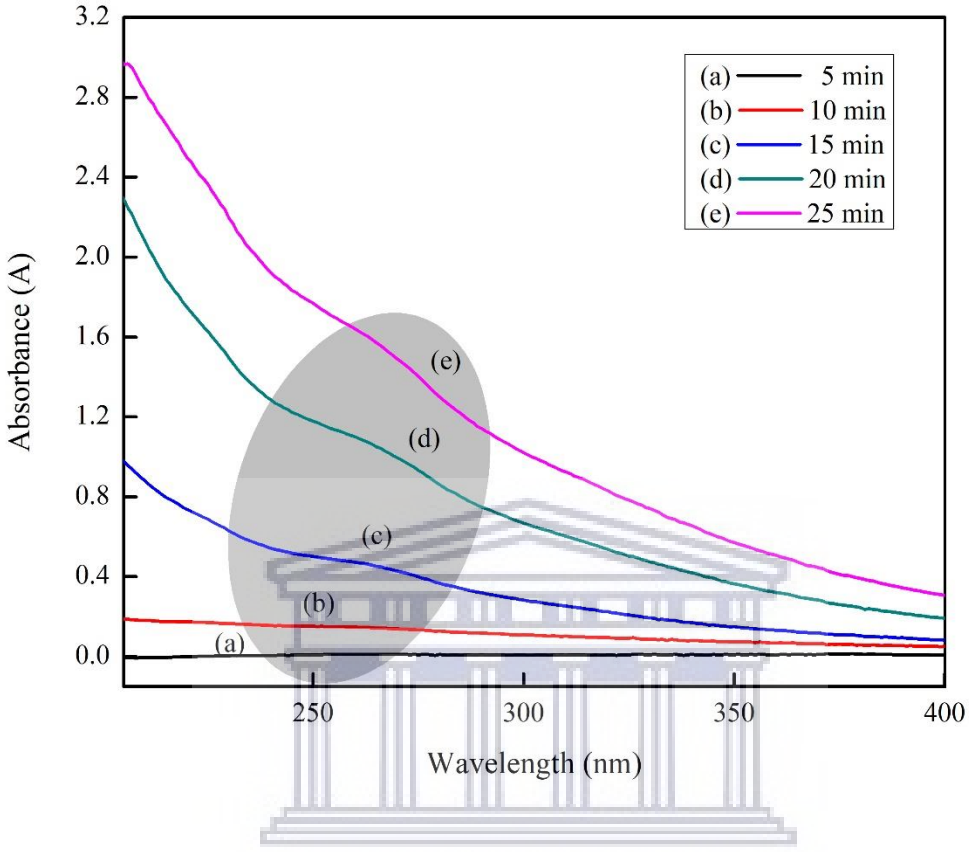

Figure 24. Ultraviolet-visible spectra for unfunctionalised carbon dots (CDs) (synthesised in a 10:1 ratio of Gly:NaH_2PO_4 at 720 W) for a number of reaction times, namely (a) 5 minutes, (b) 10 minutes, (c) 15 minutes, (d) 20 minutes and (e) 25 minutes.

In Figure 24, the optical absorption peak is visible between 220 nm and 270 nm, which is in agreement with the peak observed for CDs in previous studies (Ismail *et al* 2020, Sutanto *et al* 2020, De and Karak 2013, Joseph and Anappara 2016, Zhou *et al* 2007). The transitions remained the same as described for the power optimisation study in Section 4.1.1.2. As the reaction time was increased from 5 to 25 minutes, a hyperchromic effect (i.e., an increase in absorbance intensity) from 0.011 to 1.566 is observed as tabulated in Table 5 and indicates once again that there is an increase in concentration of CDs according to the Beer-Lambert law. Once again there is a bathochromic effect (i.e., a red shift) in the absorption band of CDs from 263 to 265 nm that occurred with an increase in reaction time and is best described by the phenomenon mentioned in Section 4.1.1.2 and relates to an increase in particle size which induces a decrease in the band gap energy, leading to a shift towards longer wavelengths.

4.1.2.2. Hydrodynamic properties – Zetasizer

The above-mentioned unfunctionalised CDs, prepared according to the method described in Section 3.4, were characterised by the Malvern Zetasizer Nano ZS90 to obtain size measurements through Dynamic Light Scattering (DLS) and zeta potential measurements through Laser Doppler Velocimetry (LDV), in determining the ideal reaction time (see Section 3.8.2 for experimental procedure). The hydrodynamic properties of CDs were studied to understand the effect of the reaction time on the average hydrodynamic diameter (D_h/Z-Ave), particle dispersity index (PDI), and zeta-potential (ZP) as tabulated in Table 6. The D_h, PDI, and ZP were plotted as functions of synthesis reaction time in Figure 25 below.

Table 6. Results on the hydrodynamic diameter, particle dispersity, and zeta potential of unfunctionalised CDs for the reaction-time optimisation study (10:1 ratio of Gly:NaH_2PO_4; 720 W).

Sample code	***Z-Ave (d.nm)***	***PDI***	***ZP (mV)***
RTOpt_A6 (5 min)	1055	0.818	−15.6
RTOpt_A7 (10 min)	379.8	0.363	−19.6
RTOpt_A8 (15 min)	296.0	0.245	−31.1
RTOpt_A9 (20 min)	223.6	0.484	−33.6
RTOpt_A10 (25 min)	313.8	0.323	−31.5

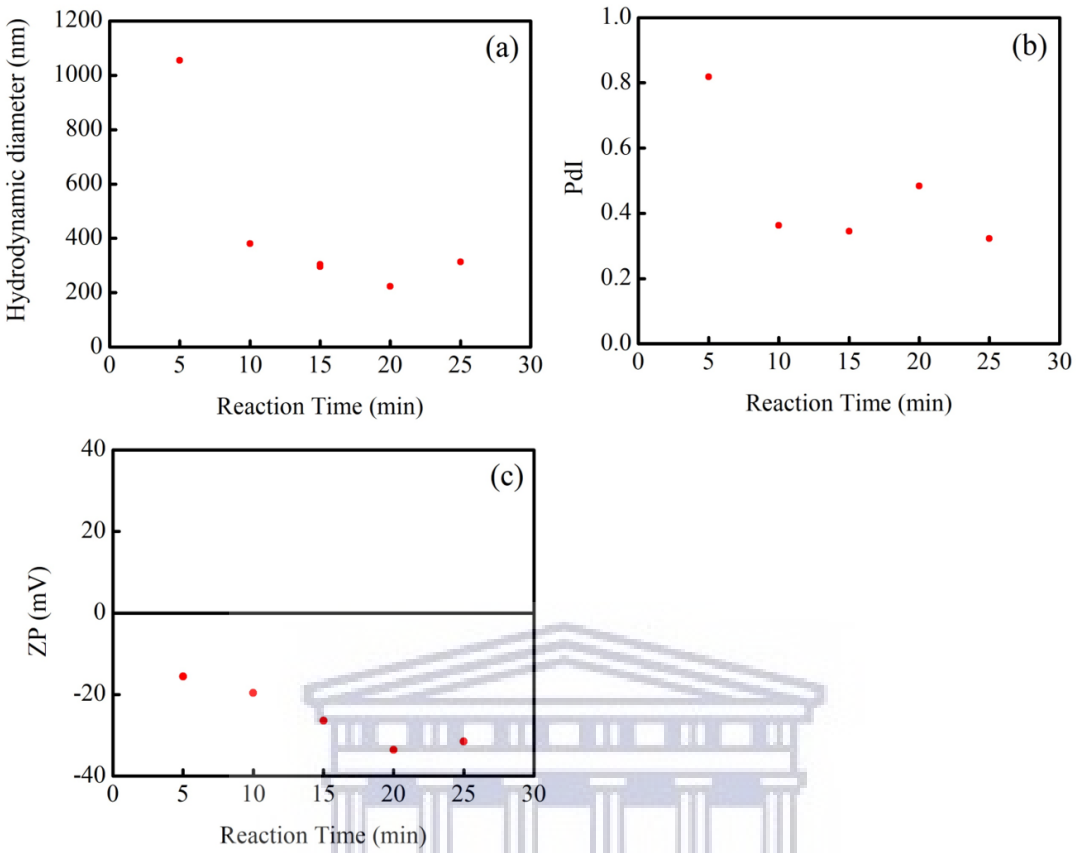

Figure 25. (a) Hydrodynamic diameter, (b) polydispersity index and (c) zeta potential of unfunctionalised CDs synthesised over a range of reaction times (from 5 to 25min) (10:1 ratio of Gly:NaH_2PO_4; 720 W).

The first parameter under investigation was the hydrodynamic diameter. In Figure 25(a), there is an overall decrease in the hydrodynamic diameter of CDs as the heating time was increased from 5 to 25 min. The very large particle size for RTOpt_A6 (prepared in 5 min) could be attributed to the occurrence of agglomeration and the formation of clusters of particles in order to obtain stability by lowering the surface energy (Filipponi and Sutherland 2012). On the other hand, for the heating-time range of 10 to 25 minutes, the particle sizes were between 200–400 nm. These large values could be attributed to agglomeration (Zook *et al* 2011) that could also be the reason for the red-shift in absorbance in Figure 24. Initially, there is a sharp decrease in D_h from 1055 nm at 5 min to 329.8 nm at 10 min which is followed by a gradual decrease in D_h to 223.6 nm at 20 min, and then there is a slight increase to 313.8 nm at 25 min, which shows that CDs were sensitive to variation in heating time. The particles show greatest stability at the reaction time of 20 min, as a smaller average particle size was reported which corresponded to the lowest zeta potential of −33.6 mV. After the optimal heating time was

reached at 20 minutes, the average particle size of CDs started to increase from 223.6 nm to 313.8 nm with a size difference of about 90 nm.

The second parameter under investigation was the polydispersity index (PDI) of CDs over the above-mentioned reaction times (as displayed in Figure 25(b)). Overall, the PDI values of unfunctionalised CDs at varied reaction times displayed narrow size distributions as their PDI values were below 0.5, with the exception of the high PDI for the sample prepared within 5 minutes. The sample with a low PDI has a narrow size distribution (as described in Section 4.1.1.3), and according to the results displayed above, the sample with the narrowest size distribution is the one prepared in 15 minutes (RTOpt_A8). The PDIs were much lower and particles were more monodisperse than those obtained for the power optimisation study. These values coincide with the sizes shown in Figure 25(a), where the smaller the hydrodynamic size, the lower the PDI, which is true for reaction times 10–25 minutes where the particle dispersity is rather low and constant between 0.2 and 0.5. Further detail on number and intensity of particle sizes in different size classes are displayed in Figure 26 and Figure 27, respectively.

Another important parameter under investigation was the ZP of CDs at varied reaction times. The ZP values of unfunctionalised CDs became more negative as the reaction time was increased from 5 to 25 min which shows their sensitivity to the time of the reaction (Figure 25(c)). There is a direct relationship visible between the hydrodynamic size of CDs and the surface charge; the smaller the CDs are, the more negative the ZP. The lowest ZP, −33.6 mV, was recorded for the sample RTOpt_A9 prepared at a reaction time of 20 minutes. Here it can be seen that the smaller and more monodispersed the particles are, the more negative the zeta potential. This decreasing trend was also observed for higher power levels of 720 W and 900 W in Figure 19(c) for the power study. It could be assumed that the higher the synthesis power and heating time for unfunctionalised CDs are, the more negative their surfaces become.

Furthermore, the size distributions of CDs over the above-mentioned range of reaction times are displayed and expressed in number (Figure 26) and intensity (Figure 27) as determined with a Malvern Zetasizer Nano ZS90 (Malvern Instruments Ltd. 2004). The objective was to examine the size distribution of particles by determining the relative amount (%) of particles found in each size range which is essential in understanding physical and chemical properties of CDs synthesised at different reaction times.

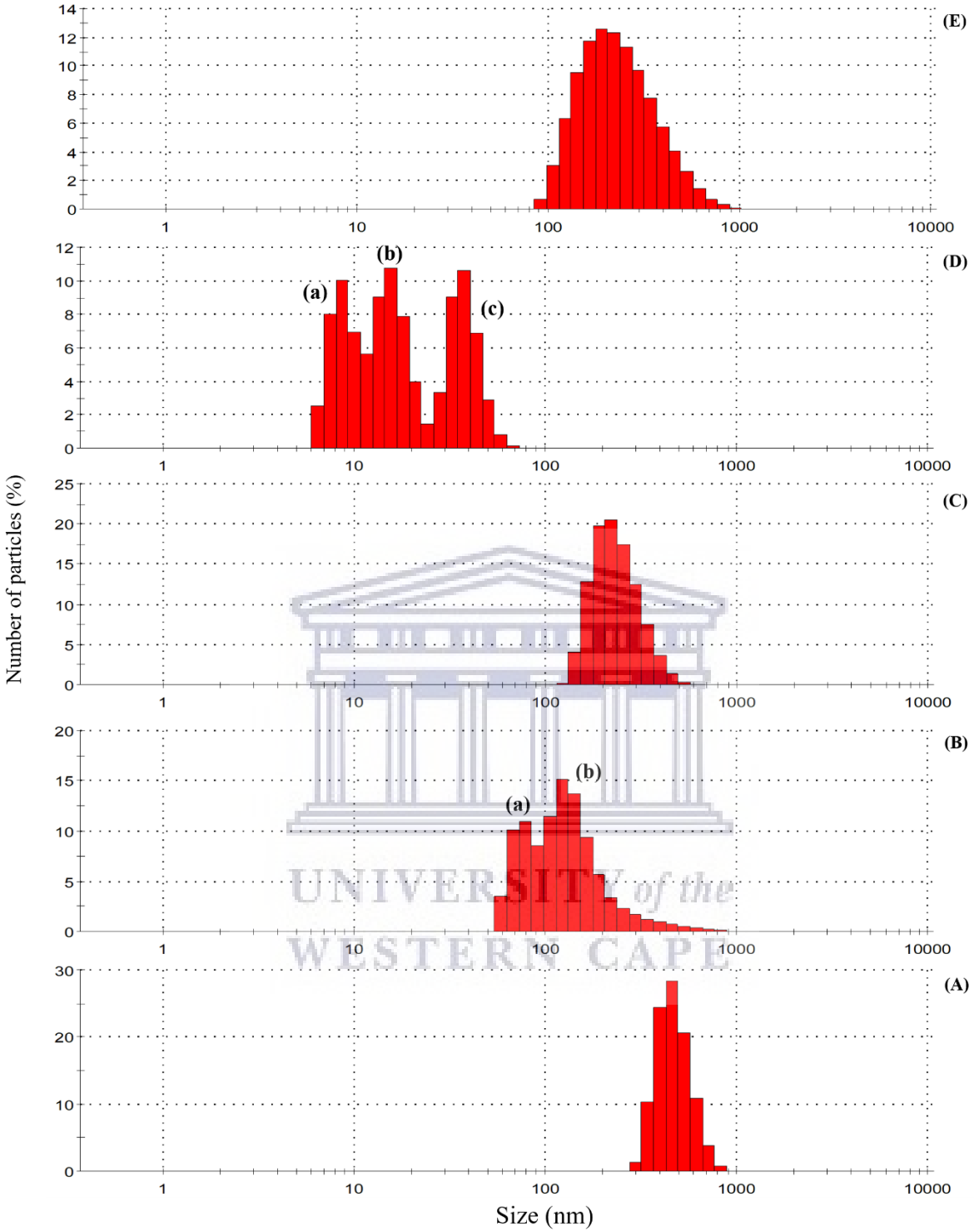

Figure 26. Particle size distribution of plain CDs with the numbers of particles present in each size class for (A) RTOpt_A6 (5 minutes), (B) RTOpt_A7 (10 minutes), (C) RTOpt_A8 (15 minutes), (D) RTOpt_A9 (20 minutes), (E) RTOpt_A10 (25 minutes) (10:1 ratio of Gly:NaH_2PO_4; 720 W).

The histograms in Figure 26 above, give the relative percentage of particles in each size class (logarithmically spaced) based on the intensity of light scattered as a function of the particle

size distribution of plain CDs. The percentage distribution is as follows: (A) RTOpt_A6 (5 minutes) in which there is one cluster of particles of the following size classes from 295.3 to 825 nm with a 28.4 % maximum at 458.7 nm; (B) RTOpt_A7 (10 minutes) in which there are two clusters of particles of the following size classes, namely (a) 58.77 to 91.28 nm (33.1 % of particles) with a 10.9 % maximum at 78.82 nm, and (b) 105.7 to 955.4 nm (66.9 % of particles) with a 15.1 % maximum at 122.4 nm; (C) RTOpt_A8 (15 minutes) in which there is one cluster of particles of the following size classes from 122.4 to 531.2 nm with a 20.5 % maximum at 220.2 nm; (D) RTOpt_A9 (20 minutes) in which there are three clusters of particles of the following size classes, namely (a) 6.503 to 11.70 nm (33.2 % of particles) with a 10.1 % maximum at 8.721 nm, (b) 13.54 to 21.04 nm (31.8 % of particles) with a 10.8 % maximum at 15.69 nm, and (c) 24.36 to 68.06 nm (35 % of particles) with a 10.6 % maximum at 37.84 nm; and (E) RTOpt_A10 (25 minutes) in which there is one cluster of particles of the following size classes from 91.28 to 955.4 nm with a 12.6 % maximum at 190.1 nm.

The overall distribution of particle size was more monodisperse than that obtained for the power optimisation study as the majority of the particles were of sizes smaller than 1000 nm which is the upper limit for colloidal suspensions. According to Hunter, the difference in behaviour of particles of 1000 nm and those that are relatively larger (and that are found in emulsions) is negligible (Hunter 1987). Sample RTOpt_A7 (10 minutes) has one cluster under 100 nm in size which approximates to about 33 % of its particles; and RTOpt_A9 (20 minutes) proved to be the best reaction time for synthesis as all of its particles were within the nano-range and were under 100 nm with the smallest size class at 6.503 nm that make up 2.5 % of the sample. Even though there were some samples that may contain large sedimenting particles or aggregates, these samples displayed much better data than those of the power optimisation study as a greater % of these samples were smaller in size.

In Figure 27 below, the relative percentage of particles in each size class based on the intensity of light scattered was plotted as a function of the particle size distribution according to logarithmically spaced size classes, as obtained by the Malvern Zetasizer Nano ZS90.

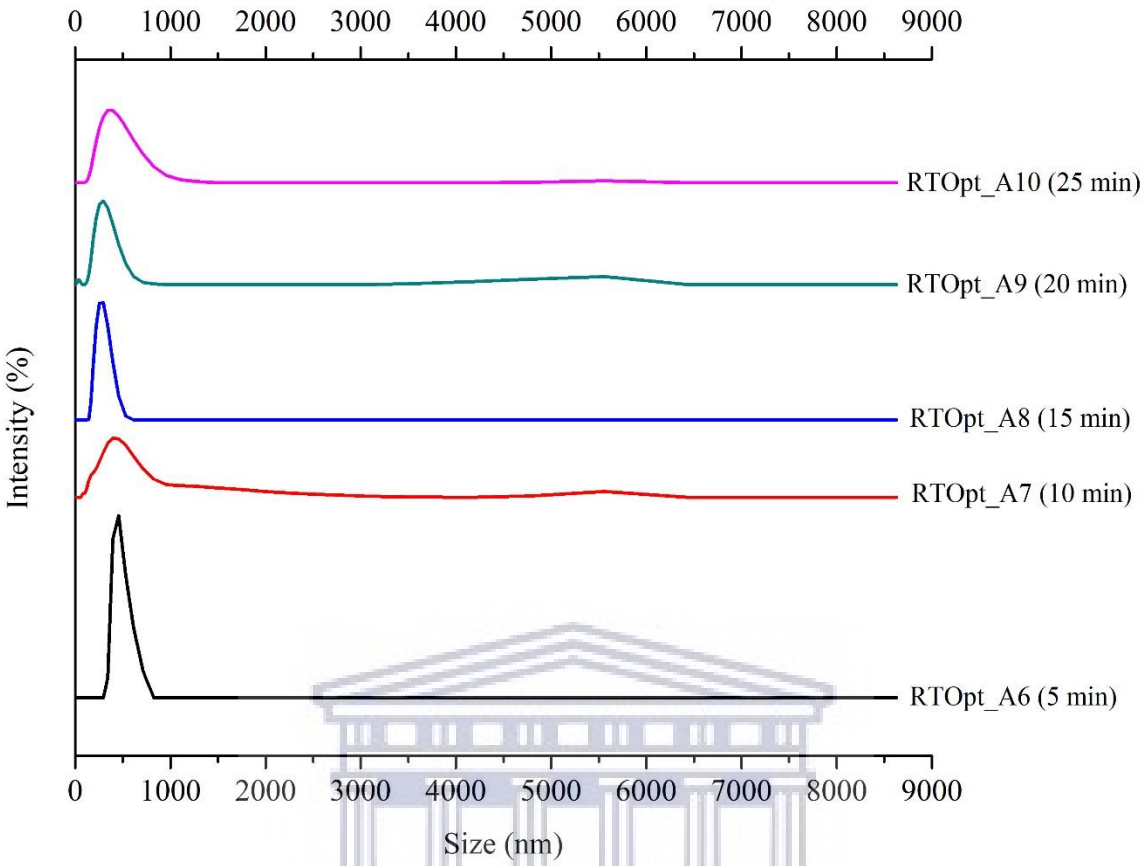

Figure 27. The particle size distribution of unfunctionalised CDs by intensity at varied reaction times (10:1 ratio of Gly:NaH_2PO_4; 720 W).

In Figure 27, the size distributions of CDs are displayed over the above-mentioned range of reaction times expressed by intensity. Notice that the majority of particles for all samples were sized below the upper limit for colloidal suspensions (i.e., 1000 nm), while the samples prepared within 15 minutes displayed particles of the smallest sizes below 500 nm in size. The sample prepared within 5 minutes displayed the sharpest peak below 1000 nm, however, as previously mentioned, could possibly be attributed to the occurrence of agglomeration.

4.1.2.3. Summary

According to literature, an increase in the reaction time of CDs significantly affects the burn-off percentage, band gap energy, absorption intensity, and emission intensity (Sutanto *et al* 2020). CDs proved to be sensitive to changes in heating time. As the heating time was increased from 5 to 25 min, several parameters were affected, such as (a) the % yield which decreased, (b) the colour of the suspension of CDs which intensified, (c) the absorbance increased and λ_{max} underwent a shift towards longer wavelengths (red-shift), (d) the hydrodynamic diameter was smallest for the sample prepared within 20 minutes, (e) the ZP became more negative with the lowest value for RTOpt_A9 (20 min), and (f) the overall size distribution of particles was narrow with all particles below the upper limit for colloidal suspensions (1000 nm) while most particles were of smaller size classes. From the absorbance data it can be deduced that as the reaction/heating time was increased, the size of particles also increased which caused a red shift in the absorbance maximum. Albeit agglomeration occurred, the size distribution of particles was towards smaller size classes than for the Power study as all particles were of sizes below the upper limit for colloidal particles. Strictly from an experimental stand point, the reaction time at which unfunctionalised CDs were fabricated without any difficulty, i.e., before the appearance of flames or yield of burnt samples, was when the CDs were prepared within 15 minutes, similar to reaction time used in a previous study (Wang *et al* 2011a). This is the point at which the sample had the desired appearance, i.e., a brown suspension with desired viscosity as seen in Figure 23(c). RTOpt_A8 (15 min) had one of the lowest ZPs of −31 mV, the 2nd lowest D_h, the lowest PDI of 0.245 (i.e., narrowest size distribution) and the best size distribution slanted most towards lower size classes below 500 nm. Even if longer reaction times yielded lower D_h and ZP, according to literature, CDs enlarge in size and emit at longer wavelengths at longer heating times (Baker and Baker 2010); and these samples also proved to be an experimental fire hazard. According to a previous study performed by So and co-workers, burnt residues were observed under normal light for CDs prepared within 16 minutes which increased over time (So *et al* 2017). Therefore, the reaction time of 14 minutes was chosen as the ideal heating time for the synthesis of CDs for further studies on the effect of environmental conditions.

4.1.3. Molar optimisation of (70 % w/w) glycerol for the synthesis of CDs

In this section, the results on the influence of the molar quantity of glycerol (Gly) on the colloidal stability of unfunctionalised CDs are discussed and the samples were prepared according to the experimental procedure described in Section 3.3.3. CDs were prepared with the following molar ratios of 70 % (w/w) Gly to 20% NaH_2PO_4, namely: 6:1, 8:1, 10:1, 12:1, and 14:1. These five samples, of increasing number of moles of Gly, i.e., 0.14, 0.18, 0.23, 0.27, and 0.32 mol (molar calculations presented in Appendix A), were labelled G_Opt_A11, G_Opt_A12, G_Opt_A13, G_Opt_A14, and G_Opt_A15, respectively. They were analysed to determine the ideal molar quantity of Gly for effective synthesis of unfunctionalised CDs. The following parameters remained fixed: (a) the concentration (70 % w/w = 7.6 $mol.L^{-1}$) of Gly, (b) the concentration (20 % w/w = 1.7 $mol.L^{-1}$) and molar quantity (5.1×10^{-3} mol) of NaH_2PO_4, (c) the synthesis power (720 W), and (d) the reaction time (14 minutes) (Wang *et al* 2011a). The aim was to determine the ideal synthesis conditions for unfunctionalised CDs and investigate the effect of the molar quantity of Gly on (a) the % yield (expressed in Table 31 in Appendix), (b) the interaction of light with the CDs through UV-Vis, (c) the hydrodynamic diameter, polydispersity index, and the surface charge. Table 31 and Figure 28 below presents the % yield (as calculated in Table 31) of the five samples prepared with increasing molar quantities of Gly.

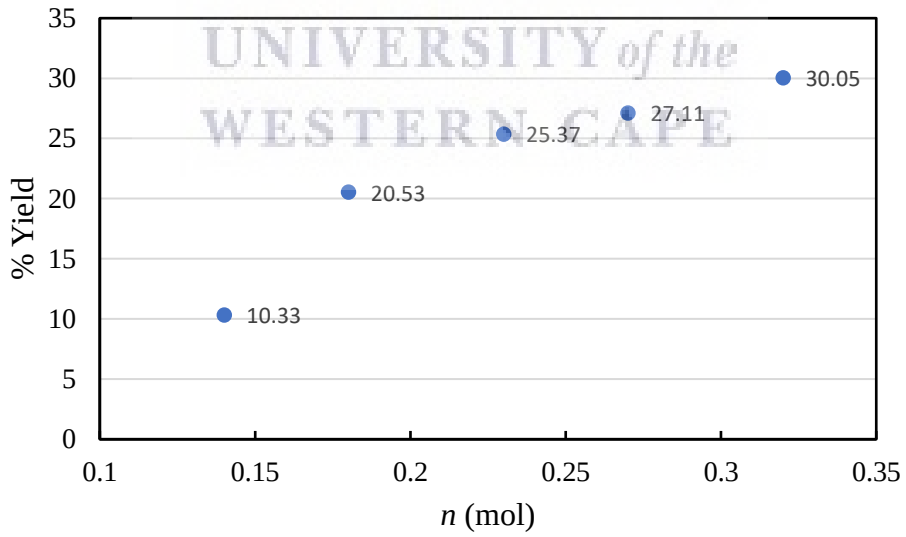

Figure 28. % Yield of unfunctionalised CDs for the molar optimisation study of glycerol (720 W; 14 minutes).

According to the results in Figure 28 above, the % yield of unfunctionalised CDs increased linearly, from 10.33 % to 30.05 %, with an increase in the number of moles of Gly from 0.14

to 0.32 mol. There is a positive correlation between the % yield of unfunctionalised CDs and the number of moles of Gly. This is expected because there is an increase in the carbon source. Typically, an increase in the number of moles of a reagent leads to an increase in the number of collisions amongst reactant molecules (Bewick *et al* 2019). Therefore, increasing the number of moles of Gly (i.e., the carbon source) in the reaction affects the overall rate of the reaction as more carbon is available for carbonisation of hydrocarbon into the graphitic structure. A low volume of the carbon source could lead to insufficient carbonisation and according to Dager et al., in turn could lead to the persistence of some functional groups of the initial source of carbon (Dager *et al* 2019). Therefore, the low % yield at low molar values could be due to insufficient carbonisation. See the effect of an increase in the molar quantity of Gly on the colour of the product as illustrated in Figure 29 below; there is a gradual lightening in the brown colour of CDs.

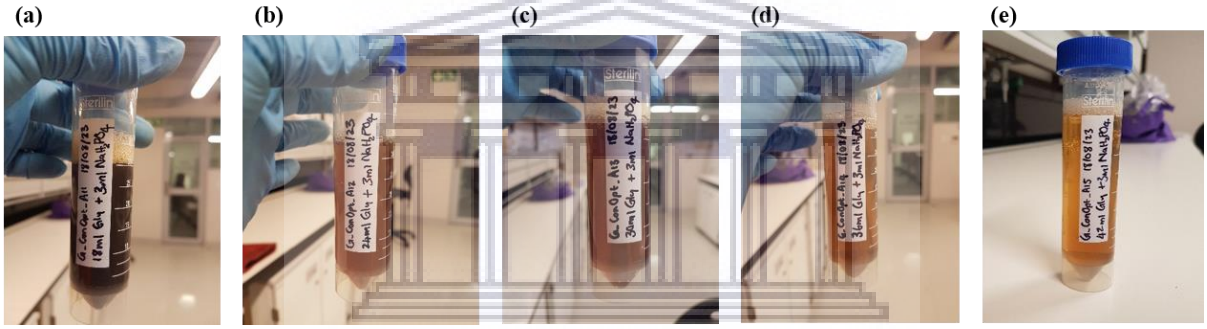

Figure 29. Molar optimisation of 70 % (w/w) glycerol for the synthesis of unfunctionalised CDs (720 W; 14 minutes); (a) 6:1 (0.14 mol), (b) 8:1 (0.18 mol), (c) 10:1 (0.23 mol), (d) 12:1 (0.27 mol), and (e) 14:1 (0.32 mol).

4.1.3.1. Absorbance study through ultraviolet-visible spectroscopy

The absorbance of unfunctionalised CDs was analysed using UV-Vis spectroscopy (as described in Section 3.8.1) to qualitatively determine whether CDs were produced and to understand the effect of variation in the molar quantity of 70 % (w/w) Gly on the absorbance of unfunctionalised CDs. The above-mentioned five samples for the molar optimisation study of Gly were studied. The absorbance data, i.e., the maximum absorption peaks of the above-mentioned samples with their respective absorbances are tabulated in Table 7 below and the absorbance spectra are shown in Figure 30.

Table 7. The absorbance values for the molar optimisation study of 70 % Gly in the synthesis of CDs (prepared at 720 W in 14 minutes) according to their wavelengths.

Sample code	***λ_{max} (nm)***	***Absorbance (A)***
G_Opt_A11	261	1.35466
G_Opt_A12	260	0.38214
G_Opt_A13	260	0.18775
G_Opt_A14	258	0.13164
G_Opt_A15	260	0.08981

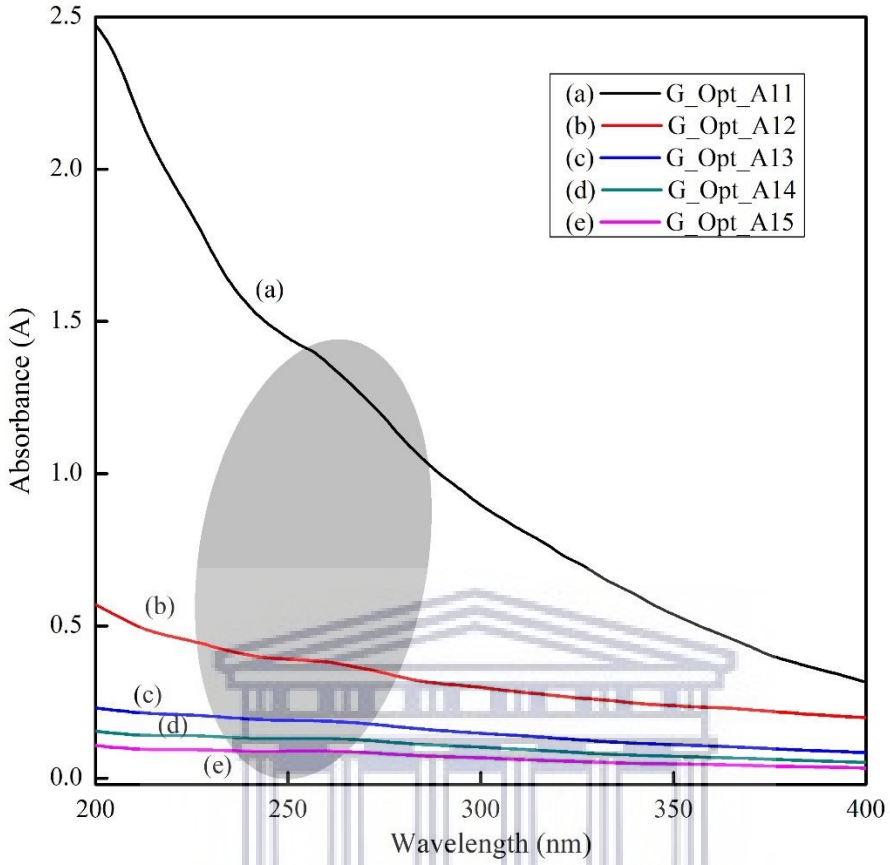

Figure 30. Ultraviolet-visible spectra for unfunctionalised carbon dots (CDs) synthesised at 720 W for 14 minutes for a number of glycerol molar quantities, namely (a) 0.14 mol (G_Opt_A11), (b) 0.18 mol (G_Opt_A12), (c) 0.23 mol (G_Opt_A13), (d) 0.27 mol (G_Opt_A14), and (e) 0.32 mol (G_Opt_A15).

In Figure 30, the optical absorption peak is visible between 220 nm and 270 nm, which is in agreement with the peak observed for CDs in previous studies (Ismail *et al* 2020, Sutanto *et al* 2020, De and Karak 2013, Joseph and Anappara 2016, Zhou *et al* 2007). As the number of moles of 70 % (w/w) Gly was increased from 0.14 to 0.32 mol, a hypochromic effect (i.e., a decrease in absorbance intensity) from 1.35 to 0.0898 is observed as tabulated in Table 7 and typically is caused by distortions in the geometry of a molecule induced by a functional group (Rouessac and Rouessac 2000). Furthermore, there is a slight hypsochromic effect (i.e., a blue shift) in the absorption band of CDs from 261 to 258 nm that occurred with an increase in the number of moles of Gly. According to literature, it could be ascribed to the greater energy demand by the $n \rightarrow \pi^*$ electronic transition, hence the shift of the absorption peak maximum towards shorter wavelengths due to the stabilisation by C^+-O^- polarisation through clustering of polar solvent (in this case water) molecules (Rouessac and Rouessac 2000).

4.1.3.2. Hydrodynamic properties – Zetasizer

The above-mentioned unfunctionalised CDs, prepared according to the method described in Section 3.3.3, were characterised by the Malvern Zetasizer Nano ZS90 to obtain size measurements through Dynamic Light Scattering (DLS) and zeta potential measurements through Laser Doppler Velocimetry (LDV), in determining the ideal molar ratio of Gly to NaH_2PO_4 (see Section 3.8.2 for experimental procedure). The hydrodynamic properties of CDs were studied to understand the effect of the molar quantity of Gly on the average hydrodynamic diameter (D_h/Z-Ave), particle dispersity index (PDI), and zeta-potential (ZP) of unfunctionalised CDs as tabulated in Table 8. The D_h, PDI, and ZP are plotted as functions of the number of moles of Gly in Figure 31 below.

Table 8. Hydrodynamic diameter, particle dispersity, and zeta potential of unfunctionalised CDs prepared at 720 W for 14 minutes for the molar optimisation study of glycerol.

Sample code	***Z-Ave (nm)***	***PDI***	***ZP (mV)***
G_Opt_A11 (6:1)	231.7	0.243	−0.737
G_Opt_A12 (8:1)	2912	0.255	+0.314
G_Opt_A13 (10:1)	3282	0.342	+5.31
G_Opt_A14 (12:1)	3293	0.569	+8.93
G_Opt_A15 (14:1)	1939	0.595	+10.3

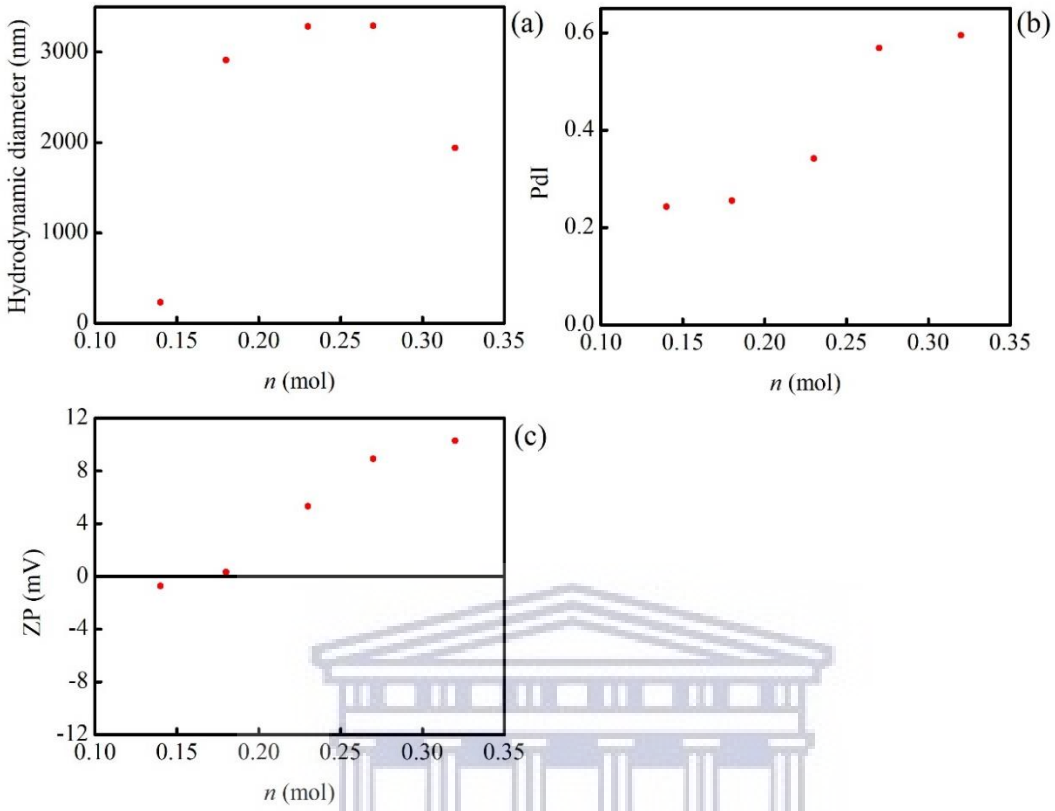

Figure 31. (a) Hydrodynamic diameter, (b) polydispersity index and (c) zeta potential over a range of 70 % (w/w) glycerol molar quantities (from 0.14 to 0.32 mol) for synthesis of plain CDs.

The first parameter under investigation was the hydrodynamic diameter. In Figure 31a, there is an overall increase in the hydrodynamic diameter of CDs as the number of moles of Gly was increased from 0.14 to 0.32 mol. Initially, there is a sharp increase in D_h from 231.7 nm for G_Opt_A11 to 2912 nm for G_Opt_A12, which is then followed by a gradual increase to 3293 nm for G_Opt_A14 and lastly, an abrupt decrease to 1939 nm for G_Opt_A15, which shows the sensitivity of CDs to variation in molar quantity of Gly. The very large particle sizes, for the samples prepared with molar values of Gly ranging from 0.18 to 0.32 mol, could be attributed to the occurrence of coagulation, i.e., the formation of clusters of particles in order to obtain stability by lowering the surface energy (Filipponi and Sutherland 2012). Due to the increase in reagent molecules, the number of collisions increase and the repulsion barrier between approaching particles is lowered, leading to more collisions resulting in a permanent particle-particle contact, which induces the formation of flocs (Hunter 1987). The particles show greatest stability for the sample produced with 0.14 mol of Gly (i.e., the smallest molar quantity of Gly), as smaller sizes were reported.

The second parameter under investigation was the polydispersity index (PDI) of CDs over the above-mentioned Gly molar quantities as displayed in Figure 31(b). The PDI values obtained for plain CDs prepared with 0.14, 0.18, and 0.23 mol of Gly displayed narrow size distributions as their PDI values were below 0.5. However, for larger molar values of Gly (i.e., 0.27 and 0.32 mol) high PDIs (i.e., wider size distributions) were obtained. There is an overall increase in the PDIs which increases exponentially for the first three molar quantities of Gly (i.e., from 0.14 to 0.23 mol) and then increases logarithmically over the last two molar values of Gly (i.e., 0.27 and 0.32 mol). This means that there is a positive correlation visible between the applied parameter (i.e. the molar quantity of Gly) and the measured property (i.e. PDI) which allows for some kind of control over the distribution of particles. Further detail on number and intensity of particle sizes in different size classes is presented in Figure 32 and Figure 33 respectively.

Another important parameter under investigation was the surface charge or ZP of CDs over the above-mentioned Gly molar quantities as displayed in Figure 31(c). The ZP values, or surfaces, of plain/unfunctionalised CDs became more positive from −0.737 mV to +10.3 mV as the number of moles of Gly was increased. Here it can once again be seen that the smaller and more monodispersed the particles are, the more negative the zeta potential as seen in previous studies (Bandi *et al* 2020). There is a clear correlation between the molar quantity of Gly and the surface charge of the synthesised CDs which shows that the ZP can be tailored according to desire. Therefore, only a small amount of Gly is necessary to obtain small-sized particles of great colloidal stability.

Compared to previous studies, i.e. power and reaction-time optimisation studies, characteristics or properties of unfunctionalised CDs could not be controlled carefully by varying the parameters. However, variation in the molar quantity study of Gly allowed better control over the particle dispersity indexes and surface charges of CDs. Furthermore, the size distributions of unfunctionalised CDs are displayed over the above-mentioned range of Gly molar quantities expressed according to number (Figure 32) and intensity (Figure 33) of particles as determined with a Malvern Zetasizer Nano ZS90 (Malvern Instruments Ltd. 2004). The objective was to examine the size distribution of particles by determining the relative number (%) of particles found in each size range which is essential in understanding physical and chemical properties of CDs synthesised with different molar quantities of Gly.

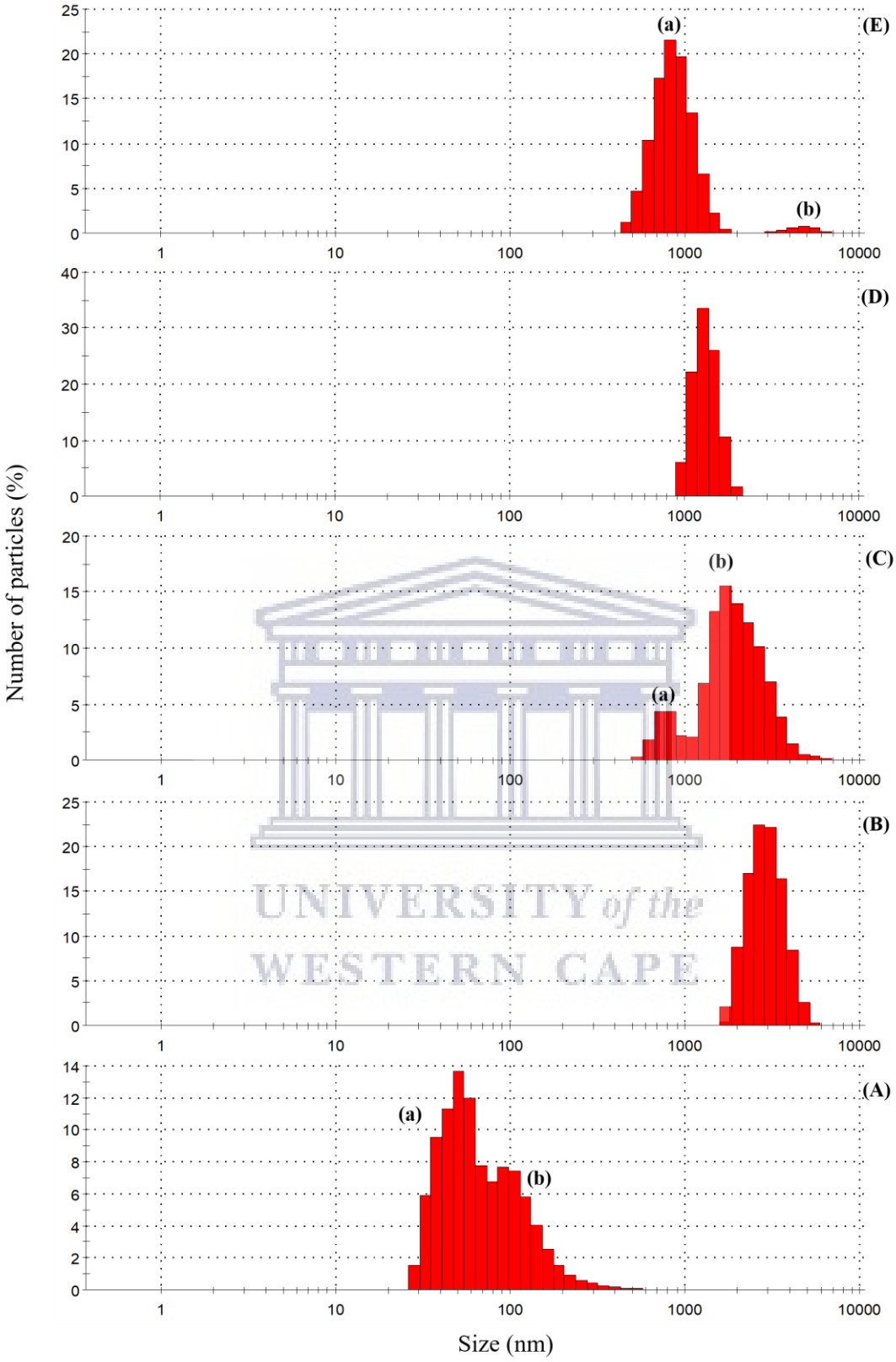

Figure 32. Particle size distribution of plain CDs by number of particles present in each size class for (A) G_Opt_A11 (0.14 mol Gly), (B) G_Opt_A12 (0.18 mol Gly), (C) G_Opt_A13 (0.23 mol Gly), (D) G_Opt_A14 (0.27 mol Gly), and (E) G_Opt_A15 (0.32 mol Gly).

The histograms in Figure 32 above show the relative percentage of particles in each size class (logarithmically spaced) based on the intensity of light scattered as a function of the particle size distribution of unfunctionalised CDs. The percentage distribution is as follows: (A) G_Opt_A11 (0.14 mol Gly) in which there are two clusters of particles of the following size classes, namely (a) 28.21 to 68.06 nm (61.6 % of particles) with a 13.6 % maximum at 50.75 nm, and (b) 78.82 to 458.7 nm (38.4 % of particles) with a 7.6 % maximum at 91.28 nm; (B) G_Opt_A12 (0.18 mol Gly) in which there is one cluster of particles of the following size classes from 1718 to 5560 nm with a 22.4 % maximum at 2669 nm; (C) G_Opt_A13 (0.23 mol Gly) in which there are two clusters of particles of the following size classes, namely (a) 531.2 to 1106 nm (14.8 % of particles) with a 4.4 % maximum at 825 nm, and (b) 1281 to 6439 nm (85.2 % of particles) with a 15.5 % maximum at 1718 nm; (D) G_Opt_A14 (0.27 mol Gly) in which there is one cluster of particles of the following size classes from 955.4 to 1990 nm with a 33.5 % maximum at 1281 nm; (E) G_Opt_A15 (0.32 mol Gly) in which there are two clusters of particles of the following size classes, namely (a) 458.7 to 1718 nm (93.9 % of particles) with a 21.6 % maximum at 825 nm, and (b) 2669 to 6439 nm (6.1 % of particles) with a 0.7 % maximum at 4801 nm.

A large percentage of particles are of larger size classes as is the case with G_Opt_A12 to G_Opt_A15 with the lowest sizes of about 500 nm to largest of 6.5 µm. For the lowest ratio of Gly to NaH_2PO_4 (i.e. 6:1) 61.6 % of particles had sizes ranging from 28.21 to 68.06 nm that were in the nano-range, whereas larger molar quantities of Gly yielded particle sizes that were far greater in size than the upper limit of the nano-range of 100 nm. However, for larger molar values of Gly, 0.23 to 0.32 mol, a small amount of the particles was sized below the upper limit for colloidal particles of 1000 nm, with the greatest % of particles being larger in size. According to Hunter, if the particle solubility is low, equilibrium might never be established and a quasi-equilibrium would exist causing the co-existence of a variety of particle sizes (Hunter 1987). Out of all five molar quantities of Gly, 0.14 mol showed the best particle dispersity with the smallest sizes which correlates with its low PDI in Figure 31(b).

In Figure 33 below, the relative percentage of particles in each size class based on the intensity of light scattered is plotted as a function of the particle size distribution according to logarithmically spaced size classes, as obtained by the Malvern Zetasizer Nano ZS90.

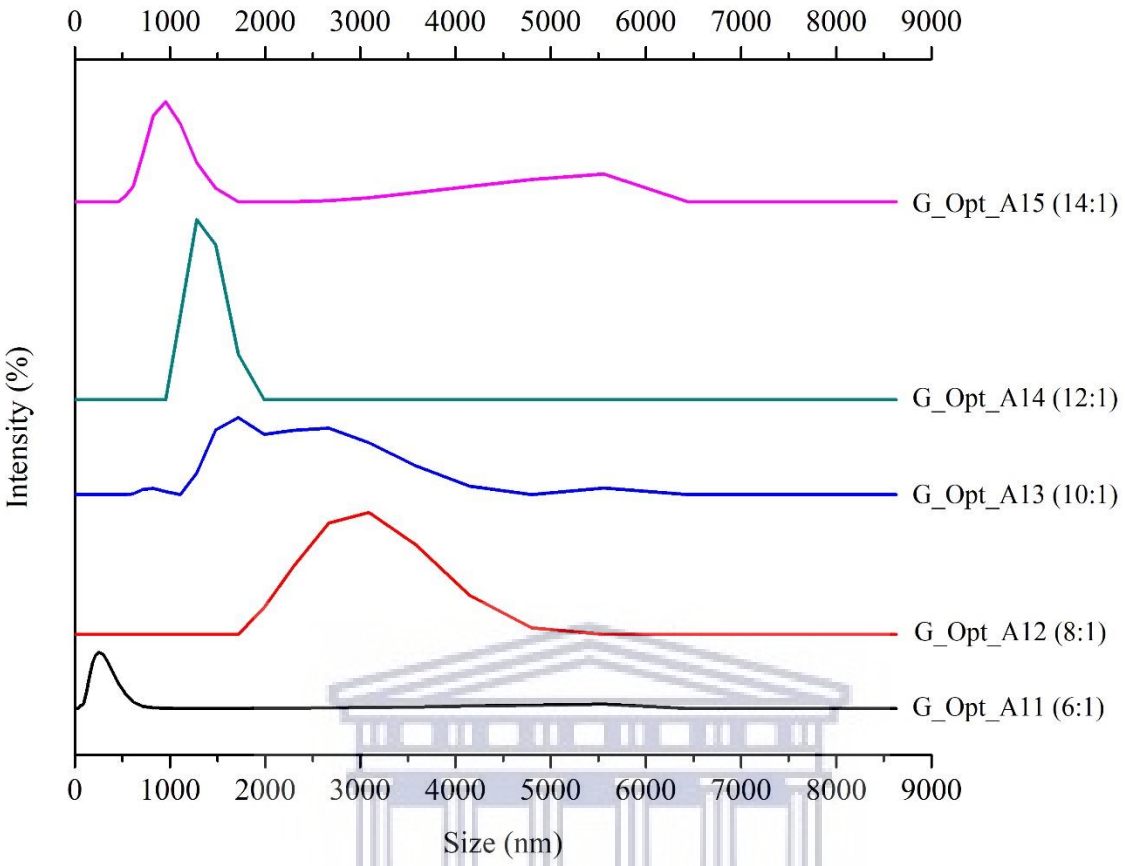

Figure 33. The particle size distribution of unfunctionalised CDs by intensity with varied molar values of glycerol.

In Figure 33, the size distributions of CDs are displayed over the above-mentioned range of molar ratios of Gly to NaH_2PO_4 and are expressed by the intensity of scattered light. Notice that the majority of particles for all samples were sized above the upper limit for colloidal suspensions (i.e. 1000 nm), while G_Opt_A11 prepared with the smallest molar ratio of Gly to NaH_2PO_4 of 6:1 presented samples of sizes below 500 nm. G_Opt_A11 proved to be the sample with the greatest degree of monodispersity towards small particle sizes and shows the greatest stability which is not expected. It is expected that intermediate values of the molar quantity of Gly would yield the most stable particles as more of the carbon source should lead to more effective collisions which at some point, i.e. at a higher molar quantity of Gly, would be excessive and result in agglomeration and later rapid agglomeration. Ideally, CDs of small sizes, low PDI, most negative ZP, a greater degree of monodispersity, and narrow size distribution towards smaller sizes is desired. The fact that agglomeration occurred from the sample prepared with 0.18 mol of Gly shows that little of the reagent is required for successful production of CDs.

4.1.3.3. Summary

According to literature, an increase in the number of moles of 70 % (w/w) Gly in the synthesis of unfunctionalised CDs significantly affects the burn-off percentage, carbonisation, band gap energy, absorption intensity, and emission intensity (Sutanto *et al* 2020). CDs proved to be very sensitive to variation in Gly molar quantity. As the ratio of 70 % (w/w) Glycerol to 20 % (w/w) NaH_2PO_4 increased from 6:1 to 14:1, several parameters were affected, such as (a) the % yield which increased linearly, (b) the colour of the suspension of CDs that lightened, (c) the absorbance which decreased and λ_{max} that underwent a blue shift towards shorter wavelengths, (d) the hydrodynamic diameter which was smallest for G_Opt_A11 prepared with 0.14 mol of Gly, (e) the ZP became more positive from −0.737 mV to +10.3 mV, and (f) the overall size distribution of particles was very broad with most particles above the upper limit for colloidal suspensions of 1000 nm. Increasing the number of moles of Gly (i.e. the carbon source) in the reaction, affected the overall rate of the reaction as more carbon was available for carbonisation of hydrocarbon into the graphitic structure, hence the increase in % yield. Albeit agglomeration occurred, the size distribution of particles prepared with the smallest molar ratio of 6:1 was shifted towards smaller size classes, while CDs prepared with higher molar values of Gly were less stable. Even though the lowest molar ratio of 6:1 for Gly to NaH_2PO_4 showed a better size distribution, the hydrodynamic size was smallest which correlated to the most negative ZP; the % yield was greatest at the largest molar ratio of 14:1. Therefore, the best course of action was to proceed with the molar ratio used in literature of 10:1 (Bayati *et al* 2018) along with better purification procedures put in place such as centrifugation.

4.1.4. Molar optimisation of (20 % w/w) sodium dihydrogen phosphate for the synthesis of plain CDs

In this section, the results on the influence of the molar quantity of sodium dihydrogen phosphate (NaH_2PO_4) on the colloidal stability of unfunctionalised CDs are discussed and the samples were prepared according to the experimental procedure described in Section 3.3.4. CDs were prepared with the following molar ratios of 70 % (w/w) Gly to 20 % NaH_2PO_4, namely: 10:0.5, 10:1, 10:2, 10:3, and 10:4. These five samples, of increasing number of moles of NaH_2PO_4, i.e. 2.6×10^{-3}, 5.1×10^{-3}, 1.02×10^{-2}, 1.53×10^{-2}, and 2.04×10^{-2} mol (molar calculations presented in Appendix), were labelled N_Opt_A16, N_Opt_A17, N_Opt_A18, N_Opt_A19, and N_Opt_A20, respectively. They were analysed to determine the ideal molar quantity of NaH_2PO_4 for effective synthesis of unfunctionalised CDs. The following parameters remained fixed: (a) the concentration (20 % w/w = 1.7 mol.L^{-1}) of NaH_2PO_4, (b) the concentration (70 % w/w = 7.6 mol.L^{-1}) and molar quantity (0.23 mol) of Gly, (c) the synthesis power (720 W), and (d) the reaction time (14 minutes) (Wang *et al* 2011a). The aim was to investigate the effect of the molar quantity of NaH_2PO_4 on (a) the % yield (expressed in Table 34 in Appendix), (b) the interaction of light with the CDs through UV-Vis, and (c) the hydrodynamic diameter, polydispersity index, and the surface charge. Table 34 (in Appendix) and Figure 34 below presents the % yield (calculated in Table 34) of the five samples prepared with increasing molar quantities of NaH_2PO_4.

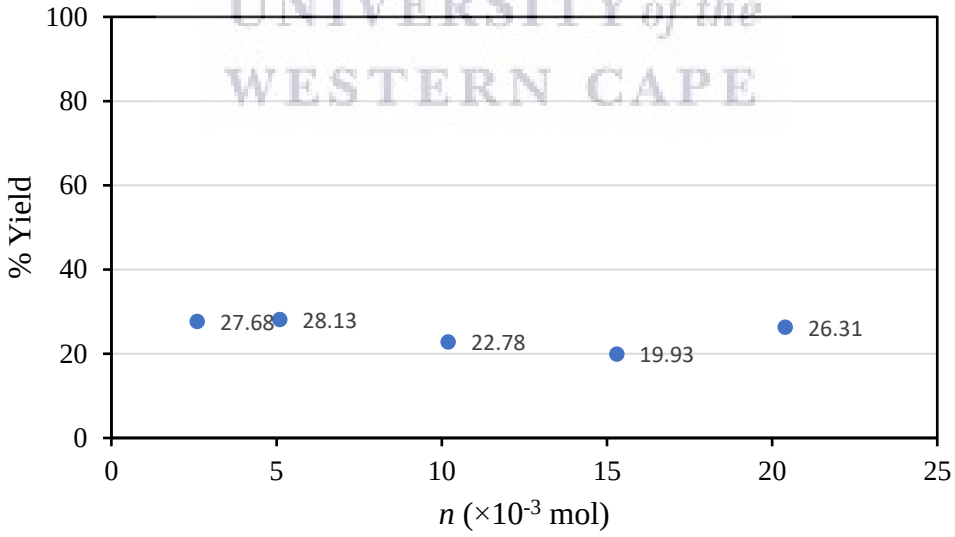

Figure 34. % Yield of unfunctionalised CDs for the molar optimisation study of NaH_2PO_4 (720 W; 14 minutes).

According to the results in Figure 34 above, there was a slight overall decrease in the % yield with an increase in the molar ratio of Gly to NaH_2PO_4 from 10:0.5 to 10:4. As the number of moles of NaH_2PO_4 increased from 2.6×10^{-3} to 5.1×10^{-3} mol, the % yield of CDs produced increased initially from 27.7 % to 28.1 %, then decreased to 20% for the sample of 1.53×10^{-2} mol of NaH_2PO_4, and lastly, increased to 26.3 % for the sample of 2.04×10^{-2} mol of NaH_2PO_4. As previously mentioned, an increase in the number of moles of a reagent leads to an increase in the number of collisions amongst reactant molecules (Bewick *et al* 2019). Therefore, increasing the number of moles of NaH_2PO_4 in the reaction affects the overall rate of the reaction as more phosphate (PO_4^{3-}) ions are available for carbonisation of hydrocarbon into the graphitic structure. According to Wang and co-workers, inorganic ions have the ability to aid in the carbonisation process by accelerating it (Wang *et al* 2011a). There were only small changes in % yield and all values are between 20 and 30 %, and could be because of the small variations in the molar quantity of NaH_2PO_4.

See the effect of an increase in the molar quantity of NaH_2PO_4 on the colour of the product as illustrated in Figure 35 below; initially there is a gradual lightening in the brown colour of CDs as the molar ratio of Gly to NaH_2PO_4 is increased from 10:0.5 to 10:2, which is followed by a deepening in the colour intensity as the number of moles of NaH_2PO_4 was doubled from 1.02×10^{-2} to 2.04×10^{-2} mol. At the lowest and highest molar quantity of 2.6×10^{-3} mol and 2.04×10^{-2} mol, respectively, the brown colour appears to be much deeper than the volumes that lie in between.

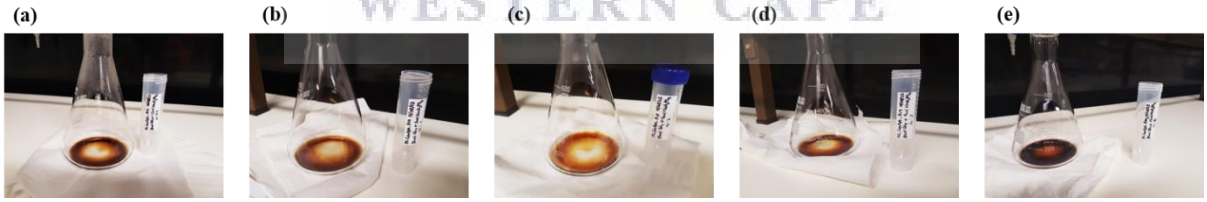

Figure 35. Molar optimisation of 20 % (w/w) NaH_2PO_4 for the synthesis of CDs; (a) 10:0.5 (2.6×10^{-3} mol), (b) 10:1 (5.1×10^{-3} mol), (c) 10:2 (1.02×10^{-2} mol), (d) 10:3 (1.53×10^{-2} mol), and (e) 10:4 (2.04×10^{-2} mol) (720 W; 14 minutes).

4.1.4.1. Absorbance study through ultraviolet-visible spectroscopy

The absorbance of unfunctionalised CDs was analysed using UV-Vis spectroscopy (as described in Section 3.8.1) to qualitatively determine whether unfunctionalised CDs were produced and to understand the effect of a variation in the molar quantity of 20 % (w/w) NaH_2PO_4 on the absorbance of unfunctionalised CDs. The above-mentioned five samples, for the molar optimisation study of NaH_2PO_4, were studied. The absorbance data, i.e., the maximum absorption peaks with their respective absorbances are tabulated in Table 9 below and the absorbance spectra are shown in Figure 36.

Table 9. The absorbance values for the molar optimisation study of 20 % NaH_2PO_4 in the synthesis of CDs according to their wavelengths (prepared at 720 W in 14 minutes).

Sample code	***λ_{max} (nm)***	***Absorbance (A)***
N_Opt_A16	260	0.195
N_Opt_A17	261	0.166
N_Opt_A18	263	0.117
N_Opt_A19	261	0.208
N_Opt_A20	260	0.236

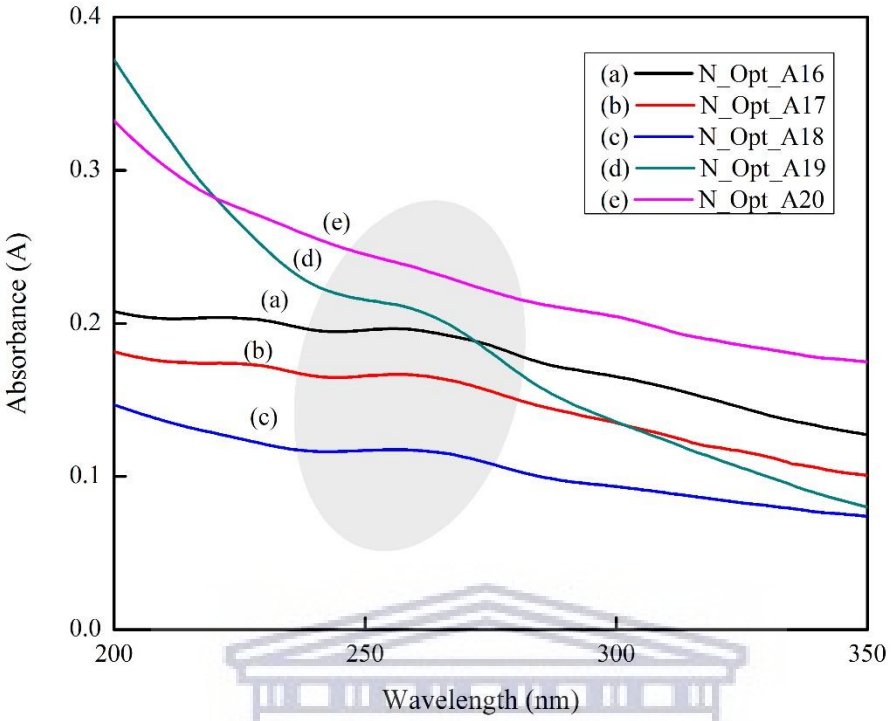

Figure 36. Ultraviolet-visible spectra for plain carbon dots (CDs) synthesised at 720 W for 14 minutes for a number of 20 % w/w NaH_2PO_4 molar quantities, namely (a) 2.6×10^{-3} mol (N_Opt_A16), (b) 5.1×10^{-3} mol (N_Opt_A17), (c) 1.02×10^{-2} mol (N_Opt_A18), (d) 1.53×10^{-2} mol (N_Opt_A19), (e) 2.04×10^{-2} mol (N_Opt_A20).

In Figure 36, the optical absorption peak is visible between 220 nm and 270 nm, which is in agreement with the peak observed for CDs in previous studies (Ismail *et al* 2020, Sutanto *et al* 2020, De and Karak 2013, Joseph and Anappara 2016, Zhou *et al* 2007). As the number of moles of 20 % w/w NaH_2PO_4 was increased from 2.6×10^{-3} to 1.02×10^{-2} mol, a hypochromic effect (i.e. a decrease in absorbance intensity) from 0.195 to 0.117 as tabulated in Table 9 is observed and is typically caused by distortions in the geometry of a molecule induced by a functional group (Rouessac and Rouessac 2000); followed by a hyperchromic effect, i.e., an increase in absorbance intensity to 0.236. Furthermore, there is a slight bathochromic effect (i.e., a red shift) in the absorption band of CDs from 260 to 263 nm that occurred as the molar quantity of NaH_2PO_4 was increased from 2.6×10^{-3} to 1.02×10^{-2} mol, which is best described by the phenomenon mentioned in Section 4.1.1.2 and that can be correlated to the increase in size observed in Figure 37(a). Wang and co-workers also reported on a bathochromic shift in the absorption band of CDs with an increase in phosphate salt and mentioned that multivalent ions such as the trivalent ion, PO_4^{3-}, have greater catalysing abilities than mono- and di-valent

ions (Wang *et al* 2011a). Moreover, a hypsochromic effect (i.e., a blue-shift) in the absorption band of CDs from 263 to 260 nm that occurred as the number of moles of NaH_2PO_4 was increased from 1.02×10^{-2} to 2.04×10^{-2} mol. This could once again be ascribed to the greater energy demand by the $n \rightarrow \pi^*$ electronic transition, hence the shift of the absorption peak maximum towards shorter wavelengths due to the stabilisation by C^+-O^- polarisation through clustering of polar solvent molecules (Rouessac and Rouessac 2000). Also, as previously mentioned, a blue-shift is a desired result typically of quantum confinement (i.e., a decrease in particle size) leading to a larger band gap energy, and, in turn, a shift of the absorbance maximum towards shorter-wavelengths. Therefore, the blue-shift correlates with the decrease in size observed in Figure 37(a).

4.1.4.2. Hydrodynamic properties – Zetasizer

The above-mentioned unfunctionalised CDs, prepared according to the method described in Section 3.3.4, were characterised by the Malvern Zetasizer Nano ZS90 to obtain size measurements through Dynamic Light Scattering (DLS) and zeta potential measurements through Laser Doppler Velocimetry (LDV), in determining the ideal molar ratio of Gly to NaH_2PO_4 (see Section 3.8.2 for experimental procedure). The hydrodynamic properties of CDs were studied to understand the effect of the molar quantity of NaH_2PO_4 on the average hydrodynamic diameter (D_h/Z-Ave), particle dispersity index (PDI), and zeta-potential (ZP) of unfunctionalised CDs as tabulated in Table 10. The D_h, PDI, and ZP are plotted as functions of the number of moles of NaH_2PO_4 in Figure 37 below.

Table 10. Hydrodynamic diameter, particle dispersity, and zeta potential of unfunctionalised CDs prepared at 720 W for 14 minutes for the molar optimisation study of NaH_2PO_4.

Sample code	***Z-Ave (nm)***	***PDI***	***ZP (mV)***
N_Opt_A16	2478	0.340	−6.38
N_Opt_A17	2496	0.300	−8.94
N_Opt_A18	2943	0.318	−23.3
N_Opt_A19	2981	1	−24.0
N_Opt_A20	2523	0.325	−32.3

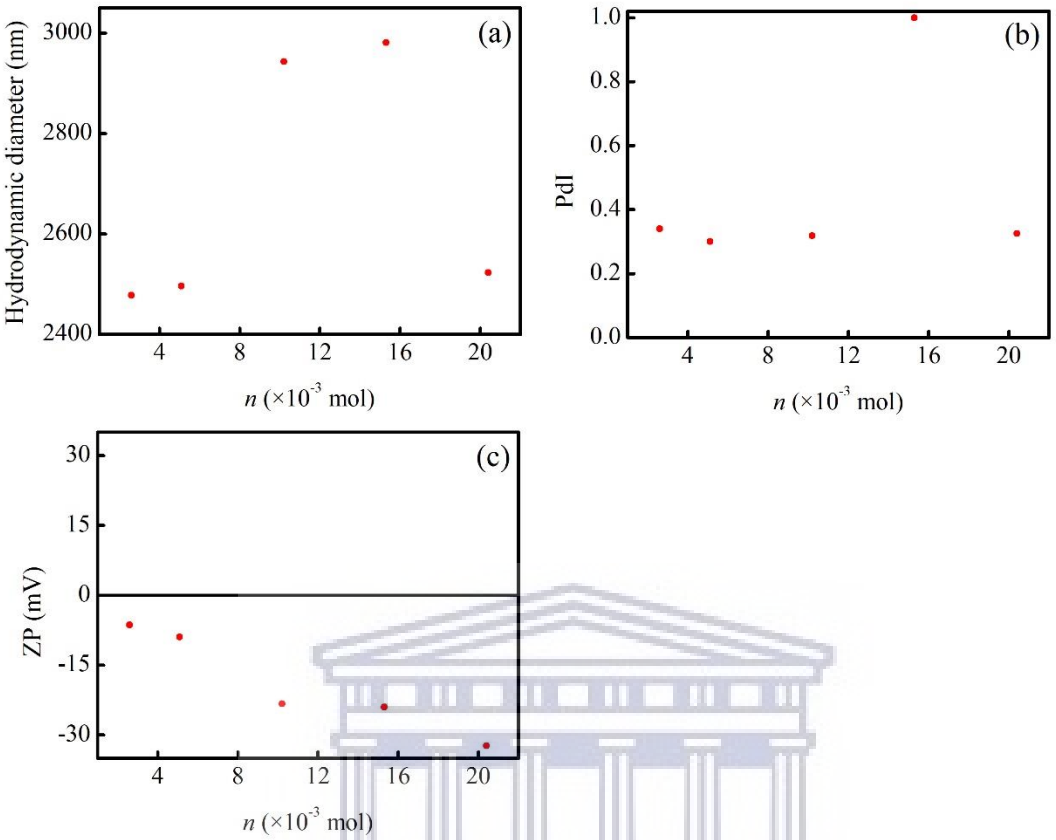

Figure 37. (a) Hydrodynamic diameter, (b) polydispersity index and (c) zeta potential over a range of 20 % w/w NaH_2PO_4 molar quantities (2.6×10^{-3} to 2.04×10^{-2} mol) for synthesis of unfunctionalised CDs.

The first parameter under investigation was the hydrodynamic diameter. In Figure 37(a), there is an overall increase in the hydrodynamic diameter of CDs as the number of moles of NaH_2PO_4 was increased from 2.6×10^{-3} to 2.04×10^{-2} mol. Initially, there is a minor increase in D_h of CDs from 2478 nm for N_Opt_A16 to 2496 nm for N_Opt_A17; then there is a sharp increase to 2943 nm for N_Opt_A18, which is followed by a slight increase to 2981 nm for N_Opt_A19, and lastly, decreases to 2523 nm for N_Opt_A20. This displays the sensitivity of CDs to variation in molar quantity of NaH_2PO_4. Correlating the hydrodynamic sizes to the % yields found in Figure 34 and the difference in colour seen in Figure 35, the D_h is smaller for samples of larger % yield and the colour a more intense brown, which is the case for the samples prepared with the lowest and highest number of moles of 20 % (w/w) NaH_2PO_4. Overall, the particle sizes are much larger than the upper limit for colloidal particles and have thus undergone agglomeration. The very large particle sizes could be attributed to the formation of clusters of particles in order to obtain stability by lowering the surface energy (Filipponi and

Sutherland 2012). As previously discussed, an increase in reagent molecules leads to an increase in the number of collisions and a lowering in the repulsion barrier between approaching particles, resulting in permanent particle-particle contact (Hunter 1987). The instability of these particles caused rapid agglomeration to occur in which each particle-particle contact is effective and flocs of particles form. Compared to the previously applied parameters, the increase in the number of moles of NaH_2PO_4 led to significantly large particles throughout whereas some of the previous parameters presented particles of either the intermediate size (i.e., between 100 and 1000 nm in size) or within the nano-range.

The second parameter under investigation was the polydispersity index (PDI) of CDs over the above-mentioned NaH_2PO_4 molar quantities as displayed in Figure 37(b). The PDI values obtained for unfunctionalised CDs displayed narrow size distributions for all samples as their PDI values were below 0.5, with the exception of N_Opt_A19 prepared with 1.53×10^{-2} mol of NaH_2PO_4 which had a larger PDI and, hence, a wider size distribution. Further detail on number and intensity of particle sizes in different size classes is presented in Figure 38 and Figure 39, respectively.

The third parameter under investigation was the surface charge or ZP of CDs over the above-mentioned NaH_2PO_4 molar quantities as displayed in Figure 37(c). The ZP values of unfunctionalised CDs became more negative from −6.38 to −32.3 mV as the number of moles of NaH_2PO_4 was increased, which opposes the trend found with an increase in the molar values of Gly. Typically, negative ZP values correlate to smaller particle sizes of CDs. However, there is no clear trend observed for the sizes of CDs as the lowest and highest molar quantities of NaH_2PO_4 yielded smaller (yet still too large) particles. Gly showed better control over particle properties than NaH_2PO_4.

Furthermore, the size distributions of CDs are displayed over the above-mentioned range of NaH_2PO_4 molar quantities expressed according to number (Figure 38) and intensity (Figure 39) of particles as determined with a Malvern Zetasizer Nano ZS90 (Malvern Instruments Ltd. 2004). The objective was to examine the size distribution of particles by determining the relative number (%) of particles found in each size range which is essential in understanding physical and chemical properties of CDs synthesised with different molar quantities of NaH_2PO_4.

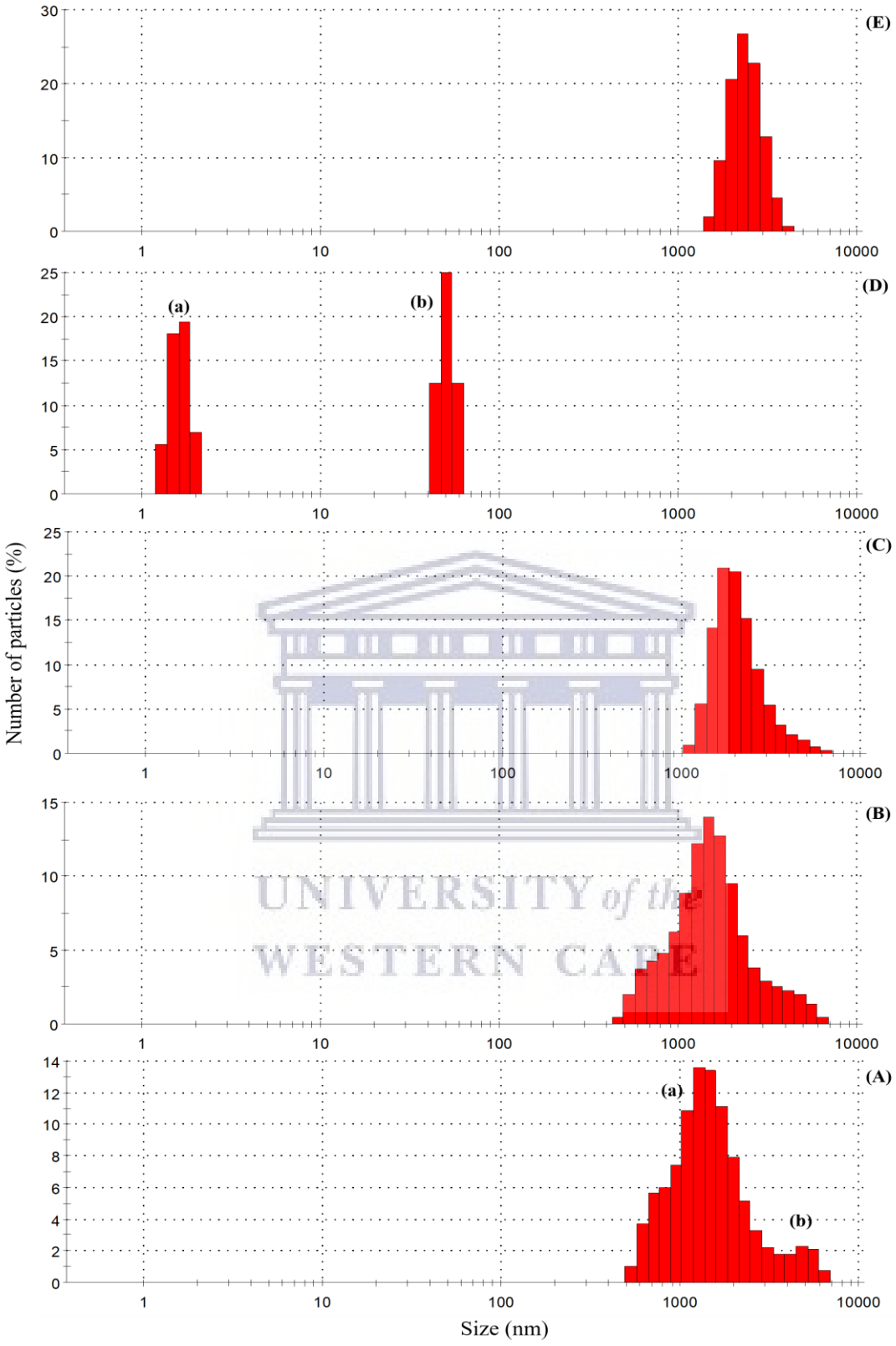

Figure 38. Particle size distribution of unfunctionalised CDs with the numbers of particles present in each size class for (A) N_Opt_A16 (2.6×10^{-3} mol), (B) N_Opt_A17 (5.1×10^{-3} mol), (C) N_Opt_A18 (1.02×10^{-2} mol), (D) N_Opt_A19 (1.53×10^{-2} mol), and (E) N_Opt_A20 (2.04×10^{-2} mol).

The histograms in Figure 38 above, show the relative percentage of particles in each size class (logarithmically spaced) based on the intensity of light scattered as a function of the particle size distribution of unfunctionalised CDs. The percentage distribution is as follows: (A) N_Opt_A16 (2.6×10^{-3} mol) in which there are two clusters of particles of the following size classes, namely (a) 531.2 to 3580 nm (93 % of particles) with a 13.6 % maximum at 1281 nm, and (b) 4145 to 6439 nm (7 % of particles) with a 2.3 % maximum at 4801 nm; (B) N_Opt_A17 (5.1×10^{-3} mol) in which there is one cluster of particles of the following size classes from 458.7 to 6439 nm with a 14 % maximum at 1484 nm; (C) N_Opt_A18 (1.02×10^{-2} mol) in which there is one cluster of particles of the following size classes from 1106 to 6439 nm with a 20.9 % maximum at 1718 nm; (D) N_Opt_A19 (1.53×10^{-2} mol) in which there are two clusters of particles of the following size classes, namely (a) 1.294 to 2.01 nm (50 % of particles) with a 19.5 % maximum at 1.736 nm, and (b) 43.82 to 58.77 nm (50 % of particles) with a 25 % maximum at 50.75 nm; and (E) N_Opt_A20 (2.04×10^{-2} mol) in which there is one cluster of particles of the following size classes from 1484 to 4145 nm with a 26.8 % maximum at 2305 nm.

A large percentage of particles are of larger size classes as is the case with all samples, apart from N_Opt_A19, with the sizes ranging from about 450 nm to 6.4 μm. For the two lowest ratios of Gly to NaH_2PO_4 (i.e., 10:0.5 and 10:1), a small % of particles had sizes that were below the upper limit for colloidal particles of 1000 nm, whereas larger molar quantities of NaH_2PO_4, i.e., N_Opt_A18 and N_Opt_A20, yielded particle sizes that were larger in size than the upper limit for colloidal particles. On the other hand, N_Opt_A19 showed particle sizes that were in the nano-range as one half of particles were between 1.294 to 2.01 nm and the other were from 43.82 to 58.77 nm in size. Once again, these large particle sizes could be due to the existence of a quasi-equilibrium which causes a variety of particle sizes to co-exist (Hunter 1987) and due to agglomeration that occurred. In terms of control and tailoring CDs with desired properties, the use of NaH_2PO_4 is not as promising. However, a better control might be established if the number of moles of NaH_2PO_4 is increased.

In Figure 39 below, the relative percentage of particles in each size class based on the intensity of light scattered is plotted as a function of the particle size distribution according to logarithmically spaced size classes, as obtained by the Malvern Zetasizer Nano ZS90.

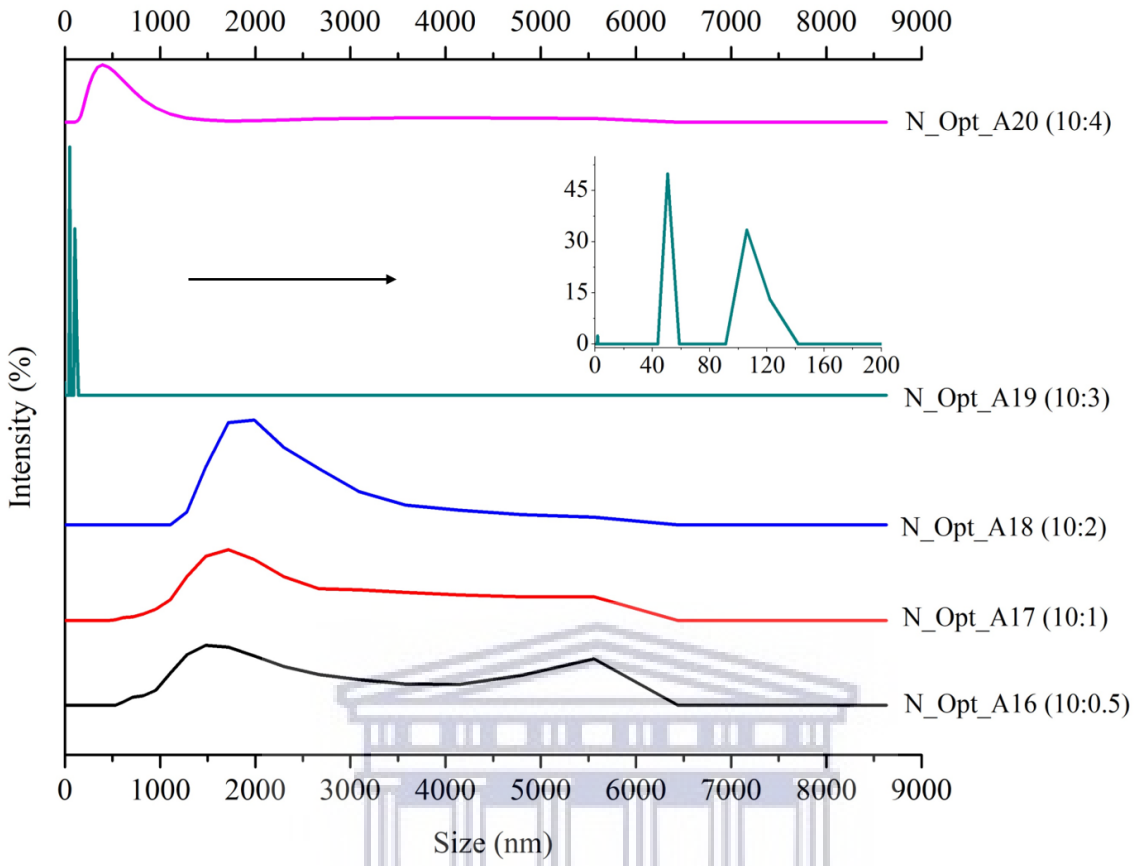

Figure 39. The particle size distribution of plain CDs by intensity with varied molar values of NaH_2PO_4.

In Figure 39, the size distributions of CDs are displayed over the above-mentioned range of molar quantities of NaH_2PO_4 and are expressed by intensity of scattered light. Notice that the majority of particles were sized above the upper limit for colloidal suspensions (i.e., 1000 nm), while N_Opt_A19 and N_Opt_A20 prepared with the largest molar ratios of Gly to NaH_2PO_4 of 10:3 and 10:4 presented samples of sizes below 500 nm. Furthermore, N_Opt_A19 presented particles of sizes as small as 50 nm.

4.1.4.3. Summary

An increase in the number of moles of 20 % (w/w) NaH_2PO_4 in the synthesis of unfunctionalised CDs significantly affects the burn-off percentage, carbonisation, band gap energy, absorption intensity, and emission intensity (Sutanto *et al* 2020). CDs proved to be slightly sensitive to variation in NaH_2PO_4 molar quantity which could be due to the small incremental changes in the number of moles of NaH_2PO_4. As the ratio of 70 % (w/w) Glycerol to 20 % (w/w) NaH_2PO_4 increased from 10:0.5 to 10:4, several parameters were affected, such as (a) the % yield which was lower for molar values between 2.6×10^{-3} to 2.04×10^{-2} mol, (b) the colour of the suspension of CDs that was darker for lower and higher ratios of Gly to NaH_2PO_4 reported in literature (Bayati *et al* 2018), (c) the absorbance which initially decreased and then increased for higher molar values of NaH_2PO_4 and λ_{max} that underwent a blue shift towards shorter wavelengths, (d) the hydrodynamic diameter which was small for N_Opt_A16, N_Opt_A17 and N_Opt_A20, (e) the ZP became more negative, and (f) the overall size distribution of particles which were rather narrow but with most particles well above the upper limit for colloidal suspensions (1000 nm). As previously mentioned, increasing the number of moles of NaH_2PO_4 in the reaction affects the overall rate of the reaction because there is more of the inorganic phosphate salt which acts to catalyse the process of carbonisation of hydrocarbon into the graphitic structure. Albeit agglomeration occurred in four of the five samples, the size distribution of particles prepared with the molar ratio of 10:3 was shifted towards smaller size classes, while CDs prepared with lower molar values of Gly were less stable. Even though the larger molar ratio of 10:3 for Gly to NaH_2PO_4 showed a better size distribution of smaller particle sizes, the decision was to proceed with the molar ratio used in literature of 10 :1 (Bayati *et al* 2018) which had the lowest polydispersity index and paired with better purification procedures such as centrifugation, smaller CDs could be produced of desired properties.

4.1.5. Comparative summary of applied parameters in synthesis of CDs

To compare the effect of each applied parameter on the characteristics of unfunctionalised CDs, the following table provides a detailed description of trends observed or the lack thereof. Table 11 serves to compare eight crucial characteristics that were studied with each applied synthesis parameter, i.e., % yield, colour of product, mass of dialysis bag, absorbance, hydrodynamic diameter, polydispersity index, surface charge, and size distribution by number and intensity.

Table 11. Comparative characteristics of unfunctionalised CDs.

Product characteristic	***Power study***	***Reaction-time study***	***Molar quantity study of 70 % w/w of Gly***	***Molar quantity study of 20 % w/w of NaH_2PO_4***
% Yield	Negative correlation Decreased from 96.62 % at 90 W to 4.34 % at 900 W	Negative correlation Decreased from 32.41 % to 2.76 % as RT increased from 5 to 25 minutes	Positive correlation Increased from 10.33 % to 30.05 % with increase in molar quantity of Gly	No trend and no sensitivity All values between 19–30 %
Colour of product	Intensified from transparent to dark brown	Intensified from light brown to dark brown	Lightening in colour of solution from dark brown to light brown	More intense for lowest and highest ratios of 10:0.5 and 10:4 of Gly to NaH_2PO_4 Most desired colour at intermediate molar ratios
Mass of dialysis bag	Initial increase due to osmotic flow into dialysis bag Constant mass reached after 30 hours	Initial increase due to osmotic flow into dialysis bag Constant mass reached after 40 hours	Initial increase due to osmotic flow into dialysis bag Constant mass reached after about 35 hours	Initial increase due to osmotic flow into dialysis bag then gradual decrease in mass Constant mass reached after about 50 hours
Absorbance & λ_{max}	Hyperchromic effect from 0.013 to 0.549 Red-shift (232 to 263 nm)	Hyperchromic effect from 0.011 to 1.566 Red-shift (260 to 265 nm)	Hypochromic effect from 1.35 to 0.0898 Blue-shift (261 to 258 nm)	Hypochromic effect from 0.195 to 0.117 accompanied by a red-shift (260 to 263 nm) for

				lower ratios of Gly to NaH_2PO_4 from 10:0.5 to 10:2 Hyperchromic effect to 0.236 accompanied by a blue-shift to 260 nm for largest ratio of Gly to NaH_2PO_4 of 10:4
D_h	Larger (above 1000 nm) for intermediate power levels Smallest at 900 W (597.6 nm) and 90 W (869.1 nm)	Very large particle size of 1055 nm for 5-min sample others sized between 200–400 nm with the smallest size of 223.6 nm for sample prepared in 20 minutes; followed by a D_h of 296 nm for 15-min sample	Smallest for lowest molar quantity of Gly with D_h of 231.7 nm Very large for intermediate number of moles (between 2900–3300 nm) and slightly smaller (still large; 1939 nm) for largest number of moles of Gly	Very large sizes recorded overall that ranged from 2478 to 2981 nm in no particular trend
PDI	Highly polydisperse and wide size distributions PDI values ranging between 0.7 and 0.94 No clear effect/trend	No particular trend Intermediate particle dispersity with more narrow size distributions PDI values between 0.2 and 0.5 with lowest PDI of 0.245 for 15-min sample greatest degree of monodispersity, and with the exception of large PDI of	More monodisperse for smaller number of moles of Gly PDIs increase from 0.243 to 0.595 Polydispersity increases as the number of moles of Gly increased	No particular trend Intermediate particle dispersity with more narrow size distributions and PDI values ranging between 0.3 and 0.34 With the exception of a very large PDI for 10:3 ratio of Gly to NaH_2PO_4

		0.818 for 5-min sample		
ZP	More positive for lower power levels Most negative for 720 W and 900 W with ZPs of −8.86 mV and −17 mV, respectively Most positive value of +8.12 mV for 450-W sample	Became more negative from −15.6 mV to the most negative of −33.6 mV for sample prepared in 20 minutes	Became more positive (from −0.737 mV to +10.3 mV) as number of moles of Gly increased	Became more negative from −6.38 mV to −32.3 mV as number of moles of NaH_2PO_4 increased
Size distribution by number & intensity	Very wide size distribution overall <u>By number</u> Sized within nano-range for 90 and 270 W Intermediate size distributions for 450 and 900 W samples and Uniform large sizes (above 1000 nm) for 720 W and a small % of particles for 270 and 450 W samples <u>By intensity</u> Large extent of polydispersity with some indication of small particles for 900-W sample with the best results and highest degree of monodispersity	Majority of intermediate size distribution between 100–1000 nm <u>By number</u> Only 20-min sample sized wholly within nano-range with some of 10-min sample sized just under upper limit of nano-range Intermediate size distributions (100–1000 nm) for samples prepared within 5, 10, 15, and 25 minutes <u>By intensity</u> Greater degree of monodispersity with majority of particles sized below upper limit for colloidal suspensions (i.e., 1000 nm)	Very wide size distributions overall <u>By number</u> Majority sized above upper limit of 1000 nm for colloidal suspensions Smallest ratio of Gly to NaH_2PO_4 of 6:1 is only sample that had particles that were sized within the nano-range <u>By intensity</u> Large degree of polydispersity Sample with smallest ratio of Gly to NaH_2PO_4 of 6:1 is only sample with narrow size distribution below 500 nm	Very wide size distributions overall <u>By number</u> Majority (10:0.5, 10:1, 10:2, and 10:4) sized above upper limit of 1000 nm for colloidal suspensions 2nd largest ratio of Gly to NaH_2PO_4 of 10:3 is only sample that had particles that were sized within the nano-range Small % of particles for 10:0.5 and 10:1 of intermediate sizes between 100 and 1000 nm <u>By intensity</u> Large degree of polydispersity with the exception of sample with 2nd

				largest ratio of Gly to NaH_2PO_4 of 10:3 is only sample with narrow size distribution within the nano-range And 10:4 sample sized below 1000 nm

As mentioned previously, CDs of small sizes, low PDI, most negative ZP, a greater degree of monodispersity, and narrow size distribution towards smaller sizes is desired. In Table 11, the % yield is affected the most by a change in power as it decreased from 96.62 to 4.34 %. A similar trend is observed for the reaction-time study because a negative correlation is observed, once again. However, the decrease occurred at a smaller gradient from 32.41 to 2.76 %. Given the lower power-levels applied within the power study, the high % yields could be attributed to incomplete conversion of reagent materials into the desired product. CDs typically possess small hydrodynamic diameters. On the other hand, the opposite trend is observed for the molar quantity study of 70 % w/w Gly, in which a positive correlation (i.e., an increase from 10.33 to 30.05 %) is observed between the % yield of CDs and the number of moles of Gly. This is expected due to the larger amount of carbon source available for effective collisions between reagent molecules leading to an increased production of CDs. Lastly, the effect of the molar quantity of NaH_2PO_4 on the % yield of CDs is negligible as CDs showed little sensitivity to an increase in the number of moles of NaH_2PO_4.

When it comes to the colour of the CDs produced, a brown coloured suspension is desired. The colour intensity of CDs intensified from transparent to dark brown as the synthesis power was increased, and from light to dark brown as the duration of the reaction was increased. However, the opposite effect was observed as the number of moles of Gly was increased, in which the colour of the product became lighter from dark brown to light brown. For the molar optimisation study of NaH_2PO_4, the colour was most intense for lowest and highest ratios of Gly:NaH_2PO_4 of 10:0.5 and 10:4 with lighter coloured suspensions at intermediate molar ratios. Overall, the colour intensity of the suspension was fairly sensitive for all applied parameters; however, it was most intense for CDs produced at higher power levels, longer reaction times, smallest number of moles of Gly and largest number of moles of NaH_2PO_4. On the contrary, a high colour intensity does not necessarily translate to the most desired size, yield, surface

charge, etc. Therefore, desired viscosity and colour was achieved at lower power levels, shorter reaction times, and intermediate molar quantities of NaH_2PO_4.

In terms of dialysis, the mass of each dialysis bag was recorded throughout the dialysis process and for all applied parameters each sample bag initially increased in mass due to osmotic flow into the bag from the surrounding solution as previously mentioned. However, notice the delay in reaching a constant mass; ranked in increasing number of hours, a constant mass was reached after 30, 35, 40, and 50 hours for the power study, molar quantity study of Gly, reaction-time study, and molar quantity study of NaH_2PO_4, respectively. A constant mass was reached earlier for the power optimisation study and latest for the molar quantity study of NaH_2PO_4. Therefore, dialysis was most successful for the power study.

The fourth characteristic studied was the effect of each applied parameter on the absorbance of CDs. A hyperchromic effect (i.e., an increase in absorbance) is observed for the power and reaction-time studies, as well as for larger molar quantities of NaH_2PO_4; whereas, a hypochromic effect (i.e., a decrease in absorbance) occurs with an increase in the number of moles of Gly and for small molar quantities of NaH_2PO_4. The reasoning behind an increase in absorbance, as previously discussed, is best explained by the Beer-Lambert law in which absorbance is directly related to the concentration of the substance under study, meaning that the increase in absorbance is induced by an increase in the concentration of CDs. An increase in the duration of the heating process imposed a greater rise in the absorbance of CDs than other applied parameters which means that better control could be achieved with variation in reaction time. Furthermore, a red shift (i.e., a shift in λ_{max} towards longer wavelengths) is observed for the power study, the reaction-time study, and for small molar quantities of NaH_2PO_4, whereas a blue shift (i.e., a shift in λ_{max} towards shorter wavelengths) is observed with an increase in the number of moles of Gly as well as for larger molar quantities of NaH_2PO_4. As previously mentioned, a red-shift is associated with an increase in particle size, hence power variation induced the largest shift and could thus be used to effectively control the size of CDs.

When it comes to the hydrodynamic diameter of CDs, large sizes were observed for each applied parameter. However, the smallest CDs were reported for the reaction-time study in which D_h values reached sizes as small as 223.6 and 296 nm for intermediate reaction times of 20 and 15 minutes, respectively, as well as for the smallest molar quantity of Gly in which CDs had an average size of 231.7 nm. Therefore, conditions under which a small D_h was observed

are for samples prepared within 15–20 minutes at 720 W with the smallest molar quantity of 0.14 mol of Gly. This is reflected in the PDI values in which a greater degree of monodispersity was found for the reaction time study, and the molar quantity studies of both Gly and NaH_2PO_4. The smallest PDIs were for samples prepared within about 15 minutes with a small number of moles of Gly. CDs became more polydisperse with an increase in the molar quantity of Gly and at lower power levels with larger PDI values that exceed 0.5. The polydispersity index was most sensitive to an increase in Gly; the polydispersity increased with the increase in Gly. The smallest D_hs of CDs in increasing order is as follows: (a) 223.6 nm for the sample prepared within 20 minutes in the reaction-time study, (b) 231.7 nm for the sample prepared with 0.14 mol of Gly (lowest molar quantity of Gly) in the Gly study, (c) 597.6 nm for the sample prepared at 900 W in the power study, and (d) 2478 nm for the sample prepared with 2.6×10^{-3} mol of NaH_2PO_4 (lowest molar quantity of NaH_2PO_4) in the NaH_2PO_4 study.

The surface charge of CDs proved to be very sensitive to all applied parameters. As mentioned before, the more negative the ZP the smaller the size of CDs. Hence, the smallest CDs were observed at the most negative ZP values of −17 mV for CDs with average size of 597.6 nm for sample prepared in the power study at 900 W, −33.6 mV for CDs with average size of 223.6 nm for sample prepared within 20 minutes in the reaction-time study, and −0.737 mV for CDs with average size of 231.7 nm prepared with the smallest molar quantity of 0.14 mol of Gly. Therefore, CDs prepared with the smallest amount of Gly of 0.14 mol at a high power such as 900 W in about 20 minutes yielded the smallest CDs. Overall, the reaction time study and molar quantity study of NaH_2PO_4 yielded ZPs that were all negative and that followed the same trend—a negative correlation between the applied parameter and surface charge, whereas more positive values were observed for the molar quantity study of Gly and the power study.

The size distribution of CDs consisted of particles that could be divided into three major size classes, i.e., the nano-range (0–100 nm), intermediate size range (100–1000 nm), and large size range (micro-sized particles or flocs; above upper limit of 1000 nm for colloidal suspensions). The overall size distribution of CDs was very wide for all applied parameters as majority of particles were of intermediate and larger sizes. As tabulated in Table 11, in the power study a large degree of polydispersity was observed in which lower power levels yielded particles that were sized within the nano-range, 450 W and 900 W yielded particles of intermediate sizes, and majority of the 720-W sample consisted of particles larger than the upper limit for colloidal suspensions. In the reaction-time study, a better control over size and a greater degree of monodispersity was observed in which most particles were sized below the upper limit for

colloidal suspensions with the exception of the sample prepared within 20 minutes that yielded CDs of sizes completely within the nano-range, while some of the 10-minute sample contained particles that were sized just below the upper limit of the nano-range. For the molar quantity study of Gly, a large degree of polydispersity and very wide size distributions were observed, wherein the majority of CDs were sized above 1000 nm with the exception of the sample with the lowest number of moles of Gly of 0.14 mol (i.e., the smallest ratio of Gly to NaH_2PO_4 of 6:1) which consisted of some particles sized within the nano-range. Lastly, in the molar quantity study of NaH_2PO_4, a large degree of polydispersity and very wide size distributions were observed in which majority of particles were sized above 1000 nm, CDs of the largest number of moles of NaH_2PO_4 were sized below 1000 nm and all particles of the sample prepared with a 10:3 ratio of Gly:NaH_2PO_4 were sized within the nano-range. The applied parameter which provided the best control over size distribution was the increase in the microwave heating time that yielded all particles of sizes below the upper limit for colloidal suspensions of 1000 nm. The best synthesis conditions for the most monodisperse particles with sizes within the nano-range is CDs synthesised with Gly and NaH_2PO_4 in a 6:1 (the smallest number of moles of Gly of 0.14 mol) or 10:3 ratio at about 720 W within 20 minutes.

4.2. Optimisation of synthesis conditions for amine-capped CDs

In the interest of comparing the effect of synthesis parameters on both unfunctionalised and functionalised CDs, results on the optimisation procedures for the applied synthesis parameters on functionalised (or amine-capped) CDs will be discussed in this section. A similar aim to that of synthesis studies performed on unfunctionalised (or plain) CDs was undertaken in which a search was conducted in determining the optimal synthesis conditions for amine-capped CDs (prepared by the method described in Section 3.5) and effectively examining the colloidal stability of the prepared materials under the aforementioned conditions, i.e., synthesis temperature, reaction duration, molar quantity of citric acid (CA) and molar quantity of branched polyethylenimine (BPEI).

4.2.1. Temperature optimisation for the synthesis of a-CDs

In this section, results for the effect of temperature on the colloidal stability of a-CDs are presented. The samples were prepared according to the experimental procedure described in Section 3.3.5. Five different temperatures were analysed to determine the ideal temperature-setting for effective synthesis of a-CDs; the synthesis temperature was varied as follows: 130 °C, 150 °C, 170 °C, 190 °C and 210 °C. Several other parameters remained fixed, such as the molar quantity of CA (1.1×10^{-2} mol), the molar quantity of BPEI (1.3×10^{-2} mol), and the heating time of the reaction (2 h). The aim was to investigate the effect of synthesis temperature on (a) the % yield (expressed in Table 37 in Appendix), (b) mass of dialysis bags throughout dialysis, (c) the interaction of light with CDs through UV-Vis, and (d) the hydrodynamic diameter, polydispersity index (PDI) and surface charge (i.e., zeta potential). Figure 40 below presents the % yield (as calculated in Table 37) of the five samples prepared at above-mentioned temperatures.

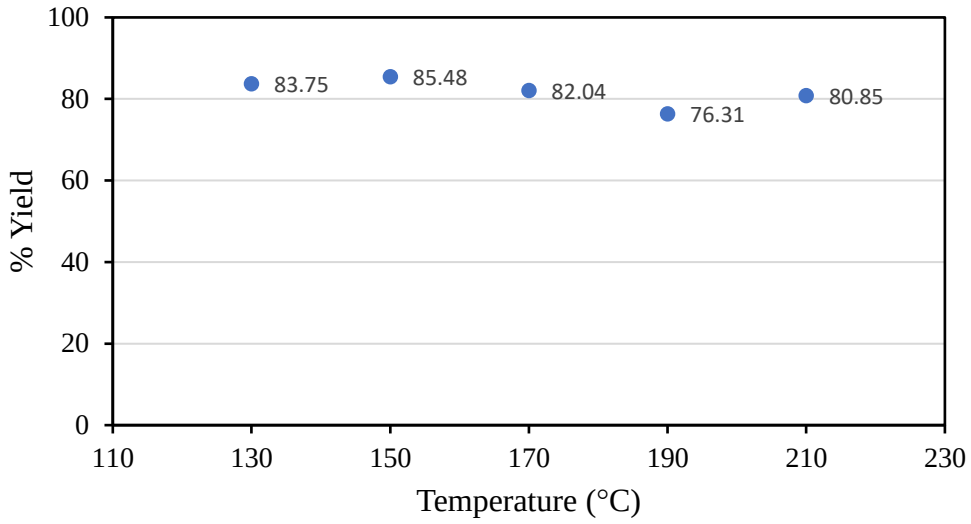

Figure 40. % Yield of a-CDs (prepared with 2.1 g of 10 mM CA and 10 mL BPEI in 2 hours) for the temperature optimisation study.

According to the results shown in Figure 40 above, the % yield remained rather high and stable between 76 and 85 % with an increase in synthesis temperature of a-CDs from 130 °C to 210 °C. The a-CDs showed negligible sensitivity to the applied parameter which could be due to the small incremental increase in temperature. In comparison with the power study performed on plain/unfunctionalised CDs, these % yield values are very high and could be due to the drastically different synthesis procedures; a microwave reaches much higher temperatures than a Si-oil bath, and the experimental set-up is more confined and controlled than that of a domestic microwave. Furthermore, these high % yields could be attributed to (a) a lower temperature (and activation energy) that is required for the reaction to occur between reagent molecules, and (b) the prevention of product losses by the use of a reflux condenser. In addition and according to literature, microwave irradiation offers uniform heating of the solution reaction molecules by raising the temperature of the whole solution simultaneously compared to the use of an oil bath that heats the parts of the reaction mixture which is in contact with the vessel wall first (Schanche 2003). Hence, the lower burn-off percentage of a-CDs compared to that of CDs. Moreover, according to Bewick, the rate of a reaction is accelerated with a raise in temperature as the particles within a solution move faster and increases the frequency of effective collisions between reacting particles (Bewick *et al* 2019). Therefore, the overall high temperatures possibly allowed for a greater number of successful collisions.

The colour of a-CDs in Figure 41 below shows an increase in the intensity from light yellow at 130 °C to deep yellow at 210 °C and according to literature it is known that the formation of a-CDs is represented by the appearance of a yellow colour (Bayati *et al* 2018).

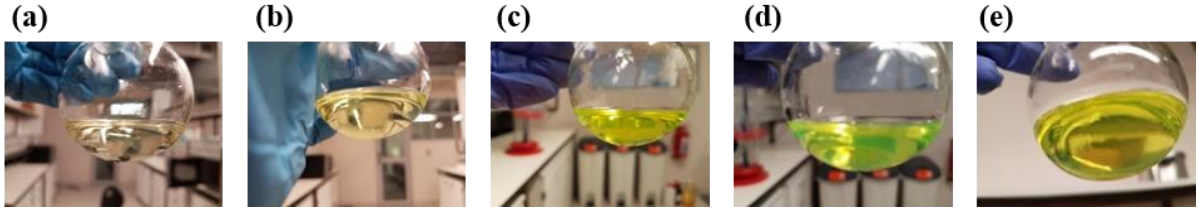

Figure 41. Temperature optimisation of a-CDs from the lowest to the highest temperature, (a) TpOpt_B1 (130 °C), (b) TpOpt_B2 (150 °C), (c) TpOpt_B3 (170 °C), (d) TpOpt_B4 (190 °C) and (e) TpOpt_B5 (210 °C).

4.2.1.1. Absorbance study through ultraviolet-visible spectroscopy

The absorbance of a-CDs was analysed using UV-Vis spectroscopy (as described in Section 3.8.1) to qualitatively determine whether a-CDs were produced, as determined by the specific wavelength at which a-CDs absorb UV light, and to understand the influence of the synthesis temperature on the absorbance of a-CDs. The five samples (of above) for the temperature optimisation study, i.e., TpOpt_B1 (130 °C) to TpOpt_B5 (210 °C), were studied. The absorbance data, i.e., the maximum absorption peaks of the above-mentioned samples with their respective absorbances are tabulated in Table 12 below and the absorbance spectra are shown in Figure 42.

Table 12. The absorbance values for the temperature optimisation study of a-CDs (prepared with 2.1 g of 10 mM CA and 10 mL BPEI in 2 hours) with respect to their wavelengths.

Sample code	***λ_{max} (nm)***	***Absorbance (A)***
TpOpt_B1 (130 °C)	285	0.027
TpOpt_B2 (150 °C)	285	0.027
TpOpt_B3 (170 °C)	285	0.040
TpOpt_B4 (190 °C)	285	0.032
TpOpt_B5 (210 °C)	285	0.051

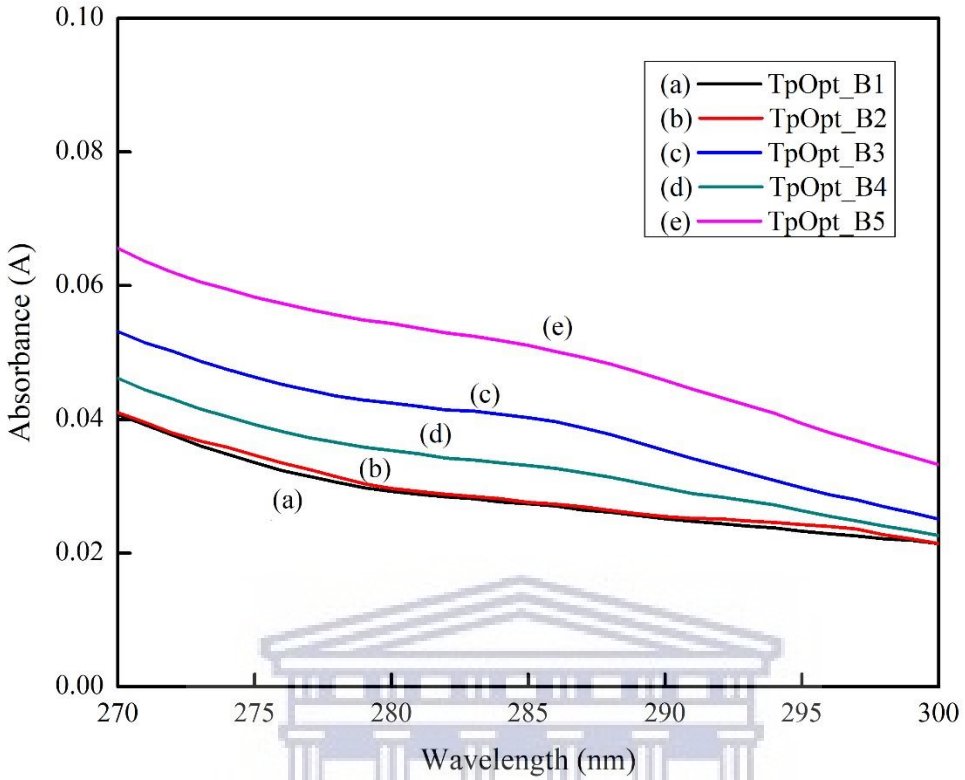

Figure 42. Ultraviolet-visible spectra for a-CDs synthesised at varied temperatures of (a) 130 °C (TpOpt_B1), (b) 150 °C (TpOpt_B2), (c) 170 °C (TpOpt_B3), (d) 190 °C (TpOpt_B4), and (e) 210 °C (TpOpt_B5). a-CDs were prepared with 2.1 g of 10 mM CA and 10 mL BPEI within 2 hours.

In Figure 42, there is a small absorbance peak visible around 285 nm, which is in agreement with the peak observed for a-CDs in previous studies (Zhu *et al* 2009). The absorbance peak of a-CDs is found at a longer wavelength compared to that of unfunctionalised CDs which was around 260 nm; this could be due to amine ($–NH_2$) groups that exist on the surface of a-CDs (Emam *et al* 2017). Similarly to unfunctionalised CDs, a-CDs have also been reported to undergo n–π* transitions of the C=O bands and π–π * transitions of the conjugated C=C bands (Pang *et al* 2017, Song *et al* 2017a, Manioudakis *et al* 2019, Bhattacharyya *et al* 2017). As previously mentioned, the $n \rightarrow \pi^*$ transition is observed in molecules with a heteroatom connected to an unsaturated system and is usually due to a carbonyl band between 270 and 295 nm (Rouessac and Rouessac 2000). As the synthesis temperature was increased from 130 to 210 °C, a hyperchromic effect (i.e., an increase in absorbance intensity) from 0.027 to 0.051 is observed in Figure 42 as tabulated in Table 12. According to the Beer-Lambert law, $A = \varepsilon lC$, there is a direct proportionality between absorbance and concentration; hence, the increase in

absorbance is directly related to an increase in the concentration of a-CDs. The desired outcome would be for the particles to be of smaller sizes which goes hand in hand with an increased band gap energy that ultimately leads to a shift towards shorter wavelengths, i.e., a blue-shift. However, no shift in absorbance occurred towards longer or shorter wavelengths. This only speaks to the insensitivity of the prepared a-CDs to an applied parameter such as temperature. On the contrary, one expects to see the desired result to be achieved with an increase in temperature as more effective collisions should be occurring but the small incremental increase in temperature might not be sufficient in determining the overall effect of the applied parameter.

4.2.1.2. Hydrodynamic properties – Zetasizer

The above-mentioned a-CDs, prepared according to the method described in Section 3.5, were characterised at various synthesis temperatures to obtain size measurements through Dynamic Light Scattering (DLS) and zeta potential measurements through Laser Doppler Velocimetry (LDV) by the Malvern Zetasizer Nano ZS90, to determine the ideal synthesis temperature (see Section 3.8.2 for experimental procedure). The hydrodynamic properties of a-CDs were studied to understand the effect of the synthesis temperature on the average hydrodynamic diameter (D_h/Z-Ave), particle dispersity index (PDI), and zeta-potential (ZP) as tabulated in Table 13. The D_h, PDI, and ZP are plotted as functions of synthesis temperature in Figure 43 below.

Table 13. Results for the hydrodynamic diameter, particle dispersity, and zeta potential of amine-capped CDs (prepared with 2.1 g of 10 mM CA and 10 mL BPEI in 2 hours) for the temperature optimisation study.

Sample code	***Z-Ave (nm)***	***PDI***	***ZP (mV)***
TpOpt_B1 (130 °C)	570.9	0.818	−3.36
TpOpt_B2 (150 °C)	821.1	0.960	−0.117
TpOpt_B3 (170 °C)	1190	0.954	+0.714
TpOpt_B4 (190 °C)	952.5	0.899	+1.42
TpOpt_B5 (210 °C)	1605	1.000	+1.10

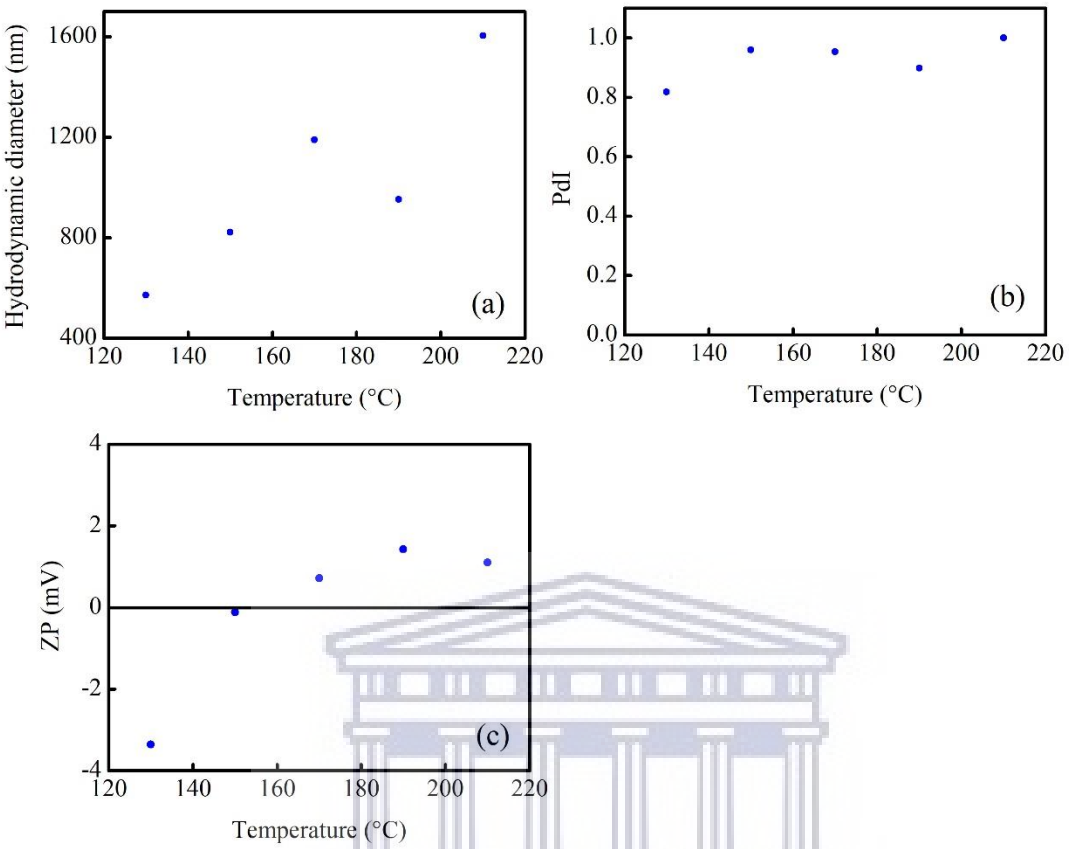

Figure 43. (a) Hydrodynamic diameter, (b) polydispersity index and (c) zeta potential over a range of temperatures (from 130 °C to 210 °C) for the synthesis of amine-capped CDs (prepared with 2.1 g of 10 mM CA and 10 mL BPEI in 2 hours).

The first parameter under investigation was the hydrodynamic diameter of a-CDs. In Figure 43a, there is an overall increase in the hydrodynamic diameter (D_h) of a-CDs from 570.9 to 1605 nm as the temperature was increased from 130 to 210 °C, with the exception of the sample prepared at 190 °C. This shows that the size of a-CDs is sensitive to changes in synthesis temperature and could thus serve as a means of size-control—at low temperatures a-CDs tend to be smaller in size. As discussed previously, collisions of small particles remain discrete due non-permanent associations. However, a colloidally unstable system undergoes collisions that result in permanent associations or the formation of aggregates (Hunter 1987). a-CDs seem to show greater stability at low temperatures as indicated by their small diameters which in turn shows that the particles remain discrete under such conditions. In contrast, the increase in size at higher temperatures could be attributed to the occurrence of agglomeration (or permanent associations) and the formation of clusters of particles in order to obtain stability by lowering the surface energy (Filipponi and Sutherland 2012). These particles seem to have undergone

agglomeration as their hydrodynamic sizes fall out of the nano-range. The particles show greatest stability at the lowest temperature of 130 °C, as smaller sizes were reported which corresponded to the lowest zeta potential value of −3.36 mV, and could be attributed to the electrical double layer compression, as predicted by classical colloidal theory.

In Figure 43b, the PDIs of a-CDs over the above-mentioned synthesis temperatures are displayed. As previously mentioned, the lower the PDI, the more monodisperse the particles are which translates to narrow size distributions—the desired outcome. However, the overall PDI values of a-CDs exhibited very broad size distributions with PDIs between 0.8 and 1, meaning that the particles were more polydisperse. Similar PDI values were observed for the power study on unfunctionalised CDs and thus shows that temperature does not provide control over the degree of polydispersity.

In Figure 43c, the ZP of a-CDs at various synthesis temperatures as measured by a Zetasizer using Laser Doppler Velocimetry (LDV) is shown. The ZP values proved to be temperature sensitive as they became more positive with an increase in temperature from −3.36 mV at 130 °C to +1.42 mV at 190 °C, then slightly decreases to +1.10 mV at 210 °C. There is a direct relationship between the hydrodynamic size of a-CDs and the ZP; it can be deduced that the larger and more polydisperse the particles are, the more positive the zeta potential. According to Verwey, when particles approach one another there will be an attraction between them and London-van der Waals potential will prevail for small double layer values and could lead to flocculation. On the other hand, if double layer potential values are large, the potential barrier is high and coagulation is prevented (Verwey 1947). Therefore, it can be deduced that the potential barrier of a-CDs lowered and van der Waals attraction increased with an increase in temperature causing coagulation. Compared to the power study performed on unfunctionalised CDs, temperature served as a better control over surface potential than power did on unfunctionalised CDs.

Furthermore, the size distributions of a-CDs are displayed over the above-mentioned range of temperatures expressed in number (Figure 44) and intensity (Figure 45) as determined with a Malvern Zetasizer Nano ZS90. Once again, the objective was to examine the distribution of particles by determining the relative amounts (%) of particles found in each size range, essential in understanding physical and chemical properties of a-CDs synthesised at different temperatures.

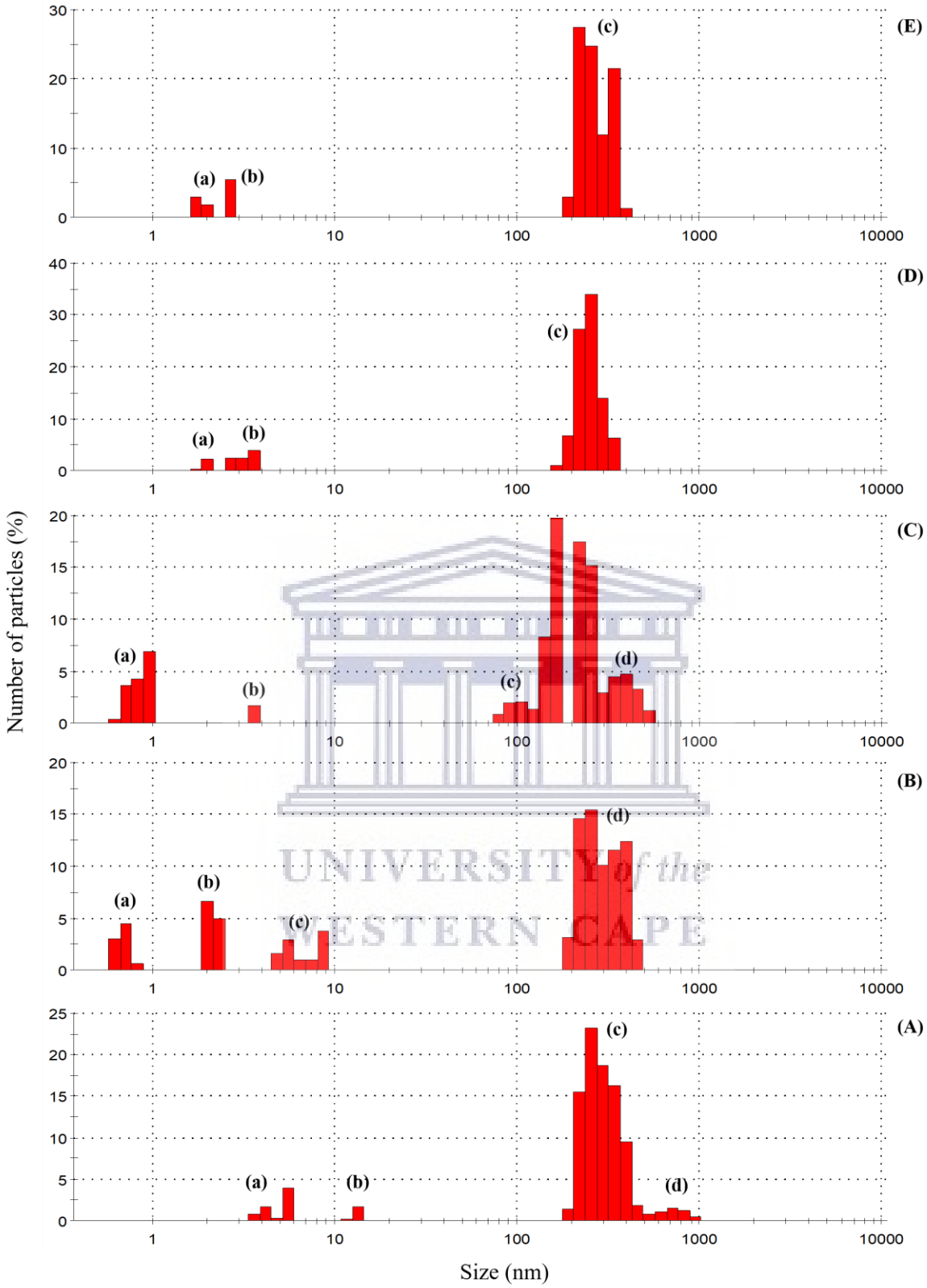

Figure 44. Particle size distribution of a-CDs with the numbers of particles present in each size class for (A) TpOpt_B1 (130 °C), (B) TpOpt_B2 (150 °C), (C) TpOpt_B3 (170 °C), (D) TpOpt_B4 (190 °C), and (E) TpOpt_B5 (210 °C).

The histograms in Figure 44 above show the relative percentage of particles in each size class (logarithmically spaced) based on the intensity of light scattered as a function of the particle size distribution of a-CDs. The percentage distribution is as follows: (A) TpOpt_B1 (130 °C) in which there are four clusters of particles of the following size classes, namely (a) 3.615 to 5.615 nm (6.6 % of particles) with a 4 % maximum at 5.615 nm, (b) 11.70 to 13.54 nm (1.8 % of particles) with a 1.6 % maximum at 13.54 nm, (c) 190.1 to 458.7 nm (86.3 % of particles) with a 23.1 % maximum at 255 nm, and (d) 531.2 to 955.4 nm (5.2 % of particles) with a 1.5 % maximum at 712.4 nm; (B) TpOpt_B2 (150 °C) in which there are four clusters of particles of the following size classes, namely (a) 0.6213 to 0.8332 nm (8 % of particles) with a 4.4 % maximum at 0.7195 nm, (b) 2.01 to 2.328 nm (11.5 % of particles) with a 6.6 % maximum at 2.01 nm, (c) 4.849 to 8.721 nm (10.2 % of particles) with a 3.7 % maximum at 8.721 nm, and (d) 190.1 to 458.7 nm (70.2 % of particles) with a 15.4 % maximum at 255 nm; (C) TpOpt_B3 (170 °C) in which there are four clusters of particles of the following size classes, namely (a) 0.6213 to 0.9649 nm (15.1 % of particles) with a 6.9 % maximum at 0.9649 nm, (b) 3.615 nm (1.7 % of particles), (c) 78.82 to 164.2 nm (34.1 % of particles) with a 19.7 % maximum at 164.2 nm, and (d) 220.2 to 531.2 nm (49.3 % of particles) with a 17.5 % maximum at 220.2 nm; (D) TpOpt_B4 (190 °C) in which there are three clusters of particles of the following size classes, namely (a) 1.736 to 2.01 nm (2.3 % of particles) with a 2.2 % maximum at 2.01 nm, (b) 2.696 to 3.615 nm (8.7 % of particles) with a 4 % maximum at 3.615 nm, and (c) 164.2 to 342 nm (89 % of particles) with a 33.9 % maximum at 255 nm; and (E) TpOpt_B5 (210 °C) in which there are three clusters of particles of the following size classes, namely (a) 1.736 to 2.01 nm (4.5 % of particles) with a 2.8 % maximum at 1.736 nm, (b) 2.696 nm (5.5 % of particles), and (c) 190.1 to 396.1 nm (90 % of particles) with a 27.5 % maximum at 220.2 nm.

Overall, the size distribution of particles for a-CDs were all sized below the upper limit for colloidal suspensions of 1000 nm. However, the majority of particles were of intermediate sizes between 100 nm (the upper limit for the nano-range) and 1000 nm. Looking at the % distribution of particles in the nano-range (0–100 nm), the % of particles present in increasing order are 8.4 % (130 °C), 10 % (210 °C), 11 % (190 °C), 19.5 % (170 °C), and 29.7 % (150 °C). At higher temperatures larger particle sizes are seen, whereas at intermediate temperatures the largest percentages of particles were sized in the nano-range with the smallest sizes recorded for 150 °C and 170 °C. This shows that high synthesis temperatures are not required for effective synthesis of a-CDs. In fact, a-CDs are formed for the lowest applied temperature

of 130 °C while larger percentages of a-CDs are formed for intermediate synthesis temperatures.

In Figure 45 below, the relative percentage of particles in each size class based on the intensity of light scattered is plotted as a function of the particle size distribution according to logarithmically spaced size classes, as obtained by the Malvern Zetasizer Nano ZS90.

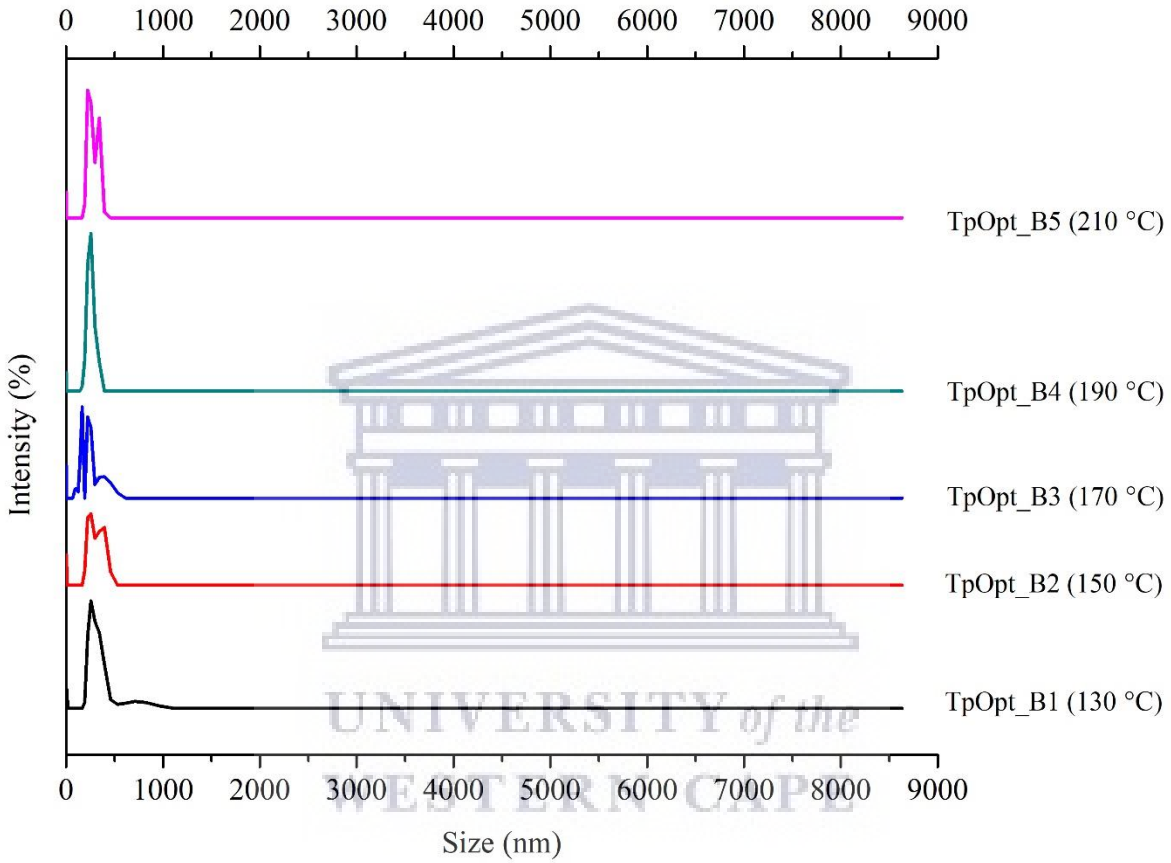

Figure 45. The particle size distribution of a-CDs (prepared with 2.1 g of 10 mM CA and 10 mL BPEI in 2 hours) by intensity with varied temperatures.

In Figure 45, the size distributions of a-CDs are displayed over the above-mentioned range of temperatures expressed by intensity. Notice that all particles for all samples were smaller than the upper limit for colloidal particles of 1000 nm. Compared to all the studies performed on unfunctionalised CDs, a-CDs showed greater stability with the smallest particles which could be attributed to their capping with amine functional groups.

4.2.1.3. Summary

In contrast to unfunctionalised CDs, an increase in the synthesis temperature of a-CDs had an insignificant effect on the burn-off percentage. However, certain characteristics of a-CDs proved to be sensitive to changes in synthesis temperature. As the synthesis temperature was increased from 130 to 210 °C, several parameters were affected, such as (a) the colour of the suspension of a-CDs which intensified, (b) the absorbance that increased, (c) the hydrodynamic diameter which increased, (d) the ZP that became more positive, and (e) the overall size distribution of particles was very wide with most particles in larger size classes but smaller than the upper limit for colloidal materials. The % yield was unaffected by an increase in temperature, which could be due to the synthesis method compared to unfunctionalised CDs—a microwave reaches higher temperatures than a Si-oil bath. However, these values were very high possibly due to the use of a reflux condenser which prevented loss of product. From the colour observed under normal lighting, it can be deduced that as the synthesis temperature was increased, the size of particles also increased which led to a-CDs of a deeper yellow colour as different particle sizes scatter different wavelengths of light (Filipponi and Sutherland 2012). Albeit agglomeration occurred, the extent thereof is much smaller compared to unfunctionalised CDs, which shows that a-CDs have greater stability due to their amine capping. This experiment showed that temperature could be an effective means of control over the hydrodynamic diameter, surface charge as well as size distribution of a-CDs. The samples prepared at intermediate synthesis temperatures of 150 and 170 °C displayed the narrowest size distributions as their surfaces had ZPs closest to the point of zero charge. In comparison, the samples prepared at 190 °C behaved differently from the trends observed for the rest of the samples as there is some correlation between the hydrodynamic size thereof, the % yield and the lower absorbance. Due to the larger number of nanoparticles produced at 170 °C, it was chosen as the ideal synthesis temperature for the synthesis of a-CDs. In essence, high temperatures above 170 °C is not necessary for effective synthesis of a-CDs, and the amine functional groups certainly improved stability of CDs.

4.2.2. Reaction-time optimisation for synthesis of amine-capped CDs

In this section, the results on the effect of synthesis reaction time on the colloidal stability of a-CDs are discussed and the samples were prepared according to the experimental procedure described in Section 3.3.6. Five different reaction times were analysed to determine the ideal reaction duration for effective synthesis of a-CDs. a-CDs were prepared within the following reaction times: 1, 1.5, 2, 2.5, and 3 hours; while several other parameters remained fixed, such as the molar quantity of CA (1.1×10^{-2} mol), the molar quantity of BPEI (1.3×10^{-2} mol), and the synthesis temperature (170 °C). The aim was to investigate the effect of heating time on (a) the % yield (expressed in Table 40 in Appendix), (b) the interaction of light with the a-CDs through UV-Vis, and (c) the hydrodynamic diameter, polydispersity index, and zeta potential. Figure 46 below presents the % yield of the five samples prepared at different reaction times (as calculated in Table 40 in Appendix).

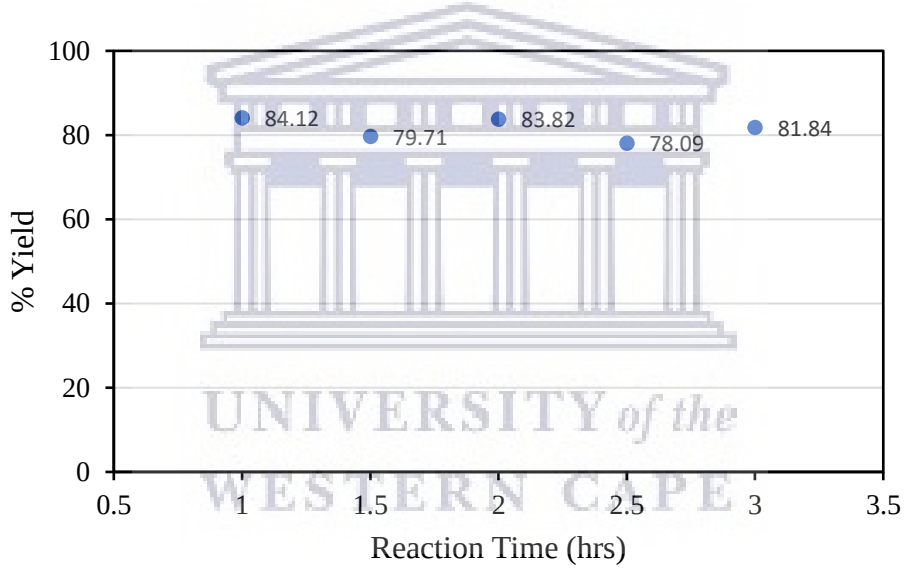

Figure 46. % Yield of a-CDs (prepared with 2.1 g of 10 mM CA and 10 mL BPEI at 170 °C) for the reaction time optimisation study.

According to the results in Figure 46 above, the % yield remained rather high and stable between 78 and 84 % with an increase in reaction time from 1 to 3 hours. This is similar to the % yield observed in the study of the effect of synthesis temperature. Overall, the duration of the reaction had a negligible influence on the % yield and could therefore not be used as a means to control the output of a-CDs. However, in comparison with similar studies performed on unfunctionalised CDs, more a-CDs were produced and could be attributed to aforementioned reasons that pertains to the difference in synthesis method. Typically, the desire is to achieve the highest possible yield for products prepared in the shortest possible time

with the lowest energy consumption and wastage. Therefore, according to the results above, a high % yield is still found at shorter reaction times which means that higher reaction times are not necessary.

As mentioned before, the formation of a-CDs is represented by the appearance of a yellow colour (Bayati *et al* 2018) which can once again be observed in Figure 47 below. Also, as the heating time was increased from 1 to 3 hours, the intensity of the colour of the product (under normal lighting) deepened from light yellow to deep yellow.

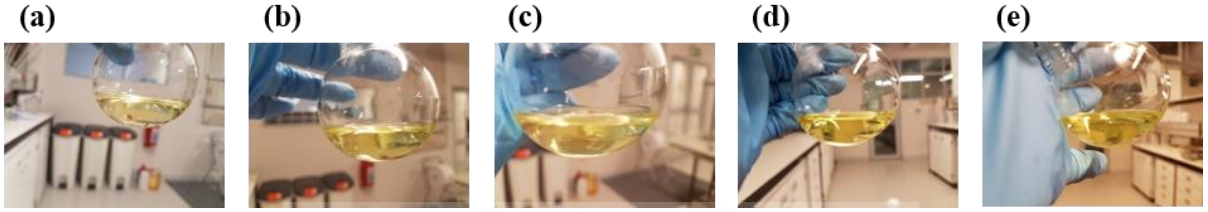

Figure 47. The reaction-time optimisation of a-CDs (prepared with 2.1 g of 10 mM CA and 10 mL BPEI at 170 °C). The reaction time was varied as follows: (a) 1 hr (RTOpt_B6), (b) 1.5 hr (RTOpt_B7), (c) 2 hr (RTOpt_B8), (d) 2.5 hr (RTOpt_B9) and (e) 3 hr (RTOpt_B10).

4.2.2.1. Absorbance study through ultraviolet-visible spectroscopy

The absorbance of a-CDs was analysed using UV-Vis spectroscopy (as described in Section 3.8.1) to qualitatively determine whether a-CDs were produced and to understand the effect of variation in the reaction/heating time on the absorbance of a-CDs. The five samples (of above) for the reaction-time optimisation study, i.e., RTOpt_B6 (1 h) to RTOpt_B10 (3 h), were studied. The absorbance data, i.e., the maximum absorption peaks of the above-mentioned samples with their respective absorbances are tabulated in Table 14 below and the absorbance spectra are shown in Figure 48.

Table 14. The absorbance values for the reaction-time optimisation study of a-CDs (prepared with 2.1 g of 10 mM CA and 10 mL BPEI at 170 °C) with respect to their wavelengths.

Sample code	***λ_{max} (nm)***	***Absorbance***
RTOpt_B6 (1 h)	280	0.037
RTOpt_B7 (1.5 h)	282	0.029
RTOpt_B8 (2 h)	282	0.032
RTOpt_B9 (2.5 h)	281	0.037
RTOpt_B10 (3 h)	283	0.033

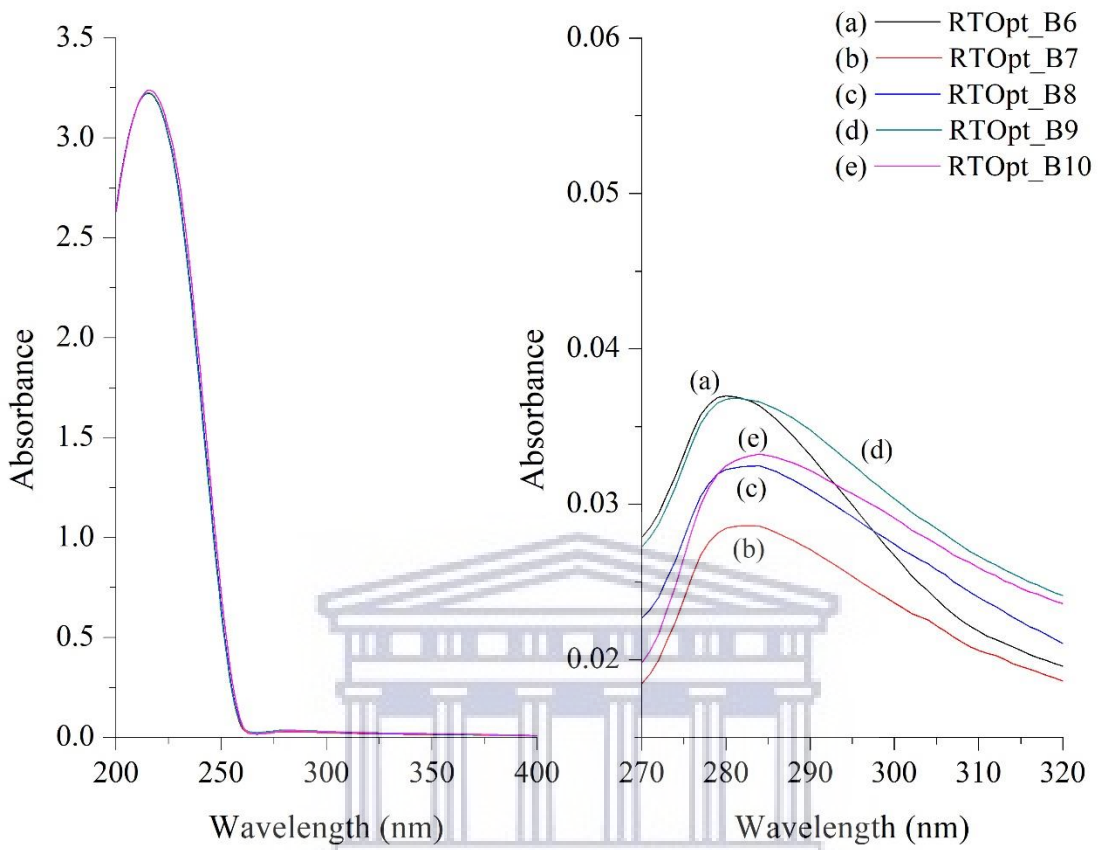

Figure 48. Ultraviolet-visible spectra for a -CDs synthesised at 170 °C for various reaction times, namely for (a) 1 h, (b) 1.5 h, (c) 2 h, (d) 2.5 h and (e) 3 h.

In Figure 48, the absorption spectra of all prepared a-CDs display a prominent absorption band at ~ 220 nm and a weak shoulder at longer wavelengths (~ 280 nm) which is in agreement with literature (Zhu *et al* 2009, Bhattacharyya *et al* 2017). As stated before, the absorbance peak of a-CDs is found at a longer wavelength compared to that of unfunctionalised CDs which was around 260 nm; which could be due to amine ($–NH_2$) groups that exist on the surface of a-CDs (Emam *et al* 2017). Similarly to unfunctionalised CDs and according to literature, a-CDs have also been reported to undergo n–π* transitions of the C=O bands and π–π * transitions of the conjugated C=C bands (Pang *et al* 2017, Song *et al* 2017a, Manioudakis *et al* 2019, Bhattacharyya *et al* 2017). As previously mentioned, the $n \rightarrow \pi^*$ transition is observed in molecules with a heteroatom connected to an unsaturated system and is usually due to a carbonyl band between 270 and 295 nm (Rouessac and Rouessac 2000). As the heating time was increased from 1 to 3 hours, an initial hypochromic effect (i.e., a decrease in absorbance intensity) from 0.037 to 0.029 is observed in Figure 48 as tabulated in Table 14, and could be

attributed to groups that caused distortion in geometry on a molecular level. The absorbance fluctuates with an increase in reaction time and there is no specific overall trend observed. Moreover, no shift in absorbance occurred towards longer or shorter wavelengths with an increase in heating time. Therefore, the duration of synthesis did not have a pronounced effect on the wavelength or absorbance intensity, which implies that shorter synthesis times are adequate.

4.2.2.2. Hydrodynamic properties – Zetasizer

The above-mentioned a-CDs, prepared at various reaction times, were characterised to obtain size measurements through Dynamic Light Scattering (DLS) and zeta potential measurements through Laser Doppler Velocimetry (LDV) by the Malvern Zetasizer Nano ZS90, to determine the ideal reaction time for synthesis (see Section 3.8.2 for experimental procedure). The hydrodynamic properties of a-CDs were studied to understand the effect of heating time on the average hydrodynamic diameter (D_h/Z-Ave), particle dispersity index (PDI), and zeta-potential (ZP) as tabulated in Table 15. The D_h, PDI, and ZP are plotted as functions of reaction time in Figure 49 below.

Table 15. Results for the hydrodynamic diameter, particle dispersity index, and zeta potential of amine-capped CDs (prepared with 2.1 g of 10 mM CA and 10 mL BPEI at 170 °C) for the reaction-time optimisation study.

Sample code	***Z-Ave (nm)***	***PDI***	***ZP (mV)***
RTOpt_B6 (1 h)	1715	1.000	+0.609
RTOpt_B7 (1.5 h)	1345	0.835	+0.252
RTOpt_B8 (2 h)	1542	1.000	+0.289
RTOpt_B9 (2.5 h)	518.8	0.774	+0.278
RTOpt_B10 (3 h)	1112	1.000	+0.215

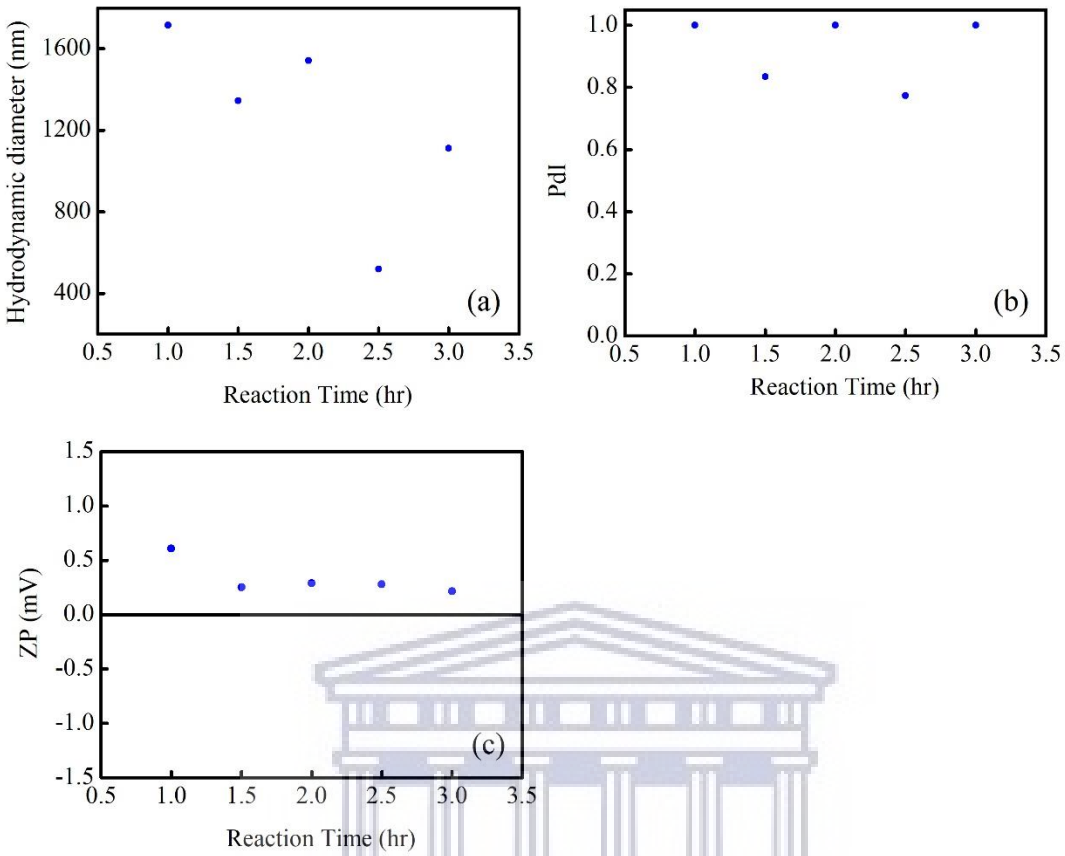

Figure 49. (a) Hydrodynamic diameter, (b) polydispersity index and (c) zeta potential over a range of reaction times (from 1 to 3 hours) for the synthesis of amine-capped CDs.

In Figure 49a, the hydrodynamic diameter (D_h) of a-CDs was plotted against the reaction time. As the reaction time was increased from 1 to 3 hours, no specific trend was observed in the data points as it was scattered. Generally, it is desired for the reaction time to be as short as possible in order to minimise energy consumption. However, shorter reaction times yielded particles of larger diameters. These particles seem to have undergone agglomeration (as permanent associations have formed between particles as discussed in Section 4.1.1.3). From the data the only reliable conclusion to make is that a-CDs showed greatest stability at the heating time of 2.5 hours with the smallest reported average particle size of 518.8 nm.

In Figure 49b, the PDI of a-CDs is displayed as a function of reaction time. As previously stated, the lower the PDI, the more monodisperse the particles are which translates to narrow size distributions. Out of all samples, the sample prepared within 2.5 hours showed the greatest stability with the lowest PDI of 0.774, which is still very high. However, compared to other samples, it has the narrowest size distribution. Overall, the PDIs of a-CDs displayed very broad size distributions which means that the particles were more polydisperse with PDIs between

0.7 and 1. Compared to PDI values found for unfunctionalised CDs, a-CDs have much larger PDIs than CDs. This behaviour is unexpected, as the capping of a-CDs should provide greater stability and greater control over particle size and in turn over particle size distribution.

The ZP of a-CDs, as obtained through Laser Doppler Velocimetry (LDV), was plotted as a function of reaction time of a-CDs (Figure 49c). The ZP values were not that sensitive to changes in reaction time as they became slightly more negative with all values remaining positive at ~0.2 mV with the exception of the most positive value at +0.603 mV for the 1-h sample. As mentioned before, the larger and more polydisperse the particles are, the more positive the zeta potential, which is evident in this experiment. It can once again be deduced that the potential barrier was low and van der Waals attraction dominated and caused coagulation (Verwey 1947).

Furthermore, the size distributions of a-CDs are displayed over the above-mentioned range of reaction times expressed in number (Figure 50) and intensity (Figure 51) as determined with a Malvern Zetasizer Nano ZS90. Once again, the objective was to examine the distribution of particles by determining the relative amounts (%) of particles found in each size range to understand the physical and chemical properties of a-CDs synthesised at different reaction times.

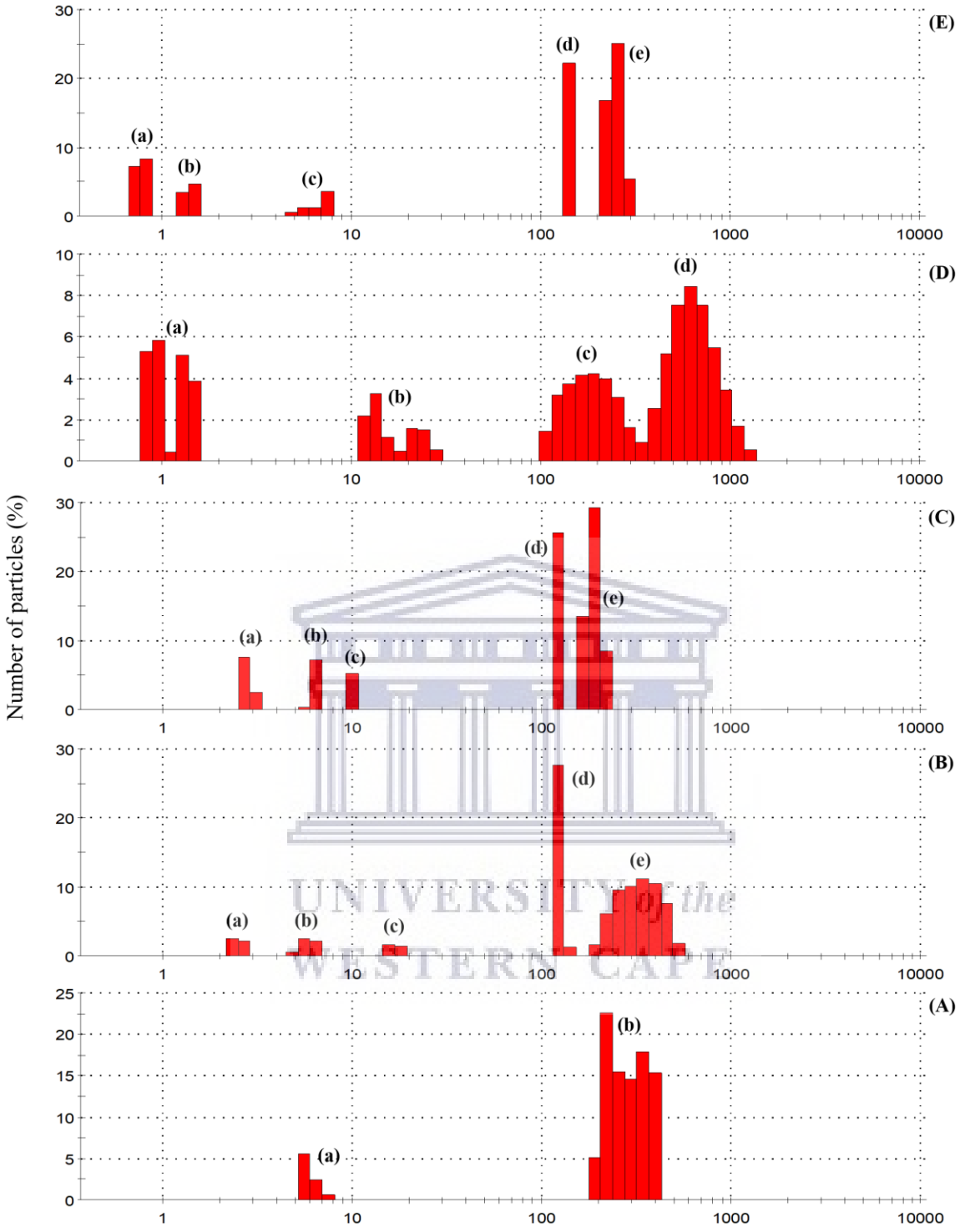

Figure 50. Particle size distribution of amine-capped CDs for the reaction-time optimisation study with the numbers of particles present in each size class for (A) RTOpt_B6 (1 h), (B) RTOpt_B7 (1.5 h), (C) RTOpt_B8 (2 h), (D) RTOpt_B9 (2.5 h), and (E) RTOpt_B10 (3 h).

The histograms in Figure 50 above show the relative percentage of particles in each size class (logarithmically spaced) based on the intensity of light scattered as a function of the particle size distribution of amine-capped CDs. The percentage distribution is as follows: (A)

RTOpt_B6 (1 h) in which there are two clusters of particles of the following size classes, namely (a) 5.615 to 7.531 nm (8.8 % of particles) with a 5.6 % maximum at 5.615 nm, and (b) 190.1 to 396.1 nm (91.2 % of particles) with a 22.6 % maximum at 220.2 nm; (B) RTOpt_B7 (1.5 h) in which there are five clusters of particles of the following size classes, namely (a) 2.328 to 2.696 nm (4.6 % of particles) with a 2.5 % maximum at 2.328 nm, (b) 4.849 to 6.503 nm (5.3 % of particles) with a 2.6 % maximum at 5.615 nm, (c) 15.69 to 18.17 nm (3.1 % of particles) with a 1.6 % maximum at 15.69 nm, (d) 122.4 to 141.8 nm (28.8 % of particles) with a 27.6 % maximum at 122.4 nm, and (e) 190.1 to 531.2 nm (58.2 % of particles) with an 11.2 % maximum at 342 nm; (C) RTOpt_B8 (2 h) in which there are five clusters of particles of the following size classes, namely (a) 2.696 to 3.122 nm (10.1 % of particles) with a 7.6 % maximum at 2.696 nm, (b) 5.615 to 6.503 nm (7.7 % of particles) with a 7.3 % maximum at 6.503 nm, (c) 10.10 nm (5.3 % of particles), (d) 122.4 nm (25.6 % of particles), and (e) 164.2 to 220.2 nm (51.3 % of particles) with a 29.2 % maximum at 190.1 nm; (D) RTOpt_B9 (2.5 h) in which there are four clusters of particles of the following size classes, namely (a) 0.8332 to 1.499 nm (20.4 % of particles) with a 5.8 % maximum at 0.9649 nm, (b) 11.7 to 28.21 nm (10.7 % of particles) with a 3.2 % maximum at 13.54 nm, (c) 105.7 to 295.3 nm (25.4 % of particles) with a 4.2 % maximum from 164.2 to 190.1 nm, and (d) 342 to 1281 nm (43.5 % of particles) with an 8.5 % maximum at 615.1 nm; and (E) RTOpt_B10 (3 h) in which there are five clusters of particles of the following size classes, namely (a) 0.7195 to 0.8332 nm (15.4 % of particles) with an 8.3 % maximum at 0.8332 nm, (b) 1.294 to 1.499 nm (8.2 % of particles) with a 4.8 % maximum at 1.499 nm, (c) 4.849 to 7.531 nm (6.6 % of particles) with a 3.5 % maximum at 7.531 nm, (d) 141.8 nm (22.3 % of particles), and (e) 220.2 to 295.3 nm (47.5 % of particles) with a 25.1 % maximum at 255 nm.

Overall, the size distribution of particles for a-CDs were all sized below the upper limit for colloidal suspensions of 1000 nm. However, as in the case of the temperature study for a-CDs, the majority of particles were of sizes between 100 nm (the upper limit for the nano-range) and 1000 nm. Compared to a-CDs produced in the Temperature study, greater percentages of particles were sized in the nano-range, especially particles that were produced at reaction times longer than 2 hours. Looking at the % distribution of particles in the nano-range (0-100 nm), the % of particles present in increasing order are 8.8 % (1 h), 13 % (1.5 h), 23.1 % (2 h), 30.2 % (3 h), and 31.1 % (2.5 h). As the heating time for the synthesis of a-CDs was increased, the % of particles within the nano-range also increased. Nevertheless, a-CDs were produced from the shortest reaction time of 1 hour up to the longest reaction time of 3 hours. Therefore,

extended reaction time is not necessary for successful production of a-CDs, and shorter times are adequate.

In Figure 51 below, the relative percentage of particles in each size class based on the intensity of light scattered is plotted as a function of the particle size distribution according to logarithmically spaced size classes, as obtained by the Malvern Zetasizer Nano ZS90.

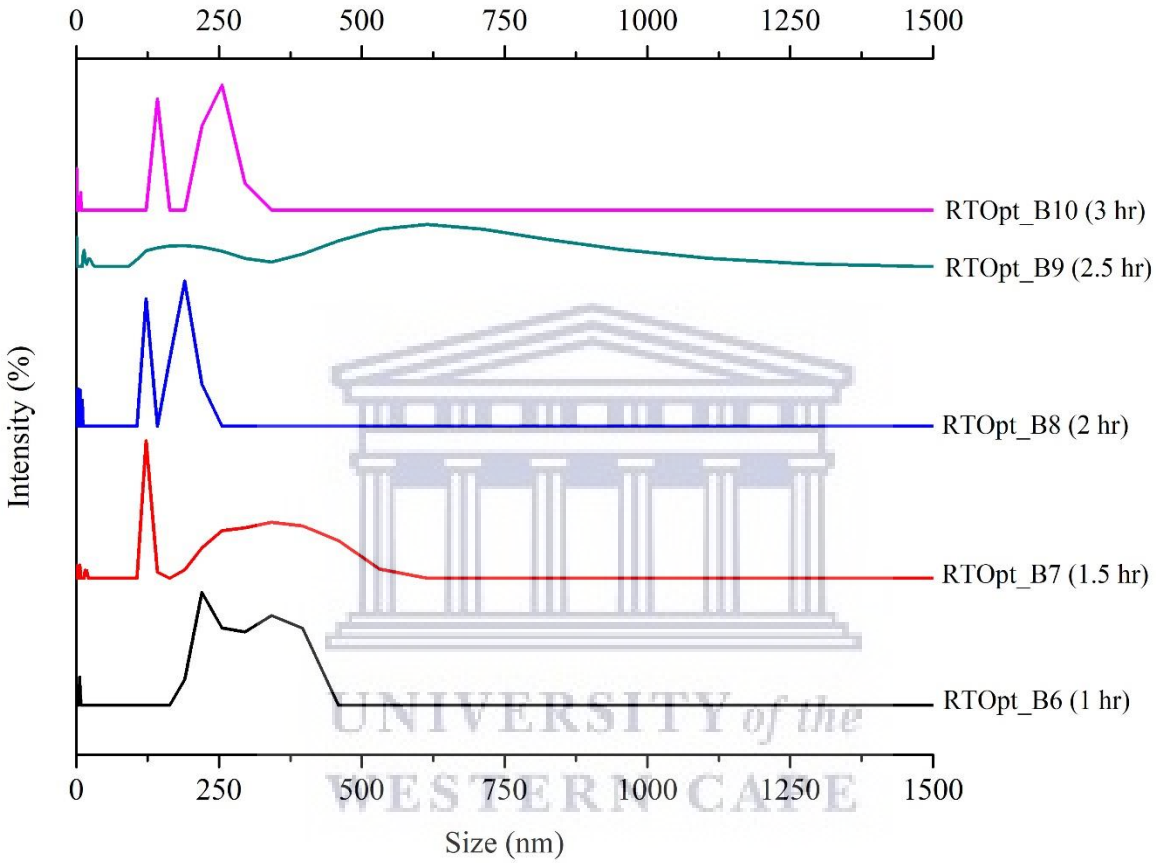

Figure 51. The particle size distribution of a-CDs by intensity with varied reaction times.

In Figure 51, the size distributions of a-CDs are displayed over the above-mentioned range of reaction times expressed by intensity. Notice, once again, that all particles for all samples were smaller than the upper limit for colloidal particles of 1000 nm. However, RTOpt_B8, i.e., the sample prepared within 2 hours, displayed the narrowest size distribution towards smaller particle sizes while all other samples showed a wide size distribution that reaches above 250 nm in particle size. Compared to a-CDs produced in the temperature study, larger amounts of particles were of relatively small sizes in the nano-range.

4.2.2.3. Summary

As previously mentioned, an increase in the reaction time of a-CDs significantly affects the burn-off percentage (Sutanto *et al* 2020). However, a-CDs proved to be relatively insensitive to changes in reaction time as majority of the data were scattered. As the reaction time was increased from 1 to 3 hours, several parameters were affected, such as (a) the colour of the suspension of a-CDs which intensified, (b) the absorbance was scattered, (c) the hydrodynamic diameter was scattered, (d) the ZP that became more negative but displayed positive surfaces throughout, and (e) the overall size distribution of particles was very wide with most particles in larger size classes but smaller than the upper limit for colloidal material. Although agglomeration occurred, a-CDs, once again displayed greater stability compared to studies performed on unfunctionalised CDs with some particles that were sized within the nano-range. Generally, shorter reaction times are desired to minimise energy consumption; as the heating time for the synthesis of a-CDs was increased, the % of particles within the nano-range also increased. Therefore, extended reaction time is not necessary for successful production of a-CDs and shorter times are adequate. The samples prepared within 2 hours had the narrowest size distribution, yielded 23.1 % of particles sized within the nano-range (according to Figure 50c) and was therefore chosen as the ideal reaction time for the synthesis of a-CDs.

4.2.3. Molar quantity optimisation of citric acid for the synthesis of a-CDs

In this section, the results for the influence of the molar quantity of citric acid (CA) on the colloidal stability of a-CDs, as prepared according to the experimental procedure described in Section 3.3.7, is discussed. a-CDs were prepared with the following molar quantities of CA, namely: 7.8×10^{-3} mol (1.5 g), 9.4×10^{-3} mol (1.8 g), 1.1×10^{-2} mol (2.1 g), 1.2×10^{-2} mol (2.4 g), and 1.4×10^{-2} mol (2.7 g) (molar calculations presented in Appendix I). These were labelled CA_Opt_B11, CA_Opt_B12, CA_Opt_B13, CA_Opt_B14, and CA_Opt_B15, respectively. They were analysed to determine the ideal molar quantity of CA for effective synthesis of a-CDs. The following parameters remained fixed: (a) the concentration (0.01 $mol.L^{-1}$) of CA, (b) the concentration (1.3 $mol.L^{-1}$) and molar quantity (1.3×10^{-2} mol) of BPEI, (c) the synthesis temperature (170 °C), and (d) the reaction time (2 hours). The aim was to determine the ideal synthesis conditions for a-CDs and investigate the effect of the molar quantity of CA on (a) the % yield (calculations in Table 43 in Appendix), (b) the interaction of light with a-CDs through UV-Vis, and (c) the hydrodynamic diameter, the polydispersity index, and the surface charge of a-CDs. Figure 52 below presents the % yield of the five samples prepared with increasing molar quantities of CA.

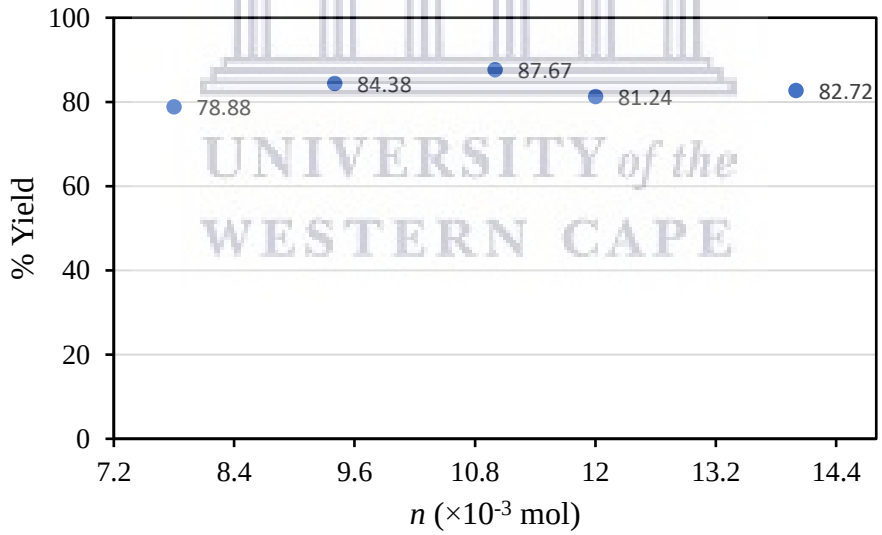

Figure 52. % Yield for the CA molar optimisation study of a-CDs (synthesised at 170 °C for 2 hours).

According to the results in Figure 52 above, the % yield increased slightly, from 78.88 % for the sample prepared with 7.8×10^{-3} mol (1.5 g) of CA to 87.67 % for the sample prepared with 1.1×10^{-2} mol (2.1 g, lit.) of CA. Then, there was a 6 % decrease to 81.24 % for the sample prepared with 1.2×10^{-2} mol (2.4 g) of CA which was followed by a slight increase in % yield

to 82.72 % for the sample containing the largest amount of CA of 1.4×10^{-2} mol (2.7 g). However, there is no real optimum as the % yield remains high and quite stable with a slight overall increasing trend as the molar value of CA was increased. This is expected because there is an increase in the carbon source. Here, the information relayed on collisions by Bewick and co-workers is of importance once more since there are more reagent molecules present for collisions to effectively accelerate the process of carbonisation (Bewick *et al* 2019). Compared to the temperature study and reaction-time study on a-CDs, there was no real change in % yield; it remains high and between 70–90 %.

See the effect of an increase in the molar quantity of CA on the colour of the product under normal lighting in Figure 53; the yellow colour is most intense for the sample prepared with 1.1×10^{-2} mol (2.1 g), which had the highest % yield of 87.67 %. This is the same amount of CA used in literature (Zheng *et al* 2014, Bayati *et al* 2018). The colour intensity of these samples corresponds to the trend found in the % yield in Figure 52 above; for higher % yields the yellow colour of the product is more intense.

Figure 53. The molar optimisation of CA for a-CDs prepared with the following molar quantities of 10 mM CA: (a) 7.8×10^{-3} mol (CA_Opt_B11), (b) 9.4×10^{-3} mol (CA_Opt_B12), (c) 1.1×10^{-2} mol (CA_Opt_B13), (d) 1.2×10^{-2} mol (CA_Opt_B14), and (e) 1.4×10^{-2} mol (CA_Opt_B15).

4.2.3.1. Absorbance study through ultraviolet-visible spectroscopy

The absorbance of a-CDs was analysed using UV-Vis spectroscopy (as described in Section 3.8.1) to qualitatively determine whether a-CDs were produced and to understand the effect of variation in the molar quantity of CA on the absorbance of a-CDs. The above-mentioned five samples, for the molar quantity optimisation study of CA, were studied. The absorbance data, i.e., the maximum absorption peaks with their respective absorbances, are tabulated in Table 16 below and the absorbance spectra are shown in Figure 54.

Table 16. The absorbance values for the CA molar optimisation study of a-CDs (synthesised at 170 °C for 2 hours) with respect to their wavelengths.

Sample code	***λ_{max} (nm)***	***Absorbance***
CA_Opt_B11	285	0.012
CA_Opt_B12	288	0.005
CA_Opt_B13	288	0.004
CA_Opt_B14	289	0.003
CA_Opt_B15	288	0.004

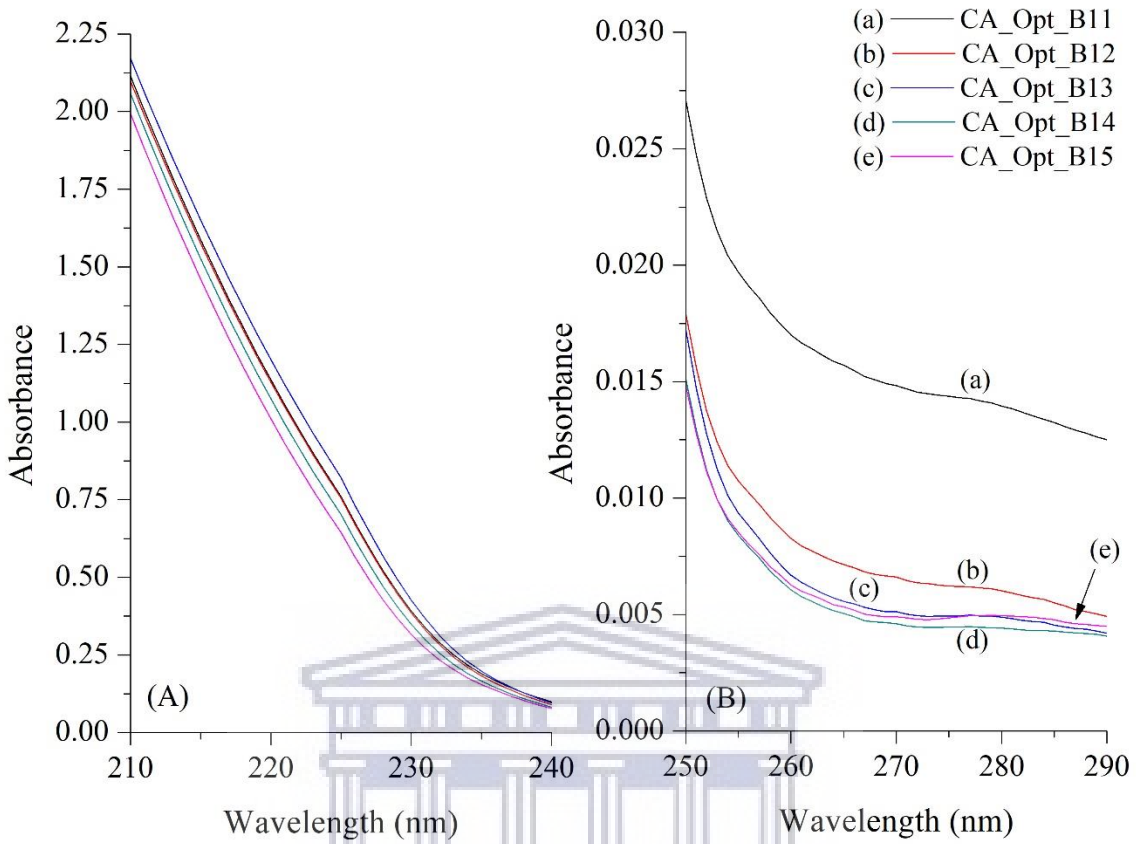

Figure 54. Ultraviolet-visible spectra for the CA molar quantity optimisation study of a-CDs in wavelength window of (A) 210–240 nm, and (B) 250–290 nm. A-CDs were synthesised with the following molar quantities of CA: (a) 7.8×10^{-3} mol (CA_Opt_B11), (b) 9.4×10^{-3} mol (CA_Opt_B12), (c) 1.1×10^{-2} mol (CA_Opt_B13), (d) 1.2×10^{-2} mol (CA_Opt_B14), and (e) 1.4×10^{-2} mol (CA_Opt_B15).

In Figure 54, the absorption spectra of all prepared a-CDs displayed strong absorption at ~ 220 nm (Figure 54A) and a weak shoulder at longer wavelengths of ~280 nm (Figure 54B) and is in agreement with previous studies (Zhu *et al* 2009, Bhattacharyya *et al* 2017). The same transitions occurred for a-CDs under the influence of the molar quantity of CA as for the temperature and reaction-time studies; n–π* transitions of the C=O bands in molecules with a heteroatom connected to an unsaturated system, and π–π * transitions of the conjugated C=C bands (Pang *et al* 2017, Song *et al* 2017a, Manioudakis *et al* 2019, Bhattacharyya *et al* 2017). As stated before, the absorbance peak of a-CDs is found at a longer wavelength compared to that of unfunctionalised CDs due to amine ($–NH_2$) groups that exist on the surface of a-CDs (Emam *et al* 2017). As the molar value of CA was increased, a hypochromic effect (i.e., a decrease in absorbance intensity) from 0.012 to 0.004 is observed at 285 nm in Figure 54 as tabulated in Table 16, and could be attributed to groups that caused distortion in geometry on

a molecular level (Rouessac and Rouessac 2000). A similar trend was observed with an increase in the molar quantity of the carbon source for unfunctionalised CDs. However, no shift in absorbance occurred towards longer or shorter wavelengths under the influence of the molar quantity of CA.

4.2.3.2. Hydrodynamic properties – Zetasizer

The above-mentioned a-CDs, prepared with different molar values of CA, were characterised to obtain size measurements through Dynamic Light Scattering (DLS) and zeta potential measurements through Laser Doppler Velocimetry (LDV) by the Malvern Zetasizer Nano ZS90 (see Section 3.8.2 for experimental procedure). The hydrodynamic properties of a-CDs were studied to understand the effect of variation in the molar quantity of CA on the average hydrodynamic diameter (D_h/Z-Ave), particle dispersity index (PDI), and zeta-potential (ZP) as tabulated in Table 17. The D_h, PDI, and ZP are plotted as functions of the number of moles of CA in Figure 55 below.

Table 17. Results for the hydrodynamic diameter, particle dispersity, and zeta potential of a-CDs (170 ºC; 2hr) for the molar quantity optimisation study of CA.

Sample code	***Z-Ave (nm)***	***PDI***	***ZP (mV)***
CA_Opt_B11	1234	1.000	+0.549
CA_Opt_B12	2466.5	1.000	+2.69
CA_Opt_B13	863.5	0.994	+1.15
CA_Opt_B14	1381	1.000	+0.815
CA_Opt_B15	1341	1.000	+1.32

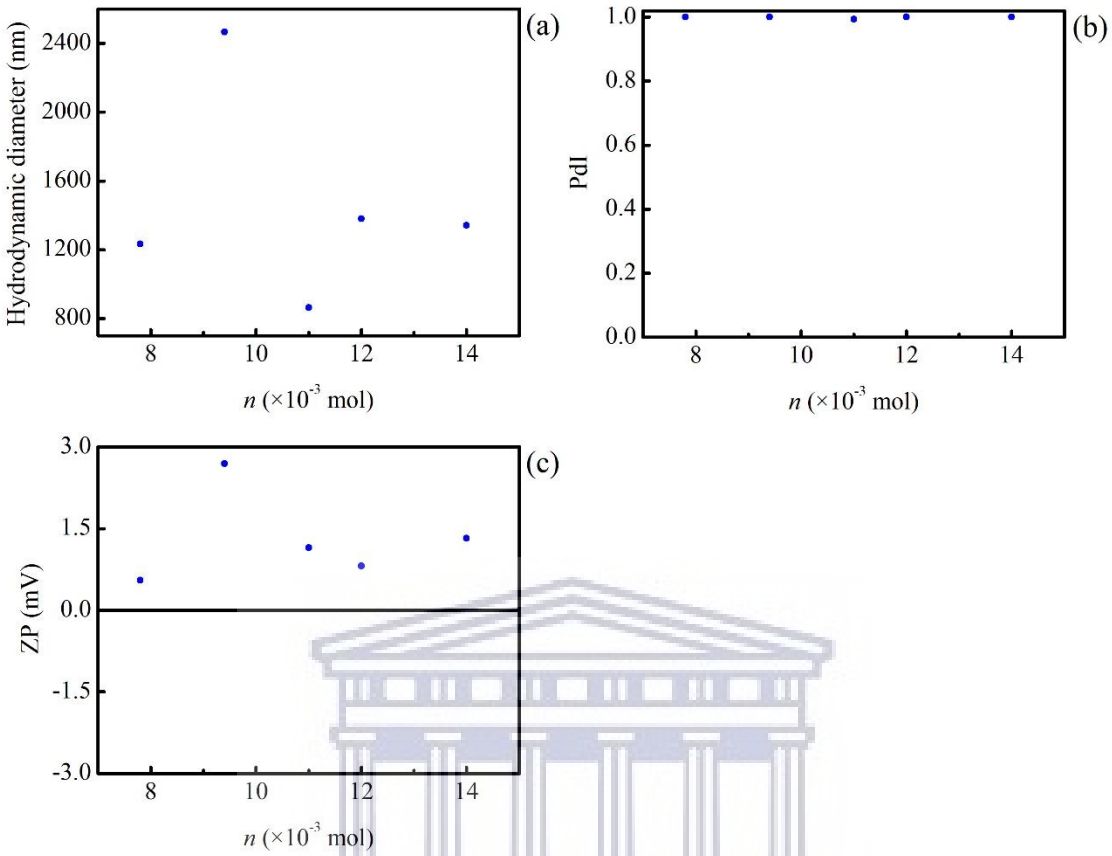

Figure 55. (a) Hydrodynamic diameter, (b) polydispersity index and (c) zeta potential over a range of CA molar quantities for the synthesis of amine-capped CDs.

In Figure 55a, as the number of moles of CA was increased from 7.8×10^{-3} to 1.4×10^{-2} mol, there is a large scatter and no trend in the hydrodynamic diameter (D_h) of a-CDs, with the largest D_h of 2466.5 nm for the sample prepared with 9.4×10^{-3} mol of CA. The a-CDs showed greatest stability for CA_Opt_B13 prepared with 1.1×10^{-2} mol of CA with the smallest reported average particle size of 863.5 nm. Overall, the samples show a large degree of agglomeration with very wide size distributions, evident by their high PDI values in Figure 55b which was the second parameter under investigation over the above-mentioned molar quantity values of CA. PDI is displayed as a function of the number of moles of CA and, as previously specified, the lower the PDI, the more monodisperse the particles are which translates to narrow size distributions. However, the PDIs of a-CDs, prepared with an increasing number of moles of CA, displayed very broad size distributions which means that the particles were more polydisperse with very high PDI values and further speaks to the large-sized particles they contain. Compared to similar studies performed on unfunctionalised CDs, a-CDs show very

wide size distributions, but they do contain a larger number of particles sized within the nano-range.

The ZP of a-CDs, obtained through Laser Doppler Velocimetry (LDV), was plotted as a function of the number of moles of CA (Figure 55c). The ZP values were insensitive to changes in CA content but they became slightly more positive from +0.549 mV to +1.32 mV with the exception of the most positive value at +2.69 mV for CA_Opt_B12. This means that the surface of the colloidal a-CDs became slightly more positive as the number of moles for CA increased. However, there is a direct relationship between the hydrodynamic size of a-CDs and the ZP; it can be deduced that the larger and more polydisperse the particles are, the more positive the zeta potential. And it can once again be deduced that agglomeration occurred due to the low potential barrier and dominating van der Waals attraction (Verwey 1947).

Furthermore, the size distributions of a-CDs are displayed over the above-mentioned range of molar quantities of CA expressed in number (Figure 56) and intensity (Figure 57) as determined with a Malvern Zetasizer Nano ZS90. Once again, the objective was to examine the distribution of particles by determining the relative amounts (%) of particles found in each size range which is essential in understanding physical and chemical properties of a-CDs synthesised with an increasing number of moles of CA.

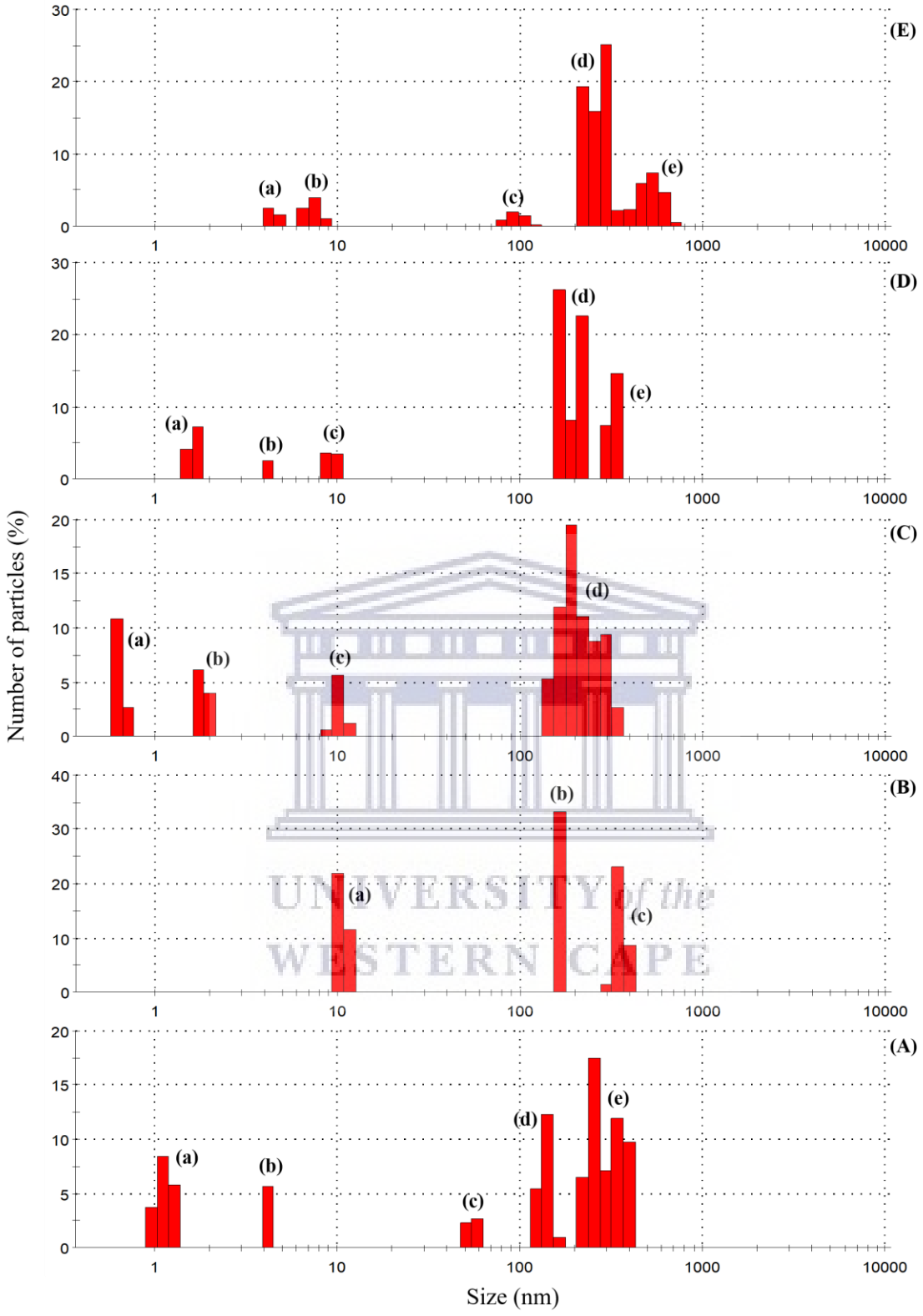

Figure 56. Particle size distribution of a-CDs (170 °C; 2 hours) with the numbers of particles present in each size class in the CA Molar Quantity Optimisation Study, for the following molar quantities (A) 7.8×10^{-3} mol (CA_Opt_B11), (B) 9.4×10^{-3} mol (CA_Opt_B12), (C) 1.1×10^{-2} mol (CA_Opt_B13), (D) 1.2×10^{-2} mol (CA_Opt_B14), and (E) 1.4×10^{-2} mol (CA_Opt_B15).

The histograms in Figure 56 above show the relative percentage of particles in each size class (logarithmically spaced) based on the intensity of light scattered as a function of the particle size distribution of a-CDs. The percentage distribution is as follows: (A) CA_Opt_B11 (7.8×10^{-3} mol) in which there are five clusters of particles of the following size classes, namely (a) 0.9649 to 1.294 nm (18 % of particles) with an 8.5 % maximum at 1.117 nm, (b) 4.187 nm (5.7 % of particles), (c) 50.75 to 58.77 nm (4.9 % of particles) with a 2.7 % maximum at 58.77 nm, (d) 122.4 to 164.2 nm (18.7 % of particles) with a 12.3 % maximum at 141.8 nm, and (e) 220.2 to 396.1 nm (57.7 % of particles) with a 17.4 % maximum at 255 nm; (B) CA_Opt_B12 (9.4×10^{-3} mol) in which there are three clusters of particles of the following size classes, namely (a) 10.1 to 11.7 nm (33.3 % of particles) with a 21.8 % maximum at 10.1 nm, (b) 164.2 nm (33.3 % of particles), and (c) 295.3 to 396.1 nm (33.3 % of particles) with a 23.2 % maximum at 342 nm; (C) CA_Opt_B13 (1.1×10^{-2} mol) in which there are four clusters of particles of the following size classes, namely (a) 0.6213 to 0.7195 nm (13.6 % of particles) with a 10.9 % maximum at 0.6213 nm, (b) 1.736 to 2.01 nm (10.1 % of particles) with a 6.1 % maximum at 1.736 nm, (c) 8.721 to 11.7 nm (7.6 % of particles) with a 5.7 % maximum at 10.1 nm, and (d) 141.8 to 342 nm (68.7 % of particles) with a 19.6 % maximum at 190.1 nm; (D) CA_Opt_B14 (1.2×10^{-2} mol) in which there are five clusters of particles of the following size classes, namely (a) 1.499 to 1.736 nm (11.3 % of particles) with a 7.2 % maximum at 1.736 nm, (b) 4.187 nm (2.6 % of particles), (c) 8.721 to 10.1 nm (7.1 % of particles) with a 3.7 % maximum at 8.721 nm, (d) 164.2 to 220.2 nm (56.9 % of particles) with a 26.2 % maximum at 164.2 nm, and (e) 295.3 to 342 nm (22.1 % of particles) with a 14.7 % maximum at 342 nm; and (E) CA_Opt_B15 (1.4×10^{-2} mol) in which there are five clusters of particles of the following size classes, namely (a) 4.187 to 4.849 nm (4.2 % of particles) with a 2.5 % maximum at 4.187 nm, (b) 6.503 to 8.721 nm (7.8 % of particles) with a 4.1 % maximum at 7.531 nm, (c) 78.82 to 122.4 nm (4.6 % of particles) with a 2 % maximum at 91.28 nm, (d) 220.2 to 295.3 nm (60.3 % of particles) with a 25.1 % maximum at 295.3 nm, and (e) 342 to 712.4 nm (23.1 % of particles) with a 7.4 % maximum at 531.2 nm.

Overall, the size distribution of particles for a-CDs were all sized below the upper limit for colloidal suspensions of 1000 nm. As with the temperature and reaction time studies for a-CDs, the majority of particles were of sizes within the intermediate size range of 100–1000 nm. Even though there is no clear trend observed and a-CDs seem to be insensitive to the number of moles of CA, there were some particles that were sized in the nano-range. Looking at the % distribution of particles in the nano-range (0–100 nm), the % of particles present in increasing

order are 14.9 % (CA_Opt_B15), 21 % (CA_Opt_B14), 28.6 % (CA_Opt_B11), 31.3 % (CA_Opt_B13), and 33.3 % (CA_Opt_B12). The % of particles within the nano-range was largest for the intermediate values of CA molar quantities of 9.4×10^{-3} mol (i.e., 1.8 g) and 1.1×10^{-2} mol (i.e., 2.1 g), which means that larger molar quantities of CA are not necessary and a-CDs can be produced with low to intermediate values of CA.

In Figure 57 below, the relative percentage of particles in each size class based on the intensity of light scattered is plotted as a function of the particle size distribution according to logarithmically spaced size classes, as obtained by the Malvern Zetasizer Nano ZS90.

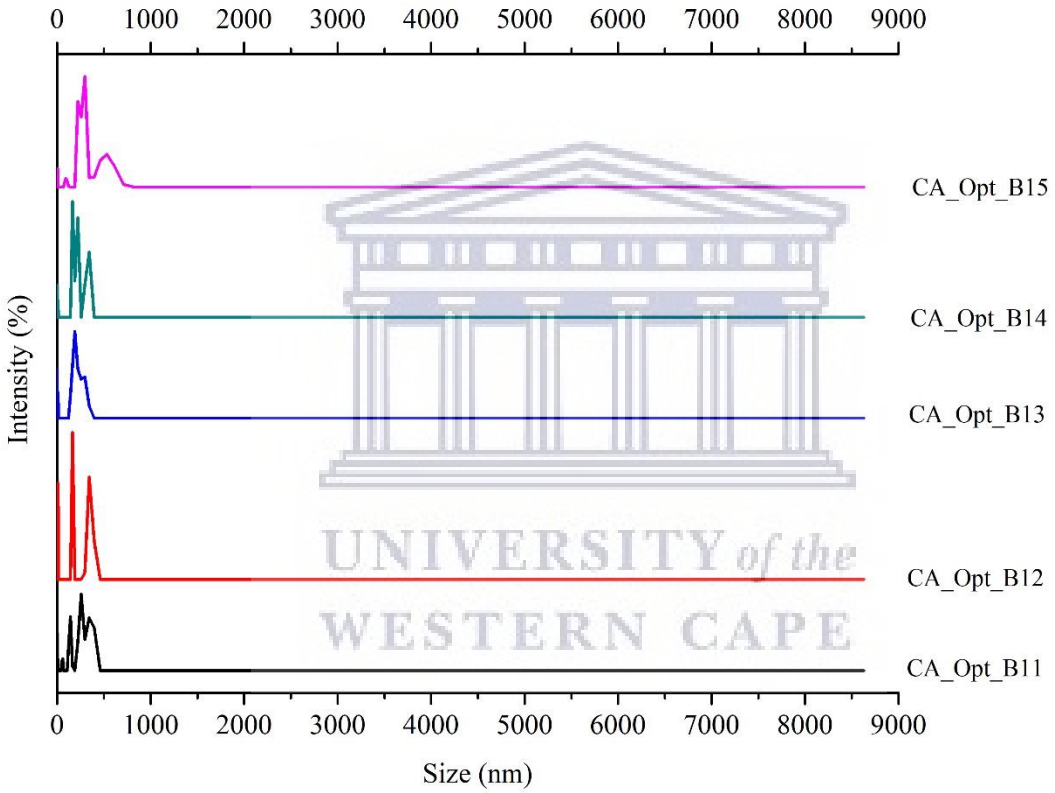

Figure 57. The particle size distribution of a-CDs by intensity with varied molar quantities of CA.

In Figure 57, the size distributions of a-CDs are displayed over the above-mentioned molar values of CA and expressed by intensity. Notice that all particles for all samples were smaller than the upper limit for colloidal particles of 1000 nm. However, CA_Opt_B13 displayed the narrowest size distribution which coincides with its slightly smaller PDI value of 0.994 and smaller average D_h of 863.5 nm. As previously mentioned, intermediate number of moles of CA yields particles that are smaller in size, that possess a narrower size distribution and larger number of particles sized within the nano-range. This provides slight control over particle size.

4.2.3.3. Summary

As previously mentioned, an increase in the number of moles of CA for the synthesis of a-CDs is expected to affect factors such as the burn-off percentage, carbonisation, band gap energy, and absorption intensity (Sutanto *et al* 2020). However, this study showed that a-CDs were relatively insensitive to increased number of moles of CA as no real optimum or correlation to the characteristic probed was found. As the number of moles of CA was increased from 7.8×10^{-3} to 1.4×10^{-2} mol, few parameters were affected, and no clear trends could be discerned in (a) the colour of the suspension of a-CDs, (b) the absorbance that slightly underwent a hypochromic effect, (c) the hydrodynamic diameter increased slightly, (d) the ZP remained positive and scattered, and (e) the overall size distribution of particles was very wide with most particles in larger size classes but smaller than the upper limit for colloidal material of 1000 nm. As stated before, increasing the number of moles of the carbon source in the reaction typically affects the overall rate of the reaction as more carbon would be available for carbonisation of hydrocarbon into the graphitic structure. However, no increase in % yield or no real effect was seen. Although agglomeration occurred, a-CDs displayed greater stability compared to the molar quantity study for the carbon source (Gly) for unfunctionalised CDs because a-CDs possessed particles that were sized within the nano-range due to the stability provided by the passivation agent (i.e., BPEI). The sample prepared with 1.1×10^{-2} mol (2.1 g) of CA had the highest % yield of 87.67 %, the smallest average hydrodynamic diameter of 863.5 nm, and the narrowest size distribution; therefore, it was chosen as the ideal molar quantity of CA for the synthesis of a-CDs. From this study, it is shown that a-CDs were adequately produced with intermediate number of moles of CA and does not require larger input of this particular reagent which inadvertently reduces the waste of reagent material.

4.2.4. Molar quantity optimisation of branched polyethylenimine for the synthesis of a-CDs

In this section, the results for the influence of the molar quantity of branched polyethylenimine (BPEI) on the colloidal stability of amine-capped carbon dots (a-CDs) are discussed. The samples were prepared according to the experimental procedure described in Section 3.3.8 in which a-CDs were prepared with the following molar quantity values of BPEI, namely: 7.9×10^{-3} mol (6 mL), 1.1×10^{-2} mol (8 mL), 1.3×10^{-2} mol (10 mL), 1.6×10^{-2} mol (12 mL), and 1.8×10^{-2} mol (14 mL) (molar quantity calculations presented in Appendix J). These were labelled BPEI_Opt_B16, BPEI_Opt_B17, BPEI_Opt_B18, BPEI_Opt_B19, and BPEI_Opt_B20, respectively. They were analysed to determine the ideal molar quantity of BPEI for effective synthesis of a-CDs. The following parameters remained fixed: (a) the concentration (1.3 mol.L^{-1}) of BPEI, (b) the concentration (0.01 mol.L^{-1}) and molar quantity (1.1×10^{-2} mol) of CA, (c) the synthesis temperature (170 °C), and (d) the reaction time (2 hours). The aim was to determine the ideal synthesis conditions for a-CDs and investigate the effect of the molar quantity of BPEI on (a) the % yield (calculated in Table 46 in Appendix), (b) the interaction of light with the a-CDs through UV-Vis spectroscopy, and (c) the hydrodynamic diameter, polydispersity index, and surface charge of a-CDs. Figure 58 below presents the % yield of the five samples prepared with increasing molar quantities of BPEI.

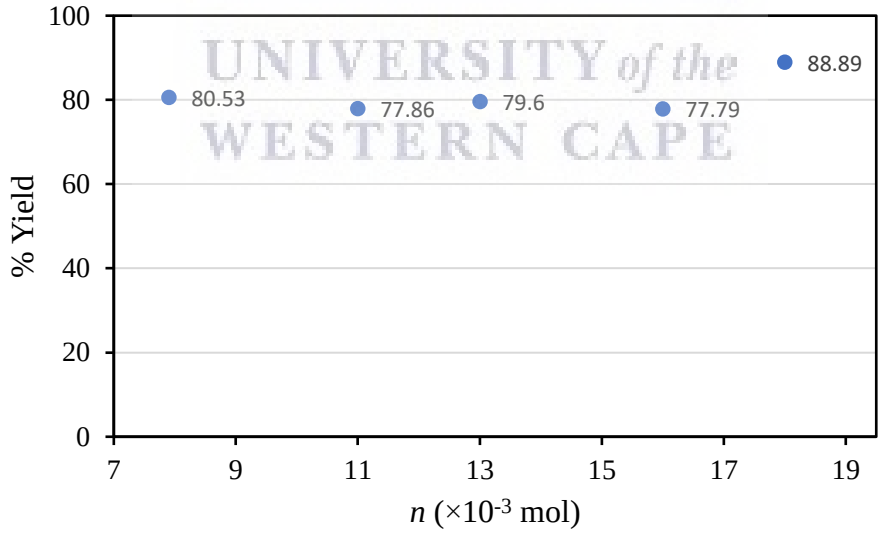

Figure 58. % Yield for the BPEI molar quantity optimisation study of a-CDs (synthesised at 170 °C for 2 hours).

According to the results in Figure 58 above, there was a slight overall increase in the % yield from 80.53 to 88.89 %, with a scatter in the data, as the molar quantity of BPEI was increased

from 7.9×10^{-3} to 1.8×10^{-2} mol. This is expected because there is an increase in the passivation or doping agent which increases the nitrogen content in the C-dot structure and increases particle stability. According to Zeng and co-workers, there is a direct relationship between the % yield and the amount of passivation agent (Zheng *et al* 2020). Their work suggests that the more passivated the surfaces of CDs are, the greater the stability and this causes an increase in the yield. Once more, the increase in reagent molecules leads to an increased frequency of collisions to effectively accelerate the process of carbonisation (Bewick *et al* 2019). See the effect of an increase in the molar quantity of BPEI on the colour of the product in normal lighting (Figure 59). There is correlation between the colour intensity and the % yield; the higher the % yield the more intense the yellow colour of the a-CDs. Notice that in Figure 59e the large volume of BPEI of 14 mL might be in excess.

Figure 59. The effect of BPEI molar quantity on the colour of a-CDs; varied as follows: (a) 7.9×10^{-3} mol (BPEI_Opt_B16), (b) 1.1×10^{-2} mol (BPEI_Opt_B17), (c) 1.3×10^{-2} mol (BPEI_Opt_B18), (d) 1.6×10^{-2} mol (BPEI_Opt_B19), and (e) 1.8×10^{-2} mol (BPEI_Opt_B20).

4.2.4.1. Absorbance study through ultraviolet-visible spectroscopy

The absorbance of a-CDs was analysed using UV-Vis spectroscopy (as described in Section 3.8.1) to qualitatively determine whether a-CDs were produced and to understand the effect of the molar quantity of BPEI on the absorbance of a-CDs. The above-mentioned five samples, for the molar optimisation study of BPEI, were studied. The absorbance data, i.e., the maximum absorption peaks with their respective absorbances are tabulated in Table 18 below and the absorbance spectra are shown in Figure 60.

Table 18. The absorbance values for the BPEI molar quantity optimisation study of a-CDs (synthesised at 170 °C for 2 hours) with respect to their wavelengths.

Sample code	***λ_{max} (nm)***	***Absorbance***
BPEI_Opt_B16	353	0.0181
BPEI_Opt_B17	353	0.0132
BPEI_Opt_B18	357	0.0264
BPEI_Opt_B19	362	0.0290
BPEI_Opt_B20	367	0.0362

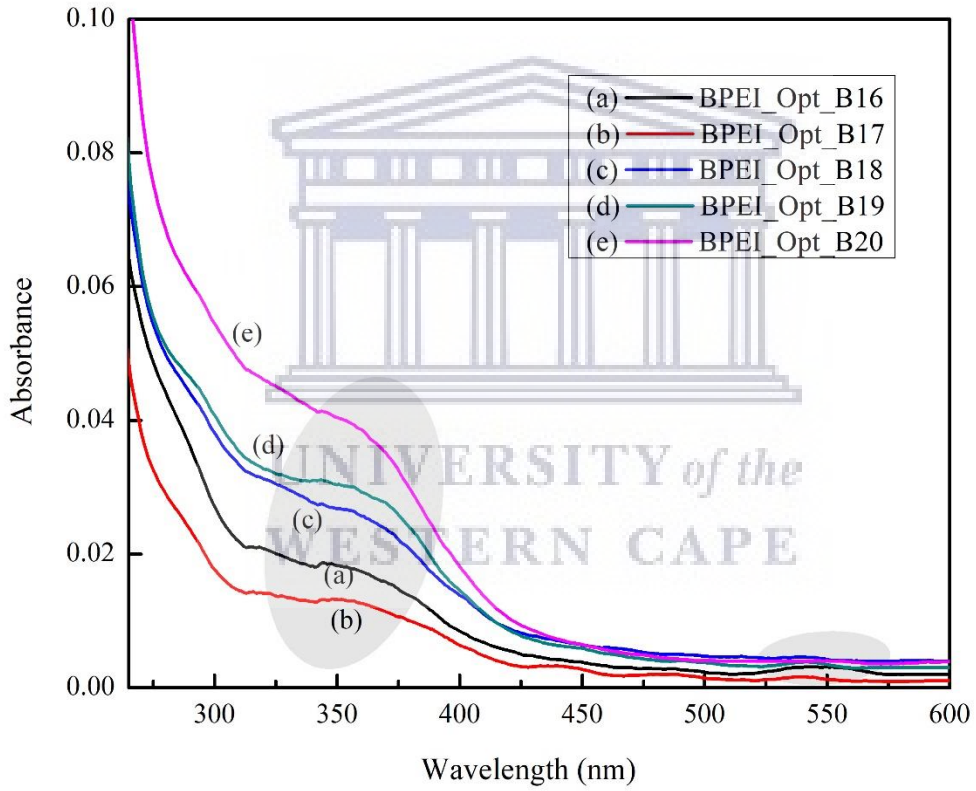

Figure 60. Ultraviolet-visible spectra for amine-capped carbon dots (a-CDs) (synthesised for 2 hours at 170 °C) with increasing molar quantities of BPEI as follows: (a) 7.9×10^{-3} mol (BPEI_Opt_B16), (b) 1.1×10^{-2} mol (BPEI_Opt_B17), (c) 1.3×10^{-2} mol (BPEI_Opt_B18), (d) 1.6×10^{-2} mol (BPEI_Opt_B19), and (e) 1.8×10^{-2} mol (BPEI_Opt_B20).

In Figure 60, the absorption spectra of all prepared a-CDs display a prominent band at ~ 350 nm, a weak shoulder at longer wavelengths (~ 550 nm) and strong absorption below 270 nm, which is in accordance to results found in literature (Zheng *et al* 2014, Bhattacharyya *et al*

2017, Bayati *et al* 2018). Corroborated in previous studies, the prominent band is typical for CDs and is generally assigned to the π–π* transitions of the conjugated C=C bands (Bhattacharyya *et al* 2017, Manioudakis *et al* 2019, Pang *et al* 2017, Zheng *et al* 2014). As the nitrogen content was increased from 7.9×10^{-3} to 1.8×10^{-2} mol, a hyperchromic effect (i.e., an increase in absorbance intensity) from 0.0181 to 0.0362 is observed as tabulated in Table 18. A bathochromic effect (i.e., a red shift) in the absorption band of a-CDs from 353 to 367 nm occurred with an increase in the number of moles of BPEI and according to literature could be attributed to the presence of amide and amine groups on the surface of a-CDs as well as phase fluctuation of amorphous sp^3 (Bhattacharyya *et al* 2017). As stated before, the absorbance peak of a-CDs is found at a longer wavelength compared to that of unfunctionalised CDs which was around 260 nm due to amine ($–NH_2$) groups that exist on the surface of a-CDs (Emam *et al* 2017). Compared to other applied parameters on a-CDs, the number of moles of BPEI had the greatest influence on the absorbance of a-CDs; finally, a trend is seen in λ_{max}, i.e., a shift towards longer wavelengths and an increase in absorbance. For further comparisons, see the conclusions drawn at the end of this Section on page 156.

4.2.4.2. Hydrodynamic properties – Zetasizer

The above-mentioned a-CDs, prepared with different molar quantities of BPEI, were characterised to obtain size measurements through Dynamic Light Scattering (DLS) and zeta potential measurements through Laser Doppler Velocimetry (LDV) by the Malvern Zetasizer Nano ZS90 (see Section 3.8.2 for experimental procedure). In order to determine the ideal molar quantity of BPEI for effective synthesis of a-CDs the hydrodynamic properties of a-CDs were studied; to understand the effect of the molar quantity of BPEI on the average hydrodynamic diameter (D_h/Z-Ave), particle dispersity index (PDI), and zeta-potential (ZP) as tabulated in Table 19. The D_h, PDI, and ZP are plotted as functions of the number of moles of BPEI in Figure 61 below.

Table 19. Results for the hydrodynamic diameter, particle dispersity, and zeta potential of a-CDs for the BPEI molar quantity optimisation study.

Sample code	***Z-Ave (nm)***	***PDI***	***ZP (mV)***
BPEI_Opt_B16	1207	1.000	+0.981
BPEI_Opt_B17	1073	1.000	+0.449
BPEI_Opt_B18	932.2	0.922	−0.181
BPEI_Opt_B19	1447	0.953	+0.897
BPEI_Opt_B20	1181	0.985	+0.252

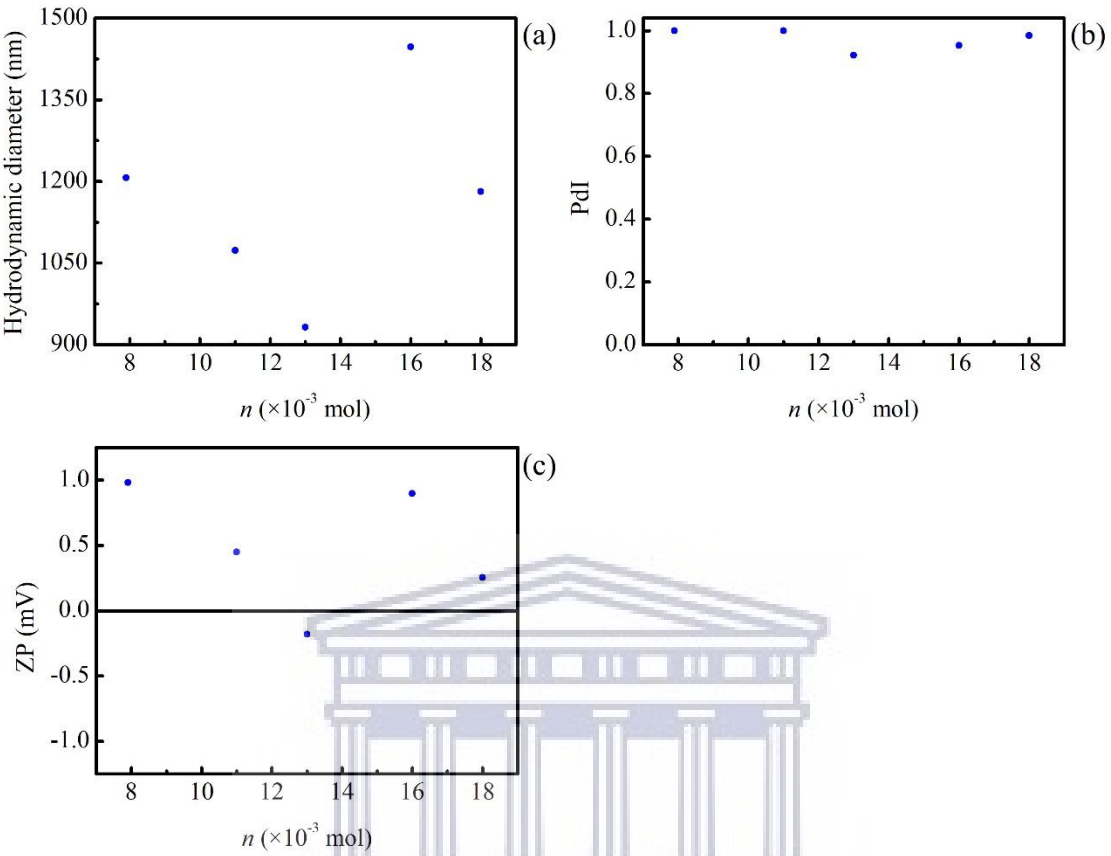

Figure 61. (a) Hydrodynamic diameter, (b) polydispersity index and (c) zeta potential over a range of BPEI molar quantities for the synthesis of amine-capped CDs.

In Figure 61a, there was a scatter in the hydrodynamic diameter (D_h) of a-CDs from 1207 nm for 7.9×10^{-3} mol of BPEI to 1181 nm for 1.8×10^{-2} mol of BPEI. The sample prepared with 1.3×10^{-2} mol (10 mL) of BPEI displayed the smallest D_h (i.e., the smallest reported average particle size) and, hence, is the molar quantity at which a-CDs showed the greatest colloidal stability. These values correspond greatly with the ZP values seen in Figure 61b; the smaller the Dh, the more negative the ZP with the most negative a-CD surface of −0.181 mV. Overall, these particles have undergone agglomeration with the formation of permanent associations (as discussed in Section 4.1.1.3).

The second parameter under investigation was the PDI of a-CDs over the above-mentioned molar quantities of BPEI (Figure 61b). PDI is displayed as a function of the number of moles of BPEI, and, as previously specified: the lower the PDI, the more monodisperse the particles are which translates to narrow size distributions. However, the PDIs of a-CDs, prepared with an increasing number of moles of BPEI, displayed very broad size distributions which means

that the particles were more polydisperse with very high PDIs between 0.9 and 1 and further speaks to the large-sized particles they contain. The sample prepared with 1.3×10^{-2} mol of BPEI displayed the lowest PDI of all a-CD samples and thus had the narrowest size distribution of all five samples. Granted, these PDI values are large but that only speaks to the magnitude of the size distribution, whereas Figure 62 provides more information on the size classes found in each sample.

Another important characteristic under investigation was the ZP of a-CDs at various molar quantities of BPEI as obtained through Laser Doppler Velocimetry (LDV). ZP was plotted as a function of the number of moles of BPEI (Figure 61c). The ZP values were slightly sensitive to changes in nitrogen content and it can be assumed that the smaller and more monodisperse the particles were, the more negative the zeta potential (as mentioned above). And, once again, according to Verwey, an overall deduction can be made that van der Waals attraction dominated due to a low potential barrier causing coagulation (Verwey 1947).

Furthermore, the size distributions of a-CDs are displayed over the above-mentioned range of molar quantities of BPEI expressed in number (Figure 62) and intensity (Figure 63) as determined with a Malvern Zetasizer Nano ZS90. Once again, the objective was to examine the distribution of particles by determining the relative amounts (%) of particles found in each size range essential in understanding physical and chemical properties of a-CDs synthesised with an increasing number of moles of BPEI.

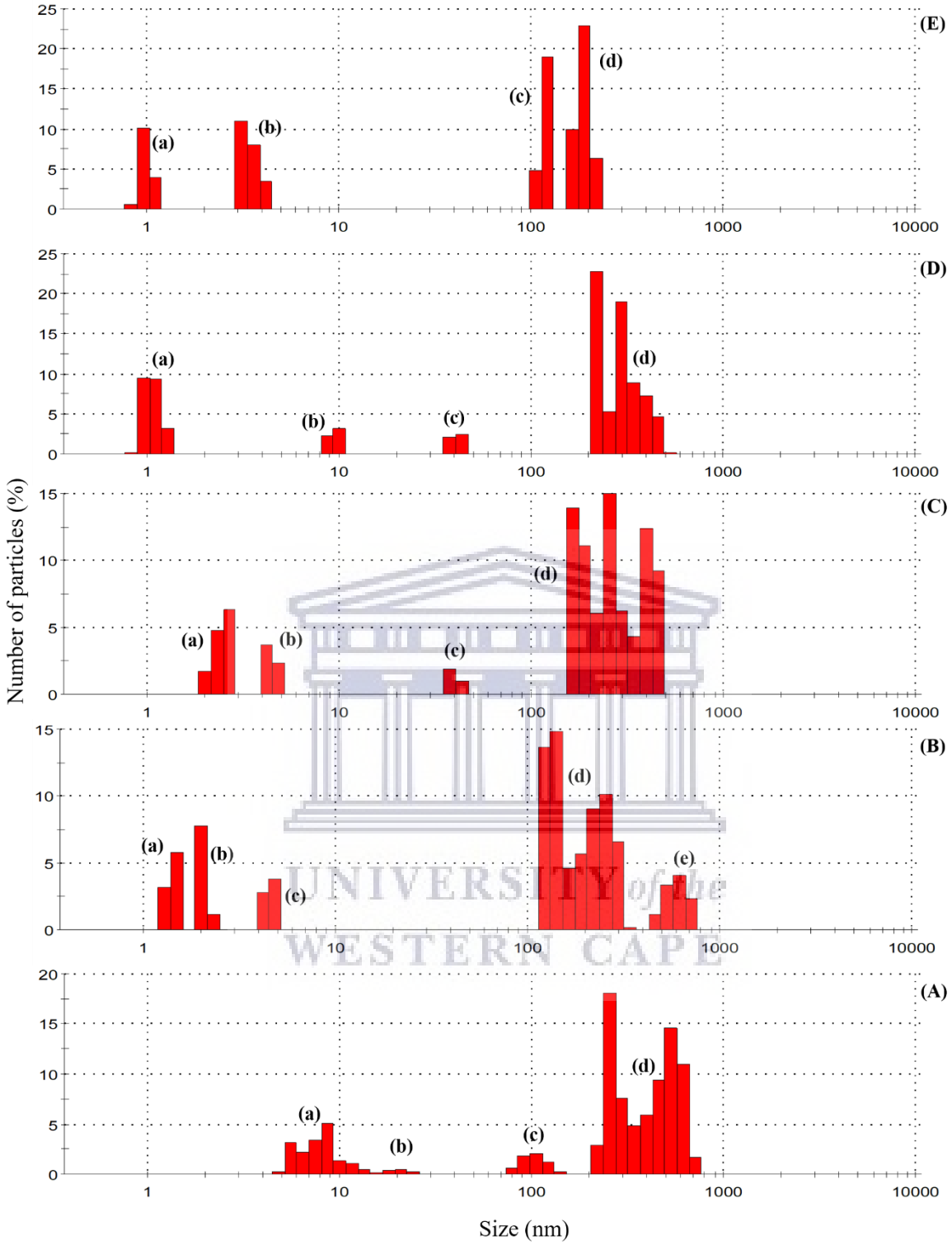

Figure 62. Particle size distribution of amine-capped CDs in the molar quantity optimisation study of BPEI with the numbers of particles present in each size class for (A) 7.9×10^{-3} mol (BPEI_Opt_B16), (B) 1.1×10^{-2} mol (BPEI_Opt_B17), (C) 1.3×10^{-2} mol (BPEI_Opt_B18), (D) 1.6×10^{-2} mol (BPEI_Opt_B19), and (E) 1.8×10^{-2} mol (BPEI_Opt_B20).

The histograms in Figure 62 above show the relative percentage of particles in each size class (logarithmically spaced) based on the intensity of light scattered as a function of the particle

size distribution of a-CDs. The percentage distribution is as follows: (A) BPEI_Opt_B16 (7.9×10^{-3} mol) in which there are four clusters of particles of the following size classes, namely (a) 4.849 to 13.54 nm (17 % of particles) with a 5.1 % maximum at 8.721 nm, (b) 15.69 to 24.36 nm (1.2 % of particles) with a 0.5 % maximum at 21.04 nm, (c) 78.82 to 141.8 nm (5.9 % of particles) with a 2.1 % maximum at 105.7 nm, and (d) 220.2 to 712.4 nm (75.9 % of particles) with a 18.1 % maximum at 255 nm; (B) BPEI_Opt_B17 (1.1×10^{-2} mol) in which there are five clusters of particles of the following size classes, namely (a) 1.294 to 1.499 nm (8.8 % of particles) with an 5.7 % maximum at 1.499 nm, (b) 2.010 to 2.328 nm (9 % of particles) with an 7.8 % maximum at 2.010 nm, (c) 4.187 to 4.849 nm (6.6 % of particles) with a 3.8 % maximum at 4.849 nm, (d) 122.4 to 342 nm (64.7 % of particles) with a 14.8 % maximum at 141.8 nm, and (e) 458.7 to 712.4 nm (10.9 % of particles) with a 4.1 % maximum at 615.1 nm; (C) BPEI_Opt_B18 (1.3×10^{-2} mol) in which there are four clusters of particles of the following size classes, namely (a) 2.01 to 2.696 nm (12.9 % of particles) with a 6.3 % maximum at 2.696 nm, (b) 4.187 to 4.849 nm (6.1 % of particles) with a 3.7 % maximum at 4.187 nm, (c) 37.84 to 43.82 nm (2.9 % of particles) with a 1.9 % maximum at 37.84 nm, and (d) 164.2 to 458.7 nm (78.1 % of particles) with a 15 % maximum at 255 nm; (D) BPEI_Opt_B19 (1.6×10^{-2} mol) in which there are four clusters of particles of the following size classes, namely (a) 0.8332 to 1.294 nm (22.1 % of particles) with a 9.5 % maximum at 0.9649 nm, (b) 8.721 to 10.10 nm (5.4 % of particles) with a 3.2 % maximum at 10.10 nm, (c) 37.84 to 43.82 nm (4.6 % of particles) with a 2.5 % maximum at 43.82 nm, and (d) 220.2 to 531.2 nm (67.9 % of particles) with a 22.7 % maximum at 220.2 nm; and (E) BPEI_Opt_B20 (1.8×10^{-2} mol) in which there are four clusters of particles of the following size classes, namely (a) 0.8332 to 1.117 nm (14.7 % of particles) with a 10.1 % maximum at 0.9649 nm, (b) 3.122 to 4.187 nm (22.4 % of particles) with an 11 % maximum at 3.122 nm, (c) 105.7 to 122.4 nm (23.8 % of particles) with a 19 % maximum at 122.4 nm, and (d) 164.2 to 220.2 nm (39.1 % of particles) with a 22.8 % maximum at 190.1 nm.

Once again, the overall size distribution of particles for a-CDs were all sized below the upper limit for colloidal suspensions of 1000 nm. As with the temperature and reaction time studies for a-CDs, the majority of particles were of sizes between 100 nm (the upper limit for the nano-range) and 1000 nm. Looking at the % distribution of particles in the nano-range (0–100 nm), the % of particles present in increasing order is as follows: 20.6 % (BPEI_Opt_B16), 21.9 % (BPEI _Opt_B18), 24.4 % (BPEI _Opt_B17), 32.1 % (BPEI _Opt_B19), and 37.1 % (BPEI _Opt_B20). There was an overall increase in the % of particles within the nano-range as the

molar quantity of BPEI increased from 7.9×10^{-3} to 1.8×10^{-2} mol. Even though the % of NPs increased with an increase in the number of moles of BPEI, larger quantities thereof are not necessary for effective production of a-CDs, which obeys green chemistry principles to reduce wastage of reagent materials.

In Figure 63 below, the relative percentage of particles in each size class based on the intensity of light scattered is plotted as a function of the particle size distribution according to logarithmically spaced size classes, as obtained by the Malvern Zetasizer Nano ZS90.

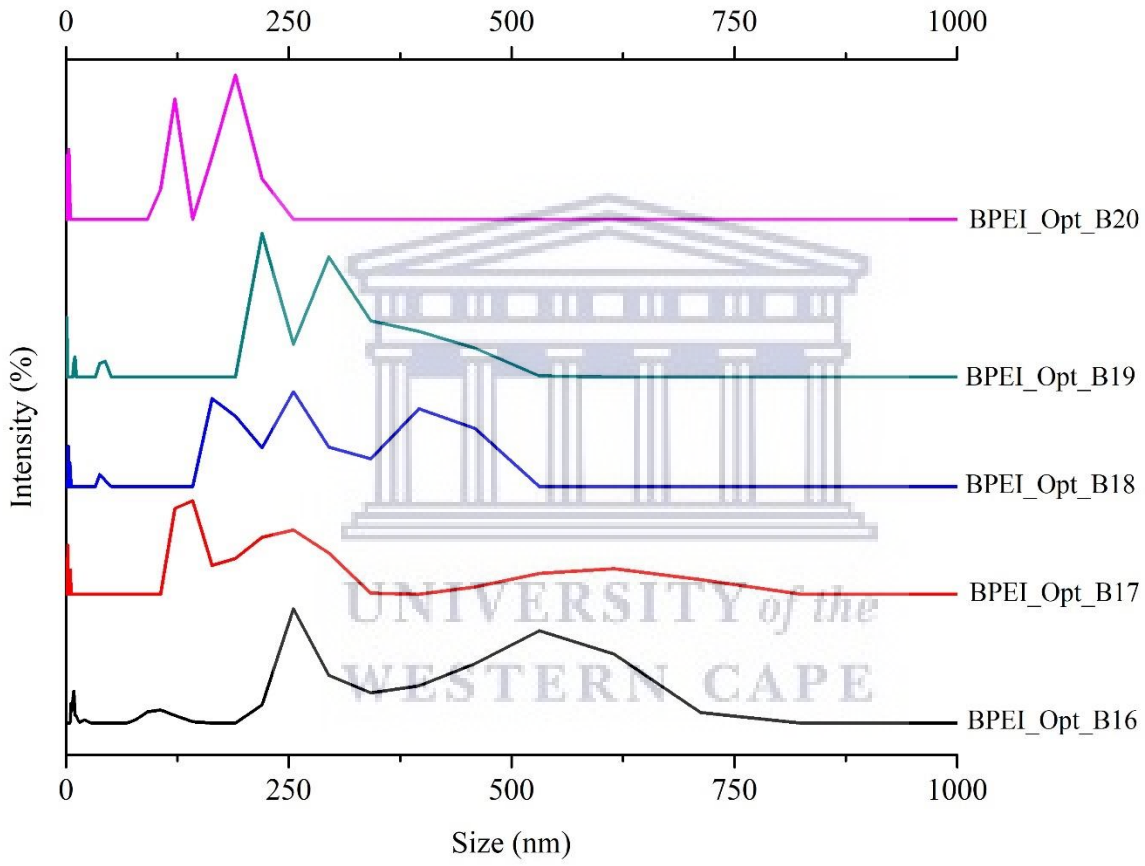

Figure 63. The particle size distribution of a-CDs by intensity with varied molar quantities of BPEI.

In Figure 63, the size distributions of a-CDs are displayed over the above-mentioned molar quantities of BPEI and expressed by intensity. Notice that all particles for all samples were, once again, smaller than the upper limit for colloidal particles of 1000 nm. Even though BPEI_Opt_B20 displayed the narrowest size distribution, excessive amounts of BPEI are not necessary for effective production of a-CDs because adequate amounts of a-CDs are produced with smaller number of moles of BPEI. Also notice in Figure 62 that 14.7 % of particles in the

nano-range for BPEI_Opt_B20 were sized between 0.8332 to 1.117 nm which could be attributed to the presence of excess reagent molecules. This means that a-CDs were effectively produced with smaller amounts of BPEI and the larger quantities used for BPEI_Opt_B19 and BPEI_Opt_B20 largely comprised of excess reagent material.

4.2.4.3. Summary

A-CDs proved to be relatively insensitive to the influence of the molar quantity of BPEI. As the number of moles of BPEI was increased from 7.9×10^{-3} to 1.8×10^{-2} mol, some characteristics were affected, such as (a) the absorbance that underwent a hypochromic effect and a red-shift towards longer wavelengths, (b) the hydrodynamic diameter which scattered, (c) the ZP that scattered, and (d) the overall size distribution of particles that was very wide with most particles in larger size classes but smaller than the upper limit for colloidal material of 1000 nm. It can be deduced that as the number of moles of BPEI was increased, the size of particles decreased and became more stable; this led to a-CDs of a deeper yellow colour. Typically, an increase in the number of moles of the passivation agent in the reaction affects the overall rate of the reaction as more nitrogen content is available to induce greater colloidal stability. Although agglomeration occurred, a-CDs displayed greater stability compared to unfunctionalised CDs due to the presence of particles in the nano-range and the stability provided by the passivation agent (i.e., BPEI). It can be deduced that an increase in the number of moles of BPEI towards intermediate molar quantity values of BPEI of about 1.3×10^{-2} mol (10 mL) shows that particles tend to become smaller with more negative surfaces, and that they are larger at molar quantities above this point, meaning that excess BPEI is not necessary for effective production of a-CDs. This is evident by the number of particles sized within the nano-range in which excess reagent molecules are present for a-CDs produced with larger number of moles of BPEI, i.e., 1.6×10^{-2} mol and 1.8×10^{-2} mol for BPEI_Opt_B19 and BPEI_Opt_B20, respectively. Therefore, the sample prepared with 1.3×10^{-2} mol (10 mL) of BPEI with the smallest average hydrodynamic diameter, most negative ZP and the narrowest size distribution was chosen as the ideal molar quantity of BPEI for effective/adequate synthesis of a-CDs.

4.2.5. Comparative summary of applied parameters in synthesis of a-CDs

In order to compare the effect of each applied parameter on the characteristics of a-CDs, the following table provides a detailed description of trends observed or the lack thereof. Table 20 serves to compare eight crucial characteristics that were studied with each applied synthesis parameter, i.e., % yield, colour of product, mass of dialysis bag, absorbance, hydrodynamic diameter, polydispersity index, surface charge, and size distribution by number and intensity.

Table 20. Comparative characteristics of a-CDs.

Product characteristic	***Temperature study***	***Reaction-time study***	***Molar quantity study of 10 mM CA***	***Molar quantity study of BPEI***
% Yield	No trend and no sensitivity All values between 76–86 %	No trend and no sensitivity All values between 78–84 %	No trend and some sensitivity for samples of lowest three molar quantities of CA slight increase from 78 to 87 % All values between 78–88 %	No trend and no sensitivity All values between 77–89 %
Colour of product	Intensified from light yellow to dark yellow	Intensified from light yellow to dark yellow	Intensified from light yellow to dark yellow for first three samples of lowest molar quantities of CA but then gets lighter and darker again Irregular colour pattern	Intensified from light yellow to dark yellow
Dialysis (see Appendix for results)	Initial increase due to osmotic flow into dialysis bag Constant mass reached after 30 hours with the exception of samples prepared at 130	Initial increase due to osmotic flow into dialysis bag Somewhat constant mass reached after 40 hours	Initial increase due to osmotic flow into dialysis bag then a gradual decrease	Initial increase due to osmotic flow into dialysis bag then a gradual decrease

	°C and 170 °C which continued to decrease gradually			
Absorbance	No clear trend Hyperchromic effect from 0.027 to 0.040 and Hypochromic effect to 0.032 followed by Hyperchromic effect to 0.051 No shift in wavelength	Irregularity; no clear trend Hypochromic effect from 0.037 to 0.029 and Hyperchromic effect to 0.032 followed by Hypochromic effect to 0.033 Initial red-shift, then blue-shift and last red-shift	Hypochromic effect from 0.012 to 0.003 Overall red-shift	Initial hypochromic effect from 0.0181 to 0.0132 and Hyperchromic effect to 0.0362 Red-shift
D_h	Increase in hydrodynamic diameter as temperature increased from 130 °C to 210 °C with exception of slight decrease for sample prepared at 190 °C Smallest D_h at 130 °C of 570.9 nm	Very large particle sizes with the smallest size of 518.8 nm for sample prepared in 2.5 hours	Large particle sizes above 1000 nm with the smallest size of 863.5 nm for sample prepared with 1.1×10^{-2} mol (intermediate molar quantity of CA)	Large particle sizes above 1000 nm with the smallest size of 932.2 nm for sample prepared with 1.3×10^{-2} mol (intermediate molar quantity of BPEI)
PDI	Highly polydisperse and wide size distributions No clear effect	Very wide size distributions No particular trend Largely polydisperse	More monodisperse for smaller number of moles of CA PDIs increase, hence, polydispersity increases as the number of moles of CA increased	Very wide size distributions No particular trend Largely polydisperse

ZP	Became more positive with most negative value for sample prepared at 130 °C with ZP of −3.36 mV	Practically unchanged All positive surfaces throughout	Became more positive; most negative (−0.737 mV) for smallest number of moles of CA	Initially, became more negative with only negative value of −0.181 mV for sample prepared with 1.3×10^{-2} mol (intermediate molar quantity of BPEI). Positive surfaces for lower and higher molar quantities of BPEI
Size distribution by number & intensity	By number All particles sized below 1000 nm which is the upper limit for colloidal suspensions with majority thereof of intermediate sizes between 100–1000 nm By intensity Greater degree of monodispersity towards smaller sizes	By number All particles sized below 1000 nm which is the upper limit for colloidal suspensions with majority thereof of intermediate sizes between 100–1000 nm By intensity Large degree of polydispersity	By number All particles sized below 1000 nm which is the upper limit for colloidal suspensions with majority thereof of intermediate sizes between 100–1000 nm By intensity Greater degree of monodispersity towards smaller sizes	By number All particles sized below 1000 nm which is the upper limit for colloidal suspensions with majority thereof of intermediate sizes between 100–1000 nm By intensity Greater degree of monodispersity towards smaller sizes

The first characteristic under study was the % yield of a-CDs under the influence of the applied parameters. Throughout all studies (temperature, reaction time, number of moles of CA, and number of moles of BPEI) the % yield remained high between 76–90 % and no specific trends were observed with the exception of the influence of the number of moles of CA, in which some sensitivity, i.e., an increase in % yield from 78–87 %, was observed for the samples prepared with the lowest three molar quantities of CA, i.e., 7.8×10^{-3} to 1.1×10^{-2} mol. Therefore, of all the applied parameters, the increase in the number of moles of CA had the greatest influence on the % yield.

The second characteristic under observation was the colour intensity of the produced a-CDs. Throughout all four studies, mentioned above, the colour of the suspension intensified from light to dark yellow. The colour intensity somehow is a reflection of the % yield and was more intense the larger the % yield. Once again, the number of moles of CA had a slightly different effect on the % yield because an irregular colour pattern was observed. This shows that the colour of a-CDs followed the same trend throughout with some instability under the influence of an increased number of moles of CA. The colour intensity of the suspension of a-CDs is not a characteristic that one necessarily seeks out to alter but it could be a good indication/reflection of trends observed for other characteristics, such as the % yield, particle size, etc.

The mass of dialysis bag for every sample in each study was monitored for the sole purpose of determining the effectiveness of purification, which is typically expected when a constant mass and pH is reached. Throughout all four synthesis parameter studies performed on a-CDs, there was an initial increase in the mass of each dialysis bag due to osmotic flow into the membrane which was followed by a gradual decrease until a constant mass was reached that occurred after about 30–40 hours.

Another characteristic under study was the absorbance of a-CDs. Throughout all studies absorbance was measured to obtain qualitative information such as whether a-CDs were produced (as determined by absorbance at a specific wavelength of ~280 nm), whether there is a shift in absorbance towards longer or shorter wavelengths, and if there is an increase or decrease in absorbance. For an increase in temperature and reaction time, an irregular pattern, i.e., fluctuations in absorbance, is observed which means that there is no clear trend. However, in the cases of an increase in CA and BPEI, an overall red shift, i.e., a shift of λ_{max} towards longer wavelengths, is observed. Also, a contrast in absorbance intensity; a hypochromic effect is observed with an increase in the number of moles of the carbon source, CA, and a hyperchromic effect is observed with an increase in the number of moles of the passivation agent, BPEI. In order to have control over size, a red-shift, i.e., a shift of λ_{max} towards longer wavelengths, is desired. One would want to adhere to the green chemistry principles as far as possible for the effective synthesis of small NPs which means the minimal use of (a) reagents and (b) harsh synthesis conditions such as high temperature and longer reaction times. A red-shift means that the band gap energy is smaller and particle size increases with an increase in temperature, reaction-time, and reagent. The influence of CA and BPEI had better control over absorbance, because in both studies specific trends were observed.

The next characteristic under study was the hydrodynamic diameter of a-CDs. Overall, the hydrodynamic diameter of a-CDs, under the influence of the above-mentioned applied synthesis parameters, is scattered and no specific trend was observed; except for the temperature study in which an increase in D_h is observed with an increase in temperature. Typically, a smaller particle size is desired as it shows greater stability; however, the average particle sizes of a-CDs were very large (above the upper limit for colloidal suspensions of 1000 nm), with the smallest D_hs in increasing order: (a) 518.8 nm for the sample prepared within 2.5 hours in the reaction-time study, (b) 570.9 nm for the sample prepared at 130 °C in the temp. study, (c) 863.5 nm for the sample prepared with 1.1×10^{-2} mol of CA (intermediate molar quantity of CA) in the CA study, and (d) 932.2 nm for the sample prepared with 1.3×10^{-2} mol of BPEI (intermediate molar quantity of BPEI) in the BPEI study. Even though the smallest average particle size was observed for the reaction-time study, temperature provided better control over size as it was the only study in which a trend was observed.

Another characteristic under study was the PDI of a-CDs which is an indication of the dispersity of particles; a high PDI (above 0.5) indicates that a sample is more polydisperse and has a very wide size distribution whereas a small PDI (below 0.5) indicated that a sample is more monodisperse with a narrow size distribution. This value needs to be considered with further size distribution data that provides more insight into the size classes present in a sample. Nevertheless, looking at the overall particle dispersity of a-CDs, it presented very polydisperse samples with very wide size distributions with negligible control achieved. Therefore, none of the applied synthesis parameters displayed good control over the PDI; however, a slight increase in PDI is observed with an increase in temperature.

The zeta-potential or surface charge of a-CDs was another characteristic under study of the applied synthesis parameters. Typically, the larger the particle size, the more positive the ZP, which was observed throughout all studies. With that said, a-CDs either possessed positive surfaces throughout or became more positive under certain conditions, such as with an increase in temperature, for samples prepared with smaller number of moles of CA, and for smaller and larger molar quantities of BPEI. According to Peng and Travas-Sejdic, the more positive surface charge is an indication of the conversion of carboxylic acid groups to amide groups (Peng and Travas-Sejdic 2009). Temperature provided the best control over ZP as it was the only parameter for which there was a trend.

Lastly, the size distribution was studied by number and intensity and provided vital information regarding the size classes of a-CDs. For all synthesis parameter studies, all particles of a-CDs were sized below the upper limit for colloidal suspensions of 1000 nm with majority thereof of intermediate sizes between 100–1000 nm, and between 20–30 % of particles sized within the nano-range (0–100 nm). For the temperature study and the two molar quantity studies, i.e., for CA and BPEI, there was a greater degree of monodispersity towards smaller sizes; whereas for the reaction time study, a-CDs showed a large degree of polydispersity.

4.3. Comparison between CDs and a-CDs – the effects of applied synthesis parameters

When comparing unfunctionalised CDs and amine-capped CDs, it is of great importance to remember that these two types of carbon-based nanomaterials underwent different synthesis routes with dissimilar reagent materials. Granted, there were similarities between the two procedures—both required a carbon source and underwent some kind of heating procedure. However, the main difference between the two was that the latter possessed a protective layer or a capping of amine groups on its surface. The expectation is that the capping would lend greater stability to a-CDs compared to unfunctionalised CDs, hence the importance of examining their behaviour or characteristics under the influence of several synthesis parameters.

4.3.1. % yield

The % yield of unfunctionalised CDs was mostly influenced by power, as it decreased from 96.62 to 4.34 %. To a smaller degree it was also influenced by reaction time, with a decrease from 32.41 to 2.76 %; and by the molar quantity of 70 % w/w Gly, in which a positive correlation (i.e., an increase from 10.33 to 30.05 %) was observed due to the larger amount of carbon source available for effective collisions between reagent molecules leading to an increased production of CDs. However, the molar quantity of NaH_2PO_4 had a negligible effect on the % yield of CDs. On the other hand, the % yield of a-CDs remained high between 76–90 % and no specific trends were observed throughout all synthesis parameter studies, except for some sensitivity for lower molar quantities of CA. Therefore, an increase in the number of moles of CA had the greatest influence on the % yield of a-CDs.

4.3.2. Colour

Due to drastically different synthesis routes of CDs and a-CDs, CDs were recognised by the formation of a brown coloured suspension, whereas the effective synthesis of a-CDs was observed by the formation of a yellow-coloured suspension. Overall, the colour intensity of

CDs was fairly sensitive to all applied parameters; however, it was most intense for CDs produced at higher power levels, longer reaction times, smallest number of moles of Gly and largest number of moles of NaH_2PO_4. On the other hand, the colour intensity of a-CDs intensified from light to dark yellow throughout all studies, with some irregularity seen under the influence of the number of moles of CA, and somehow reflected the % yield, meaning that it was more intense the larger the % yield. Granted, a high colour intensity does not necessarily translate to the most desired size, yield, or surface charge; however, as previously mentioned, it could be a good indication of trends observed for other characteristics, such as the % yield, particle size, etc.

4.3.3. Dialysis

The mass of dialysis bag for every sample in each study was monitored for the sole purpose of determining the effectiveness of purification, which is typically expected when a constant mass and pH is reached. Throughout all studies performed on both CDs and a-CDs, there was an initial increase in the mass of each dialysis bag due to osmotic flow into the membrane which was followed by a gradual decrease until a constant mass was reached that occurred after about 30–40 hours.

4.3.4. Absorbance

In order to have control over size, a red-shift, i.e., a shift of λ_{max} towards longer wavelengths, is desired. One would want to adhere to the green chemistry principles as far as possible for the effective synthesis of small NPs with the minimal use of reagents and refraining from harsh synthesis conditions such as high temperature and longer reaction times. A red-shift means that the band gap energy is smaller and particle size increases with the applied parameter.

Under the influence of power and temperature, the desire is to avoid synthesis routes that require high power or temperature input, while still effectively producing CDs and a-CDs. Therefore, high absorbance at low power/temperature along with a red shift in λ_{max} would be ideal. In the case of CDs, a hyperchromic effect (i.e., an increase in absorbance) and a red shift (i.e., a shift in λ_{max} towards longer wavelengths) was observed for the power study; whereas for a-CDs, an irregular pattern, i.e., fluctuations in absorbance, was observed with no clear trend and no shift in λ_{max} occurred. This means that under the influence of power/temperature,

the absorbance of unfunctionalised CDs was easier to control, whereas that of a-CDs were relatively unchanged, meaning that a-CDs showed greater stability.

Under the influence of reaction time, the desire is to adhere to green chemistry principles by avoiding synthesis routes that require longer reaction times, while still adequately producing CDs and a-CDs. Therefore, high absorbance at shorter reaction times would be ideal with a red shift in λ_{max}. In the case of CDs, a hyperchromic effect and a red shift from 260 to 265 nm was observed; whereas a-CDs, once again, displayed fluctuations in absorbance with an overall red shift in λ_{max} from 280 nm for the sample prepared within 1 hour to 283 nm for the one produced in 3 hours. This means that for both CDs and a-CDs smaller particle sizes are expected to be found at shorter reaction times. However, unfunctionalised CDs were more sensitive to the change in reaction time due to the 5-nm shift in absorbance as compared to the 3-nm overall shift for a-CDs, granted, one needs to keep in mind that different synthesis routes were undertaken. Once again, a-CDs displayed superior stability compared to unfunctionalised CDs.

Under the influence of the carbon source, the desire is to avoid synthesis routes that require larger quantities thereof, while still adequately producing CDs and a-CDs. Therefore, high absorbance at smaller molar quantities of the carbon source would be ideal with a red shift in λ_{max}. In the case of CDs, a hypochromic effect (i.e., a decrease in absorbance) occurred with an increase in the number of moles of Gly, meaning that at lower molar quantities of Gly a higher absorbance was observed. Also, a blue shift (i.e., a shift in λ_{max} towards shorter wavelengths) is observed with an increase in the number of moles of Gly, meaning that larger particle sizes are expected for samples prepared with a smaller number of moles of Gly, which goes against what is desired. On the other hand, a-CDs showed an overall red shift in absorbance with a hypochromic effect with an increase in the number of moles of the carbon source, CA. This meant that samples prepared with a smaller number of moles CA yielded smaller particle sizes of higher absorbance.

Furthermore, with an increase in number of moles of the inorganic salt, NaH_2PO_4, in the synthesis of CDs, and an increase in the molar quantity of the passivation agent, BPEI, in the production of a-CDs, the absorbance was studied. In the case of CDs, a hypochromic effect from 0.195 to 0.117 accompanied by a red-shift from 260 to 263 nm for smaller number of moles of NaH_2PO_4 was observed, while the highest absorbance occurred at larger molar quantities and a blue-shift was observed. This meant that particles were smaller in size at low and high molar quantities of NaH_2PO_4. Therefore, small amounts of NaH_2PO_4 would suffice

for effective fabrication of CDs. On the other hand, a-CDs showed highest absorbance for the sample prepared with the largest number of moles of BPEI and second highest absorbance for the one prepared with the smallest number of moles of BPEI; also, a red shift in absorbance, from 353 to 367 nm, was observed. This shows that smaller molar quantities of BPEI would be effective for adequate production of a-CDs of smaller sizes.

4.3.5. D_h & PDI

As previously mentioned, CDs and a-CDs of small particle sizes, low PDI, most negative ZP, a greater degree of monodispersity, and narrow size distribution towards smaller particle sizes is desired. When comparing the average hydrodynamic diameter (D_h) and PDI values of CDs and a-CDs, one needs to bear in mind that (a) these D_h values are averages and that there might be smaller particles present, and (b) these PDI values, as mentioned before, only speak to the degree of polydispersity of the sample under study and does not provide information regarding the size classes of particles. However, this information will be further discussed in Section 4.3.7 below. With that said, CDs displayed much smaller average D_h values than a-CDs; and their PDI values were much lower than those of a-CDs. Hence, CDs presented more monodisperse samples of narrower size distributions than a-CDs, which were largely polydisperse. CDs showed the greatest stability in the reaction time study with the smallest overall particle sizes that ranged from 200–400 nm. Throughout all applied parameter studies, CDs were smallest for samples prepared within 15–20 minutes at 720 W with the smallest molar quantity of 0.14 mol of Gly. Their average particle sizes reflected in their PDI values in which a greater degree of monodispersity was found for reaction time study. Their PDI values were most sensitive to an increase in Gly in which the polydispersity increased with the increase in Gly. On the other hand, the average D_h of a-CDs was most sensitive to temperature as no specific trends in D_h were observed under the influence of other applied synthesis parameters. Compared to unfunctionalised CDs, a-CDs presented much larger D_h values and highly polydisperse samples throughout all studies, with the smallest D_h of 518.8 nm for the sample prepared within 2.5 hours in the reaction-time study. However, temperature provided better control over average particle size as it was the only study in which a trend was observed, and none of the applied synthesis parameters displayed good control over the PDI.

4.3.6. ZP

As mentioned before, the smaller the particle size, the more negative the ZP. Overall, CDs displayed more negative surfaces, whereas a-CDs mostly possessed positive surfaces throughout all studies. According to Peng and Travas-Sejdic, the negative ZP of CDs could be owed to the presence of carboxylic groups on their surfaces, whereas a-CDs possess more positive surfaces due the conversion of carboxylic acid groups to amide groups (Peng and Travas-Sejdic 2009). As mentioned in Section 4.3.5, smaller average D_h values were observed for CDs than for a-CDs, which meant that on average a-CDs contained a greater number of particles of larger particle sizes, which correlated to their positive surfaces. The surface charge of unfunctionalised CDs proved to be very sensitive to all applied parameters; however, the smallest CDs were observed at the most negative ZP value of −33.6 mV with an average particle size of 223.6 nm for sample prepared within 20 minutes in the reaction-time study. On the other hand, temperature provided the best control over the ZP of a-CDs, as it was the only parameter for which a trend was observed.

4.3.7. Size distribution

Overall, a-CDs were sized below the upper limit for colloidal suspensions of 1000 nm with majority thereof of intermediate sizes between 100–1000 nm, and between 20–30 % of particles sized within the nano-range (0–100 nm). On the other hand, the majority of particles of CDs were of intermediate to larger sizes with a very small percentage thereof attributed to particles sized within the nano-range. Also, the reaction-time study provided a better control over size and a greater degree of monodispersity was observed with most particles sized below 1000 nm and some particles sized within the nano-range. However, in the molar quantity studies of Gly and NaH_2PO_4, a large degree of polydispersity and very wide size distributions were observed in which majority of particles were sized above 1000 nm. Whereas for a-CDs, the temperature study and both molar quantity studies presented a greater degree of monodispersity towards smaller sizes, and a larger degree of polydispersity for the reaction-time study.

In conclusion, the reaction-time study had the greatest influence over the characteristics of unfunctionalised CDs, whereas the temperature study had the greatest influence on the characteristics of a-CDs.

Chapter 5 – Environmental Influences on Colloidal Stability of Unfunctionalised Carbon Dots and Amine-Capped Carbon Dots

5. Environmental influences

5.1. Introduction

Having looked at the influence of several synthesis parameters on the colloidal stability of unfunctionalised carbon dots (CDs) and amine-capped carbon dots (a-CDs) in effectively determining ideal/adequate synthesis conditions; this chapter focuses on the influence of environmental factors, such as pH, salinity, and the presence of natural organic matter, on the colloidal stability of the aforementioned materials. According to Bayati, nanomaterials tend to undergo agglomeration rapidly under natural water conditions which leads to sedimentation of aggregates that would typically affect benthic organisms; whereas, when they remain suspended and highly stable, they would affect organisms such as fish, marine mammals and planktonic species. In addition, if they remain stable and in suspension, they could be transported to other ecosystems far from their initial point of contamination (Bayati et al 2018). Therefore, recall, the core of this dissertation is to examine the behaviour of both unfunctionalised CDs and a-CDs under the influence of the above-mentioned environmental conditions.

5.2. The influence of centrifugation on colloidal stability of CDs & a-CDs

In this section, the results for the effect of centrifugation on the colloidal stability of CDs and a-CDs is measured and presented, over a number of time-intervals, after centrifugation. The purpose of this experiment was to see how the hydrodynamic diameter of CDs and a-CDs would be affected after centrifugation in order to achieve separation of particles from solution. As discussed previously, a large degree of aggregation has occurred especially for unfunctionalised CDs. Therefore, the samples were characterised at different time-frames after centrifugation, using the Malvern Zetasizer Nano ZS90, to examine whether a purification process such as centrifugation could (a) yield particles that are smaller in diameter, (b) reverse any agglomeration processes that might have taken place, and (c) see how long it would take for the particles to re-agglomerate. In Figure 64 and Figure 65 below, the hydrodynamic diameter was plotted as a function of time-elapsed. This study was performed on four samples of CDs (i.e., PowOpt_A5, RTOpt_A8, G_Opt_A13, and N_Opt_A18) and four samples of a-

CDs (i.e., TpOpt_B3, RTOpt_B8, CA_Opt_B13, and BPEI_Opt_B17), prepared in the optimisation studies according to the methods described in Section 3.3.

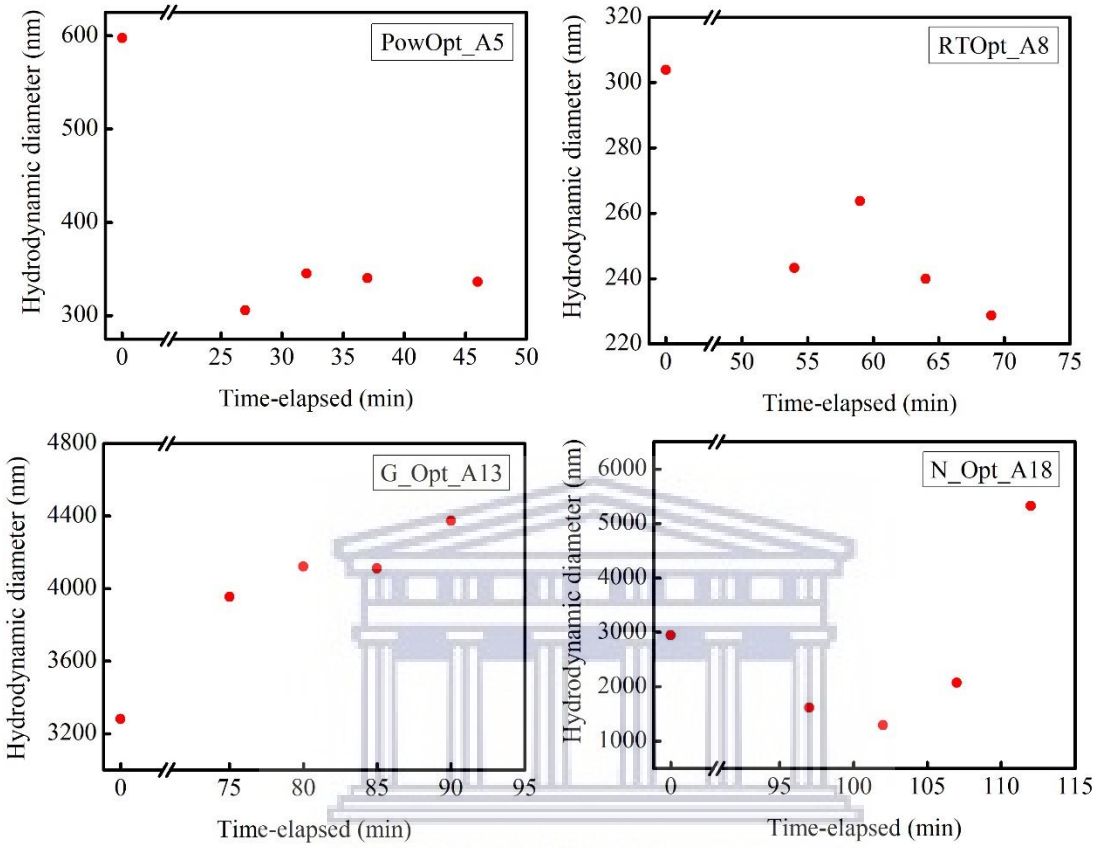

Figure 64. The effect of centrifugation (at 3300 rpm for 1 hour) on the colloidal stability of CDs.

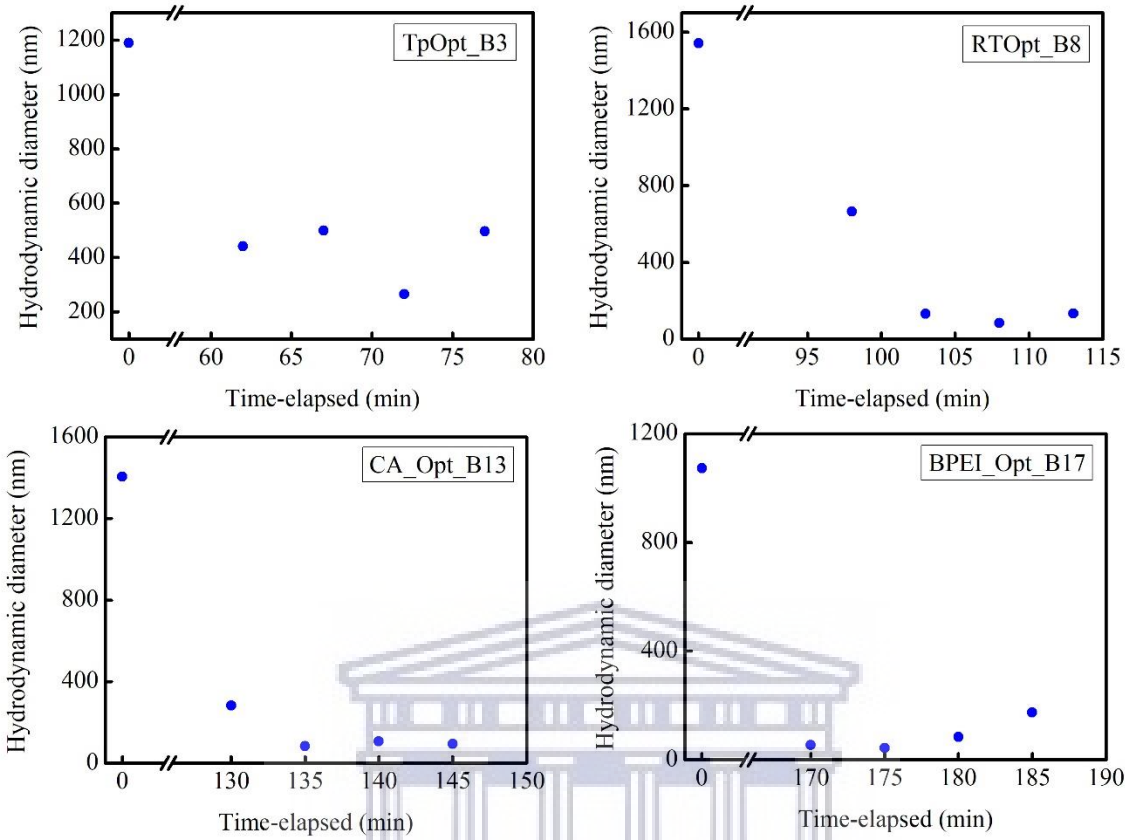

Figure 65. The effect of centrifugation on the colloidal stability of a-CDs (at 3300 rpm for 1 hour).

It is important to note that the first data point of each graph represents the hydrodynamic diameter before centrifugation, and the readings of CDs were conducted 27 minutes after centrifugation, whereas the readings of a-CDs were only conducted 62 minutes after centrifugation (factoring in time lost due to the walk between buildings, setting up and additional time for the waiting period for authorized personnel to log into the computer). All samples, except sample G_Opt_A13, displayed a sharp decrease in the hydrodynamic diameter of particles after centrifugation, which was followed by a slow increase after about 60 minutes for CDs and 100 minutes for a-CDs. In the case of G_Opt_A13, the increase in particle size could either be due to (a) a strong attraction between particles that causes further agglomeration of particles under centrifugation, or (b) some form of contamination. According to Hunter, this slow increase in the hydrodynamic diameter could be attributed to a process called Ostwald ripening in which aggregates undergo dissolution and reprecipitation due to linkages formed between particles (Hunter 1987). Notice that centrifugation does prove to drastically decrease the hydrodynamic diameter of both CDs and a-CDs, and, therefore, proves to be a suitable

method to actively reduce the size of particles or revert agglomerated particles. If there is a weak attraction between particles their agglomeration process could be slow and they tend to form structures that are compact with little solvent entrapped. Alternatively, for particles with strong attraction, rapid coagulation could occur with the formation of loose structures that entraps a larger amount of the dispersion medium (Hunter 1987).

5.3. The influence of pH on the colloidal behaviour of CDs and a-CDs

As you may recall from the problem statement (see Section 1.3), the importance of this project was to investigate the behaviour of the synthesised carbon-based nanomaterials, i.e., CDs and a-CDs, under the influence of several environmental factors; one of which was the examination of the effect of pH on the colloidal stability of CDs and a-CDs. A pH study provides vital information regarding the behaviour of the synthesised materials in acidic and basic environments, should they succumb to their fate of eventually ending up in certain ecosystems. In understanding their behaviour in various kinds of environments, simulated by variations in pH (as discussed in this section), ionic strength (IS) (as discussed in Section 5.4), and the presence of NOM (as discussed in Section 5.5); one can model/anticipate their aggregating behaviour in ecosystems or living organisms.

With that said, this section presents the results on the effect of pH on the colloidal stability of CDs and a-CDs, in the presence of 0.01 M NaCl and 0.01 M $CaCl_2$, after centrifugation (see the experimental procedure described in Section 3.7). This study was performed on samples prepared under synthesis conditions (established in Section 4.1.5 and Section 4.2.5, for CDs and a-CDs, respectively). Table 21 shows the results on the effect of pH on factors such as hydrodynamic diameter (D_h), polydispersity index (PDI), and zeta potential (ZP) for both CDs and a-CDs, which are illustrated in Figure 66 to Figure 68.

Table 21. The influence of pH on the hydrodynamic diameter, polydispersity index, and zeta potential of CDs and a-CDs.

	0.01 M NaCl			*0.01 M $CaCl_2$*		
pH	***D_h (nm)***	***PDI***	***ZP (mV)***	***D_h (nm)***	***PDI***	***ZP (mV)***
			Carbon dots (CDs)			
1	354.9	0.736	−1.15	169	0.877	−1.68
3	353.7	0.793	−10.7	339.1	0.777	−7.10
5	371.8	0.314	−13.7	386.7	0.284	−8.11
7	387.8	0.271	−18.4	399.8	0.490	−11.4
9	403.6	0.560	−17.2	389.2	0.555	−9.40
11	407.4	0.560	−19.9	402.2	0.706	−12.9
13	467.1	0.665	−13.4	5221	0.266	−19.7
			Amine-capped carbon dots (a-CDs)			
1	375.3	1.000	+4.26	539.1	0.966	+13.41
3	589.5	0.788	−1.32	9.3	0.906	−0.0984
5	453.4	0.777	−0.642	871.4	0.697	+0.175
7	656.4	0.699	+0.918	849.5	0.926	+0.816
9	1421	0.341	−4.21	1541	0.325	−3.36
11	825.4	0.557	−0.0801	1157	0.521	+0.0711
13	273.4	0.706	−4.97	1625	0.788	−0.819

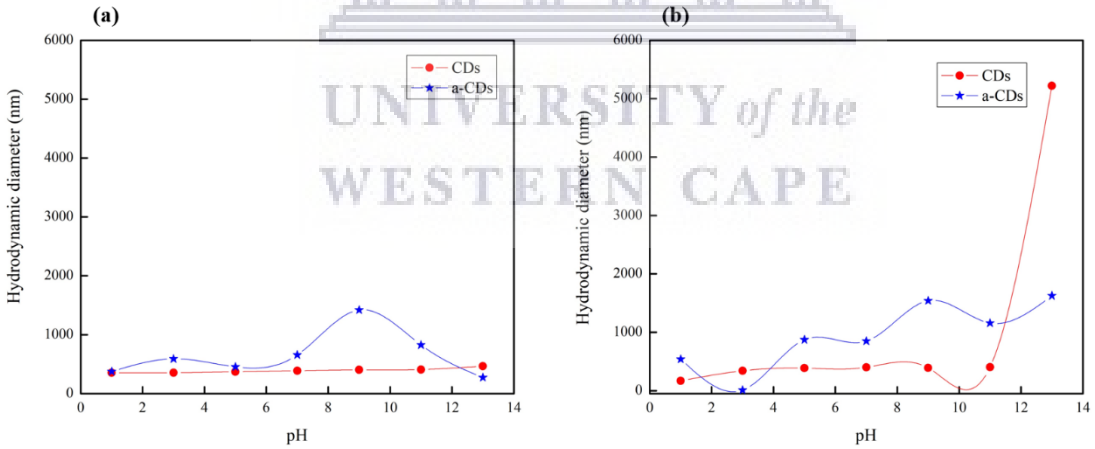

Figure 66. Hydrodynamic diameter of CDs, a-CDs as a function of pH with 0.01 M ionic strength given by (a) NaCl, and (b) $CaCl_2$.

Due to the potential imprecision of pH determinations for low IS solutions, i.e., ultrapure water, these studies were performed in a 0.01 M NaCl environment, which serves as an indifferent electrolyte condition for comparison (Bayati *et al* 2018). According to literature, aggregation is not expected for CDs in environments where IS is lower than 0.01 M which is the case for a majority of natural freshwater bodies (Chowdhury *et al* 2013). On the other hand,

agglomeration can be expected in environments of higher IS such as seawater or groundwater (Bayati *et al* 2018).

In the presence of 0.01 M IS given by NaCl (Figure 66a), the stability of CDs over the pH range from 1 to 13 is not noticeably affected, as the D_h thereof remained stable. However, a-CDs have shown to be pH sensitive as the D_h values were larger from pH 7 to 9 (i.e., in a basic environment) with the greatest stability seen from pH 1 to 3 and at pH 13, where the measured D_h was small.

In a 0.01 M IS environment created by $CaCl_2$ (Figure 66b), CDs displayed good stability in their D_h from pH 1 to 11, with a drastic increase in D_h at pH 13. On the other hand, a-CDs were more pH sensitive as their D_h increased with the increase in pH from 1 to 13 with their greatest stability at pH 3 with the smallest D_h of 9.3 nm. The presence of divalent cations thus influenced a-CDs greater than CDs.

The second characteristic under investigation was the effect of pH on the ZP of CDs and a-CDs. The zeta potential was measured by a Malvern Zetasizer Nano ZS90 using Laser Doppler Velocimetry (LDV) which involves an electrophoresis experiment in which the velocity of particles (i.e., the electrophoretic mobility) was determined and the Henry equation was applied. ZP was plotted as a function of pH, adjusted by HCl and NaOH, with fixed molar quantities of CDs and a-CDs (Figure 67).

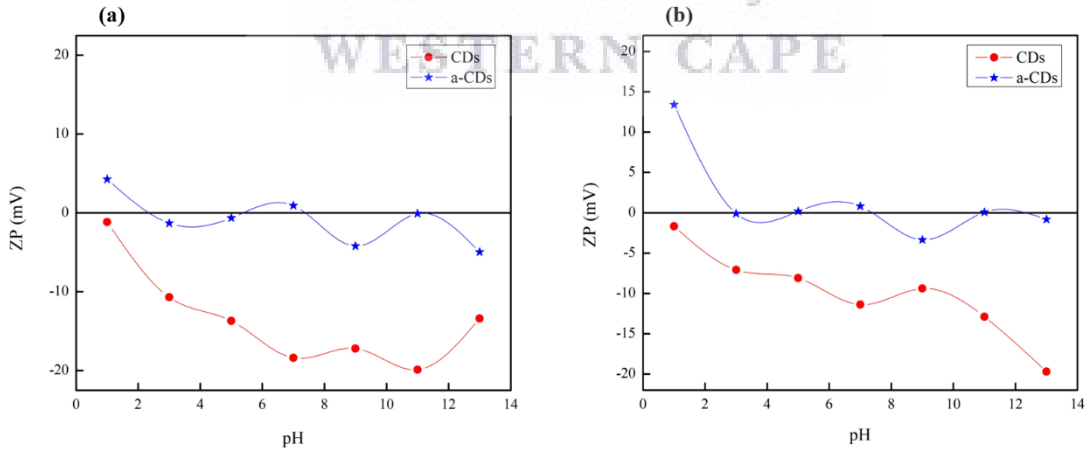

Figure 67. Zeta potential of CDs, a-CDs as a function of pH with 0.01 M ionic strength given by (a) NaCl, and (b) $CaCl_2$.

In Figure 67, the ZP values of both CDs and a-CDs were pH sensitive as their surfaces became more negative with an increase in pH. In the presence of 0.01 M ionic strength given by NaCl (Figure 67a), as the pH was increased from 1 to 13, the ZP decreased from −1.15 mV to −19.9

mV with a slight increase to −13.4 mV at pH 13 for CDs; and it decreased from +4.26 mV to −4.97 mV for a-CDs. In a 0.01 M IS environment created by $CaCl_2$ (Figure 67b), CDs were more pH sensitive than a-CDs; as the pH was increased from 1 to 13, the ZP became more negative from −1.68 mV to −19.7 mV. For a-CDs surface charge was most positive at +13.41 mV for pH 1 and most negative at −3.36 mV for pH 9 but remained constant for pH 3, 5, 7, 11 and 13 (the stability at higher pHs is in correlation with results in literature) (Bayati *et al* 2018). The surface functional groups on CDs and a-CDs determined their surface charge as protonation or deprotonation could occur, which significantly influenced pH (Bayati *et al* 2018, Jia *et al* 2012). According to literature, the decrease in ZP from pH 1 to 13 could be attributed to the deprotonation of surface functional groups such as hydroxyl and carboxyl groups (Bayati *et al* 2018). On the other hand, the presence of amino groups on the surfaces of a-CDs, with pK_a value typically between 9 and 10 (Bayati *et al* 2018, Stark 1965, Wang *et al* 2011a), lead to protonation thereof at lower pHs, which yielded surfaces that were more positively charged (Bayati *et al* 2018). Furthermore, the process of carbonisation is catalysed by the presence of H^+ ions which aids in the formation of CDs (Wang *et al* 2011a). The addition of more alkali to a system containing negatively charged particles leads to the surface attaining a more negative charge. Whereas in the case of an addition of an acid, such as HCl, there would be a point where the negative charge would be neutralised and further addition of acid yields a more positively-charged surface (Malvern Instruments Ltd. 2004). Also, from these measurements, it is evident that divalent cations have a greater effect on the stability of nanomaterials than monovalent cations, which could be attributed to the fact that divalent cations have a greater impact on the coagulation of negatively charged nanomaterials than do monovalent cations (Bayati *et al* 2018, Hunter 1987).

Another important factor to study was the polydispersity of CDs and a-CDs over the above-mentioned range of pH levels. The PDI is a width parameter obtained by a Zetasizer which refers to the degree of dispersity of particles. The PDI of CDs and a-CDs was displayed as a function of pH, adjusted by HCl and NaOH (Figure 68).

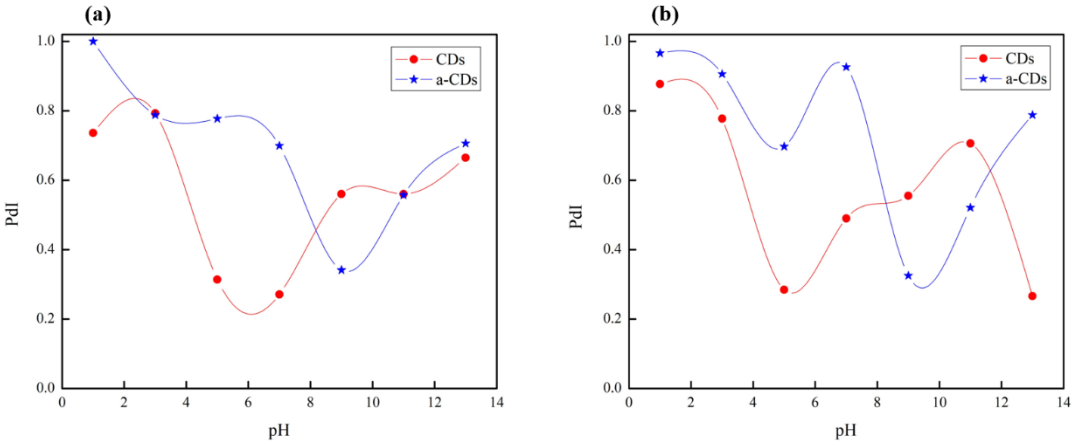

Figure 68. Polydispersity index of CDs, a-CDs as a function of pH with 0.01 M ionic strength given by (a) NaCl, and (b) $CaCl_2$.

In the presence of 0.01 M IS given by NaCl (Figure 68a), the polydispersity of CDs is best at pH 5 and 7 with PDIs of 0.314 and 0.271 respectively. Recall that the lower the PDI, the more monodisperse and less polydisperse the particles, which translates to narrow size distributions and greater colloidal stability. At lower pH (i.e., in an acidic environment) and at higher pH (i.e., in a basic environment) from 9 to 13 the particles were more polydisperse and possessed wider size distributions. For a-CDs the lowest PDI was 0.341 at pH 9 while PDIs for ranges > pH 9 and < pH 9 were higher than 0.5 which means that the particles showed greater stability at pH 9.

In a 0.01 M IS environment created by $CaCl_2$ (Figure 68b), the polydispersity of CDs is lower and displays narrower size distributions at pH 5 and 13 with PDIs of 0.284 and 0.266, respectively. The lowest value of 0.266 at pH 13 is corroborated by the lowest ZP of −19.7 mV which supports the idea that the lower PDI corresponds to more negative ZPs. At pH 5 and 13 the CDs showed greater monodispersity and possessed narrow size distributions. On the other hand, the lowest PDI for a-CDs in a 0.01 M IS given by $CaCl_2$ is 0.325 at pH 9 which is the pH at which the narrowest size distribution and greatest monodispersity of particles is seen as all pH values below and above pH 9 produced particles of wider size distributions.

Furthermore, the size distributions of CDs (Figure 69) and a-CDs (Figure 70) are displayed over the above-mentioned range of pH levels and expressed as intensity and is determined with the Malvern Zetasizer nano ZS90. The objective was to examine the distribution of particles

by determining the relative amounts (%) of particles found in each size range. This was essential in understanding physical and chemical properties of unmodified and modified CDs.

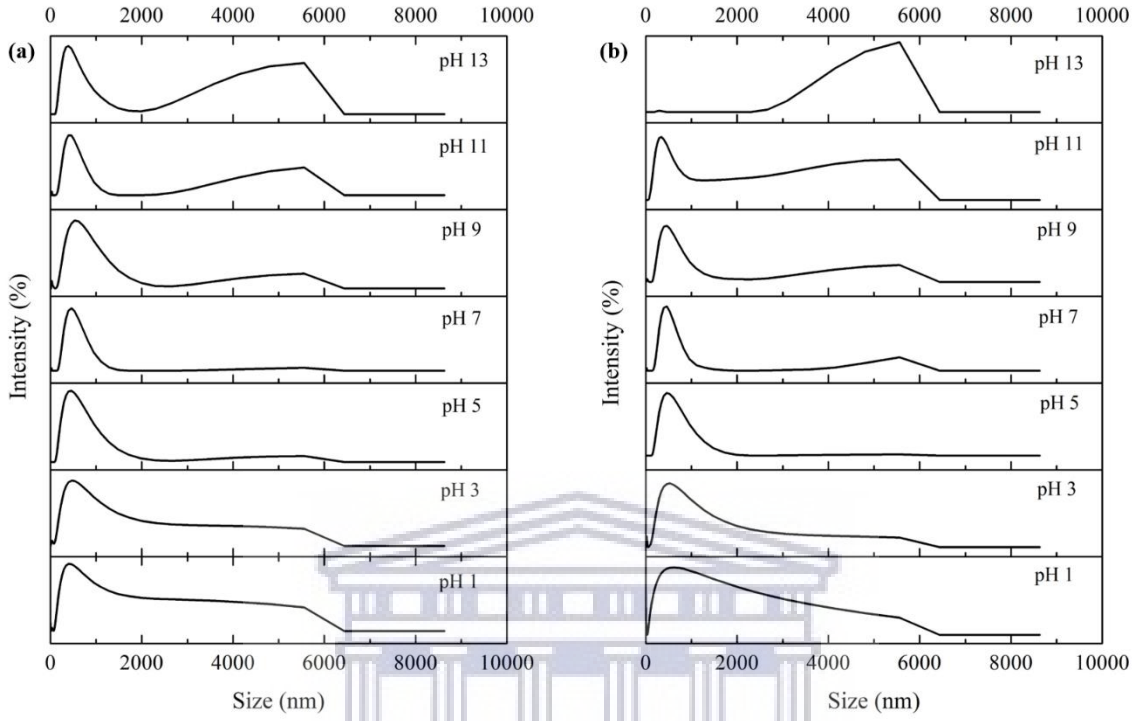

Figure 69. Size distribution of unfunctionalised CDs for pH study with ionic strength given by (a) 0.01 M NaCl, and (b) 0.01 M $CaCl_2$.

In the presence of 0.01 M ionic strength given by NaCl (Figure 69a), CDs displayed the best size distribution of the narrowest size distribution for pH 5 and 7, which correlates to the low PDI values seen at these pH levels (Figure 68a). The size distributions displayed for CDs in Figure 69a coincide greatly with their PDIs. The polydispersity for CDs ranked in decreasing order from the samples that displayed the widest size distribution and particles of greater polydispersity (i.e., highest PDI) to those of size distributions that are narrower and possess particles that are more monodisperse (i.e., lowest PDI) are as follows: pH 3, 1, 13, 9/11, 5 and 7 with their respective PDIs of 0.793, 0.736, 0.665, 0.56/0.56, 0.314, and 0.271. Therefore, notice that the samples at pH 3 and 1 displayed a wider range of particles that stretches from 0 to just over 6000 nm in size, whereas at pH 7 and 5 CDs have the narrowest size distributions of all samples, which corresponds to the lowest PDIs and lowest degree of polydispersity. There are two peaks visible for samples in the pH range from 9 to 13, with the second peak increasing in amplitude as the pH increases. This second peak is much wider and it represents the % of particles that are greater in size. Therefore, it should be noted that the area of the peak

at about 5500 nm is much larger than the peak at about 500 nm, because large particles scatter way more light than small particles with the scattering intensity proportional to the sixth power of a particle's diameter as described by Rayleigh's approximation (Malvern Instruments Ltd. 2004). Also, according to Ray et al., broad size distributions and large particle sizes mask the presence of small particles because DLS considers average hydrodynamic diameter which may include sizes of small particles along with particles that might have molecules and ions adsorbed to their surfaces (Ray *et al* 2009). Compared to the average D_hs (in Table 21) for the samples subjected to an alkaline environment (i.e., pH 9-13), larger D_hs are reported, which speaks to the lack of stability of particles and the onset of agglomeration. Under the applied parameter, i.e., pH variation, CDs retained their nanostructure best at pH 5 and 7.

On the other hand, in a 0.01 M ionic strength environment created by $CaCl_2$ (Figure 69b), CDs displayed the best size distribution for pH 5 and 7, which once again correlates to their low PDIs (Figure 68a) and hence, narrow size range that is slanted more towards particle sizes that are smaller in diameter. The size distributions displayed in Figure 69b coincides greatly with their PDIs. The polydispersity for CDs ranked in increasing order is as follows: pH 13, 5, 7, 9, 11, 3, and 1 with their respective PDIs of 0.266, 0.284, 0.49, 0.555, 0.706, 0.777, and 0.877. Notice that the samples at pH 13 had the lowest PDI but that is only because the distribution is narrow but towards the larger size classes. The particles of pH 5, however, has the second lowest PDI and therefore has a narrow size distribution but in the desired size classes of particles with smaller diameter. Therefore, it is important to discuss PDI along with size distribution graphs to accurately examine the size distribution of particles. pH 5 displayed particles of the narrowest size distribution which was slanted towards smaller particle sizes and hence contained particles of greater colloidal stability.

Comparing the presence of divalent cations to that of monovalent cations, it is clear that unfunctionalised CDs displayed the greatest stability at pH 5 with particles that are more monodisperse and smaller in size. In the presence of divalent cations, the distribution is slanted more towards smaller particle sizes for pH 1; as the pH increased from pH 7 to 13, more particles were of the larger sizes due to the occurrence of agglomeration whereas the distribution at pH 3 was unchanged.

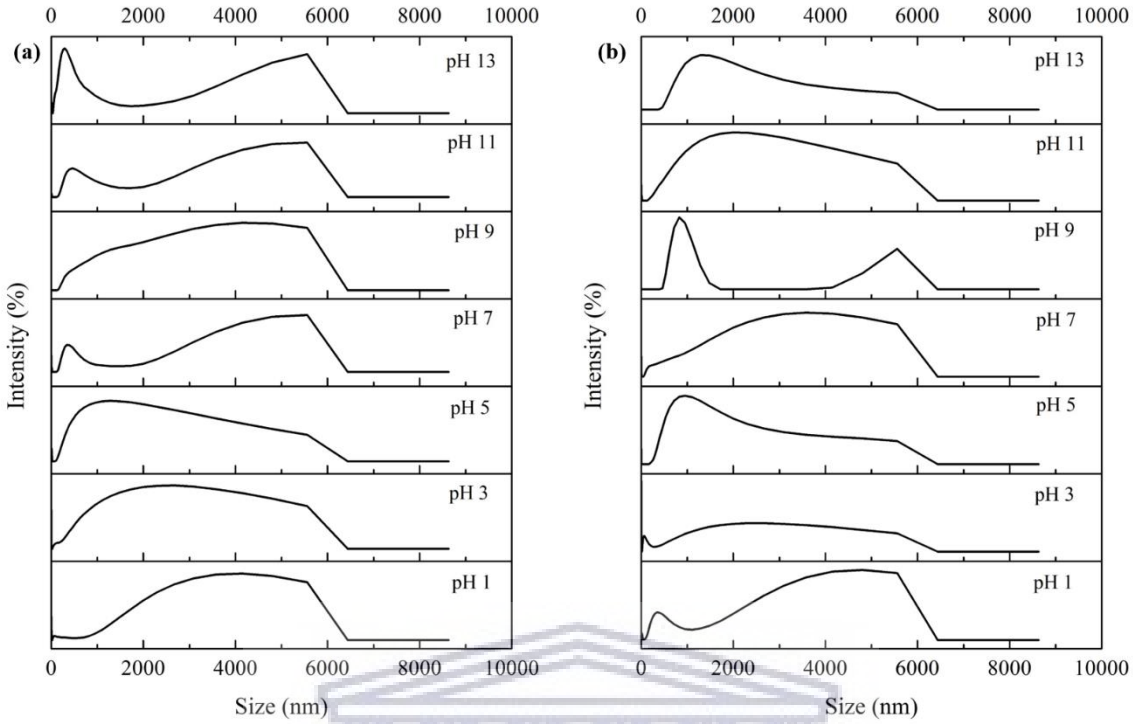

Figure 70. Size distribution of a-CDs for pH study with ionic strength given by (a) 0.01 M NaCl, and (b) 0.01 M $CaCl_2$.

In the presence of 0.01 M IS given by NaCl (Figure 70a), a-CDs displayed bimodal size distribution for pH 13, but possessed the largest number of particles of the smallest particle sizes, as evidenced by the narrow but large peak towards smaller size classes. The polydispersity for a-CDs ranked in increasing order from the samples that displayed the narrowest size distribution and particles of greater monodispersity (i.e., lowest PDI) to those of size distributions that are wider and possess particles that are more polydisperse (i.e., highest PDI) are as follows: pH 9, 11, 7, 13, 5, 3, and 1 with their respective PDIs of 0.341, 0.557, 0.699, 0.706, 0.777, 0.788, and 1. Therefore, notice that the samples at pH 1 and 9 displayed a wide range of particles that slanted more towards larger size classes due to a larger degree of agglomeration that occurred, whereas pH 3 and 5 also display wide size distributions but that slants more towards smaller size classes, whereas pH 7, 11 and 13 displayed similar bimodal trends in which there are two peaks visible with a greater % of particles of larger diameters. The large second peak can once again be attributed to Rayleigh's approximation as described above (Malvern Instruments Ltd. 2004). The large size distributions at pH 1, 3 and 5 coincides with their large PDIs that indicate wide size distributions and greater polydispersity. There are

two peaks visible for samples in the pH range from 9 to 13, with the second peak increasing in size as the pH increases.

On the other hand, in a 0.01 M IS environment created by $CaCl_2$ (Figure 70b), a-CDs displayed the best colloidal stability and narrowest size distribution towards smaller size classes at pH 9 with particles remaining in the nano-range, which correlates to the low PDI of 0.325 (Figure 68b). The size distributions displayed in Figure 70b to some extent coincides with their PDIs. The polydispersity for a-CDs ranked in increasing order is as follows: pH 9, 11, 5, 13, 3, 7, and 1 with their respective PDIs of 0.325, 0.521, 0.697, 0.788, 0.906, 0.926, and 0.966. Therefore, notice that the samples at pH 1 and 7 displayed a wide range of particles that slanted more towards larger size classes, whereas pH 5, 13, and 11 also display wide size distributions but that slants more towards smaller size classes, and pH 9 displayed a bimodal size distribution with a greater % of particles of smaller diameters. The large size distributions from pH 1 to 7 and 11 to 13 coincide with their large PDIs that indicate wide size distributions and a larger degree of polydispersity.

Comparing the presence of divalent cations with that of monovalent cations, it is clear that a-CDs displayed the greatest stability at pH 9 with particles that are monodisperse and smaller in size. In the presence of divalent cations, the distribution is slanted more towards smaller particle sizes for pH 1, 5, 9, and 11, whereas for pH 1 and 7 a greater % of particles were of the larger sizes while the distribution at pH 3 remained wide but of lower intensity. Albeit a-CDs in a pH-9 environment displayed the best colloidal stability among all samples, comparing a-CDs at pH 9 in NaCl with those in $CaCl_2$, agglomeration still occurred as particles were not found within the nano-range anymore even though they consisted of particles of smaller size classes.

In conclusion, when comparing CDs with a-CDs, the greatest stability with particles that were smaller, more monodisperse, and possessed narrower size distributions towards smaller size classes, occurred at pH 5 for CDs and pH 9 (in a basic environment) for a-CDs. Also, the presence of divalent cations (introduced by $CaCl_2$) had a greater influence on the D_h, ZP, PDI, and size distribution of both CDs and a-CDs, than monovalent cations (introduced by NaCl). Lastly, the amino groups on a-CDs didn't seem to provide improved or superior stability over unfunctionalised CDs or greater protection from aggregation in the environment when pH was varied as a larger degree of agglomeration was observed in a-CDs.

5.4. The influence of ionic strength on the colloidal behaviour of CDs and a-CDs

In this section, results on the effect of ionic strength (IS) on the colloidal stability of CDs and a-CDs were characterised using a Malvern Zetasizer Nano ZS90 at pH 5 for CDs and pH 9 for a-CDs (determined as pH environments of greater stability—see conclusion of Section 5.3). This study was performed on CDs (RTOpt_A8) prepared with 0.15 mol of Gly and 3.4×10^{-3} mol of NaH_2PO_4 at 720 W for 15 minutes; and on a-CDs (TpOpt_B3) prepared with 1.1×10^{-2} mol of CA and 1.3×10^{-2} mol of BPEI at 170 °C within 2 hours (see Section 3.7 for experimental procedure). Table 22 shows the results on the effect of IS on factors such as hydrodynamic diameter (D_h), polydispersity index (PDI), and zeta potential (ZP) for CDs and a-CDs, which is illustrated in Figure 71, Figure 72, and Figure 73; in which the D_h, ZP, and PDI of particles are respectively plotted as functions of IS.

Table 22. The influence of IS on the hydrodynamic diameter, polydispersity index, and zeta potential of CDs (pH 5) and a-CDs (pH 9).

	NaCl			***$CaCl_2$***		
IS (M)	***D_h (nm)***	***PDI***	***ZP (mV)***	***D_h (nm)***	***PDI***	***ZP (mV)***
			Carbon nanodots (CDs)			
0.001	404.1	0.491	−26.9	414.6	0.412	−19.4
0.01	388.6	0.438	−20.5	371.6	0.646	−9.19
0.1	395.5	0.991	−15	310.9	0.749	−1.53
1	360.9	0.557	−4.57	520	0.613	−2.47
			Amine-capped carbon dots (a-CDs)			
0.001	1196	0.753	−0.633	1096	0.414	−3.81
0.01	1312	0.978	−2.6	1328	0.520	−2.93
0.1	1123	0.639	−2.26	861	0.756	+0.236
1	1066	1	+1.42	1291	0.522	+0.648

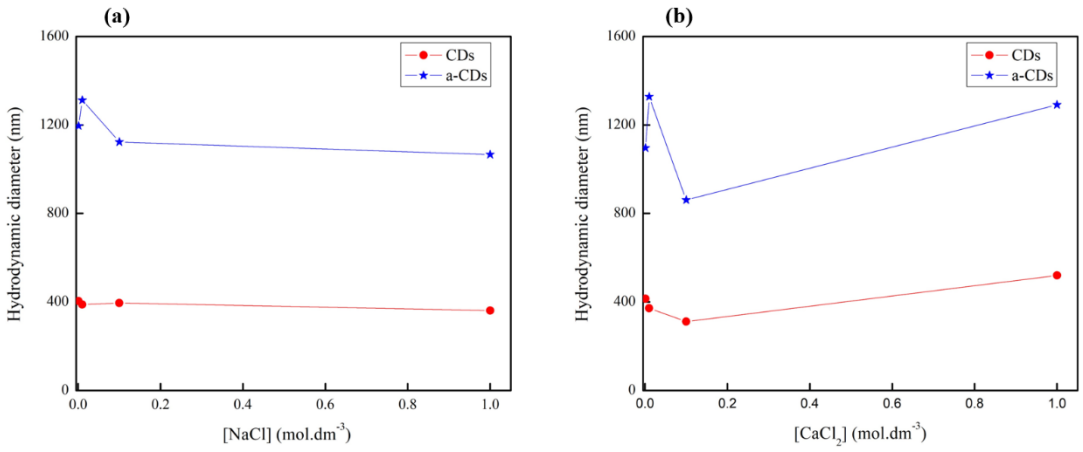

Figure 71. Hydrodynamic diameter of CDs (pH 5), a-CDs (pH 9) as a function of IS given by (a) NaCl, and (b) $CaCl_2$.

In the presence of NaCl (Figure 71a), CDs displayed good stability in their hydrodynamic diameter (D_h) over the IS range from 0.001 to 1 M, as evident in their D_h which remained constant between 300–400 nm. However, a-CDs reached much larger sizes and proved to be more sensitive to the presence of Na^+ ions as their D_h values were larger for lower IS of 0.001 and 0.01 M NaCl, which proceeded to decrease for 0.1 and 1 M NaCl.

In the presence of $CaCl_2$ (Figure 71b), CDs were more sensitive to changes in IS as the D_h is influenced more noticeably by the presence of Ca^{2+}-ions than Na^+-ions. Hence, the D_h of CDs decreased from 414.6 to 310.9 nm as the IS increased from 0.001 to 0.1 M, which was followed by a significant increase to 520 nm in a 1 M IS environment. On the other hand, a-CDs were more IS sensitive than CDs and sizes were influenced more significantly in the presence of divalent cations (Ca^{2+}) than monovalent cations (Na^+). At 0.001 M $CaCl_2$ there is a 100 nm decrease in D_h for a-CDs compared to the same conditions for NaCl. Furthermore, a-CDs displayed a considerably lower D_h in the 0.1 M IS environment of $CaCl_2$ than for NaCl, whereas the outcome for at 0.01 M was relatively uninfluenced. Moreover, in 1 M $CaCl_2$ there was an increase in D_h of approximately 200 nm compared to that in NaCl.

The use of different pH levels limits comparison between CDs and a-CDs in terms of examining possible superior stability of a-CDs over unfunctionalised CDs brought about by the amine-functionality of a-CDs. Nevertheless, one could still individually examine the effect of IS on CDs and a-CDs by investigating the influence of the presence of ions that differ in valency. That being said, even if there were no specific trends observed, the presence of divalent cations influenced both CDs and a-CDs more greatly than monovalent cations.

According to Hunter, an electrolyte with coagulating abilities is more effective when it consists of multivalent ions (Hunter 1987). Furthermore, it seems as though both CDs and a-CDs underwent agglomeration at high IS provided by divalent ions. Therefore, in a high IS environment these nanomaterials are expected to undergo agglomeration, which could greatly affect a multitude of living organisms in the environment. As previously mentioned, agglomeration can be expected in environments of higher IS such as seawater or groundwater that could affect benthic organisms; whereas, in freshwater bodies (i.e., at low IS, lower than 0.01 M) they remain suspended, more stable and could affect organisms such as fish, marine mammals and planktonic species or be transported to other ecosystems far from their initial point of contamination (Bayati *et al* 2018).

The second characteristic under investigation was the effect of IS on the surface charge or ZP of CDs and a-CDs, as measured by a Malvern Zetasizer Nano ZS90. In Figure 72, ZP is plotted as a function of IS introduced by NaCl and $CaCl_2$.

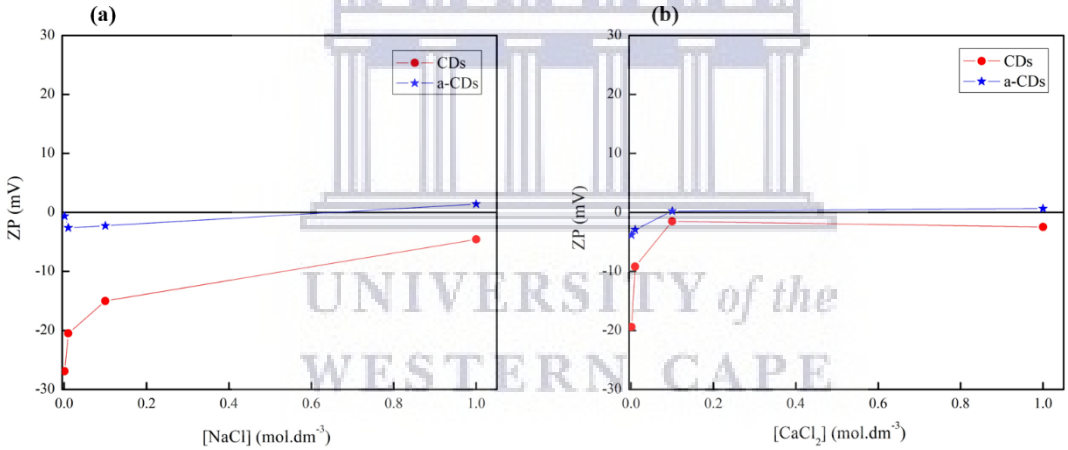

Figure 72. Zeta potential of CDs (pH 5) and a-CDs (pH 9) as a function of IS given by (a) NaCl, and (b) $CaCl_2$.

The ZP values of CDs and a-CDs were slightly IS sensitive because they increased with an increase in IS. CDs displayed negatively charged surfaces throughout all IS measurements for NaCl and $CaCl_2$, whereas 3/8 (37.5 %) of the data points of a-CDs were positively charged.

In the presence of NaCl (Figure 72a), as the concentration of NaCl increased from 0.001 M to 1 M, the ZP values of CDs became more positive from −26.9 to −4.57 mV. According to classical colloid theory, electrical double layer (EDL) compression occurs as the IS increases and surface charge becomes more positive due to interaction of NPs with surrounding or dissolved electrolytes (Bayati *et al* 2018, Verwey 1947). The thickness of the EDL is dependent

on IS and diminishes with an increase in IS, which leads to a rapid decline in potential energy with respect to distance from the surface of a colloid (Bayati *et al* 2018). This causes a relocation of the slip plane, the point where the stern layer and diffuse layer meet and where the ZP is measured (Zeta-Meter, Inc. 1993), to a lower absolute potential value (Bayati *et al* 2018). On the other hand, at low IS there was an initial decrease in the ZP values of a-CDs from −0.633 to −2.6 mV as the concentration of NaCl increased from 0.001 to 0.01 M; which was followed by an increase to +1.42 mV at the highest IS of 1 M NaCl. This decrease could be due to the fact that at low IS the EDL is thick, the potential barrier is large, and repulsion occurs between particles which yields more negative ZPs. As the electrolyte concentration increases, the potential barrier shifts towards interparticle distances that are smaller until it is completely suppressed and the charge in the liquid is very dense close to particle surfaces. This shifts the repulsive field fully into the attractive sphere of van der Waals forces which inactivates it. When this occurs, then agglomeration is no longer prevented by the maximum electrolyte concentration but strongly depends on the valency of the potential-determining ions (i.e., ions of opposite charge to the colloids or particles) and rapid agglomeration occurs (Schultze-Hardy rule) (Hunter 1987, Verwey 1947). This perfectly explains why a-CDs generally have more positively charged surfaces than unfunctionalised CDs, due to their thinner EDL layers.

In the presence of $CaCl_2$ (Figure 72b), CDs were significantly affected by the presence of Ca^{2+} ions as ZP values for each concentration was more positive for $CaCl_2$ than for NaCl, while the ZP values of a-CDs increased moderately. The ZP values of CDs increased from −19.4 to −1.53 mV, as IS (i.e., [$CaCl_2$]) increased from 0.001 to 0.1 M and decreased to −2.47 mV at 1 M. The approach of ZP to zero could be explained by the adsorption of Ca^{2+} onto the negatively charged surfaces of CDs (Bayati *et al* 2018). On the other hand, ZP values of a-CDs became more positive from −3.81 mV at the lowest IS of 0.001 M to +0.236 mV at 0.1 M and remained fairly constant from 0.1 M to 1 M; a similar trend was observed in the work of Bayati et al. in 2018.

From these measurements, it is evident that divalent cations have a greater effect on the stability of CDs and a-CDs than monovalent cations. The ZPs of a-CDs showed greater stability in IS variation than did CDs, which could be attributed to the intricate surface chemistry of a-CDs (Bayati *et al* 2018). Therefore, it could be concluded that the amine-functionality of a-CDs provided greater stability in their surface charges over that of CDs.

Another important factor to study was the polydispersity of CDs and a-CDs over the above-mentioned IS ranges. The PDI is displayed as a function of IS with fixed pH values for CDs (pH 5) and a-CDs (pH 9) (Figure 73).

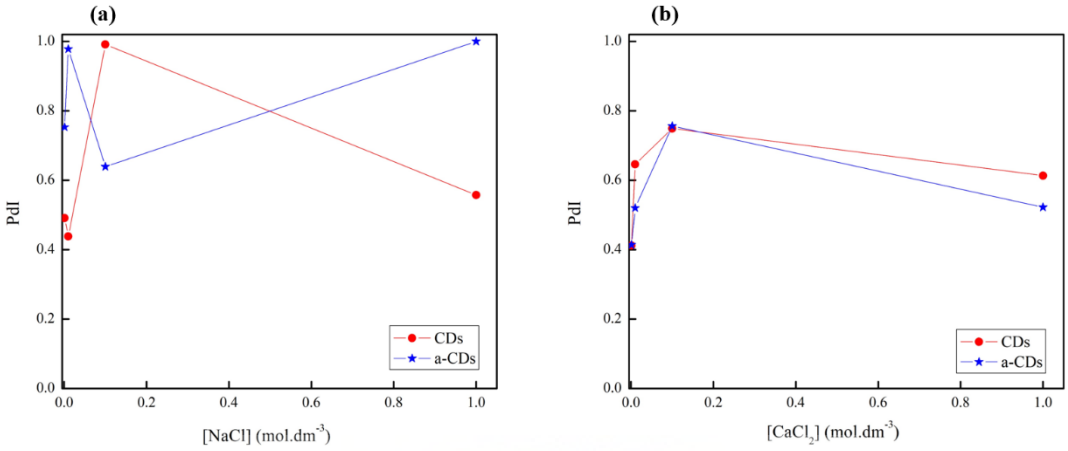

Figure 73. Polydispersity index of CDs (pH 5) and a-CDs (pH 9) as a function of IS given by (a) NaCl, and (b) $CaCl_2$.

Recall that the lower the PDI, the more monodisperse and less polydisperse the particles, which translates to narrow size distributions. In the presence of NaCl (Figure 73a), CDs displayed the narrowest size distribution in a 0.01 M IS environment with a PDI of 0.438. At lower and higher IS (i.e., at 0.001, 0.01, and 1 M) the particles were more monodisperse, had narrower size distributions, and showed greater stability. For a-CDs the greatest stability was observed with the lowest PDI of 0.639 in a 0.1 M IS environment given by NaCl, while other samples displayed larger PDIs, wider size distributions and a greater degree of polydispersity. The intricate surface chemistry of a-CDs could be the reason for stability thereof in a higher IS environment than CDs.

In the presence of $CaCl_2$ (Figure 73b), the PDI of CDs was lowest for the lowest IS environment of 0.001 M with a PDI of 0.412 which coincides with the lowest ZP of −19.4 mV, whereas the particles became more polydisperse and PDI values increased from 0.412 to 0.749 as IS was increased to 0.1 M and was followed by a slight decrease to 0.613 at 1 M. On the other hand, as IS increased from 0.001 to 0.1 M the PDI values of a-CDs also increased from 0.414 at 0.001 M to 0.756 at 0.1 M, which was followed by a significant decrease to 0.522 at 1 M. Both CDs and a-CDs displayed the same trend in which there is an initial increase in PDI from 0.001 to 0.1 M meaning that with an increase in IS, particles become more polydisperse and have wider

size distributions with the widest size distribution observed at 0.1 M with a PDI of approximately 0.7; then there is a decrease in PDI at the greatest IS of 1 M.

Furthermore, the size distributions of CDs (Figure 74) and a-CDs (Figure 75) are displayed over the above-mentioned range of IS levels, expressed in intensity as determined with a Malvern Zetasizer Nano ZS90. Once again, the objective was to examine the distribution of particles by determining the relative amounts (%) of particles found in each size range. This was essential in understanding physical and chemical properties of modified and unmodified CDs.

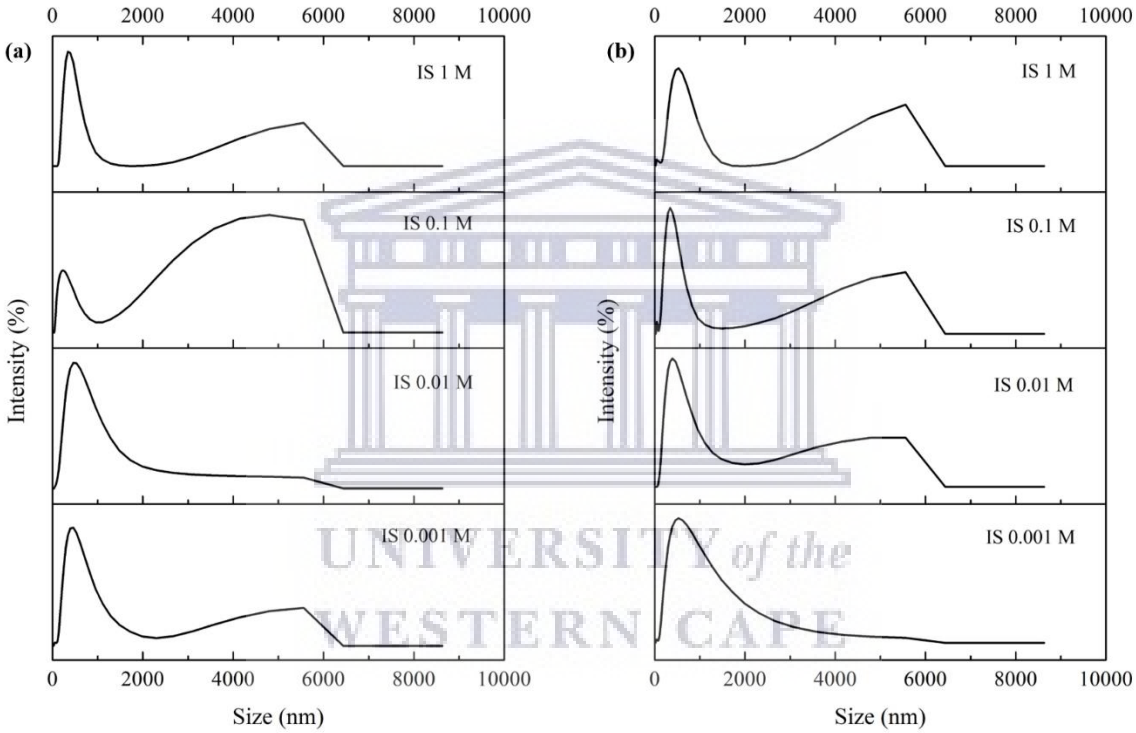

Figure 74. Size distribution of CDs (pH 5) for IS study (a) NaCl, and (b) $CaCl_2$.

In the presence of NaCl (Figure 74a), CDs displayed the narrowest size distribution in an IS environment of 0.01 M NaCl and for IS of 0.001 M $CaCl_2$, which correlates to their low PDIs (Figure 73). Overall, the size distributions displayed in Figure 74a coincide greatly with their PDIs (Figure 73a). The polydispersity for CDs ranked in increasing order from the samples that displayed the narrowest size distribution and particles of greater monodispersity (i.e., lowest PDI) to those of size distributions that were wider and possessed particles that were more polydisperse (i.e., highest PDI) are as follows: IS 0.01, 0.001, 1, and 0.1 M with their respective PDIs of 0.438, 0.491, 0.557, and 0.991. Particles in the 0.01 M IS NaCl environment displayed the best colloidal stability with particles that were monodisperse with majority

exhibiting hydrodynamic diameters of size classes below 1000 nm. The size distribution of particles of samples in environments of IS 0.001 and 1 M showed wider size ranges that encompassed smaller particles below 1000 nm as well as large particles of sizes from 3000 to 6000 nm. In an IS environment of 0.1 M, a large percentage of particles were of larger sizes.

On the other hand, in the presence of $CaCl_2$ (Figure 74b), CDs displayed the narrowest size distribution for IS 0.001 M, which once again coincides with the low PDI of 0.412 (Figure 73b), and has a narrow size range that consisted of smaller particles of sizes below 2000 nm. As the IS was increased from 0.01 M to 1 M, the size distribution of particles became much wider and stretched more to larger size classes.

Overall, it is safe to say that an increase in IS induced aggregation and that in high IS environments CDs tend to aggregate under dominant van der Waals forces. Also, in the presence of divalent cations and monovalent cations, it is clear that CDs displayed the greatest colloidal stability with particles that are monodisperse in lower IS environments of 0.001 M and 0.01 M. In the presence of divalent cations, the particle size distribution is slanted more towards smaller size classes meaning that a greater % of particles are smaller in size.

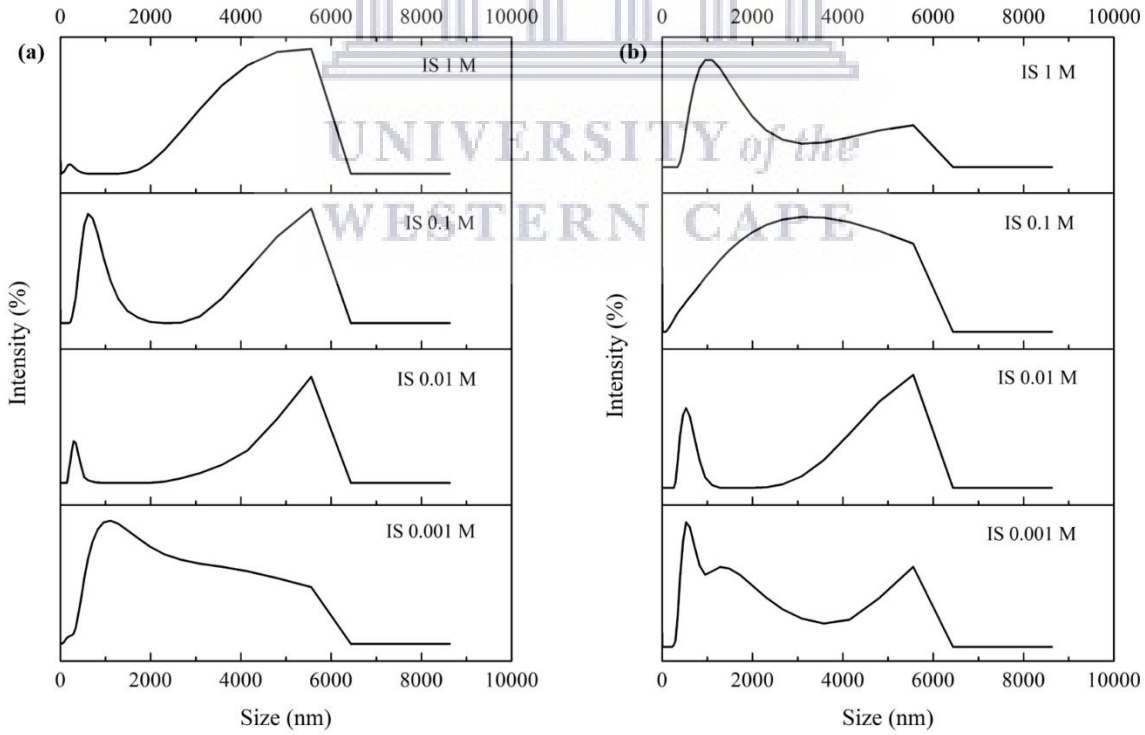

Figure 75. Size distribution of a-CDs (pH 9) for IS study (a) NaCl, and (b) $CaCl_2$.

In the presence of NaCl (Figure 75a), a-CDs displayed the best colloidal stability and narrowest size distribution for IS of 0.1 M; compared to other concentrations of NaCl. Also, the IS 0.1 M sample had the highest % of particles in size classes smaller than 1000 nm. As the IS was increased from 0.001 M to 1 M of NaCl, a greater % of particles were of larger size classes. The polydispersity for a-CDs ranked in increasing order from the samples that displayed the narrowest size distribution and particles of greater monodispersity (i.e., lowest PDI) to those of size distributions that are wider and possess particles that are more polydisperse (i.e., highest PDI) are as follows: IS 0.1, 0.001, 0.01, and 1 M with their respective PDIs of 0.639, 0.753, 0.978, and 1. a-CDs in a 0.001 M IS environment displayed a very wide distribution of particles over a large range from 1000 to 6000 nm, whereas in an environment of 0.01 M, a small peak is visible around 500 nm but of a very small percentage compared to the large peak that stretches from about 4000 to 6000 nm; which could once again be attributed to the fact that large particles scatter more light than small particles with the scattering intensity proportional to the sixth power of a particle's diameter as described by Rayleigh's approximation (Malvern Instruments Ltd. 2004). Furthermore, at an IS of 1 M, practically all particles were of greater sizes and were sized within greater size classes and yielded a very large and wide peak stretching from 2000 to just above 6000 nm. The large size distributions overall coincide with their large PDIs which suggests that the samples possess particles that are polydisperse to a large extent.

On the other hand, in the presence of $CaCl_2$ (Figure 75b), a-CDs displayed the best colloidal stability and narrowest size distribution at the lowest IS of 0.001 M (which correlates with the low PDI of 0.414 in Figure 73b), and narrow size range with the presence of a greater % of smaller particles. The size distributions displayed in Figure 75b to some extent coincide with their PDIs. The polydispersity for a-CDs ranked in increasing order is as follows: IS 0.001, 0.01, 1, and 0.1 M with their respective PDIs of 0.414, 0.52, 0.522, and 0.756. As the IS was increased from 0.001 to 1 M, the degree of polydispersity increased and the size distributions were wider. However, at lower IS a greater % of particles are found in smaller size classes, while at an IS of 0.1 M the size distribution is very wide and ranges from about 200 to 6000 nm.

Comparing the presence of divalent and monovalent cations, a-CDs were more monodisperse and smaller in size in the presence of $CaCl_2$. In the presence of divalent cations, the distribution is slanted more towards smaller particle sizes in comparison to the presence of monovalent cations with very little nanosized particles in IS of 0.01 M and 1 M NaCl, and 0.1 M $CaCl_2$.

5.5. The influence of the presence of natural organic matter on the colloidal behaviour of CDs and a-CDs

In this section, results on the effect of the concentration of humic acid (HA, i.e., natural organic matter, NOM), on the colloidal stability of CDs and a-CDs were studied at a neutral pH of 7 in the absence of any salts, using a Malvern Zetasizer Nano ZS90. This study was performed on samples prepared under synthesis conditions according to the method described in Section 3.7. Table 23 shows the results of the effect of NOM on factors such as hydrodynamic diameter (D_h) and zeta potential (ZP) of CDs and a-CDs, as illustrated in Figure 76, and plotted as a function of the concentration of HA.

Table 23. The influence of humic acid on the hydrodynamic diameter and zeta potential of CDs and a-CDs at neutral pH.

	CDs		***a-CDs***	
[HA] (mg/L)	***D_h (nm)***	***ZP (mV)***	***D_h (nm)***	***ZP (mV)***
20	343.5	−9.97	448.7	−8.01
60	423	−24.6	546.7	−3.01
100	407.8	−26.7	495.3	−5.65
140	511.6	−33.6	613.5	−5.09
200	518.9	−36.9	860.6	−6.2

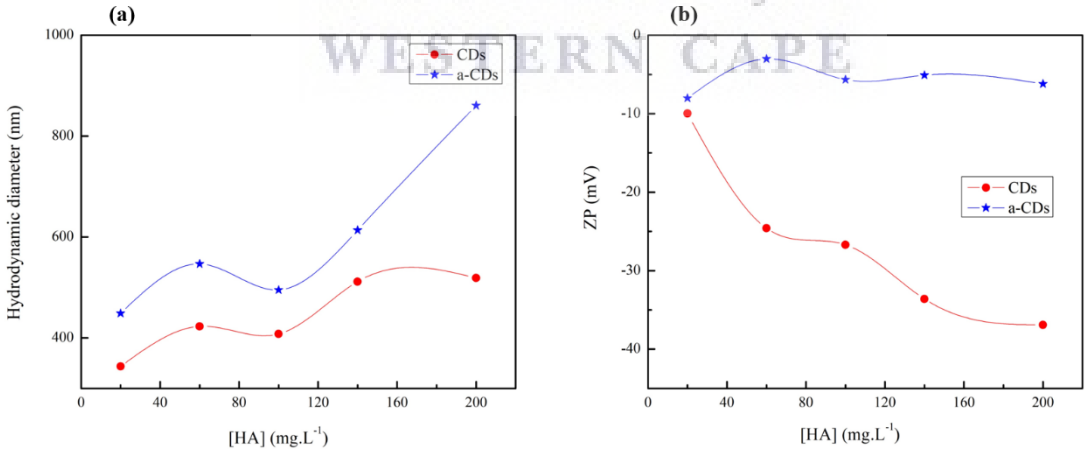

Figure 76. (a) Hydrodynamic diameter, and (b) zeta potential of CDs and a-CDs as a function of the concentration of humic acid at neutral pH.

In the absence of electrolytes and at a circumneutral pH (Figure 76a), CDs displayed greater stability in their D_h over the HA concentration range from 20 to 200 mg/L than a-CDs, as the

D_h of a-CDs were influenced greater by the presence of HA than CDs. However, as the concentration of HA increased from 20 to 200 mg/L, the D_h of CDs as well as a-CDs increased from 343.5 nm to 518.9 nm and 448.7 nm to 860.6 nm, respectively. CDs and a-CDs seem to follow the same trend with an approximate 100-nm difference between them. a-CDs reached considerably larger particle sizes and proved to be more sensitive to the presence of HA with their overall D_h values being larger than those of CDs.

The ZP values were plotted as a function of the concentration of HA (Figure 76b). The ZP values of CDs were more sensitive to the presence of HA and is inversely proportional to the concentration of HA as the colloid surfaces became more negatively charged, from −9.97 to −36.9 mV, with an increase in HA concentration. On the other hand, a-CDs displayed good stability in their ZP over the [HA] range from 20 to 200 mg/L, as their ZP values remained fairly constant between 0 and −10 mV. CDs and a-CDs displayed negatively charged surfaces throughout all [HA] measurements. NOM is present in all potable water and is normally produced from decomposed plant materials that can be adsorbed onto the surfaces of CDs and a-CDs. These HA molecules have a variety of functional groups on their surfaces, such as carboxylic acids, that can be deprotonated in natural water. According to Benjamin and Lawler, because NOM carry multiple negative charges on its surface it can lead to the replacement of hydroxyl groups on the surfaces of CDs (Benjamin and Lawler 2013). Furthermore, it has been reported that NOM adsorbs onto carbon nanotubes to stabilise particles, therefore these large organic molecules could interact with the surfaces of CDs though π–π bonding because of the presence of C=C double bonds and aromatic rings (Bayati *et al* 2018), which could be what occurred in the case of a-CDs in Figure 76b. The binding strength of NOM is greater because of its multiple functional groups that provide multiple binding sites. Moreover, the tendency of NOM to adsorb is increased in environments of higher IS induced by the presence of divalent cations and also depends on the number of available surface sites and the build-up of a negative charge (Benjamin and Lawler 2013).

5.6. Summary

Overall, the applied environmental parameters influenced the characteristics of the synthesised materials to different extents with the most significant impact induced by high IS environments. Recall that agglomeration is expected in environments of higher IS such as seawater or groundwater that could affect benthic organisms and according to Bayati et al. CDs remain suspended in freshwater bodies (i.e., at low IS, lower than 0.01 M) but could still affect organisms such as fish, marine mammals and planktonic species or be transported to other ecosystems far from their initial point of contamination (Bayati *et al* 2018).

From the data presented on the behaviour of CDs and a-CDs under the applied environmental conditions it could be deduced that:

a) centrifugation does prove to revert the effects of agglomeration and actively reduces the hydrodynamic diameter of the synthesised materials;
b) unfunctionalised CDs are more stable, more monodisperse, and smaller in an environment of pH 5, whereas a-CDs show greater stability under basic conditions (i.e., at pH 9);
c) divalent cations (introduced by $CaCl_2$) had a greater influence on the D_h, ZP, PDI, and size distribution of both CDs and a-CDs, than monovalent cations (introduced by NaCl);
d) contrary to expectations and literature, the amine-functionality of a-CDs didn't seem to provide superior stability over unfunctionalised CDs against the process of agglomeration under pH variation; however, a-CDs showed greater stability in their surface charge under IS variation due to their intricate surface chemistry;
e) both CDs and a-CDs were susceptible to agglomeration at high IS of divalent ions as expected due to dominant van der Waals forces, and displayed the greatest colloidal stability with particles that are monodisperse in lower IS environments of 0.001 M and 0.01 M;
f) in the presence of natural organic matter (NOM, i.e., HA), the hydrodynamic diameter of a-CDs were more sensitive than that of unfunctionalised CDs, however, the ZP of CDs were more sensitive to an increase in the concentration of HA than that of a-CDs.

Table 24 serves to compare four characteristics, i.e., hydrodynamic diameter (D_h), zeta potential (ZP), polydispersity index (PDI), and size distribution by intensity of CDs and a-CDs,

that were studied with each applied environmental parameter, such as variation in pH, ionic strength (IS), and the presence of natural organic matter (NOM).

Table 24. The influence of pH, IS, and the presence of NOM on the D_h, ZP, PDI, and size distribution of CDs and a-CDs.

Characteristic	***CDs***	***a-CDs***
	The influence of pH	
D_h	In the presence of 0.01 M NaCl: D_h stable for all pH values In the presence of 0.01 M $CaCl_2$: D_h stable from pH 1–11 but very large at pH 13	In the presence of 0.01 M NaCl: D_h sensitive at pH 9 In the presence of 0.01 M $CaCl_2$: D_h slightly sensitive to pH variation, larger as pH increases
ZP	In the presence of 0.01 M NaCl: ZP decrease with increase in pH, therefore pH-sensitive In the presence of 0.01 M $CaCl_2$: ZP decrease with increase in pH, therefore pH-sensitive	In the presence of 0.01 M NaCl: ZP remains rather stable throughout pH variation In the presence of 0.01 M $CaCl_2$: ZP remains rather stable throughout pH variation with exception of more positive value at pH 1
PDI	In the presence of 0.01 M NaCl: PDI under 0.5 for pH 5 and 7; hence, more monodisperse at neutral pH In the presence of 0.01 M $CaCl_2$: PDI under 0.5 for pH 5 and 13	In the presence of 0.01 M NaCl: PDI under 0.5 for pH 9; hence, more monodisperse at larger pH (in basic environment) In the presence of 0.01 M $CaCl_2$: PDI under 0.5 for pH 9; hence, more monodisperse at larger pH (in basic environment)
Size distribution by intensity	In the presence of 0.01 M NaCl: more monodisperse and of smaller particle sizes below 1000 nm for pH 5 and 7 In the presence of 0.01 M $CaCl_2$: more monodisperse and of smaller particle sizes below 1000 nm for pH 5 and 7	In the presence of 0.01 M NaCl: more monodisperse and of smaller particle sizes below 1000 nm for pH 13 In the presence of 0.01 M $CaCl_2$: more monodisperse and of smaller particle sizes below 1000 nm for pH 9
	The influence of IS	
D_h	In a pH 5 environment with increasing [NaCl]: D_h stable for all IS values	In a pH 9 environment with increasing [NaCl]: D_h higher for environments of 0.001 M & 0.01 M IS; largest D_h in 0.01 M IS environment

	In a pH 5 environment with increasing [$CaCl_2$]: D_h stable from IS 0.001–0.1 M but larger in 1 M IS environment	In a pH 9 environment with increasing [$CaCl_2$]: D_h smaller in a 0.1 M IS environment and largest in 0.01 M IS environment
ZP	In a pH 5 environment with increasing [NaCl]: ZP became more positive with increasing IS In a pH 5 environment with increasing [$CaCl_2$]: ZP became more positive with increasing IS	In a pH 9 environment with increasing [NaCl]: ZP slightly more positive for high IS of 1 M; more negative for intermediate IS environments of 0.01 and 0.1 M In a pH 9 environment with increasing [$CaCl_2$]: ZP became slightly more positive with increasing IS
PDI	In a pH 5 environment with increasing [NaCl]: Particles more monodisperse at lower IS of 0.001 M and 0.01 M In a pH 5 environment with increasing [$CaCl_2$]: Particles monodisperse at low IS of 0.001 M	In a pH 9 environment with increasing [NaCl]: Particles polydisperse for all IS environments In a pH 9 environment with increasing [$CaCl_2$]: Increase in polydispersity of particles from 0.001 to 0.01 M of $CaCl_2$
Size distribution by intensity	In a pH 5 environment with increasing [NaCl]: Particles more monodisperse in a 0.01 M IS environment; increase in aggregation; contain small particles throughout In a pH 5 environment with increasing [$CaCl_2$]: Particles more monodisperse in a 0.001 M IS environment; increase in aggregation; contain small particles throughout	In a pH 9 environment with increasing [NaCl]: A larger number of smaller-sized particles at low IS; bimodal size distribution for intermediate IS of 0.01 and 0.1 M; largely agglomerated in 1 M IS environment In a pH 9 environment with increasing [$CaCl_2$]: Particles more polydisperse throughout with a larger quantity of smaller-sized particles (below 1000 nm) at low IS of 0.001 M and 0.01 M
The influence of NOM		
D_h	D_h increase with increase in the concentration of HA	D_h increase with increase in the concentration of HA
ZP	ZP decrease with increase in the concentration of HA	ZP remain stable with increase in the concentration of HA

Comparing the characteristics of CDs and a-CDs under the above-mentioned environmental factors, a-CDs were larger in size and more positively charged, than unfunctionalised CDs and presented more particles that were more monodisperse and of smaller hydrodynamic diameters at pH 9. On the contrary, unfunctionalised CDs showed greater colloidal stability under several applied environmental conditions as they were smaller in size, remained negatively charged throughout all environmental studies and possessed more monodisperse particles of smaller sizes at pH 5 and 7. As mentioned above, IS had a greater influence on the colloidal stability of the synthesised materials. Divalent cations had a greater effect on the D_h and ZP of both unfunctionalised CDs and a-CDs, and they were less polydisperse in the presence of divalent ions than monovalent ions. CDs showed greater stability in their D_h and size distribution under the influence of IS than a-CDs, which showed greater stability in their surface charge under the same conditions. Now, what does this all mean?

Granted, both CDs and a-CDs underwent agglomeration in high IS environments. Overall, CDs showed greater stability over a-CDs regardless of the fact that a-CDs possessed a so-called protective layer consisting of amino-groups. Furthermore, CDs are more stable at pH 5 and 7 whereas a-CDs are more stable in a basic environment of pH 9. Lastly, in the presence of NOM, even though CDs were smaller in size compared to a-CDs, both CDs and a-CDs showed an increase in their hydrodynamic diameter with an increase in HA, and their ZP values were negative throughout all HA studies, with CDs showing greater sensitivity than a-CDs. That being said, in high IS environments of pH lower and higher than pH 5–7, and in the presence of a larger concentration of NOM, CDs tend to undergo agglomeration at which point they would pose a threat to benthic organisms on the floor of water bodies such as seawater or groundwater (as mentioned at the beginning of this summary). On the other hand, in high IS and lower pH environments (below pH 9), and in the presence of a larger concentration of NOM, a-CDs tend to undergo agglomeration. These materials would be expected to remain in suspension in freshwater bodies and could thus affect organisms such as fish, marine mammals and planktonic species or be transported to other ecosystems far from their initial point of contamination (Bayati *et al* 2018), at low IS, low concentration of NOM, and pH 5–7 and 9, for CDs and a-CDs respectively.

Chapter 6 – Conclusions and Recommendations

6. Introduction

In this chapter the main findings on the studies performed is summarised and answers to research questions, posed at the beginning of this project, presented. Furthermore, recommendations are provided for future work on carbon-based nanomaterials and their colloidal stability.

6.1. Main findings of this study

The concept of nanotechnology and nanoscience, introduced many years ago, is for the progression or advancement of science and technology through manipulation of matter at the smallest scale possible to produce materials that work faster, react better, and possess unique properties. Technology needs to progress and reach greater heights but not at the cost of an unhealthy environment. Therefore, these nanomaterials have to undergo studies on their colloidal stability to accurately model and predict their behaviour in similar environmental conditions. This study provided great detail on the behaviour of carbon-based nanomaterials with the following research questions answered:

Q1: How is the colloidal stability of CDs and a-CDs affected by changes in their synthesis conditions?

Toxicity studies go far beyond just the materials under investigation. It has been discovered that the choice of reference materials, dispersion medium, and route of synthesis could heavily influence the degree of toxicity the material could possess (Filipponi and Sutherland 2012). Due to their small size, these carbon-based nanomaterials have been proved to have unique properties such as increased surface area and chemical reactivity. This higher chemical reactivity means that these small materials could be unstable under certain conditions. Therefore, various synthesis conditions were studied to determine their influence on a number of characteristics of CDs and a-CDs and their effective production.

As mentioned before, one would want to adhere to the green chemistry principles as far as possible for the effective synthesis of small NPs which means the minimal use of (a) reagents and (b) harsh synthesis conditions such as high temperature and longer reaction times. Therefore, to synthesise particles of small sizes, a large % yield, a red-shift, i.e., a shift of λ_{max} towards longer wavelengths, a smaller D_h, a smaller PDI value i.e., a larger degree of monodispersity, more negative surface charges, and narrow size distributions towards smaller

particle sizes, is desired for lower synthesis temperatures, shorter reaction times, and smaller reagent quantities.

In this study, plain/unfunctionalised CDs proved to be sensitive to changes in the microwave power; as the power was increased from 90 to 900 W, several parameters were affected such as the burn-off percentage, band gap energy, and absorption intensity (Sutanto *et al* 2020). The higher the power, the more viscous the product became until a dried product was obtained for the highest power level of 900 W. The position of the absorbance peak maximum proved that CDs were synthesised and red-shifted towards longer wavelengths with an increase in power. Furthermore, the small hydrodynamic diameters along with the more negative surface charges at higher power levels showed that CDs displayed greater stability at higher power. However, agglomeration occurred to a large extent and could be halted by the introduction of further purification through a method such as centrifugation which proved to yield particles of smaller hydrodynamic sizes. To adhere to green chemistry principles as far as possible, utilisation of a lower synthesis power is desired for the effective or adequate production of CDs. Therefore, while lower power-levels yielded particles of a wider size distribution, at a power of 720 W an effective production of CDs was observed and it was therefore identified as an adequate synthesis power for this procedure which has proved to be very successful in previous studies (Chen *et al* 2019, Liu *et al* 2016, Wang *et al* 2019, Xu *et al* 2015).

This study has shown that an increase in the heating time from 5 to 25 minutes for the synthesis of plain CDs affected several parameters such as (a) the % yield which decreased, (b) the colour of the suspension of CDs which intensified, (c) the absorbance increased and λ_{max} underwent a shift towards longer wavelengths (red-shift), (d) the hydrodynamic diameter was smallest for the sample prepared within 20 minutes, (e) the ZP became more negative with the lowest value for RTOpt_A9 (20 min), and (f) the overall size distribution of particles was narrow with all particles below the upper limit for colloidal suspensions (1000 nm) while most particles were of smaller size classes. The trends observed for this study was similar to what has been observed for the power optimisation study. However, although agglomeration occurred, the size distribution of particles leaned more towards smaller size classes than for the power study. Due to experimental difficulty at longer reaction times, the adequate reaction time for the synthesis of CDs was determined as 15 minutes which had the narrowest size distribution, a small D_h, the most negative surface charge and was similar to the reaction time used for a previous study (Wang *et al* 2011a).

CDs also proved to be very sensitive to variation in the Gly molar quantity. As the ratio of 70 % (w/w) Gly to 20 % (w/w) NaH_2PO_4 increased from 6:1 to 14:1, an opposite trend was observed to those of the power and reaction-time studies. The % yield increased, the colour of the suspension of CDs lightened, the absorbance decreased and λ_{max} underwent a blue-shift towards shorter wavelengths, the surface charge became more positive from −0.737 mV to +10.3 mV, and the overall size distribution of particles was very broad with most particles above the upper limit for colloidal suspensions (1000 nm). As previously mentioned, an increase in the number of moles of Gly (i.e., the carbon source) in the reaction affects the overall rate of the reaction as more carbon was available for carbonisation of hydrocarbon into the graphitic structure, hence the increase in % yield. Even though the most negative surfaces were observed for the lowest reagent ratio of 6:1, the 10:1 reagent ratio was chosen as the ideal/adequate ratio for effective synthesis of CDs as more of the carbon source is available for carbonisation.

In this study, the increase in the number of moles of 20 % (w/w) NaH_2PO_4 in the synthesis of plain CDs showed that CDs were also sensitive to variation in the molar quantity of NaH_2PO_4. Increasing the number of moles of NaH_2PO_4 in the reaction affected the overall rate of the reaction because there were more of the inorganic phosphate salt which acted to catalyse the process of carbonisation of hydrocarbon into the graphitic structure. Therefore, as the ratio of 70 % (w/w) Glycerol to 20 % (w/w) NaH_2PO_4 increased from 10:0.5 to 10:4, several parameters were affected, such as the % yield which was lower for intermediate molar values between 2.6×10^{-3} to 2.04×10^{-2} mol; the colour of the suspension of CDs that was darker for lower and higher ratios of Gly to NaH_2PO_4 as reported in literature (Bayati *et al* 2018), the absorbance which initially decreased and then increased for higher molar values of NaH_2PO_4 and λ_{max} blue-shifted towards shorter wavelengths; the hydrodynamic diameter which was small for larger molar quantities of NaH_2PO_4; the ZP became more negative; and the overall size distribution of particles which was rather narrow but with most particles above the upper limit for colloidal suspensions (1000 nm).

a-CDs were very sensitive to changes in synthesis temperature; as the synthesis temperature was increased from 130 °C to 210 °C, the average hydrodynamic diameter of particles increased which was corroborated by the more positive zeta potentials and this could be attributed to the occurrence of agglomeration. However, the overall size distribution is narrower than that measured for the plain unfunctionalised CDs which could be owed to greater stability induced by amine groups on the surface of a-CDs. Greatest stability was observed for the samples prepared at 150 °C and 170 °C.

As the reaction time for the synthesis of a-CDs was increased from 1 to 3 hours, the average hydrodynamic diameter of particles decreased, and the surfaces of a-CDs became more negative but remained positive throughout. Although agglomeration occurred, a-CDs still displayed greater stability compared to the reaction time study done on unfunctionalised CDs because a-CDs possessed particles that were sized within the nano-range.

Once again, an increase in the number of moles of CA for the synthesis of a-CDs significantly affected the process of carbonisation and a-CDs proved to be sensitive to changes in the molar values of CA. As the number of moles of CA was increased from 7.8×10^{-3} to 1.4×10^{-2} mol, there was a hypochromic effect observed in the absorbance spectra of a-CDs, there was a slight increase in the average hydrodynamic diameter which correlated to surface charges that became more positive. As in the case of plain CDs, increasing the number of moles of the carbon source in the reaction affected the overall rate of the reaction as more carbon was available for carbonisation of hydrocarbon into the graphitic structure, hence the increase in % yield. The sample prepared with 1.1×10^{-2} mol (2.1 g) of CA was determined as the ideal molar quantity of CA for the synthesis of a-CDs and has been successful in previous studies (Bayati *et al* 2018, Zheng *et al* 2014).

An increase in the number of moles of BPEI for the synthesis of a-CDs significantly affected the carbonisation process. As the number of moles of BPEI was increased from 7.9×10^{-3} to 1.8×10^{-2} mol, the absorbance maximum underwent a hypochromic effect and red-shifted towards longer wavelengths with an overall decrease in the average hydrodynamic diameter as corroborated by the more negative surface charges. As stated previously, increasing the number of moles of the passivation agent in the reaction, affected the overall rate of the reaction as more nitrogen content was available to induce greater colloidal stability. Agglomeration occurred to a large extent, however, a-CDs displayed greater stability compared to plain/unfunctionalised CDs due to the presence of nano-sized particles and the stability

provided by the passivation agent (i.e., BPEI). The sample prepared with 1.3×10^{-2} mol (10 mL) of BPEI possessed the smallest average hydrodynamic diameter, most negative ZP and the narrowest size distribution; therefore, it was chosen as the ideal molar quantity of BPEI for the synthesis of a-CDs and has been successful in previous studies (Bayati *et al* 2018, Zheng *et al* 2014).

Q2: How is the colloidal stability of plain CDs and a-CDs affected by changes in environmental conditions, such as the influence of pH, salinity (introduced by monovalent and divalent cations from NaCl and $CaCl_2$, respectively), and the presence of natural organic matter, i.e., humic acid?

Typically, nanoparticles undergo aggregation due to their small size and their large amount of surface atoms that gives rise to a high surface energy but aggregation could be hindered or halted by coatings or adsorbed material such as NOM. According to Bayati, the stability of NMs greatly depends on the presence of NOM and Ca^{2+} ions; NOM could provide stability whereas Ca^{2+} could cause aggregation especially in surface waters (Bayati *et al* 2018).

CDs displayed greater stability in water suspensions of a circumneutral pH, whereas, a-CDs showed higher stability in water suspensions of a basic nature. As the pH was increased from 1 to 13, in the presence of 10 mM ionic strength given by NaCl, CDs showed greater stability in their hydrodynamic diameter. However, the hydrodynamic diameter (D_h) values of a-CDs were pH sensitive as their D_h increased with the increase in pH from 1 to 13. The presence of divalent cations influenced a-CDs greater than CDs. Furthermore, the surfaces of both CDs and a-CDs became more negatively charged with an increase in pH. According to Bayati, the decrease in ZP with an increase in pH could be attributed to the deprotonation of surface functional groups such as hydroxyl and carboxyl groups (Bayati *et al* 2018). In the case of a-CDs, at lower pH values, protonation of amino groups occurred and yielded surfaces that were more positively charged. It was evident that divalent cations had a greater impact on the coagulation of negatively charged nanomaterials than monovalent cations which is in agreement with literature (Bayati *et al* 2018, Hunter 1987). Throughout the pH study a-CDs displayed surfaces that were more positively charged than CDs. CDs had lowest PDI values at pH 5 and 7, and a-CDs displayed their lowest PDI value at pH 9 under basic conditions. This meant that under circumneutral conditions CDs showed greater monodispersity and had narrow size distributions, whereas a-CDs were more monodisperse under basic conditions.

In this study, the effect of ionic strength was studied as induced by NaCl and $CaCl_2$, i.e., monovalent and divalent cations, respectively. In the presence of NaCl, CDs displayed greater stability in their hydrodynamic diameter over the IS range from 0.001 to 1 M, than a-CDs. Although CDs were large in size between 300–400 nm, a-CDs proved to be more unstable and have reached much larger sizes due to their sensitivity to the presence of Na^+ ions. In the presence of the divalent Ca^{2+} ions, CDs were slightly more sensitive to changes in IS as the D_h was influenced more noticeably by the presence of Ca^{2+}-ions than Na^+-ions. Hence, the D_h of CDs initially decreased as the IS increased from 0.001 to 0.1 M, and then significantly increased in a 1 M IS environment. On the other hand, a-CDs were more IS sensitive than CDs and were greater influenced by the presence of divalent cations (Ca^{2+}) than monovalent cations (Na^+). The presence of divalent cations influenced both CDs and a-CDs greater than monovalent cations, which, according to previous studies, greatly influences coagulation and catalytic abilities for carbonisation (Hunter 1987, Wang *et al* 2011a).

Moreover, the ZP values of CDs and a-CDs were IS sensitive because they increased with an increase in IS. CDs displayed negatively charged surfaces throughout all IS measurements in the presence of NaCl and $CaCl_2$, whereas a-CDs were more positively charged. According to classical colloid theory, electrical double layer compression occurs as the IS increases and surface charge becomes more positive due to interaction of NPs with surrounding or dissolved electrolytes (Bayati *et al* 2018, Verwey 1947). At low IS an initial decrease in the surface potential values of a-CDs occurred due to the thickening of the EDL and the large potential barrier which is caused by repulsion that occurs between particles yielding more negative ZPs. Due to the dependency on the valency of the potential-determining ions (i.e., ions of opposite charge to the colloids or particles) at high IS rapid agglomeration could occur according to the Schultze-Hardy rule (Hunter 1987, Verwey 1947). According to Bayati et al., rapid aggregation of NMs in natural water could cause them to sediment and affect benthic organisms. In the presence of $CaCl_2$, CDs were significantly affected by the presence of Ca^{2+} ions as ZP values for each concentration was more positive for $CaCl_2$ than for NaCl, while the surface charge values of a-CDs increased moderately. Furthermore, all surfaces approached the point of zero charge due to the adsorption of Ca^{2+} onto the negatively charged surfaces of CDs (Bayati *et al* 2018). It was found that divalent cations have a greater influence on the stability of CDs and a-CDs than monovalent cations, and a-CDs showed greater stability in IS variation than did CDs.

In addition, the stability of particles is better understood by studying the degree of polydispersity and size distribution in which greater stability is recognised by particles that possess narrow size distributions towards smaller size classes. In NaCl suspensions, CDs displayed the best size distribution in a 0.01 M IS environment, whereas, a-CDs showed greater stability in a 0.1 M IS environment, showing that the amine-capping of a-CDs provided greater stability under these conditions. In $CaCl_2$ solutions, both CDs and a-CDs displayed particles that were more monodisperse and of narrow size distributions in a 0.001 M IS environment. The overall size distribution of particles in the presence of divalent cations was slanted more towards smaller size classes meaning that a greater % of particles were smaller in size. Also, a-CDs were more monodisperse and smaller in size in the presence of $CaCl_2$.

In this study, the influence of natural organic matter on the colloidal stability of CDs and a-CDs was studied by varying the concentration of HA from 20 to 200 mg/L in the absence of electrolytes. As the concentration of HA increased from 20 to 200 mg/L, the D_h of CDs as well as a-CDs increased, while a-CDs reached considerably larger sizes and proved to be more sensitive to the presence of HA with their overall hydrodynamic diameter values being larger than those of CDs. On the other hand, as the concentration of HA was increased the surface charge of CDs became more negative, while a-CDs displayed good stability in their surface charge with more positive surfaces (at fairly constant ZP values between 0 and −10 mV) than plain/unfunctionalised CDs. Both CDs and a-CDs displayed negatively charged surfaces throughout all [HA] measurements. As previously mentioned, NOM is commonly found in natural water bodies and they have a variety of functional groups on their surfaces that can be deprotonated. Hence, NOM adsorbed onto colloidal particles due to its high binding strength inducing aggregation at lower concentrations and stability at higher concentrations which is why the application of CDs in natural water-sensing is restricted (Benjamin and Lawler 2013, Bayati *et al* 2018).

In summary, as stated in a previous paper written by Bayati et al., literature has mainly been focused on stability studies performed on inorganic nanoparticles, and other carbon-based nanomaterials such as fullerenes, carbon nanotubes, and graphene oxides while information on the colloidal stability of CDs have been greatly neglected over the years (Bayati *et al* 2018). Therefore, the information gathered on the aggregation behaviour of both unfunctionalised and functionalised carbon dots in this study, with a thorough investigation into several particle characteristics under the above-mentioned applied environmental conditions, further broadens the understanding on its colloidal stability—speaking to its novelty.

6.2. Recommendations for future work

This study shed some light on important parameters in the synthesis of carbon-based materials and the colloidal stability thereof. However, further research into the colloidal stability of CDs and a-CDs and the following notes should be taken under consideration:

1. Having synthesised CDs and a-CDs from glycerol, and citric acid, respectively, greener reagents are suggested for use as the carbon source. Literature is full of a variety of reagents that are extracted straight from the fruit or vegetation rich in carbon. These are readily available and could still yield a large amount of the product, i.e., CDs.
2. Furthermore, the use of a domestic microwave for the synthesis of plain CDs exposes the researcher to a possible fire hazard. Higher power levels and longer heating periods increases the possibility of one experiencing the eruption of a flame. In this study, higher power levels yielded better results for CDs; however, further investigation into the use of other reagents at lower power levels might produce promising data and other heating equipment is suggested for safer synthesis procedures.
3. Also, during this study there was some difficulty in drying CDs in a freeze-drier, hence, the studies being done on wet samples as some of the initial samples of CDs were found to retain water. Future work on this topic could make use of other drying techniques.
4. In terms of the purification procedure used within this study, i.e., dialysis, one could introduce longer dialysis periods better regulated and introduce a stirring mechanism if a small number of samples are studied, but in this study a stirring mechanism could not be introduced due to the lack of access to magnetic stirring equipment that could accommodate the large group of samples. Other purification procedures could be introduced if the structural integrity of the material under study is not a big concern or great priority, such as centrifugation or ultracentrifugation which might alter the shape or integrity of the materials under study.
5. The narrow scope of characterisation techniques used in this study has left areas in need of further characterisation. For future work, the CDs prepared in this study should be analysed by HR-TEM or HR-SEM to more accurately investigate the size distribution of samples. These characterisation techniques could also shed some light on the degree of aggregation in the sample. Ray et al. reported on their difficulty in finding isolated small carbon particles during TEM analysis due to the strong tendency of the particles to undergo agglomeration during grid preparation (Ray *et al* 2009). However, they have suggested that a monitored dropping process does allow for better control over

aggregation and have reported that single drop samples were of smaller sizes than successive multiple drops.

Furthermore, materials such as graphene could serve as a comfortable means of transportation for pollutants such as pharmaceuticals. Currently there are few studies done on the adsorption of pharmaceuticals onto the surface of LIG, as graphene had been prepared by many different methods but only very recently have been prepared from a CO_2 laser, hence the novelty and necessity of its study. Therefore, be on the look-out for an article that I will have published in the near future on adsorption studies I performed on graphene during my masters.

"No matter how sophisticated knowledge is, it will always be subject to some degree of ignorance. To be alert to—and humble about— the potential gaps in those bodies of knowledge that are included in our decision-making is fundamental. Surprise is inevitable. Just as one basis for scientific research is the anticipation of positive surprises—'discoveries'—so it will always yield the corresponding prospect of negative surprises. By their nature, complex, cumulative, synergistic or indirect effects in particular have traditionally been inadequately addressed in regulatory appraisal."

– The European Environment Agency, from the 2001 report, "Late Lessons from Early Warnings: The Precautionary Principle 1896-2000"

References

Arivazhagan V 2014 *Investgation of Quantum Confinement Effect in pbse znse multiple Quantum Well Structures Prepared by Thermal Evaporation technique* (Karunya University) Online: http://hdl.handle.net/10603/23484

Ayala P, Arenal R, Loiseau A, Rubio A and Pichler T 2010 The physical and chemical properties of heteronanotubes *Rev. Mod. Phys.* **82** 1843–85

Baker S N and Baker G A 2010 Luminescent carbon nanodots: Emergent nanolights *Angew. Chemie - Int. Ed.* **49** 6726–44

Bandi S P, Kumbhar Y S and Venuganti V V K 2020 Effect of particle size and surface charge of nanoparticles in penetration through intestinal mucus barrier *J. Nanoparticle Res.* **22** 1–11 Online: https://link.springer.com/article/10.1007/s11051-020-04785-y

Barman M K and Patra A 2018 Current status and prospects on chemical structure driven photoluminescence behaviour of carbon dots *J. Photochem. Photobiol. C Photochem. Rev.* **37** 1–22 Online: https://www.sciencedirect.com/science/article/pii/S1389556718300418

Bawa A S and Anilakumar K R 2013 Genetically modified foods: Safety, risks and public concerns - A review *J. Food Sci. Technol.* **50** 1035–46 Online: /pmc/articles/PMC3791249/?report=abstract

Bayati M, Dai J, Zambrana A, Rees C and Fidalgo de Cortalezzi M 2018 Effect of water chemistry on the aggregation and photoluminescence behavior of carbon dots *J. Environ. Sci. (China)* **65** 223–35 Online: https://www.researchgate.net/publication/315960299_Effect_of_water_chemistry_on_the_aggregation_and_photoluminescence_behavior_of_carbon_dots

Bayati M, Peng H, Deng H, Lin J and Fidalgo de Cortalezzi M 2020 Laser induced graphene /ceramic membrane composite: Preparation and characterization *J. Memb. Sci.* **595**

Bayda S, Adeel M, Tuccinardi T, Cordani M and Rizzolio F 2020 The History of Nanoscience and Nanotechnology: From Chemical-Physical Applications to Nanomedicine *Molecules* **25** 112 Online: /pmc/articles/PMC6982820/?report=abstract

Benjamin M M and Lawler D F 2013 *Water Quality Engineering: Physical / Chemical*

Treatment Processes (John Wiley & Sons, Inc.) Online: https://www.wiley.com/en-us/Water+Quality+Engineering%3A+Physical+Chemical+Treatment+Processes-p-9781118169650

Bewick S, Parsons R, Forsythe T, Robinson S and Dupon J 2019 Factors Affecting Reaction Rate - Chemistry LibreTexts *Chem. Libr.* Online: https://chem.libretexts.org/Bookshelves/Introductory_Chemistry/Book%3A_Introductory_Chemistry_(CK-12)/18%3A_Kinetics/18.6%3A_Factors_Affecting_Reaction_Rate

Bhattacharyya S, Ehrat F, Urban P, Teves R, Wyrwich R, Döblinger M, Feldmann J, Urban A S and Stolarczyk J K 2017 Effect of nitrogen atom positioning on the trade-off between emissive and photocatalytic properties of carbon dots *Nat. Commun.* **8** 1–9 Online: www.nature.com/naturecommunications

Biener J, Wittstock A, Baumann T F, Weissmüller J, Bäumer M and Hamza A V. 2009 Surface chemistry in nanoscale materials *Materials (Basel).* **2** 2404–28

Binnig G and Rohrer H 1986 *Scanning Tunneling Microscopy - From Birth to Adolescence*

Binnig G, Rohrer H, Gerber C and Weibel E 1982 Tunneling through a controllable vacuum gap *Appl. Phys. Lett.* **40** 178–80 Online: http://aip.scitation.org/doi/10.1063/1.92999

Biswas J K and Sarkar D 2019 Nanopollution in the Aquatic Environment and Ecotoxicity: No Nano Issue! *Curr. Pollut. Reports* **5** 4–7 Online: http://link.springer.com/10.1007/s40726-019-0104-5

Cameron J S 2012 Thomas Graham (1805-1869)- The "father" of dialysis *Dialysis: History, Development and Promise* (World Scientific Publishing Co.) pp 19–26 Online: https://www.researchgate.net/publication/288491362_Thomas_Graham_1805-1869_-_The_Father_of_Dialysis

Chen C Y, Tsai Y H and Chang C W 2019 Evaluating the dialysis time required for carbon dots by HPLC and the properties of carbon dots after HPLC fractionation *New J. Chem.* **43** 6153–9 Online: https://pubs.rsc.org/en/content/articlehtml/2019/nj/c9nj00434c

Chen K L and Elimelech M 2006 Aggregation and deposition kinetics of fullerene (C60) nanoparticles *Langmuir* **22** 10994–1001 Online: https://pubs.acs.org/doi/10.1021/la062072v

Choi G S, Oak C, Chun B K, Wilson D, Jang T W, Kim H K, Jung M, Tutkun E and Park E

K 2014 Titanium dioxide exposure induces acute eosinophilic lung inflammation in rabbits *Ind. Health* **52** 289–95 Online: /pmc/articles/PMC4243014/?report=abstract

Chowdhury I, Duch M C, Mansukhani N D, Hersam M C and Bouchard D 2013 Colloidal properties and stability of graphene oxide nanomaterials in the aquatic environment *Environ. Sci. Technol.* **47** 6288–96 Online: https://pubs.acs.org/doi/abs/10.1021/es400483k

Dager A, Uchida T, Maekawa T and Tachibana M 2019 Synthesis and characterization of Mono-disperse Carbon Quantum Dots from Fennel Seeds: Photoluminescence analysis using Machine Learning *Sci. Rep.* **9** 1–12 Online: www.nature.com/scientificreports

De B and Karak N 2013 A green and facile approach for the synthesis of water soluble fluorescent carbon dots from banana juice *RSC Adv.* **3** 8286–90 Online: https://www.researchgate.net/publication/236960085_A_green_and_facile_approach_for_the_synthesis_of_water_soluble_fluorescent_carbon_dots_from_banana_juice

Delahay P 1957 *Instrumental Analysis* (Canada: The Macmillan Company)

Deng J, Lu Q, Mi N, Li H, Liu M, Xu M, Tan L, Xie Q, Zhang Y and Yao S 2014 Electrochemical synthesis of carbon nanodots directly from alcohols *Chem. - A Eur. J.* **20** 4993–9 Online: https://www.researchgate.net/publication/260761175_Electrochemical_Synthesis_of_Carbon_Nanodots_Directly_from_Alcohols

Edwards P P and Thomas J M 2007 Gold in a Metallic Divided State-From Faraday to Present-Day Nanoscience *Angew. Chemie - Int. Ed.* **46** 5480–6

Ellenbecker M and Tsai S 2011 Engineered nanoparticles: Safer substitutes for toxic materials, or a new hazard? *J. Clean. Prod.* **19** 483–7 Online: http://dx.doi.org/10.1016/j.jclepro.2010.11.004

Emam A N, Loutfy S A, Mostafa A A, Awad H and Mohamed M B 2017 Cyto-toxicity, biocompatibility and cellular response of carbon dots-plasmonic based nano-hybrids for bioimaging *RSC Adv.* **7** 23502–14

European Defence Agency 2019 *Preparatory Action on Defence Research (PADR) Programme - Guidance on How to complete your self-assessment on "ethics, legal and societal aspects (ELSA)"*

Faraday M 1857 The Bakerian Lecture: Experimental Relations of Gold (and Other Metals) to Light *Philos. Trans. R. Soc. London* 145–81 Online: https://www.jstor.org/stable/pdf/108616.pdf

Feynman R P 1960 There's Plenty of Room at the Bottom *Eng. Sci.* 22–36 Online: https://calteches.library.caltech.edu/1976/1/1960Bottom.pdf

Filipponi L and Sutherland D 2012 *Nanotechnologies: Principles, Applications, Implications and Hands-on Activities* (Luxembourg: EU Publications) Online: https://op.europa.eu/en/publication-detail/-/publication/39ee677e-4e6c-4c2c-97d1-6669057c09b3/language-en

Freestone I, Meeks N, Sax M and Higgitt C 2008 The Lycurgus Cup - A Roman nanotechnology *Gold Bull.* **40** 270–7 Online: http://link.springer.com/10.1007/BF03215599

Galdiero S, Falanga A, Vitiello M, Cantisani M, Marra V and Galdiero M 2011 Silver nanoparticles as potential antiviral agents *Molecules* **16** 8894–918 Online: /pmc/articles/PMC6264685/?report=abstract

Gao J, Gu H and Xu B 2009 Multifunctional magnetic nanoparticles: design, synthesis, and biomedical applications *Acc. Chem. Res.* **42** 1097–107 Online: https://pubs.acs.org/doi/abs/10.1021/ar9000026

Georgakilas V, Perman J A, Tucek J and Zboril R 2015 Broad Family of Carbon Nanoallotropes: Classification, Chemistry, and Applications of Fullerenes, Carbon Dots, Nanotubes, Graphene, Nanodiamonds, and Combined Superstructures *Chem. Rev.* **115** 4744–822

Gong N, Wang H, Li S, Deng Y, Chen X, Ye L and Gu W 2014 Microwave-assisted polyol synthesis of gadolinium-doped green luminescent carbon dots as a bimodal nanoprobe *Langmuir* **30** 10933–9 Online: https://pubmed.ncbi.nlm.nih.gov/25157595/

Gottlieb M A and Pfeiffer R 1963 The Brownian Movement - The Feynman Lectures on Physics Vol. I *Calif. Inst. Technol.* Online: https://www.feynmanlectures.caltech.edu/I_41.html

Hasanuzzaman M, Rafferty A, Sajjia M and Olabi A G 2016 Properties of Glass Materials *Ref. Modul. Mater. Sci. Mater. Eng.* 1–12 Online:

https://www.sciencedirect.com/science/article/pii/B9780128035818039989

Hassellöv M, Readman J W, Ranville J F and Tiede K 2008 Nanoparticle analysis and characterization methodologies in environmental risk assessment of engineered nanoparticles *Ecotoxicology* **17** 344–61 Online: https://link.springer.com/article/10.1007/s10646-008-0225-x

Hazari A 2017 Electronics are about to reach their limit in processing power—but there's a solution *Quartz Media, Inc.* Online: https://qz.com/852770/theres-a-limit-to-how-small-we-can-make-transistors-but-the-solution-is-photonic-chips/

He H, Wang X, Feng Z, Cheng T, Sun X, Sun Y, Xia Y, Wang S, Wang J and Zhang X 2015 Rapid microwave-assisted synthesis of ultra-bright fluorescent carbon dots for live cell staining, cell-specific targeting and in vivo imaging *J. Mater. Chem. B* **3** 4786–9 Online: http://dx.doi.org/10.1039/C5TB00570A

Helmenstine A M 2019 An Introduction to Brownian Motion *ThoughtCo.* Online: https://www.thoughtco.com/brownian-motion-definition-and-explanation-4134272

Hu S L, Niu K Y, Sun J, Yang J, Zhao N Q and Du X W 2009 One-step synthesis of fluorescent carbon nanoparticles by laser irradiation *J. Mater. Chem.* **19** 484–8 Online: https://pubs.rsc.org/en/content/articlehtml/2009/jm/b812943f

Hullmann A 2008 *European activities in the field of ethical, legal and social aspects (ELSA) and governance of nanotechnology* Online: http://cordis.europa.eu./nanotechnology2/48

Hunter R J 1987 *Foundations of Colloid Science* (New York, United States: Oxford University Press, New York)

Ismail N S, Husain U S, Selvan S I S, Mordani N A, Juhari N and Halim N H A 2020 Effect of heating power towards synthesis of carbon dots through microwave pyrolysis method for optical-based biosensor *AIP Conference Proceedings* vol 2203 (American Institute of Physics Inc.) p 020057 Online: http://aip.scitation.org/doi/abs/10.1063/1.5142149

ISO/TS 80004-1:2015 2015 Nanotechnologies-Vocabulary-Part 1: Core terms. Online: https://www.iso.org/obp/ui/#iso:std:iso:ts:80004:-1:ed-2:v1:en

Jaiswal A, Sankar Ghosh S and Chattopadhyay A 2012 One step synthesis of C-dots by microwave mediated caramelization of poly(ethylene glycol) *Chem. Commun.* **48** 407–9

Jia X, Li J and Wang E 2012 One-pot green synthesis of optically pH-sensitive carbon dots with upconversion luminescence *Nanoscale* **4** 5572–5 Online: https://pubs.rsc.org/en/content/articlehtml/2012/nr/c2nr31319g

Joseph J and Anappara A A 2016 White light emission of carbon dots by creating different emissive traps *J. Lumin.* **178** 128–33 Online: https://www.researchgate.net/publication/303780703_White_light_emission_of_carbon_dots_by_creating_different_emissive_traps

Kandasamy G 2019 Recent Advancements in Doped/Co-Doped Carbon Quantum Dots for Multi-Potential Applications *C* **5** 24 Online: https://www.mdpi.com/2311-5629/5/2/24

Khan I, Saeed K and Khan I 2019 Nanoparticles: Properties, applications and toxicities *Arab. J. Chem.* **12** 908–31

Lab Manager 2009 Working with Laboratory Glassware Online: https://www.labmanager.com/lab-health-and-safety/working-with-laboratory-glassware-20359

Leon L, Chung E J and Rinaldi C 2019 A brief history of nanotechnology and introduction to nanoparticles for biomedical applications *Nanoparticles for Biomedical Applications: Fundamental Concepts, Biological Interactions and Clinical Applications* (Elsevier) pp 1–4 Online: https://linkinghub.elsevier.com/retrieve/pii/B9780128166628000011

Li D and Kaner R B 2008 Graphene-Based Materials *Science (80-.).* **320** 1170–1 Online: https://science.sciencemag.org/content/320/5880/1170

Li H, Zhang Y, Wang L, Tian J and Sun X 2011 Nucleic acid detection using carbon nanoparticles as a fluorescent sensing platform *Chem. Commun.* **47** 961–3

Li L L, Ji J, Fei R, Wang C Z, Lu Q, Zhang J R, Jiang L P and Zhu J J 2012 A facile microwave avenue to electrochemiluminescent two-color graphene quantum dots *Adv. Funct. Mater.* **22** 2971–9

Liu C, Zhang P, Tian F, Li W, Li F and Liu W 2011a One-step synthesis of surface passivated carbon nanodots by microwave assisted pyrolysis for enhanced multicolor photoluminescence and bioimaging *J. Mater. Chem.* **21** 13163–7

Liu H, He Z, Jiang L P and Zhu J J 2015 Microwave-assisted synthesis of wavelength-tunable photoluminescent carbon nanodots and their potential applications *ACS Appl.*

Mater. Interfaces **7** 4913–20

Liu H, Ye T and Mao C 2007 Fluorescent carbon nanoparticles derived from candle soot *Angew. Chemie - Int. Ed.* **46** 6473–5 Online: https://pubmed.ncbi.nlm.nih.gov/17645271/

Liu S, Wang L, Tian J, Zhai J, Luo Y, Lu W and Sun X 2011b Acid-driven, microwave-assisted production of photoluminescent carbon nitride dots from N,N-dimethylformamide *RSC Adv.* **1** 951–3

Liu X, Li T, Hou Y, Wu Q, Yi J and Zhang G 2016 Microwave synthesis of carbon dots with multi-response using denatured proteins as carbon source *RSC Adv.* **6** 11711–8 Online: https://pubs.rsc.org/en/content/articlehtml/2016/ra/c5ra23081k

Loos M 2015 Nanoscience and Nanotechnology *Carbon Nanotube Reinforced Composites: CNR Polymer Science and Technology* (Elsevier Inc.) pp 1–36 Online: https://linkinghub.elsevier.com/retrieve/pii/B9781455731954000011

López C, Zougagh M, Algarra M, Rodríguez-Castellón E, Campos B B, Esteves Da Silva J C G, Jiménez-Jiménez J and Ríos A 2015 Microwave-assisted synthesis of carbon dots and its potential as analysis of four heterocyclic aromatic amines *Talanta* **132** 845–50 Online: http://dx.doi.org/10.1016/j.talanta.2014.10.008

Malvern Instruments Ltd. 2004 Zetasizer Nano Series User Manual *Biofutur* **1999** 54

Manioudakis J, Victoria F, Thompson C A, Brown L, Movsum M, Lucifero R and Naccache R 2019 Effects of nitrogen-doping on the photophysical properties of carbon dots *J. Mater. Chem. C* **7** 853–62 Online: https://pubs.rsc.org/en/content/articlehtml/2019/tc/c8tc04821e

Mao Y, Bao Y, Han D, Li F and Niu L 2012 Efficient one-pot synthesis of molecularly imprinted silica nanospheres embedded carbon dots for fluorescent dopamine optosensing *Biosens. Bioelectron.* **38** 55–60 Online: https://linkinghub.elsevier.com/retrieve/pii/S0956566312002722

Michalet X, Pinaud F F, Bentolila L A, Tsay J M, Doose S, Li J J, Sundaresan G, Wu A M, Gambhir S S and Weiss S 2005 Quantum dots for live cells, in vivo imaging, and diagnostics *Science (80-.).* **307** 538–44 Online: https://pubmed.ncbi.nlm.nih.gov/15681376/

Mitra S, Chandra S, Kundu T, Banerjee R, Pramanik P and Goswami A 2012 Rapid microwave synthesis of fluorescent hydrophobic carbon dots *RSC Adv.* **2** 12129–31

Mohajerani A, Burnett L, Smith J V., Kurmus H, Milas J, Arulrajah A, Horpibulsuk S and Kadir A A 2019 Nanoparticles in construction materials and other applications, and implications of nanoparticle use *Materials (Basel).* **12** Online: /pmc/articles/PMC6804222/?report=abstract

Mohan Bhagyaraj S and Oluwafemi O S 2018 Nanotechnology: The Science of the Invisible *Synthesis of Inorganic Nanomaterials* (Elsevier) pp 1–18

NobelPrize.org Press release: The 1996 Nobel Prize in Chemistry *Nobel Media AB 2020* Online: https://www.nobelprize.org/prizes/chemistry/1996/press-release/

Nowack B and Bucheli T D 2007 Occurrence, behavior and effects of nanoparticles in the environment *Environ. Pollut.* **150** 5–22

Pang Y, Gao H, Wu S and Li X 2017 Facile synthesis the nitrogen and sulfur co-doped carbon dots for selective fluorescence detection of heavy metal ions *Mater. Lett.* **193** 236–9

Peng H and Travas-Sejdic J 2009 Simple aqueous solution route to luminescent carbogenic dots from carbohydrates *Chem. Mater.* **21** 5563–5 Online: https://www.researchgate.net/publication/231242610_Simple_Aqueous_Solution_Route_to_Luminescent_Carbogenic_Dots_from_Carbohydrates

Pramanik P and Maity A 2013 Nanopollution - A Growing Issue *NESA Newsl.* Online: https://www.researchgate.net/publication/280640298_nanopollution-_A_growing_issue

Qu S, Wang X, Lu Q, Liu X and Wang L 2012 A biocompatible fluorescent ink based on water-soluble luminescent carbon nanodots *Angew. Chemie - Int. Ed.* **51** 12215–8 Online: https://onlinelibrary.wiley.com/doi/full/10.1002/anie.201206791

Ralston W R S 1883 *Krilof and his fables : Krylov, Ivan Andreevich, 1768-1844* (London: Cassell & Company, Ltd.) Online: https://archive.org/details/krilofhisfables00kryluoft/page/43/mode/1up

Ravina L 1993 Everything you want to know about Coagulation & Flocculation *Zeta-m. Inc.* Online: http://www.zeta-meter.com/

Ray S C, Saha A, Jana N R and Sarkar R 2009 Fluorescent carbon nanoparticles: Synthesis, characterization, and bioimaging application *J. Phys. Chem. C* **113** 18546–51 Online: https://pubs.acs.org/doi/abs/10.1021/jp905912n

Rouessac F and Rouessac A 2000 *Chemical Analysis: Modern Instrumental Methods and Techniques* (England: John Wiley & Sons, Ltd.)

Schanche J S 2003 Microwave synthesis solutions from Personal Chemistry *Mol. Divers.* **7** 293–300 Online: https://pubmed.ncbi.nlm.nih.gov/14870861/

Science History Institute 2017 Richard E. Smalley, Robert F. Curl, and Harold W. Kroto | Science History Institute Online: https://www.sciencehistory.org/historical-profile/richard-smalley-robert-curl-harold-kroto

Shen L, Zhang L, Chen M, Chen X and Wang J 2013 The production of pH-sensitive photoluminescent carbon nanoparticles by the carbonization of polyethylenimine and their use for bioimaging *Carbon N. Y.* **55** 343–9

So R C, Sanggo J E, Jin L, Diaz J M A, Guerrero R A and He J 2017 Gram-Scale Synthesis and Kinetic Study of Bright Carbon Dots from Citric Acid and Citrus japonica via a Microwave-Assisted Method *ACS Omega* **2** 5196–208 Online: https://pubs.acs.org/sharingguidelines

Song J, Li J, Guo Z, Liu W, Ma Q, Feng F and Dong C 2017a A novel fluorescent sensor based on sulfur and nitrogen co-doped carbon dots with excellent stability for selective detection of doxycycline in raw milk *RSC Adv.* **7** 12827–34

Song Y, Li H, Lu F, Wang H, Zhang M, Yang J, Huang J, Huang H, Liu Y and Kang Z 2017b Fluorescent carbon dots with highly negative charges as a sensitive probe for real-time monitoring of bacterial viability *J. Mater. Chem. B* **5** 6008–15 Online: https://pubs.rsc.org/en/content/articlehtml/2017/tb/c7tb01092c

Soutter W 2019 Nanopollution: Hype or Health Risk? *AZoNano* Online: https://www.azonano.com/article.aspx?ArticleID=3138

Stark G R 1965 Reactions of Cyanate with Functional Groups of Proteins. III. Reactions with Amino and Carboxyl Groups *Biochemistry* **4** 1030–6 Online: https://pubs.acs.org/doi/abs/10.1021/bi00882a008

Sun Y P, Zhou B, Lin Y, Wang W, Fernando K A S, Pathak P, Meziani M J, Harruff B A,

Wang X, Wang H, Luo P G, Yang H, Kose M E, Chen B, Veca L M and Xie S Y 2006 Quantum-sized carbon dots for bright and colorful photoluminescence *J. Am. Chem. Soc.* **128** 7756–7 Online: https://www.researchgate.net/publication/7013064_Quantum-Sized_Carbon_Dots_for_Bright_and_Colorful_Photoluminescence

Sutanto H, Alkian I, Romanda N, Lewa I W L, Marhaendrajaya I and Triadyaksa P 2020 High green-emission carbon dots and its optical properties: Microwave power effect *AIP Adv.* **10** 055008 Online: http://aip.scitation.org/doi/10.1063/5.0004595

Tofighy M A and Mohammadi T 2019 Barrier, diffusion, and transport properties of rubber nanocomposites containing carbon nanofillers *Carbon-Based Nanofillers and Their Rubber Nanocomposites: Fundamentals and Applications* (Elsevier) pp 253–85 Online: https://linkinghub.elsevier.com/retrieve/pii/B9780128173428000093

United States National Nanotechnology Initiative What is Nanotechnology? *Nano.gov* Online: https://www.nano.gov/nanotech-101/what/definition

UV-1800 Series 2008 Instruction Manual System User's Guide UV-1800 SHIMADZU SPECTROPHOTOMETER Online: http://www.sustainable-desalination.net/wp-content/uploads/2013/05/UV-1800.pdf

Verwey E J W 1947 Theory of the stability of lyophobic colloids *J. Phys. Colloid Chem.* **51** 631–6 Online: https://pubs.acs.org/doi/abs/10.1021/j150453a001

Wang J, Cheng C, Huang Y, Zheng B, Yuan H, Bo L, Zheng M W, Yang S Y, Guo Y and Xiao D 2014a A facile large-scale microwave synthesis of highly fluorescent carbon dots from benzenediol isomers *J. Mater. Chem. C* **2** 5028–35

Wang Q, Yang Z, Yang Y, Long C and Li H 2014b A bibliometric analysis of research on the risk of engineering nanomaterials during 1999-2012 *Sci. Total Environ.* **473**–**474** 483–9 Online: http://dx.doi.org/10.1016/j.scitotenv.2013.12.066

Wang T, Wang A, Wang R, Liu Z, Sun Y, Shan G, Chen Y and Liu Y 2019 Carbon dots with molecular fluorescence and their application as a "turn-off" fluorescent probe for ferricyanide detection *Sci. Rep.* **9** 1–9 Online: https://doi.org/10.1038/s41598-019-47168-7

Wang X, Qu K, Xu B, Ren J and Qu X 2011a Microwave assisted one-step green synthesis of cell-permeable multicolor photoluminescent carbon dots without surface passivation

reagents *J. Mater. Chem.* **21** 2445–50 Online: https://pubs.rsc.org/en/content/articlehtml/2011/jm/c0jm02963g

Wang Y, Anilkumar P, Cao L, Liu J H, Luo P G, Tackett K N, Sahu S, Wang P, Wang X and Sun Y P 2011b Carbon dots of different composition and surface functionalization: Cytotoxicity issues relevant to fluorescence cell imaging *Exp. Biol. Med.* **236** 1231–8 Online: https://pubmed.ncbi.nlm.nih.gov/22036734/

Wang Y, Bao L, Liu Z and Pang D W 2011c Aptamer biosensor based on fluorescence resonance energy transfer from upconverting phosphors to carbon nanoparticles for thrombin detection in human plasma *Anal. Chem.* **83** 8130–7 Online: https://pubmed.ncbi.nlm.nih.gov/21923110/

Wang Y and Hu A 2014 Carbon quantum dots : Synthesis, properties and applications *J. Mater. Chem. C Mater. Opt. Electron. devices* **2** 6921–39 Online: http://dx.doi.org/10.1039/C4TC00988F

Wayne C E and Wayne R P 1996 *Photochemistry* ed R G Compton, S G Davies, J Evans and L F Gladden (New York, United States: Oxford University Press Inc., New York)

Willard H H, Merritt Jr L L, Dean J A and Settle Jr F A 1988 *Instrumental Methods of Analysis* ed J Carey, V Friedberg, C Reitz and I Imfeld (United States of America: Wadsworth, Inc.)

Xu X, Ray R, Gu Y, Ploehn H J, Gearheart L, Raker K and Scrivens W A 2004 Electrophoretic analysis and purification of fluorescent single-walled carbon nanotube fragments *J. Am. Chem. Soc.* **126** Online: https://pubmed.ncbi.nlm.nih.gov/15469243/

Xu Z, Wang C, Jiang K, Lin H, Huang Y and Zhang C 2015 Microwave-Assisted Rapid Synthesis of Amphibious Yellow Fluorescent Carbon Dots as a Colorimetric Nanosensor for Cr(VI) *Part. Part. Syst. Charact.* **32** 1058–62 Online: http://doi.wiley.com/10.1002/ppsc.201500172

Yang Y, Cui J, Zheng M, Hu C, Tan S, Xiao Y, Yang Q and Liu Y 2012a One-step synthesis of amino-functionalized fluorescent carbon nanoparticles by hydrothermal carbonization of chitosan *Chem. Commun.* **48** 380–2 Online: https://pubmed.ncbi.nlm.nih.gov/22080285/

Yang Y, Cui J, Zheng M, Hu C, Tan S, Xiao Y, Yang Q and Liu Y 2012b One-step synthesis

of amino-functionalized fluorescent carbon nanoparticles by hydrothermal carbonization of chitosan *Chem. Commun.* **48** 380–2 Online: https://pubs.rsc.org/en/content/articlehtml/2012/cc/c1cc15678k

Yin J Y, Liu H J, Jiang S, Chen Y and Yao Y 2013 Hyperbranched polymer functionalized carbon dots with multistimuli- responsive property *ACS Macro Lett.* **2** 1033–7 Online: https://pubs.acs.org/doi/abs/10.1021/mz400474v

Zhang M, Zhao X, Fang Z, Niu Y, Lou J, Wu Y, Zou S, Xia S, Sun M and Du F 2017 Fabrication of HA/PEI-functionalized carbon dots for tumor targeting, intracellular imaging and gene delivery *RSC Adv.* **7** 3369–75

Zhao H X, Liu L Q, de Liu Z, Wang Y, Zhao X J and Huang C Z 2011 Highly selective detection of phosphate in very complicated matrixes with an off–on fluorescent probe of europium-adjusted carbon dots *Chem. Commun.* **47** 2604–6 Online: https://pubmed.ncbi.nlm.nih.gov/21234476/

Zhao Q L, Zhang Z L, Huang B H, Peng J, Zhang M and Pang D W 2008 Facile preparation of low cytotoxicity fluorescent carbon nanocrystals by electrooxidation of graphite *Chem. Commun.* 5116–8 Online: https://pubmed.ncbi.nlm.nih.gov/18956040/

Zheng J, Xie Y, Wei Y, Yang Y, Liu X, Chen Y and Xu B 2020 An Efficient Synthesis and Photoelectric Properties of Green Carbon Quantum Dots with High Fluorescent Quantum Yield *Nanomaterials* **10** 82 Online: https://www.mdpi.com/2079-4991/10/1/82

Zheng M, Liu S, Li J, Qu D, Zhao H, Guan X, Hu X, Xie Z, Jing X and Sun Z 2014 Integrating oxaliplatin with highly luminescent carbon dots: An unprecedented theranostic agent for personalized medicine *Adv. Mater.* **26** 3554–60 Online: https://www.onlinelibrary.wiley.com/doi/full/10.1002/adma.201306192

Zhou J, Booker C, Li R, Zhou X, Sham T K, Sun X and Ding Z 2007 An electrochemical avenue to blue luminescent nanocrystals from multiwalled carbon nanotubes (MWCNTs) *J. Am. Chem. Soc.* **129** 744–5 Online: https://pubmed.ncbi.nlm.nih.gov/17243794/

Zhu H, Wang X, Li Y, Wang Z, Yang F and Yang X 2009 Microwave synthesis of fluorescent carbon nanoparticles with electrochemiluminescence properties *Chem. Commun.* 5118–20 Online: https://pubmed.ncbi.nlm.nih.gov/20448965/

Zook J M, Rastogi V, MacCuspie R I, Keene A M and Fagan J 2011 Measuring agglomerate size distribution and dependence of localized surface plasmon resonance absorbance on gold nanoparticle agglomerate size using analytical ultracentrifugation *ACS Nano* **5** 8070–9

Appendix

A. Glycerol calculation for synthesis of plain CDs

The amount of glycerol necessary for the experiment was calculated as follows:

For a 70 % (w/w) glycerol solution; 70 g of glycerol needed to be mixed with 100 g of deionized water.

Density of water: 1 $g.mL^{-1}$ → 100 g of water = 100 mL of water

Density of glycerol: 1.25 $g.mL^{-1}$

1.25 g : 1 mL

70 g : x

1.25 g × (x mL) = 70 g × (1 mL)

x.1.25 g = 70 g.mL

$x = \frac{70\ g.mL}{1.25\ g}$

x = 56 mL

B. Mass calculation of CA

For the preparation of the 10 mM CA stock solution:

n = C × V

= (0.010 mol/dm^3) × (0.025 L)

= 2.5×10^{-4} mol

m = n.MW

= (2.5×10^{-4} mol) × (192.12 g/mol)

= 0.048 g

C. Synthesis Power Optimisation for synthesis of plain CDs

Table 25. Mass table for the power optimisation of plain CDs.

Sample code	***PowOpt_A1***	***PowOpt_A2***	***PowOpt_A3***	***PowOpt_A4***	***PowOpt_A5***
Contents	30 mL of 70 % Gly & 3 mL of 20 % NaH_2PO_4	30 mL of 70 % Gly & 3 mL of 20 % NaH_2PO_4	30 mL of 70 % Gly & 3 mL of 20 % NaH_2PO_4	30 mL of 70 % Gly & 3 mL of 20 % NaH_2PO_4	30 mL of 70 % Gly & 3 mL of 20 % NaH_2PO_4
Power (%)	10	30	50	80	100
Power (W)	90	270	450	720	900
Reaction Time (min)	20	20	20	20	20
Mass (g) of 50 mL container	11.3794 (1) 11.2227 (2)	11.9317	11.0070	11.0320	11.0686
Mass (g) of container + reagents	46.5589 (1)	47.6690	46.3191	47.1772	46.2420
Mass (g) of 500 mL conical flask	225	225	225	225	225
Mass (g) of flask + reagents	260.1795	260.7373	260.3121	261.1452	260.1734
Mass (g) of flask + CDs	258.99	249.1245	234.8278	230.4792	226.5272
Mass (g) of flask + CDs + 30 mL DI Water	288.99	279.1245	264.8278	260.4792	256.5272
Mass (g) of container + CDs + 30 mL DI water	60.3899 (1) 26.2022 (2)	66.0562	50.8348	46.5112	42.5958
Mass (g) of 30 mL DI water (density of water = 1g.ml^{-1})	30	30	30	30	30
Mass (g) of reagents ([mass of container + reagents] – mass of container)	35.1795	35.7373	35.3121	36.1452	35.1734
Mass (g) of product (CDs) ([mass of container + CDs	33.99	24.1245	9.8278	5.4792	1.5272

+ 30 mL DI water] – mass of container – mass of 30 mL DI water)					
% yield after heating (mass of product/mass of reagents × 100)	96.62	67.51	27.83	15.16	4.34

Table 26. Table for calculations of requirements for effective dialysis of plain CDs for power optimisation study.

Sample code	***PowOpt_A1***	***PowOpt_A2***	***PowOpt_A3***	***PowOpt_A4***	***PowOpt_A5***
Mass (g) of 50 mL container(s)	11.3794 (1) 11.2227 (2)	11.9317	11.0070	11.0320	11.0686
Mass (g) of container + CDs + 30 mL DI water	60.3899 (1) 26.2022 (2)	66.0562	50.8348	46.5112	42.5958
Mass (g) of CDs + 30 mL DI water = V_1 Let's assume that 1 g = 1 mL	63.99 g ≈ 64 mL	54.1245 g ≈ 55 mL	39.8278 g ≈ 40 mL	35.4792 g ≈ 36 mL	31.5272 g ≈ 32 mL
If 200 mL is used for dialysis; $\frac{V_1}{V_1+200\ mL} << 1$	0.2424	0.2130	0.1661	0.1507	0.1362
If 200 mL is used for dialysis; $\frac{200\ mL}{V_1+200\ mL} \approx 1$	0.7576	0.7870	0.8339	0.8493	0.8638
If 300 mL is used for dialysis; $\frac{V_1}{V_1+300\ mL} << 1$	0.1758	0.1528	0.1172	0.1058	0.0951
If 300 mL is used for dialysis; $\frac{300\ mL}{V_1+300ml} \approx 1$	0.8242	0.8472	0.8828	0.8942	0.9049
Length (cm) of membrane needed V_1/6.4 mL/cm	64/6.4 = 10	55/6.4 = 8.6	40/6.4 = 6.3	36/6.4 = 5.6	32/6.4 = 5

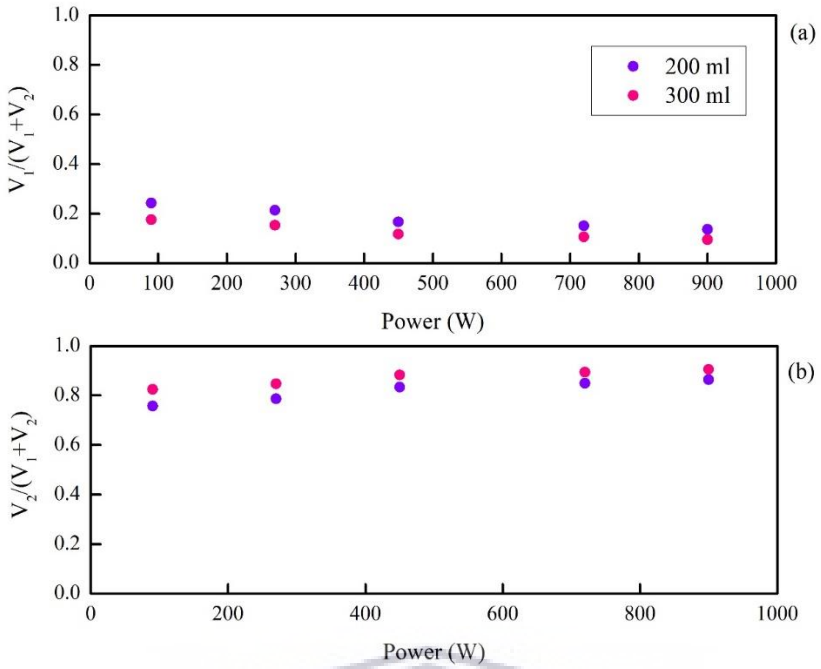

Figure 77. Illustrated above are the values for calculations pertaining to the effective dialysis of plain carbon dots for the power optimisation study; presenting the above-mentioned requirements comparing V_2 = 200 mL with V_2 = 300 mL for (a) $\frac{V_1}{V_1+V_2}$, and (b) $\frac{V_2}{V_1+V_2}$.

According to Figure 77, when V_2 is 300 mL the process of dialysis would be much more effective than when V_2 is 200 mL, as it yields much better values for the 2nd requirement of $\frac{V_1}{V_1+V_2} << 1$ with its calculated values being much smaller than 1. Moreover, for the 3rd requirement of $\frac{V_2}{V_1+V_2} \approx 1$, the values produced by calculations when V_2 = 300 mL are much closer to 1 that those calculated for V_2 = 200 mL. Therefore, 300 mL ultrapure water was used for more effective dialysis.

Table 27. Mass table for dialysis of plain CDs for power optimisation study.

Day	***Time elapsed (h)***	***Mass of dialysis bag (g)***				
		PowOpt_A1	***PowOpt_A2***	***PowOpt_A3***	***PowOpt_A4***	***PowOpt_A5***
1	0	64.4404	55.5692	41.2068	36.2589	32.4889
2	20	73.2687	67.2721	53.9892	51.3970	42.9766
	30	75.1030	69.7250	55.7350	53.1983	44.6954
3	45	71.6792	67.6752	53.5699	52.1431	45.5609
	50	70.6084	66.5322	52.7627	51.4721	45.6472

D. Reaction-time Optimisation for synthesis of plain CDs

Table 28. Mass table for the reaction-time optimisation of plain CDs synthesised at 720 W.

Sample code	***RTOpt_A6***	***RTOpt_A7***	***RTOpt_A8a***	***RTOpt_A8b***	***RTOpt_A9***	***RTOpt_A10***
Contents	20 mL of 70 % Gly & 2 mL of 20 % NaH_2PO_4	20 mL of 70 % Gly & 2 mL of 20 % NaH_2PO_4	20 mL of 70 % Gly & 2 mL of 20 % NaH_2PO_4	20 mL of 70 % Gly & 2 mL of 20 % NaH_2PO_4	40 mL of 70 % Gly & 4 mL of 20 % NaH_2PO_4	40 mL of 70 % Gly & 4 mL of 20 % NaH_2PO_4
Reaction Time (min)	5	10	15	15	20	25
Mass (g) of 50 mL container	10.4336	10.5155	10.5160	10.4356	10.5959	11.2182
Mass (g) of container + reagents	34.1140	34.4243	34.5670	34.1570	58.1511	59.3848
Mass (g) of 500 mL flask	218.6237	218.6237	218.6237	205.0459	225	225
Mass (g) of flask + reagents	240	242.5325	242.6747	228.7673	272.5552	273.1666
Mass (g) of flask + CDs	226.2995	222.2168	222.6002	205.2746	230.345	226.3293
Mass (g) of flask + CDs + 30 mL DI Water	256.2995	252.2168	252.6002	235.2746	280.345	256.3293
Mass (g) of container + CDs + 30 mL DI water	48.1094	44.1086	44.4925	40.6643	45.9409	42.5475

Mass (g) of 30 mL DI water (density of water = 1g.ml^{-1})	30	30	30	30	30	30
Mass (g) of reagents ([mass of container + reagents] – mass of container)	23.6804	23.9088	24.051	23.7214	47.5552	48.1666
Mass (g) of product (CDs) ([mass of container + CDs + 30 mL DI water] – mass of container – mass of 30 mL DI water)	7.6758	3.5931	3.9765	0.2287	5.345	1.3293
% yield after heating (mass of product/mass of reagents × 100)	32.41	15.03	16.53	0.96	11.24	2.76

Dialysis – reaction time optimisation study

The process and requirements of dialysis described in Section 3.6 was followed and the results of the calculations performed for effective dialysis with a wash liquid volume of 300 mL are presented in Table 29 below.

Table 29. Table for calculations of requirements for effective dialysis of plain CDs for reaction-time optimisation study.

Sample code	***RTOpt_A6***	***RTOpt_A7***	***RTOpt_A8a***	***RTOpt_A8b***	***RTOpt_A9***	***RTOpt_A10***
Reaction Time (min)	5	10	15	15	20	25
Mass (g) of 50 mL container	10.4336	10.5155	10.5160	10.4356	10.4732	10.5629
Mass(g) of container + CDs + 30 mL DI water	48.1094	44.1086	44.4925	44.6643	45.9409	42.5475
Mass (g) of CDs + 30 mL DI water (V_1)	37.6758 g ≈ 38 mL	33.5931 g ≈ 34 mL	33.9765 g ≈ 34 mL	34.2287 g ≈ 35 mL	35.4677 g ≈ 36 mL	31.9846 g ≈ 32 mL
If 300 mL is used for dialysis; $\frac{V_1}{V_1+300\ mL} << 1$	0.1116	0.1007	0.1017	0.1024	0.1057	0.0963
If 300 mL is used for dialysis; $\frac{300\ mL}{V_1+300\ mL} \approx 1$	0.8884	0.8993	0.8983	0.8976	0.8943	0.9037
Length (cm) of membrane needed V_1/6.4 mL/cm	38/6.4 = 5.94	34/6.4 = 5.31	34/6.4 = 5.31	35/6.4 = 5.47	36/6.4 = 5.63	32/6.4 = 5

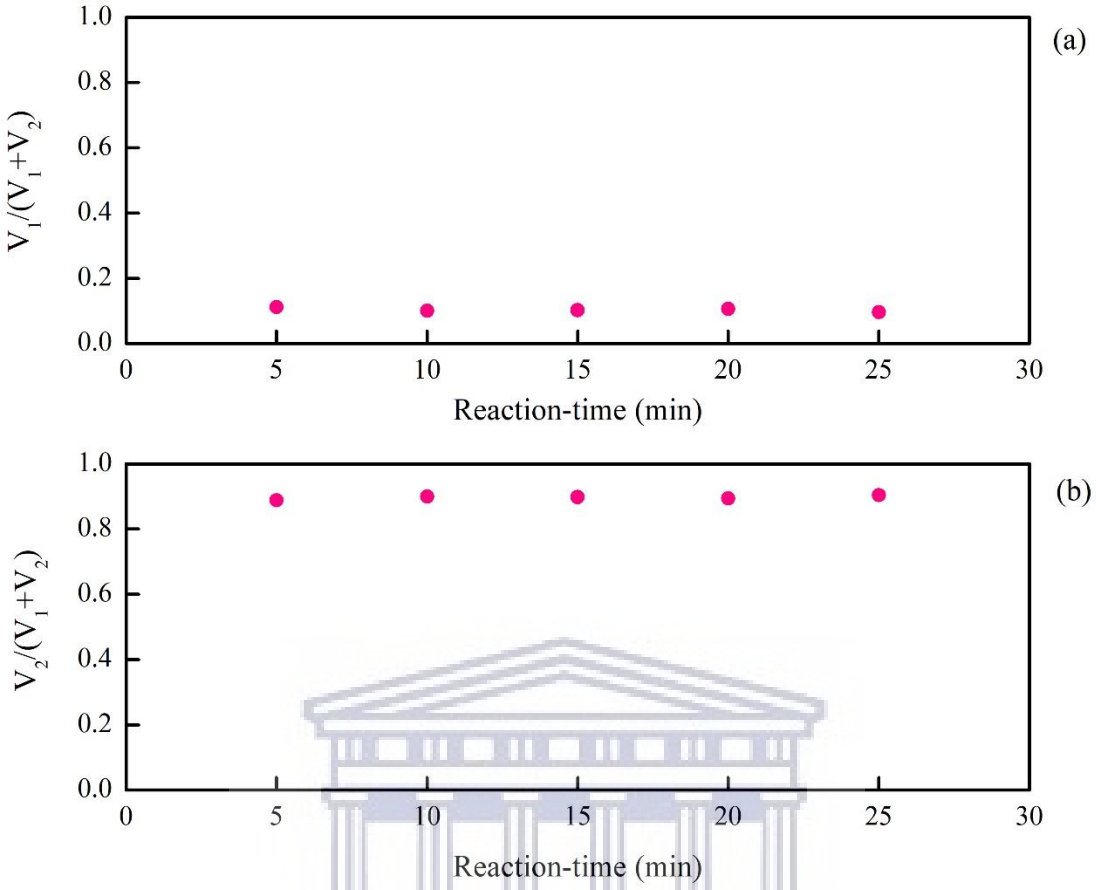

Figure 78. Illustrated above are images of the dialysis calculations for the reaction-time optimisation of plain carbon dots presenting the above-mentioned requirements and comparing V_2 = 300 mL for (a) $\frac{V_1}{V_1+V_2}$, and (b) $\frac{V_2}{V_1+V_2}$.

As established in Section 4.1.1.1, when V_2 = 300 mL the process of dialysis is more effective than for smaller amounts as it yields much better values for the 2nd and 3rd requirements of $\frac{V_1}{V_1+V_2}$ << 1 and $\frac{V_2}{V_1+V_2} \approx 1$, with its calculated values much smaller than 1 and much closer to 1, respectively.

Table 30. Mass table for dialysis of plain CDs for reaction-time optimisation study.

	Day	Time	RTOpt_A6	RTOpt_A7	RTOpt_A8a	RTOpt_A8b	RTOpt_A9	RTOpt_A10
Mass (g)	**1**	**IN 14:00**	38.3681	34.9952	31.1630	31.2580	35.7703	33.5936
Mass (g)		**OUT 20:45**	54.5629	45.9885	38.2056	38.3471	44.6275	44.9679
pH			4.11	4.18	4.88	4.34	4.41	4.78
		IN 21:15						
Mass (g)	**2**	**OUT 09:46**	52.7958	46.9993	41.9080	42.1933	53.1091	52.3362
pH			4.91	4.96	5.32	4.84	4.81	5.48
		IN 10:35						
Mass (g)		**OUT 21:07**	50.9691	46.3627	42.9315	43.5474	57.7941	55.3012
pH			6.10	6.03	6.72	6.20	5.82	6.16
		IN 21:37						
Mass (g)	**3**	**OUT 10:49**	48.6352	45.4117	43.6602	44.1193	61.2042	56.1898
pH			5.64	5.71	5.83	6.20	5.90	6.06
		IN 12:33						
Mass (g)		**OUT 21:06**	46.5525	44.4661	43.3546	43.9856	61.9894	56.5821
pH			6.31	6.50	6.53	6.77	6.60	6.58

In this section, data regarding the dialysis (as described in Section 3.6) of the above-mentioned samples for the optimisation study for the reaction time of CDs is presented. Shown in Figure 79 below are images of CDs before and after dialysis. Notice the colour of the bathing solution before and after dialysis; it transformed from transparent to light brown and could once again be attributed to diffusion that occurred through the membrane from the higher concentrated sample to the surrounding solution of lower concentration.

Figure 79. The dialysis of unfunctionalised CDs (a) before, and (b) after dialysis for the study on the effect of reaction time on the synthesis of CDs.

The masses of dialysis bags for 2-day dialysis procedure of the reaction-time optimisation study are tabulated in Table 30. In Figure 80, the masses of the dialysis bags are plotted against the time elapsed throughout the dialysis procedure.

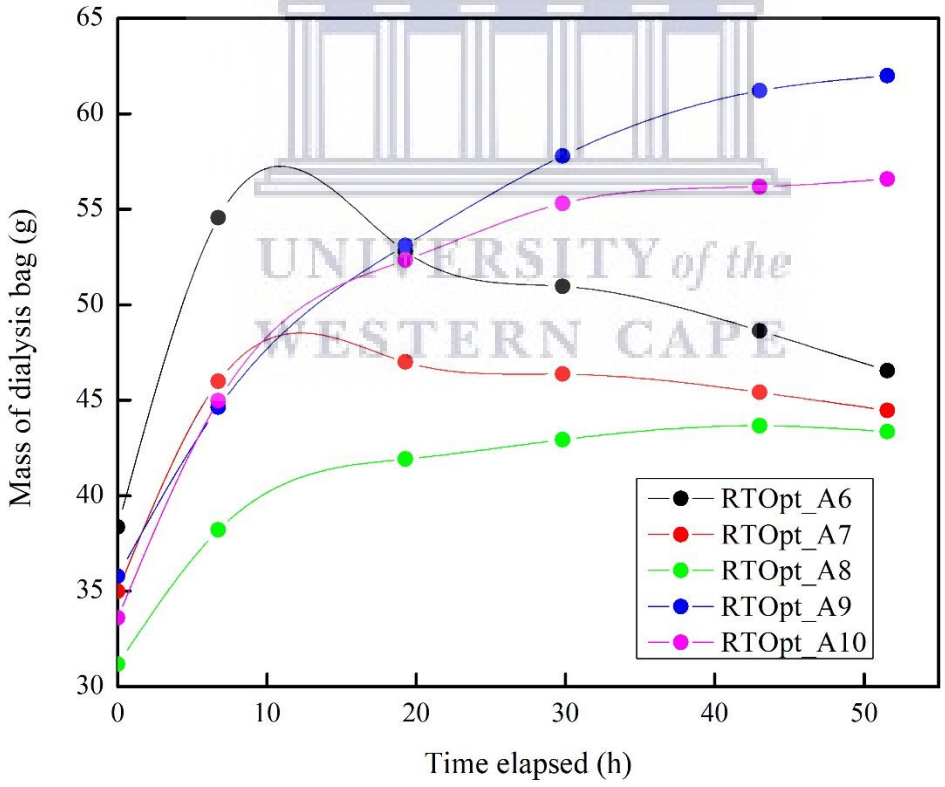

Figure 80. Mass of dialysis bags as a function of the time elapsed for dialysis of unfunctionalised CDs in the reaction-time optimisation study (10:1 ratio of Gly:NaH_2PO_4; 720 W).

According to the data displayed in Figure 80, the masses of the dialysis bags for samples RTOpt_A6 (5 min) and RTOpt_A7 (10 min) initially increased but then gradually decreased as time progressed. On the other hand, the masses of dialysis bags of the rest of the samples, namely RTOpt_A8 (15 min), RTOpt_A9 (20 min), and RTOpt_A10 (25 min), increased gradually and eventually levelled off over time. The increase in mass for all samples could be attributed to the explanation provided in Section 4.1.1.1 in which diffusion is hindered by the occurrence of osmosis into the dialysis bags (Hunter 1987). However, the mass of each bag eventually reached a somewhat constant mass, i.e., equilibrium or the point at which diffusion was complete, after the dialysis period.

E. Molar quantity Optimisation of 70 % w/w Gly

For a 70 % (w/w) Gly ($C_3H_9O_3$) solution, 70 g of Gly needed to be mixed with 100 g of deionized water.

100 g of water = 100 mL of water (Density of water = 1 $g.mL^{-1}$)

Therefore, 70 g of Gly is added to 100 mL of H_2O**.** From this, the number of moles, *n*, of Gly is given by:

$$n_{(C_3H_9O_3)} = \frac{m}{M} = \frac{70\ g}{92.09\ g.mol^{-1}} = 0.76\ mol,$$

where *m* is the mass and *M* is the molecular weight/molar mass of Gly. Consequently, the molarity or concentration, *C*, of Gly is given by:

$$C_{(C_3H_9O_3)} = \frac{n}{V} = \frac{0.76\ mol}{0.1\ L} = 7.6\ mol.L^{-1}\ ,$$

where *n* is the number of moles of solute, Gly, and *V* is the volume of solution, water. Here forth, the molar quantities for the following volumes of Gly, i.e., 18, 24, 30, 36, and 42 mL, is given by rearrangement of the previous equation:

For 18 mL of Gly:

$$n_{18\ mL} = C \cdot V = (7.6\ mol.L^{-1}) \cdot (0.018\ L) = 0.14\ mol$$

For 24 mL of Gly:

$$n_{24\ mL} = C \cdot V = (7.6\ mol.L^{-1}) \cdot (0.024\ L) = 0.18\ mol$$

For 30 mL of Gly:

$$n_{30\ mL} = C \cdot V = (7.6\ mol.L^{-1}) \cdot (0.030\ L) = 0.23\ mol$$

For 36 mL of Gly:

$$n_{36\ mL} = C \cdot V = (7.6\ mol.L^{-1}) \cdot (0.036\ L) = 0.27\ mol$$

For 42 mL of Gly:

$$n_{42\ mL} = C \cdot V = (7.6\ mol.L^{-1}) \cdot (0.042\ L) = 0.32\ mol$$

Table 31. Mass table for the molar quantity optimisation of glycerol for effective synthesis of plain CDs.

Sample code	***G_Opt_A11***	***G_Opt_A12***	***G_Opt_A13***	***G_Opt_A14***	***G_Opt_A15***
Contents	18 mL of 70 % Gly & 3 mL of 20 % NaH_2PO_4 (6:1)	24 mL of 70 % Gly & 3 mL of 20 % NaH_2PO_4 (8:1)	30 mL of 70 % Gly & 3 mL of 20 % NaH_2PO_4 (10:1)	36 mL of 70 % Gly & 3 mL of 20 % NaH_2PO_4 (12:1)	42 mL of 70 % Gly & 3 mL of 20 % NaH_2PO_4 (14:1)
Power (%)	80	80	80	80	80
Power (W)	720	720	720	720	720
Reaction Time (min)	14	14	14	14	14
Mass (g) of 50 mL container	10.2321	10.3105	10.2683	10.5154	10.3328
Mass (g) of container + reagents	32.7964	40.3402	46.0187	52.5225	58.9976
Mass (g) of 500 mL Erlenmeyer flask	225	225	225	215.7573	225
Mass (g) of flask + reagents	247.5643	255.0297	260.7504	257.7644	273.6648
Mass (g) of flask + CDs	227.3313	231.1653	234.0685	227.1472	239.6241
Mass (g) of flask + CDs + 30 mL DI Water	257.3313	261.1653	264.0685	257.1472	269.6241
Mass (g) of container + CDs	42.5634	46.4758	49.3368	51.9053	54.9569

+ 30 mL DI water					
Mass (g) of 30 mL DI water (density of water = 1g.ml^{-1})	30	30	30	30	30
Mass (g) of reagents ([mass of container + reagents] – mass of container)	22.5643	30.0297	35.7504	42.0071	48.6648
Mass (g) of product (CDs) ([mass of container + CDs + 30 mL DI water] – mass of container – mass of 30 mL DI water)	2.3313	6.1653	9.0685	11.3899	14.6241
% yield after heating (mass of product/mass of reagents × 100)	10.33	20.53	25.37	27.11	30.05

Dialysis – glycerol molar quantity optimisation study

The process and requirements of dialysis described in Section 3.6 was followed and the results of the calculations performed for effective dialysis with a wash liquid volume of 300 mL are presented in Table 32 below.

Table 32. Table for calculations of requirements for effective dialysis of plain CDs for glycerol molar quantity optimisation study.

Sample code	***G_Opt_A11***	***G_Opt_A12***	***G_Opt_A13***	***G_Opt_A14***	***G_Opt_A15***
Mass (g) of 50 mL container	10.2321	10.3105	10.2683	10.5154	10.3328
Mass (g) of container + CDs + 30 mL DI water	42.5634	46.4758	49.3368	51.9053	54.9569
Mass (g) of CDs + 30 mL DI water (V_1)	32.3313 g ≈ 33 mL	36.1653 g ≈ 37 mL	39.0685 g ≈ 40 mL	41.3899 g ≈ 42 mL	44.6241 g ≈ 45 mL
If 300 mL is used for dialysis; $\frac{V_1}{V_1+300\ mL} << 1$	0.0973	0.1076	0.1152	0.1212	0.1295
If 300 mL is used for dialysis; $\frac{300\ mL}{V_1+300\ mL} \approx 1$	0.9027	0.8924	0.8848	0.8788	0.8705
Length (cm) of membrane needed V_1/6.4 mL/cm	33/6.4 = 5.16	37/6.4 = 5.78	40/6.4 = 6.25	42/6.4 = 6.56	45/6.4 = 7.03

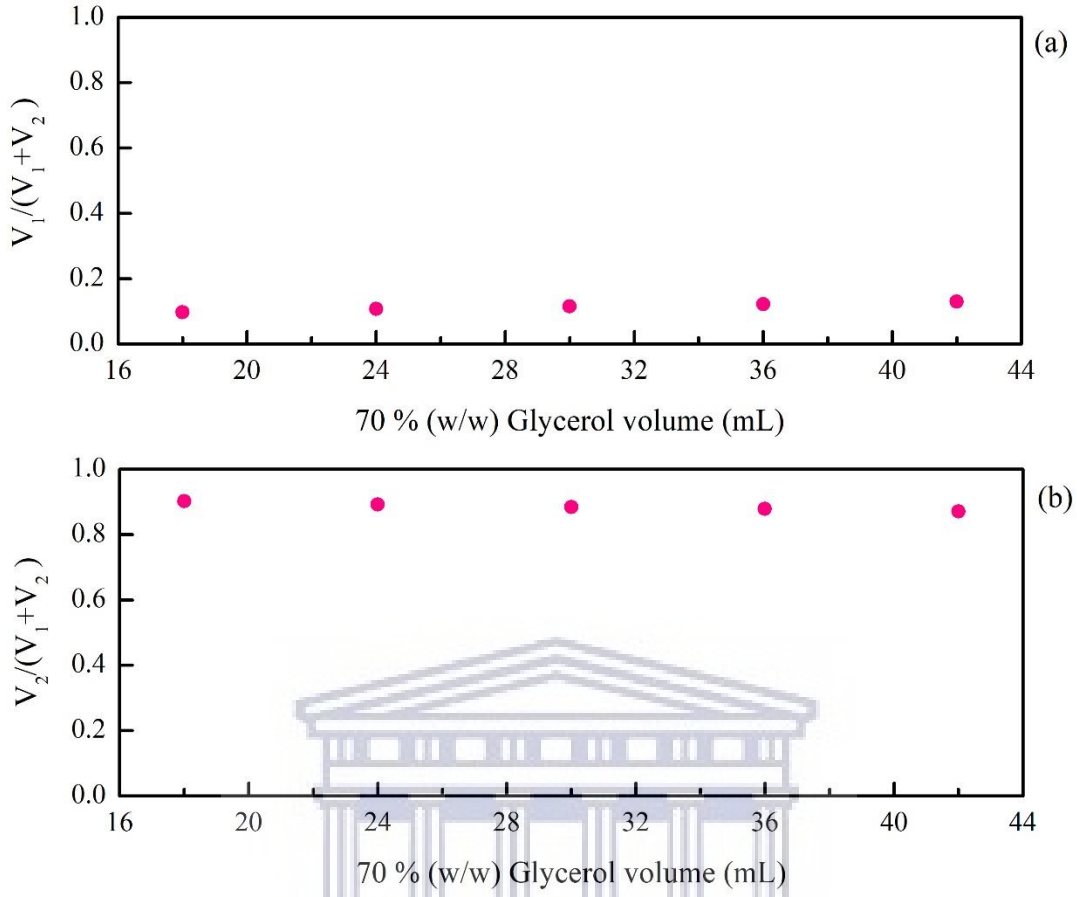

Figure 81. Illustrated above are images of the dialysis calculations for the optimisation of the molar quantity of 70 % (w/w) Gly for plain carbon dots presenting the above-mentioned requirements and comparing V_2 = 300 mL for (a) $\frac{V_1}{V_1+V_2}$, and (b) $\frac{V_2}{V_1+V_2}$.

As established in Section 4.1.1.1 and as illustrated in Figure 81 above, when V_2 = 300 mL the process of dialysis is more effective than for smaller amounts as it yields much better values for the 2nd and 3rd requirements of $\frac{V_1}{V_1+V_2} << 1$ and $\frac{V_2}{V_1+V_2} \approx 1$, with its calculated values much smaller than 1 and much closer to 1, respectively.

Table 33. Mass table for dialysis of plain CDs for glycerol molar quantity optimisation study.

	Day	Time	G_Opt_A11	G_Opt_A12	G_Opt_A13	G_Opt_A14	G_Opt_A15
Mass (g)	***1***	***IN 12:12***	33.6967	37.7299	40.1674	43.0438	46.4804
Mass (g)		***OUT 21:10***	47.6747	56.4935	60.5414	65.6730	72.4288
		IN 21:23					
Mass (g)	***2***	***OUT 14:10***	52.9378	56.6456	56.9139	61.2554	67.7916
pH			6	6	6	6	6
		IN 14:23					
Mass (g)	***3***	***OUT 12:12***	54.0677	54.8030	53.0062	56.7641	62.7418
pH			8.25	7.91	7.41	7.21	6.85

In this section, data regarding the dialysis (as described in Section 3.6) of the above-mentioned samples for the optimisation of the molar quantity of Gly in the synthesis of unfunctionalised CDs is presented. Shown in Figure 82 below are images of CDs before and after dialysis. Once again, it is noticeable that the colour of the wash liquids before and after dialysis transformed from transparent to light brown and could be due to diffusion that occurred form the higher concentrated sample inside the dialysis bag to the surrounding solution of lower concentration.

Figure 82. Dialysis of unfunctionalised CDs for molar quantity optimisation of 70 % (w/w) glycerol, (a) before dialysis, and (b) after dialysis.

The dialysis bags after dialysis are larger in size when compared to those before dialysis, and could be due to the initial osmotic flow into the bag (as described in Section 4.1.1.1). In Figure

82, the difference in the intensity of colour from the low molar quantity of 0.14 mol on the left to that of higher number of moles of 0.32 mol on the right (in both images) is quite significant. There is a lightening in intensity of the brown colour as the molar quantity of Gly is increased. The masses of dialysis bags for the 2-day dialysis procedure in the molar optimisation study of Gly are tabulated in Table 33. In Figure 83, the mass of each dialysis bag is plotted against the time elapsed throughout the dialysis procedure.

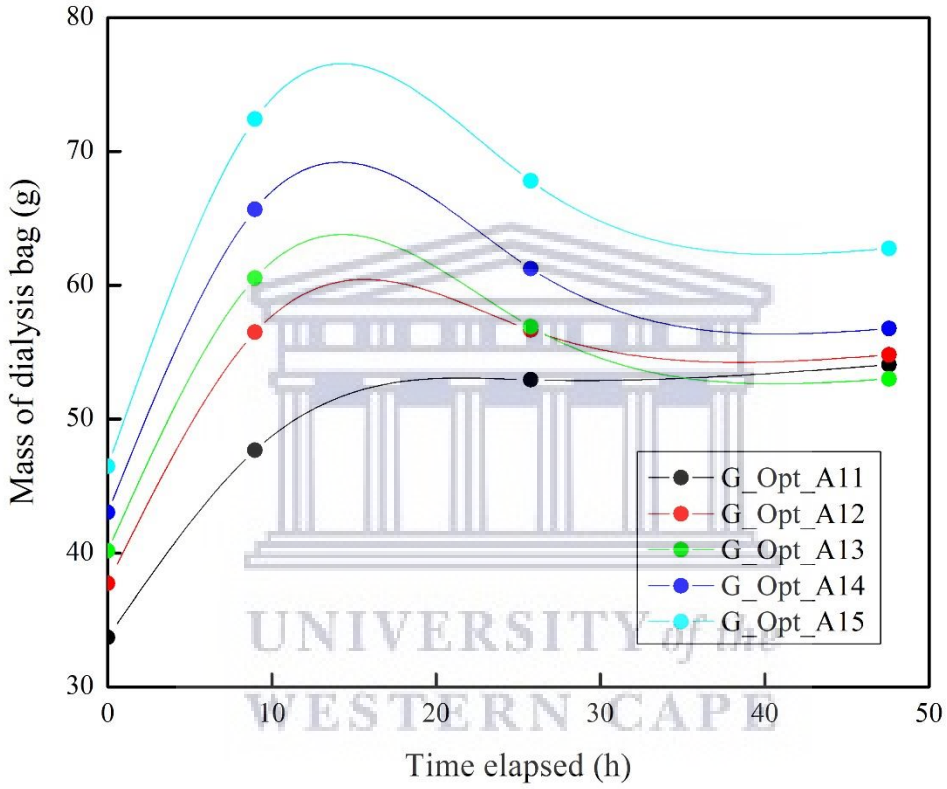

Figure 83. Dialysis of unfunctionalised CDs in molar optimisation study of 70 % (w/w) glycerol.

According to the data displayed in Figure 83, the masses of the dialysis bags for each of the above-mentioned samples initially increased and then decreased. This behaviour is expected as the initial increase in mass for all samples could once again be attributed to the explanation provided in Section 4.1.1.1 in which diffusion is hindered by the occurrence of osmosis into the dialysis bags (Hunter 1987). However, the mass of each bag eventually reached a somewhat constant mass after the dialysis period which is an indication that dialysis reached completion.

F. Molar quantity Optimisation of 20 % w/w NaH_2PO_4

Calculations for the molar quantities of 20 % (w/w) sodium dihydrogen phosphate

For a 20 % (w/w) sodium dihydrogen phosphate (NaH_2PO_4) solution, 20 g of NaH_2PO_4 needed to be mixed with 100 g of deionized water.

100 g of water = 100 mL of water (Density of water = 1 $g.mL^{-1}$)

Therefore, 20 g of NaH_2PO_4 is added to 100 mL of H_2O**.** From this, the number of moles, *n*, of NaH_2PO_4 is given by:

$$n_{(NaH_2PO_4)} = \frac{m}{M} = \frac{20\ g}{119.98\ g.mol^{-1}} = 0.17\ mol,$$

where *m* is the mass and *M* is the molecular weight/molar mass of NaH_2PO_4. Consequently, the molarity or concentration, *C*, of NaH_2PO_4 is given by:

$$C_{(NaH_2PO_4)} = \frac{n}{V} = \frac{0.17\ mol}{0.1\ L} = 1.7\ mol.L^{-1},$$

where *n* is the number of moles of solute, NaH_2PO_4, and *V* is the volume of solution, water. Here forth, the molar quantities for the following volumes of NaH_2PO_4, i.e., 1.5, 3, 6, 9, and 12 mL, is given by rearrangement of the previous equation:

For 1.5 mL of NaH_2PO_4:

$$n_{1.5\ mL} = C \cdot V = (1.7\ mol.L^{-1}) \cdot (1.5 \times 10^{-3}\ L) = 2.6 \times 10^{-3}\ mol$$

For 3 mL of NaH_2PO_4:

$$n_{3\ mL} = C \cdot V = (1.7\ mol.L^{-1}) \cdot (3 \times 10^{-3}\ L) = 5.1 \times 10^{-3}\ mol$$

For 6 mL of NaH_2PO_4:

$$n_{6\ mL} = C \cdot V = (1.7\ mol.L^{-1}) \cdot (6 \times 10^{-3}\ L) = 1.02 \times 10^{-2}\ mol$$

For 9 mL of NaH_2PO_4:

$$n_{9\ mL} = C \cdot V = (1.7\ mol.L^{-1}) \cdot (9 \times 10^{-3}\ L) = 1.53 \times 10^{-2}\ mol$$

For 12 mL of NaH_2PO_4:

$$n_{12\ mL} = C \cdot V = (1.7\ mol.L^{-1}) \cdot (1.2 \times 10^{-2}\ L) = 2.04 \times 10^{-2}\ mol$$

Table 34. Mass table for the molar quantity optimisation of NaH_2PO_4 for the effective synthesis of plain CDs.

Sample code	***N_Opt_A16***	***N_Opt_A17***	***N_Opt_A18***	***N_Opt_A19***	***N_Opt_A20***
Contents	30 mL of 70 % Gly & 1.5 mL of 20 % NaH_2PO_4 (10:0.5)	30 mL of 70 % Gly & 3 mL of 20 % NaH_2PO_4 (10:1)	30 mL of 70 % Gly & 6 mL of 20 % NaH_2PO_4 (10:3)	30 mL of 70 % Gly & 9 mL of 20 % NaH_2PO_4 (10:5)	30 mL of 70 % Gly & 12 mL of 20 % NaH_2PO_4 (10:7)
Power (%)	80	80	80	80	80
Power (W)	720	720	720	720	720
Reaction Time (min)	14	14	14	14	14
Mass (g) of 50 mL container	11.2209	11.2870	11.9246	11.2866	11.3378
Mass (g) of container + reagents	45.7517	46.9968	50.6597	53.7757	57.3046
Mass (g) of 500 mL Erlenmeyer flask	215.7573	225	215.7573	225	225
Mass (g) of flask + reagents	250.2881	260.7098	254.4924	267.4891	270.9668
Mass (g) of flask + CDs	225.3166	235.0437	224.5826	233.4673	237.093
Mass (g) of flask + CDs + 30 mL DI Water	255.3166	265.0437	254.5826	263.4673	267.093
Mass (g) of + CDs + 30 mL DI water	50.7802	51.3307	50.7499	49.7539	53.4308

Mass (g) of 30 mL DI water (density of water = 1g.ml^{-1})	30	30	30	30	30
Mass (g) of reagents ([mass of container + reagents] – mass of container)	34.5308	35.7098	38.7351	42.4891	45.9668
Mass (g) of product (CDs) ([mass of container + CDs + 30 mL DI water] – mass of container – mass of 30 mL DI water)	9.5593	10.0437	8.8253	8.4673	12.093
% yield after heating (mass of product/mass of reagents × 100)	27.68	28.13	22.78	19.93	26.31

Dialysis – NaH_2PO_4 molar quantity optimisation study

The process and requirements of dialysis described in Section 3.6 was followed and the results of the calculations performed for effective dialysis with a wash liquid volume of 300 mL are presented in Table 35 below.

Table 35. Table for calculations of requirements for effective dialysis of plain CDs for NaH_2PO_4 molar quantity optimisation study.

Sample code	***N_Opt_A16***	***N_Opt_A17***	***N_Opt_A18***	***N_Opt_A19***	***N_Opt_A20***
Mass (g) of 50 mL container	11.2209	11.2870	11.9246	11.2866	11.3378
Mass (g) of container + CDs + 30 mL DI water	50.7802	51.3307	50.7499	49.7539	53.4308
Mass (g) of CDs + 30 mL DI water (V_1)	39.5593 g ≈ 40 mL	40.0437 g ≈ 41 mL	38.8253 g ≈ 39 mL	38.4673 g ≈ 39 mL	42.093 g ≈ 43 mL
If 300 mL is used for dialysis; $\frac{V_1}{V_1+300\ mL} << 1$	0.1165	0.1178	0.1146	0.1137	0.1230
If 300 mL is used for dialysis; $\frac{300\ mL}{V_1+300\ mL} \approx 1$	0.8835	0.8822	0.8854	0.8863	0.8770
Length (cm) of membrane needed V_1/6.4 mL/cm	40/6.4 = 6.25	41/6.4 = 6.41	39/6.4 = 6.09	39/6.4 = 6.09	43/6.4 = 6.72

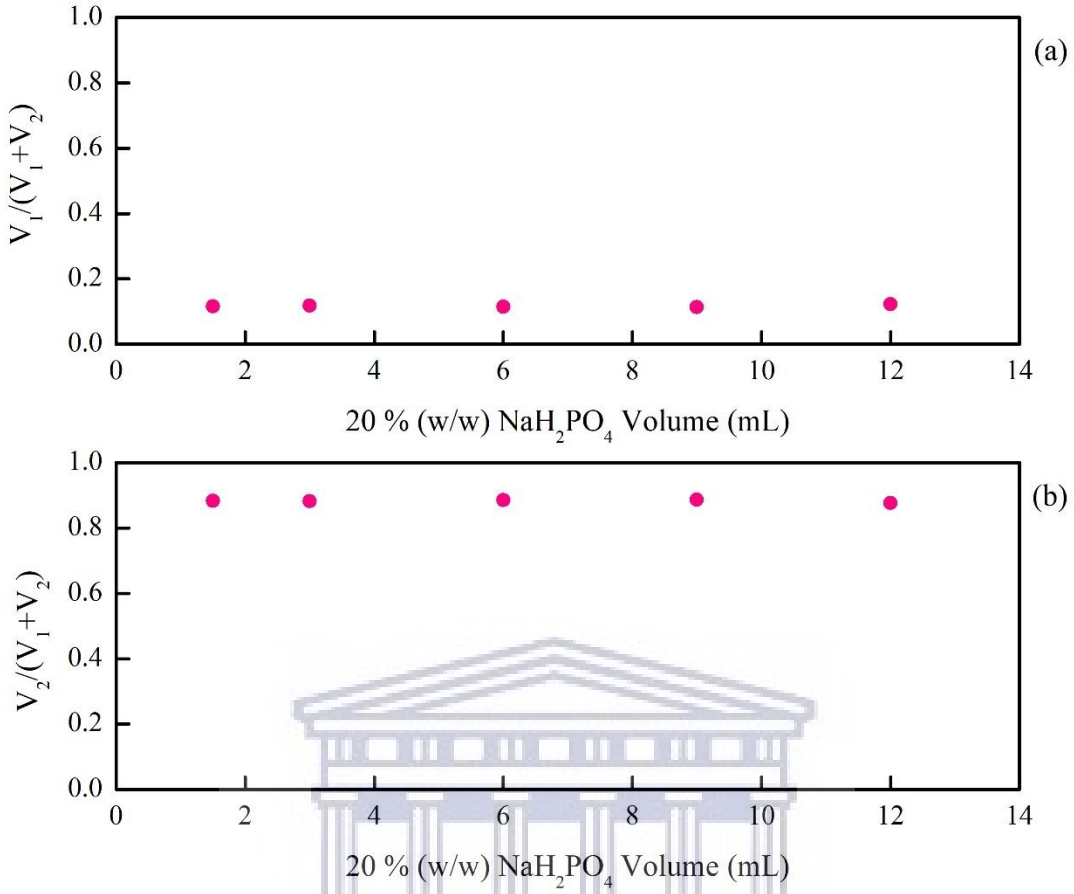

Figure 84. Illustrated above are images of the dialysis calculations for the optimisation of molar quantity of 20 % (w/w) NaH_2PO_4 for plain carbon dots presenting the above-mentioned requirements and comparing V_2 = 300 mL for (a) $\frac{V_1}{V_1+V_2}$, and (b) $\frac{V_2}{V_1+V_2}$.

As established in Section 4.1.1.1 and as illustrated in Figure 84 above, when V_2 = 300 mL the process of dialysis is more effective than for smaller amounts as it yields much better values for the 2nd and 3rd requirements of $\frac{V_1}{V_1+V_2} << 1$ and $\frac{V_2}{V_1+V_2} \approx 1$, with its calculated values much smaller than 1 and much closer to 1, respectively.

Table 36. Mass table for dialysis of plain CDs for 20 % (w/w) NaH_2PO_4 molar quantity optimisation study.

	Day	*Time*	*N_Opt_A16*	*N_Opt_A17*	*N_Opt_A18*	*N_Opt_A19*	*N_Opt_A20*
Mass (g)	***1***	***IN 11:40***	40.7820	41.5515	40.1695	39.6200	43.7413
Mass (g)		***OUT 19:55***	60.7415	63.2325	63.5359	66.6005	71.8674
pH		***IN 20:17***	4.11	4.08	4.04	3.89	5.08
Mass (g)	***2***	***OUT 08:58***	59.0712	62.0951	62.2682	64.9463	70.4921
pH		***IN 09:29***	5.10	5.06	4.81	4.49	5.34
Mass (g)		***OUT 20:23***	57.0334	60.6663	61.5924	64.8128	69.8018
pH		***IN 20:52***	6.33	6.20	5.72	5.44	5.63
Mass (g)	***3***	***OUT 09:49***	54.4785	58.4739	59.5418	63.5976	68.2355
pH		***IN 10:37***	4.65	5.03	5.34	5.39	5.70
Mass (g)		***OUT 13:56***	53.7064	57.9450	58.9953	63.3267	67.9525
pH		***IN 14:52***	5.29	6.81	6.85	6.70	6.40
Mass (g)		***OUT 20:30***	52.2448	56.5865	57.3291	62.1780	66.5898
pH			6.03	6.70	6.67	6.65	6.64

In this section, data regarding the dialysis (as described in Section 3.6) of the above-mentioned samples obtained during the optimisation of the molar quantity of the inorganic salt, NaH_2PO_4, in the synthesis of plain CDs is presented. Shown in Figure 85 below are images of CDs before and after dialysis. Notice, one more time, the colour of the wash liquids before and after dialysis; it transformed from transparent to light brown and could, once again, be due to diffusion that occurred form the higher concentrated sample inside the dialysis bag to the surrounding solution of lower concentration. One can also see that the more intense the brown colour of the product is, the darker the surrounding liquid (i.e., wash liquid).

Figure 85. Dialysis of unfunctionalised CDs for molar quantity optimisation of 20 % (w/w) NaH_2PO_4, (a) before dialysis, and (b) after dialysis.

In Figure 85, once more, the dialysis bags after dialysis are larger in size when compared to those before dialysis, and could be due to the initial osmotic flow into the bag (as described in Section 4.1.1.1). The difference in the intensity of colour amongst the median molar ratio of Gly to NaH_2PO_4 of 10:2 in the middle in comparison to those of lowest and highest molar ratios of 10:0.5 and 10:4, respectively, is quite significant as the brown colour appears to be much deeper for the lowest and highest molar quantities of NaH_2PO_4. This is also evident in the colour of the surrounding wash liquid and correlates with the trend observed for % yield in Figure 34.

The masses of dialysis bags for the 2-day dialysis procedure of the molar optimisation study of NaH_2PO_4 are tabulated in Table 36. In Figure 86, the mass of each dialysis bag is plotted against the time elapsed throughout the dialysis procedure.

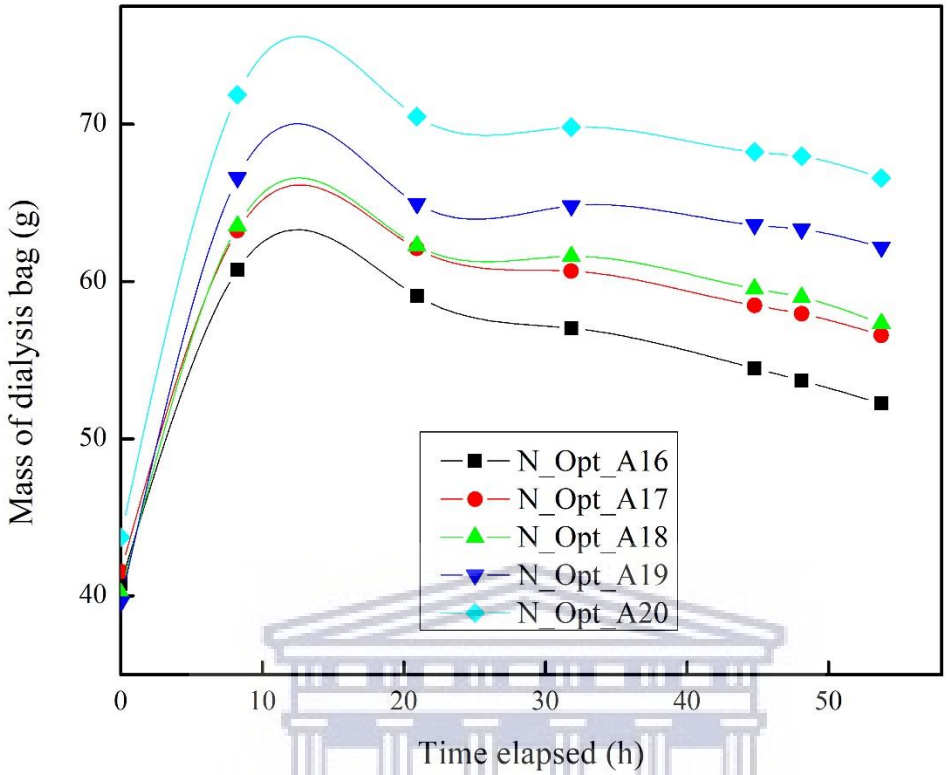

Figure 86. Dialysis of unfunctionalised CDs in molar optimisation study of 20 % (w/w) NaH_2PO_4.

According to the data displayed in Figure 86, the masses of the dialysis bags for each of the above-mentioned samples follow the same trends as the previous three studies (i.e., power, reaction-time, and molar quantity of Gly studies) in which it initially increased and then decreased to a somewhat constant mass and pH (see values in Table 36). See Section 4.1.1.1 for explanation. A neutral pH level for each sample was eventually reached within the 2-day dialysis process, which served as an indicator that the dialysis process has reached its completion. Here, the mass of dialysis bags increases as the molar quantity of NaH_2PO_4 increased, which follows the same trend as for the Gly study, as is expected with an increase in reagent; however, the power and reaction-time studies follow an opposite trend as the higher power levels and reaction durations inadvertently increases the amount of material burnt off.

G. Temperature Optimisation study for effective synthesis of a-CDs

Table 37. Mass table for the optimisation of temperature for the synthesis of amine-capped CDs.

Sample code	***TpOpt_B1***	***TpOpt_B2***	***TpOpt_B3***	***TpOpt_B4***	***TpOpt_B5***
Contents	2.1327 g of 10 mM CA & 10 mL BPEI	2.1020 g of 10 mM CA & 10 mL BPEI	2.1457 g of 10 mM CA & 10 mL BPEI	2.1043 g of 10 mM CA & 10 mL BPEI	2.1263 g of 10 mM CA & 10 mL BPEI
Temperature (ºC)	130	150	170	190	210
Reaction Time (hr)	2	2	2	2	2
Mass (g) of 50 mL container	11.4294	11.4042	11.3667	11.3690	11.3990
Mass (g) of container + reagents	22.7951	22.8131	23.0791	22.8904	22.8582
Mass (g) of container + a-CDs + 30 mL DI water	50.9479	51.1567	50.9759	50.1607	50.6641
Mass (g) of 30 mL DI water (density of water = 1g.ml^{-1})	30	30	30	30	30
Mass (g) of reagents ([mass of container + reagents] – mass of container)	11.3657	11.4089	11.7124	11.5214	11.4592
Mass (g) of product (CDs) ([mass of container + CDs + 30 mL DI water] – mass of container – mass of 30 mL DI water)	9.5185	9.7525	9.6092	8.7917	9.2651
% yield after heating (mass of product/mass of reagents × 100)	83.75	85.48	82.04	76.31	80.85

Dialysis – temperature optimisation study

The process and requirements of dialysis described in Section 3.6 was followed and the results of the calculations performed for effective dialysis are presented in Table 38 below.

Table 38. Table for calculations of requirements for effective dialysis of a-CDs for temperature optimisation study.

Sample code	***TpOpt_B1***	***TpOpt_B2***	***TpOpt_B3***	***TpOpt_B4***	***TpOpt_B5***
Mass (g) of 50 mL container	11.4294	11.4042	11.3667	11.3690	11.3990
Mass (g) of container + a-CDs + 30 mL DI water	50.9479	51.1567	50.9759	50.1607	50.6641
Mass (g) of a-CDs + 30 mL DI water (V_1)	39.5185 g ≈ 40 mL	39.7525 g ≈ 40 mL	39.6092 g ≈ 40 mL	38.7917 g ≈ 39 mL	39.2651 g ≈ 40 mL
If 300 mL is used for dialysis; $\frac{V_1}{V_1+300\ mL} << 1$	0.1164	0.1170	0.1166	0.1145	0.1157
If 300 mL is used for dialysis; $\frac{300\ mL}{V_1+300\ mL} \approx 1$	0.8836	0.8830	0.8834	0.8855	0.8843
Length (cm) of membrane needed V_1/6.4 mL.cm^{-1}	40 mL/6.4 = 6.25	40 mL/6.4 = 6.25	40 mL/6.4 = 6.25	39 mL/6.4 = 6.09	40 mL/6.4 = 6.25

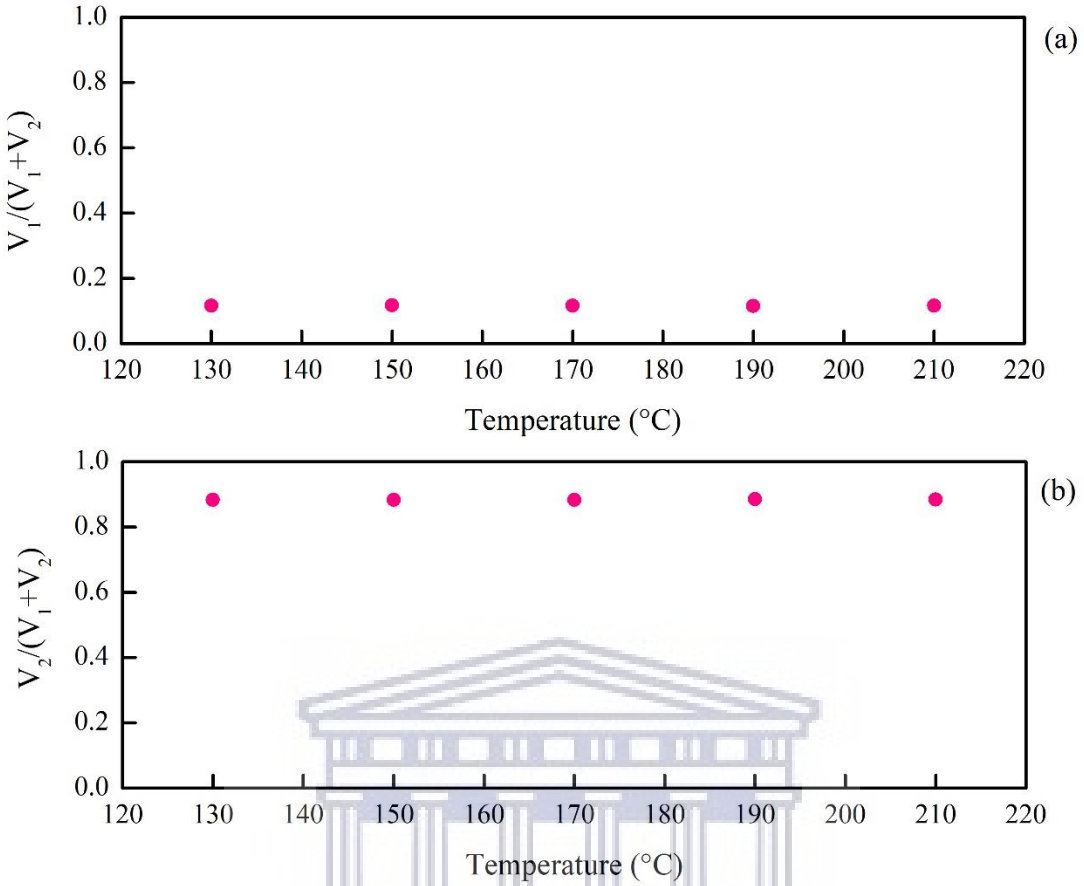

Figure 87. Illustrated above are the values for calculations pertaining to the effective dialysis of amine-capped carbon dots for the temperature optimisation study; presenting the above-mentioned requirements with V_2 = 300 mL for (a) $\frac{V_1}{V_1+V_2}$, and (b) $\frac{V_2}{V_1+V_2}$.

As established in Section 4.1.1.1 and as illustrated in Figure 87 above, when V_2 = 300 mL the process of dialysis is more effective than for smaller amounts as it yields much better values for the 2nd and 3rd requirements of $\frac{V_1}{V_1+V_2} << 1$ and $\frac{V_2}{V_1+V_2} \approx 1$, with its calculated values much smaller than 1 and much closer to 1, respectively.

Table 39. Mass table for dialysis of a-CDs for the temperature optimisation study.

	Day	***Time***	***TpOpt_B1***	***TpOpt_B2***	***TpOpt_B3***	***TpOpt_B4***	***TpOpt_B5***
Mass (g)	***1***	***15:47***	40.8750	41.3440	40.5757	39.1411	40.9454
Mass (g)	***2***	***14:00***	78.9224	79.5110	76.8172	68.5617	75.8111
Mass (g)		***21:47***	77.1832	66.7229	76.4202	59.8460	70.1639
Mass (g)	***3***	***12:51***	72.1988	66.0569	71.7642	58.8354	70.0677
Mass (g)		***19:30***	69.7833	64.4338	69.3299	57.1424	68.7657

In this section, data regarding the dialysis of the above-mentioned samples for the temperature optimisation study of a-CDs is presented. The samples underwent dialysis right after heating in a Si-oil bath (through a procedure described in Section 3.6) to ensure effective purification of a-CDs through the removal of unreacted reagent molecules and small molecular by-products from the solution mixture. Shown in Figure 88 below are images of a-CDs before and after dialysis.

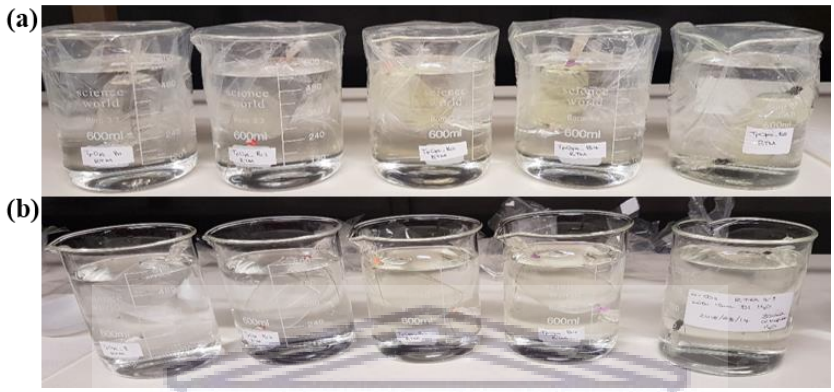

Figure 88. Dialysis of amine-capped carbon dots from the lowest temperature to the highest temperature, (a) before, and (b) after dialysis.

In Figure 88, the dialysis bags after dialysis were larger in size when compared to those before dialysis, and could once again be attributed to the initial osmotic flow into the bag (as described in Section 4.1.1.1). Compared to unfunctionalised CDs, it is not that noticeable that diffusion occurred as the colour of the samples inside the dialysis bags after dialysis was transparent. The masses of dialysis bags for the 2-day dialysis procedure for the temperature optimisation study of a-CDs are tabulated in Table 39. In Figure 89, the mass of dialysis bag is plotted against the time elapsed throughout the dialysis procedure.

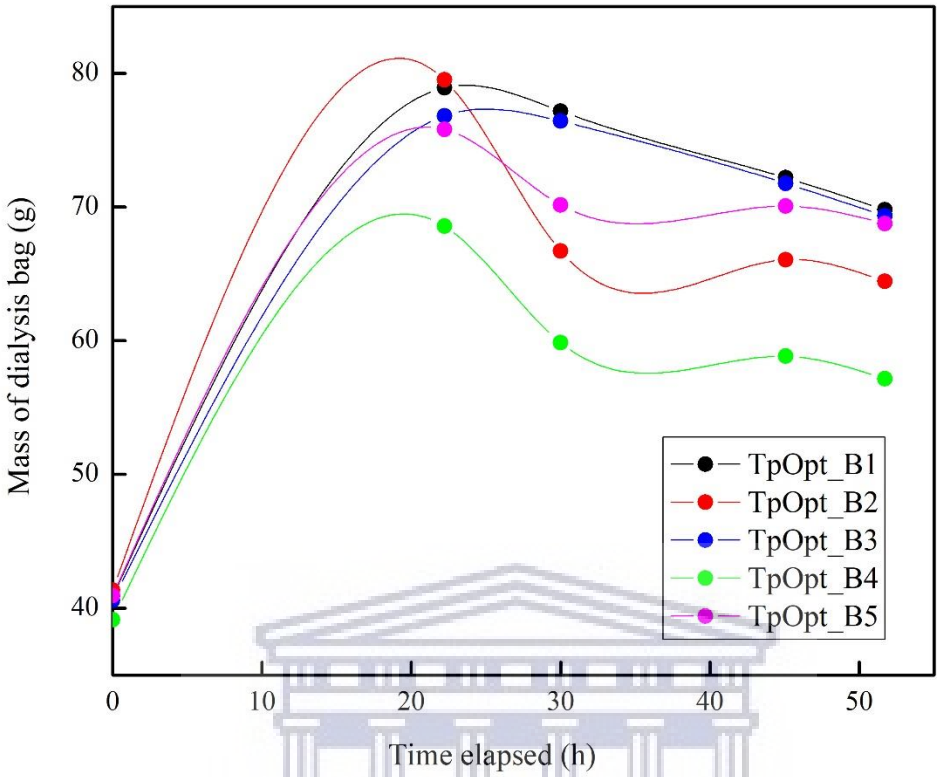

Figure 89. Dialysis of amine-capped CDs in temperature optimisation study.

According to the data displayed in Figure 89, the masses of the dialysis bags for each of the above-mentioned samples initially increased and then decreased until stable. This behaviour is expected as the initial increase in mass for all samples could once again be attributed to the explanation provided in Section 4.1.1.1 in which diffusion is hindered by the occurrence of osmosis into the dialysis bags (Hunter 1987). However, the mass of each bag eventually reached a somewhat constant mass after the dialysis period, which served as an indicator that the dialysis process had reached its completion. Notice that the masses of the dialysis bags for TpOpt_B1 and TpOpt_B3 levelled off with larger masses following somewhat the same trend which could be an indication of greater stability. Also, a neutral pH level for each sample was eventually reached within the 2-day dialysis process (see Table 39 for pH values).

H. Heating-time Optimisation for effective synthesis of a-CDs

Table 40. Mass table for the optimisation of reaction time for the synthesis of amine-capped CDs.

	RTOpt_B6	***RTOpt_B7***	***RTOpt_B8***	***RTOpt_B9***	***RTOpt_B10***
Contents	2.1195 g of 10 mM C & 10 mL BPEI	2.1902 g of 10 mM CA & 10 mL BPEI	2.1256 g of 10 mM CA & 10 mL BPEI	2.1642 g of 10 mM CA & 10 mL BPEI	2.1471 g of 10 mM CA & 10 mL BPEI
Temp (ºC)	170	170	170	170	170
Reaction Time (hr)	1	1.5	2	2.5	3
Mass (g) of 50 mL container	10.5903	10.4277	10.4050	10.4237	10.5338
Mass (g) of container + reagents	22.1736	22.2133	22.0769	22.0781	22.1677
Mass (g) of container + a-CDs + 30 mL DI water	50.3341	49.8221	50.1888	49.5245	50.0549
Mass (g) of 30 mL DI water (density of water = 1g.ml^{-1})	30	30	30	30	30
Mass (g) of reagents ([mass of container + reagents] – mass of container)	11.5833	11.7856	11.6719	11.6544	11.6339
Mass (g) of product (a-CDs) ([mass of container + a-CDs + 30 mL DI water] – mass of container – mass of 30 mL DI water)	9.7438	9.3944	9.7838	9.1008	9.5211
% yield after heating (mass of product/mass of reagents × 100)	84.12	79.71	83.82	78.09	81.84
Time elapsed before presence of yellow colour (min)	26	22	20	20	17

Dialysis – reaction-time optimisation study of a-CDs

The process and requirements of dialysis described in Section 3.6 was followed and the results of the calculations performed for effective dialysis are presented in Table 41 below.

Table 41. Table for calculations of requirements for effective dialysis of a-CDs for reaction-time optimisation study.

Sample code	***RTOpt_B6***	***RTOpt_B7***	***RTOpt_B8***	***RTOpt_B9***	***RTOpt_B10***
Reaction Time (hr)	1	1.5	2	2.5	3
Mass (g) of 50 mL container	10.5903	10.4277	10.4050	10.4237	10.5338
Mass (g) of container + a-CDs + 30 mL DI water	50.3341	49.8221	50.1888	49.5245	50.0549
Mass (g) of a-CDs + 30 mL DI water (V_1)	39.7438 g ≈ 40 mL	39.3944 g ≈ 40 mL	39.7838 g ≈ 40 mL	39.1008 g ≈ 40 mL	39.5211 g ≈ 40 mL
If 300 mL is used for dialysis; $\frac{V_1}{V_1+300\ mL} << 1$	0.1170	0.1161	0.1171	0.1153	0.1164
If 300 mL is used for dialysis; $\frac{300\ mL}{V_1+300\ mL} \approx 1$	0.8830	0.8839	0.8829	0.8847	0.8836
Length (cm) of membrane needed V_1/6.4 ml.cm^{-1}	40 ml/6.4 = 6.25	40 mL/6.4 = 6.25	40 mL/6.4 = 6.25	40 mL/6.4 = 6.25	40 mL/6.4 = 6.25

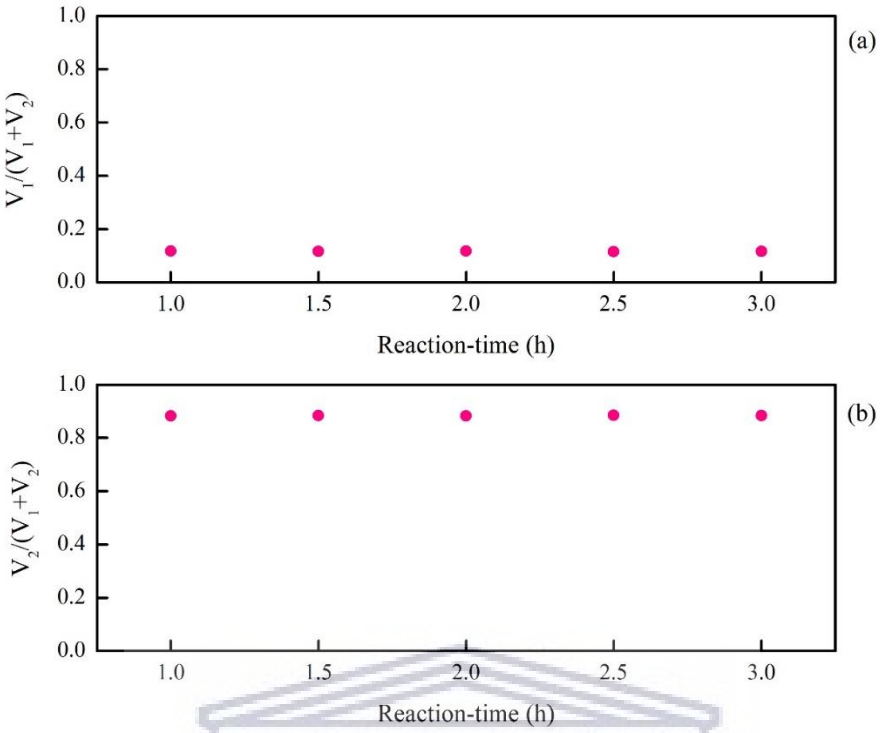

Figure 90. Illustrated above are the values for calculations pertaining to the effective dialysis of amine-capped carbon dots for the reaction-time optimisation study; presenting the above-mentioned requirements with V_2 = 300 mL for (a) $\frac{V_1}{V_1+V_2}$, and (b) $\frac{V_2}{V_1+V_2}$.

As established in Section 4.1.1.1 and as illustrated in Figure 90 above, when V_2 = 300 mL the process of dialysis is more effective than for smaller amounts as it yields much better values for the 2nd and 3rd requirements of $\frac{V_1}{V_1+V_2} << 1$ and $\frac{V_2}{V_1+V_2} \approx 1$, with its calculated values much smaller than 1 and much closer to 1, respectively.

Table 42. Mass table for dialysis of a-CDs for the reaction-time optimisation study.

	Day	***Time***	***RTOpt_B6***	***RTOpt_B7***	***RTOpt_B8***	***RTOpt_B9***	***RTOpt_B10***
Mass (g)	***1***	***IN 16:36***	41.1163	40.9100	41.3030	40.4892	39.7826
Mass (g)	***2***	***OUT 14:16***	80.1850	80.6995	81.7277	70.1770	73.6889
		IN 14:43					
Mass (g)		***OUT 20:34***	79.6911	81.8000	81.3934	67.8500	75.1310
		IN 20:55					
Mass (g)	***3***	***OUT 13:13***	74.2652	77.6951	76.1027	62.6551	72.0806
		IN 13:26					
Mass (g)		***OUT 19:30***	71.7470	75.6107	73.6247	60.6992	69.9774

In this section, data regarding the dialysis of the above-mentioned samples for the optimisation on the reaction time of a-CDs is presented. The samples underwent dialysis right after heating in a Si-oil bath (through a procedure described in Section 3.6) to ensure effective purification of a-CDs through the removal of unreacted reactant and small molecular by-products from the solution mixture. Shown in Figure 91 below are images of a-CDs before and after dialysis.

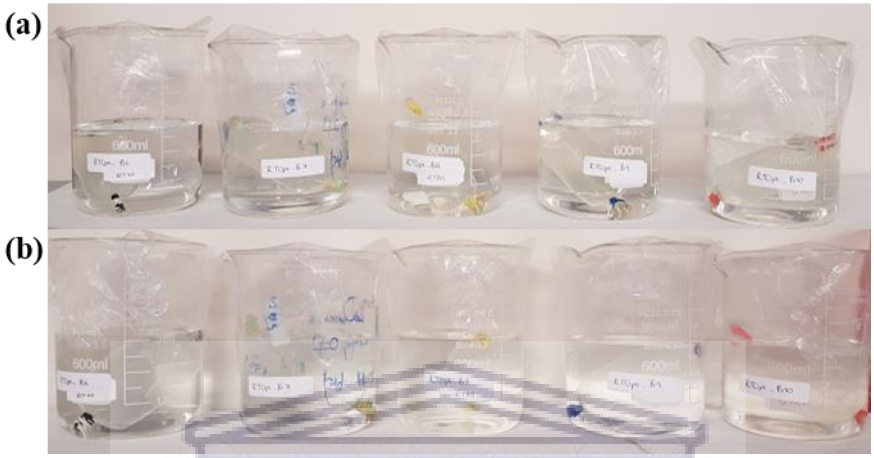

Figure 91. The dialysis of amine-capped carbon dots for the reaction-time optimisation, (a) before, and (b) after dialysis.

In Figure 91, the dialysis bags after dialysis were larger in size when compared to those before dialysis, and could once again be attributed to the initial osmotic flow into the bag (as described in Section 4.1.1.1). It is not that noticeable that diffusion occurred as the colour of the samples inside the dialysis bags after dialysis was transparent. The masses of dialysis bags for a 2-day dialysis procedure in the reaction-time optimisation study of a-CDs are tabulated in Table 42. In Figure 92, the mass of dialysis bag is plotted against the time elapsed throughout the dialysis procedure.

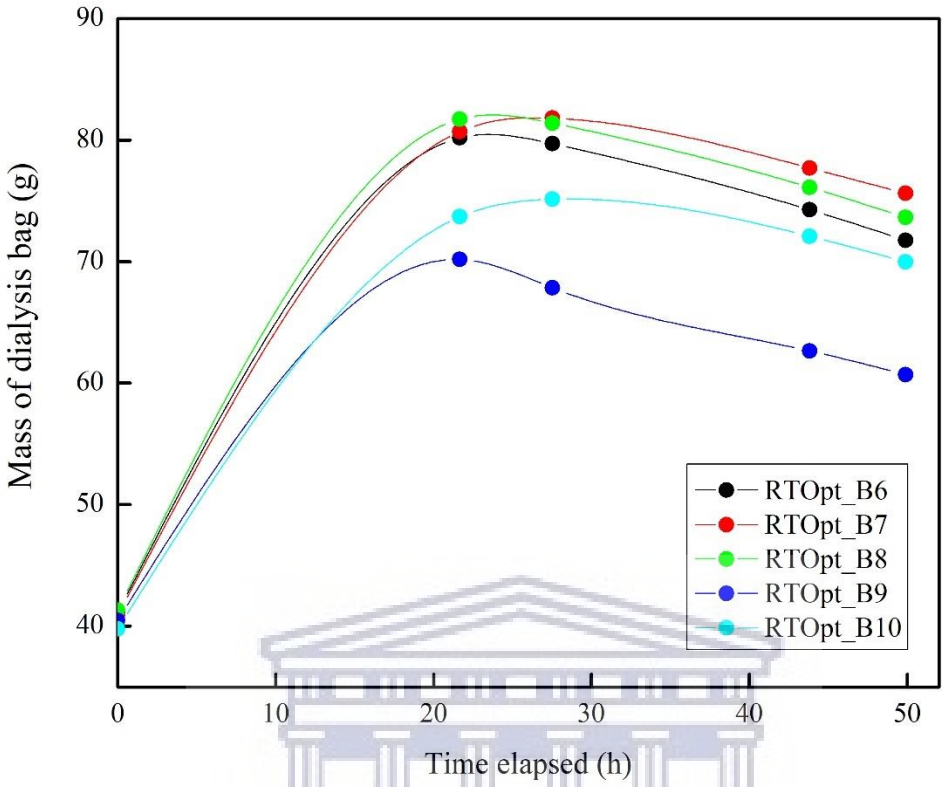

Figure 92. Dialysis of amine-capped CDs in reaction-time optimisation study.

According to the data displayed in Figure 92, the masses of the dialysis bags for each of the above-mentioned samples initially increased and then decreased until stable. This behaviour is expected as the initial increase in mass for all samples could once again be attributed to the explanation provided in Section 4.1.1.1 in which diffusion is hindered by the occurrence of osmosis into the dialysis bags (Hunter 1987). However, the mass of each bag eventually reached a somewhat constant mass after the dialysis period. A neutral pH level for each sample was eventually reached within the 2-day dialysis process, which served as an indicator that the dialysis process had reached its completion.

I. Molar Quantity Optimisation of CA for effective synthesis of a-CDs

Calculations for the molar quantities of 10 mM Citric Acid solution

For a 10 mM Citric Acid (CA, $C_6H_8O_7$) solution,

the molarity or concentration, *C*, of CA is given by:

$C_{(C_6H_8O_7)} = 10\ mM = 0.01\ M = 0.01\ mol.L^{-1}$.

Therefore, the molar quantities, *n*, for the following masses of CA, i.e., 1.5, 1.8, 2.1, 2.4, and 2.7 g, is given by:

$n_{(C_6H_8O_7)} = \frac{m}{M}$,

where *m* is the mass and *M* is the molecular weight/molar mass of CA, 192.12 g.mol^{-1}.

For 1.5 g of CA:

$n_{1.5\ g} = \frac{1.5\ g}{192.12\ g.mol^{-1}} = 7.8 \times 10^{-3}\ mol$

For 1.8 g of CA:

$n_{1.8\ g} = \frac{1.8\ g}{192.12\ g.mol^{-1}} = 9.4 \times 10^{-3}\ mol$

For 2.1 g of CA:

$n_{2.1\ g} = \frac{2.1\ g}{192.12\ g.mol^{-1}} = 1.1 \times 10^{-2}\ mol$

For 2.4 g of CA:

$n_{2.4\ g} = \frac{2.4\ g}{192.12\ g.mol^{-1}} = 1.2 \times 10^{-2}\ mol$

For 2.7 g of CA:

$n_{2.7\ g} = \frac{2.7\ g}{192.12\ g.mol^{-1}} = 1.4 \times 10^{-2}\ mol$

Table 43. Mass table for the optimisation of CA molar quantity for the synthesis of a-CDs.

Sample code	***CA_Opt_B11***	***CA_Opt_B12***	***CA_Opt_B13***	***CA_Opt_B14***	***CA_Opt_B15***
Contents	1.5176 g of 10 mM CA & 10 mL BPEI	1.8491 g of 10 mM CA & 10 mL BPEI	2.1150 g of 10 mM CA & 10 mL BPEI	2.4192 g of 10 mM CA & 10 mL BPEI	2.7251 g of 10 mM CA & 10 mL BPEI
Temp (ºC)	170	170	170	170	170
Reaction Time (hr)	2	2	2	2	2
Mass (g) of 50 mL container	7.8536	7.1426	11.3700	11.4233	11.3967
Mass (g) of container + reagents	18.6093	17.9827	22.4419	22.9570	23.0363
Mass (g) of container + a-CDs + 30 mL DI water	46.3377	46.2896	51.0768	50.7934	51.0251
Mass (g) of 30 mL DI water (density of water = 1g.ml^{-1})	30	30	30	30	30
Mass (g) of reagents ([mass of container + reagents] – mass of container)	10.7557	10.8401	11.0719	11.5337	11.6396
Mass (g) of product (a-CDs) ([mass of container + a-CDs + 30 mL DI water] – mass of container – mass of 30 mL DI water)	8.4841	9.147	9.7068	9.3701	9.6284
% yield after heating (mass of product/mass of reagents × 100)	78.88	84.38	87.67	81.24	82.72
Time elapsed before presence of yellow colour (min)	6	15	6	14	13

Dialysis – citric acid molar quantity optimisation study of a-CDs

The process and requirements of dialysis described in Section 3.6 was followed and the results of the calculations performed for effective dialysis are presented in Table 44 below.

Table 44. Table for calculations of requirements for effective dialysis of a-CDs for CA molar quantity optimisation study.

Sample code	***CA_Opt_B11***	***CA_Opt_B12***	***CA_Opt_B13***	***CA_Opt_B14***	***CA_Opt_B15***
Contents	1.5176 g of 10 mM CA & 10 mL BPEI	1.8491 g of 10 mM CA & 10 mL BPEI	2.1150 g of 10 mM CA & 10 mL BPEI	2.4192 g of 10 mM CA & 10 mL BPEI	2.7251 g of 10 mM CA & 10 mL BPEI
Mass (g) of 50 mL container	7.8536	7.1426	11.3700	11.4233	11.3967
Mass (g) of container + a-CDs + 30 mL DI water	46.3377	46.2896	51.0768	50.7934	51.0251
Mass (g) of a-CDs + 30 mL DI water (V_1)	38.4841g ≈ 39 mL	39.147 g ≈ 40 mL	39.7068 g ≈ 40 mL	39.3701 g ≈ 40 mL	39.6284 g ≈ 40 mL
If 300 mL is used for dialysis; $\frac{V_1}{V_1+300\ mL} << 1$	0.1137	0.1154	0.1169	0.1160	0.1167
If 300 mL is used for dialysis; $\frac{300\ mL}{V_1+300\ mL} \approx 1$	0.8863	0.8846	0.8831	0.8840	0.8833
Length (cm) of membrane needed V_1/6.4 ml.cm^{-1}	39 mL/6.4 = 6.09	40 mL/6.4 = 6.25	40 mL/6.4 = 6.25	40 mL/6.4 = 6.25	40 mL/6.4 = 6.25

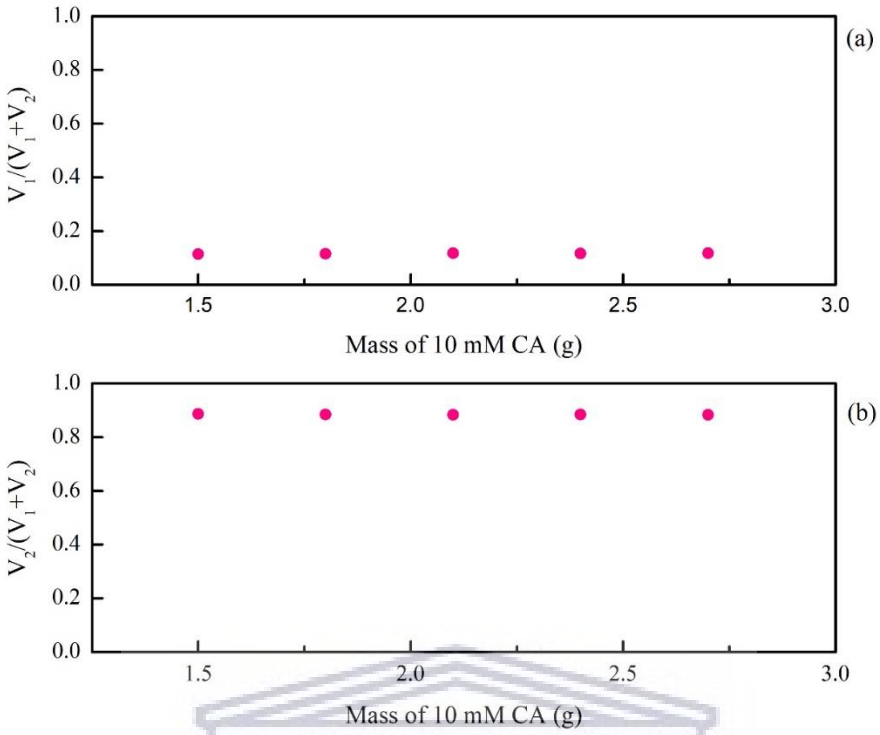

Figure 93. Illustrated above are the values for calculations pertaining to the effective dialysis of amine-capped carbon dots for the molar quantity optimisation of CA; presenting the above-mentioned requirements with V_2 = 300 mL for (a) $\frac{V_1}{V_1+V_2}$, and (b) $\frac{V_2}{V_1+V_2}$.

As established in Section 4.1.1.1 and as illustrated in Figure 93 above, when V_2 = 300 mL the process of dialysis is more effective than for smaller amounts as it yields much better values for the 2nd and 3rd requirements of $\frac{V_1}{V_1+V_2} << 1$ and $\frac{V_2}{V_1+V_2} \approx 1$, with its calculated values much smaller than 1 and much closer to 1, respectively.

Table 45. Mass table for dialysis of a-CDs for the CA molar quantity optimisation study.

	Day	***Time***	***CA_Opt_B 11***	***CA_Opt_B 12***	***CA_Opt_B 13***	***CA_Opt_B 14***	***CA_Opt_B 15***
Mass (g)	***1***	***IN 13:30***	39.9988	40.0449	41.5511	41.1433	41.6170
Mass (g)		***OUT 20:04***	67.9350	67.0813	69.0027	68.0426	66.4450
		IN 20:21					
Mass (g)	***2***	***OUT 14:47***	75.4477	76.2373	78.1561	75.8248	73.4490
		IN 15:05					
Mass (g)	***3***	***OUT 15:02***	63.1545	63.9469	65.8849	63.6293	60.9222

In this section, data regarding the dialysis of the above-mentioned samples for the optimisation of the molar quantity of CA in the synthesis of a-CDs is presented. The samples underwent dialysis right after heating in a Si-oil bath (through a procedure described in Section 3.6) to ensure effective purification of a-CDs through the removal of unreacted reagent and small molecular by-products from the solution mixture. Shown in Figure 94 below are images of a-CDs before and after dialysis.

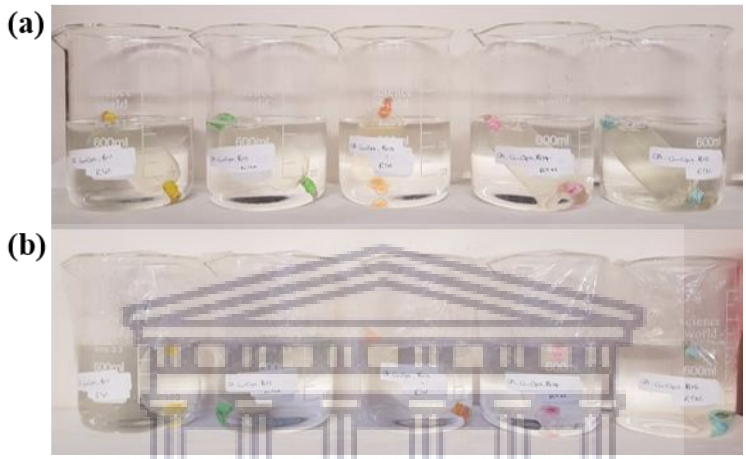

Figure 94. The dialysis of amine-capped carbon dots for the molar optimisation study of 10 mM CA, (a) before, and (b) after dialysis.

In Figure 94, the dialysis bags after dialysis were larger in size when compared to those before dialysis, and could once again be attributed to the initial osmotic flow into the bag (as described in Section 4.1.1.1). It is not that noticeable that diffusion occurred as the colour of the samples inside the dialysis bags were transparent. The masses of dialysis bags for 2-day dialysis procedure in molar quantity optimisation of CA are tabulated in Table 45. In Figure 95, the mass of dialysis bag is plotted against the time elapsed throughout the dialysis procedure.

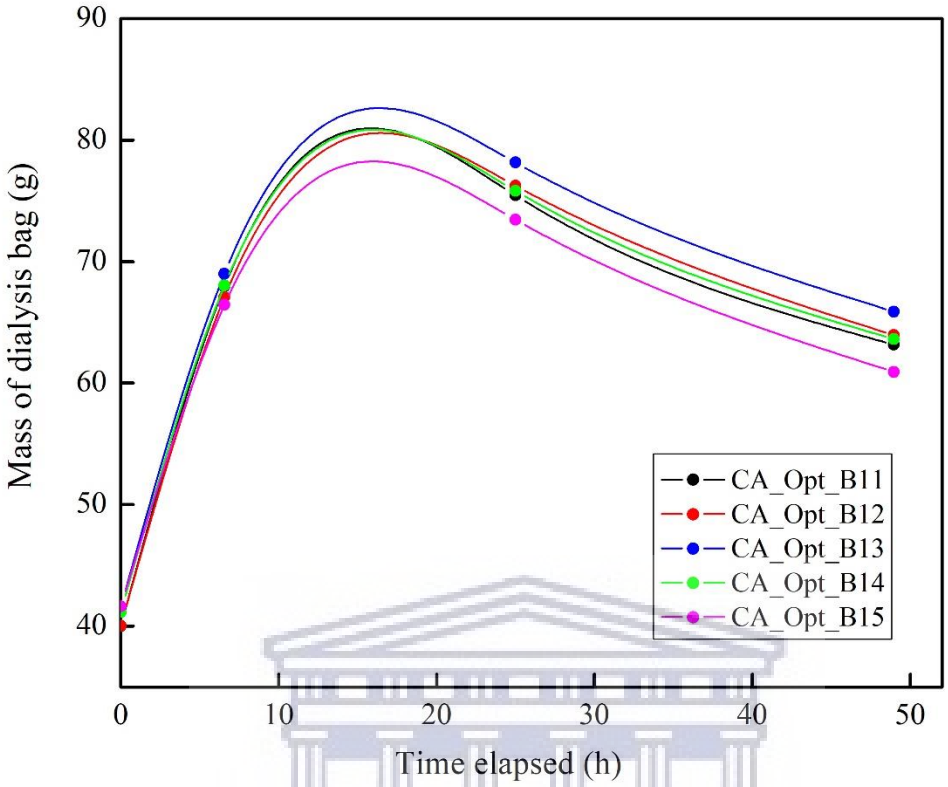

Figure 95. Dialysis of a-CDs for the CA molar quantity optimisation study of a-CDs (synthesised at 170 °C for 2 hours).

According to the data displayed in Figure 95, the masses of the dialysis bags for each of the above-mentioned samples initially increased and then decreased. This behaviour is expected as the initial increase in mass for all samples could once again be attributed to the explanation provided in Section 4.1.1.1 in which diffusion is hindered by the occurrence of osmosis into the dialysis bags (Hunter 1987). However, the mass of each bag eventually reached a somewhat constant mass after the dialysis period and there is better correlation between all samples.

J. Molar Quantity Optimisation of BPEI for effective synthesis of a-CDs

Calculations for the molar quantities of Branched polyethylenimine (BPEI)

For a BPEI solution with a molecular weight of 800 Da or 800 $g.mol^{-1}$ (because 1 Da = 1 $g.mol^{-1}$), and density of 1.05 $g.mL^{-1}$, the molar quantities, *n*, for the following volumes of BPEI, i.e., 6, 8, 10, 12, and 14 mL, is given by:

$$n_{(BPEI)} = \frac{m}{M},$$

where *m* is the mass and *M* is the molecular weight/molar mass of BPEI.

For 6 mL of BPEI:

If 1.05 g of BPEI is present in 1 mL thereof, then *x* g is found in 6 mL. To solve *x*,

$$x = \frac{(6\ mL)(1.05\ g)}{1\ mL} = 6.3\ g\ .$$

Therefore, the number of moles, *n*, for 6.3 g of BPEI is given by:

$$n_{6.3\ g} = \frac{6.3\ g}{800\ g.mol^{-1}} = 7.9 \times 10^{-3}\ mol$$

For 8 mL of BPEI:

If 1.05 g of BPEI is present in 1 mL thereof, then *x* g is found in 8 mL. To solve *x*,

$$x = \frac{(8\ mL)(1.05\ g)}{1\ mL} = 8.4\ g\ .$$

Therefore, the number of moles, *n*, for 8.4 g of BPEI is given by:

$$n_{8.4\ g} = \frac{8.4\ g}{800\ g.mol^{-1}} = 1.1 \times 10^{-2}\ mol$$

For 10 mL of BPEI:

If 1.05 g of BPEI is present in 1 mL thereof, then *x* g is found in 10 mL. To solve *x*,

$$x = \frac{(10\ mL)(1.05\ g)}{1\ mL} = 10.5\ g\ .$$

Therefore, the number of moles, *n*, for 10.5 g of BPEI is given by:

$$n_{10.5\ g} = \frac{10.5\ g}{800\ g.mol^{-1}} = 1.3 \times 10^{-2}\ mol$$

For 12 mL of BPEI:

If 1.05 g of BPEI is present in 1 mL thereof, then *x* g is found in 12 mL. To solve *x*,

$$x = \frac{(12\ mL)(1.05\ g)}{1\ mL} = 12.6\ g\ .$$

Therefore, the number of moles, *n*, for 12.6 g of BPEI is given by:

$$n_{12.6\ g} = \frac{12.6\ g}{800\ g.mol^{-1}} = 1.6 \times 10^{-2}\ mol$$

For 14 mL of BPEI:

If 1.05 g of BPEI is present in 1 mL thereof, then *x* g is found in 14 mL. To solve *x*,

$$x = \frac{(14\ mL)(1.05\ g)}{1\ mL} = 14.7\ g\ .$$

Therefore, the number of moles, *n*, for 14.7 g of BPEI is given by:

$$n_{14.7\ g} = \frac{14.7\ g}{800\ g.mol^{-1}} = 1.8 \times 10^{-2}\ mol$$

Table 46. Mass table for the optimisation of BPEI molar quantity for the synthesis of a-CDs.

Sample code	***BPEI_Opt_B16***	***BPEI _Opt_B17***	***BPEI _Opt_B18***	***BPEI _Opt_B19***	***BPEI _Opt_B20***
Contents	2.1103 g of 10 mM CA & 6 mL BPEI	2.1040 g of 10 mM CA & 8 mL BPEI	2.1107 g of 10 mM CA & 10 mL BPEI	2.1114 g of 10 mM CA & 12 mL BPEI	2.1102 g of 10 mM CA & 14 mL BPEI
Temperature (ºC)	170	170	170	170	170
Reaction Time (hr)	2	2	2	2	2
Mass (g) of 50 mL container	11.0744	10.9617	11.0646	11.0750	11.1191
Mass (g) of container + reagents	19.0546	20.5550	22.1765	24.4584	26.8130
Mass (g) of container + a-CDs + 30 mL DI water	47.5005	48.4312	49.9102	51.4865	55.0695
Mass (g) of 30 mL DI water	30	30	30	30	30
Mass (g) of reagents ([mass of container + reagents] – mass of container)	7.9802	9.5933	11.1119	13.3834	15.6939
Mass (g) of product (a-CDs) ([mass of container + a-CDs + 30 mL DI water] – mass of container – mass of 30 mL DI water)	6.4261	7.4695	8.8456	10.4115	13.9504
% yield after heating (mass of product/mass of reagents × 100)	80.53	77.86	79.60	77.79	88.89

Dialysis – branched polyethylenimine molar quantity optimisation study of a-CDs

The process and requirements of dialysis described in Section 3.6 was followed and the results of the calculations performed for effective dialysis are presented in Table 47 below.

Table 47. Table for calculations of requirements for effective dialysis of a-CDs for molar quantity optimisation of BPEI.

Sample code	***BPEI _Opt_B16***	***BPEI _Opt_B17***	***BPEI _Opt_B18***	***BPEI _Opt_B19***	***BPEI _Opt_B20***
Contents	2.1103 g of 10 mM CA & 6 mL BPEI	2.1040 g of 10 mM CA & 8 mL BPEI	2.1107 g of 10 mM CA & 10 mL BPEI	2.1114 g of 10 mM CA & 12 mL BPEI	2.1102 g of 10 mM CA & 14 mL BPEI
Mass (g) of 50 mL container	11.0744	10.9617	11.0646	11.0750	11.1191
Mass (g) of container + a-CDs + 30 mL DI water	47.5005	48.4312	49.9102	51.4865	55.0695
Mass (g) of a-CDs + 30 mL DI water (V_1)	36.4261 g ≈ 37 mL	37.4695 g ≈ 38 mL	38.8456 g ≈ 39 mL	40.4115 g ≈ 41 mL	43.9504 g ≈ 44 mL
If 300 mL is used for dialysis; $\frac{V_1}{V_1+300\ mL} << 1$	0.1083	0.1110	0.1146	0.1187	0.1278
If 300 mL is used for dialysis; $\frac{300\ mL}{V_1+300\ mL} \approx 1$	0.8917	0.8890	0.8854	0.8813	0.8722
Length (cm) of membrane needed V_1/6.4 mL.cm^{-1}	37 mL/6.4 = 5.78	38 mL/6.4 = 5.94	39 mL/6.4 = 6.09	41 mL/6.4 = 6.41	44 mL/6.4 = 6.88

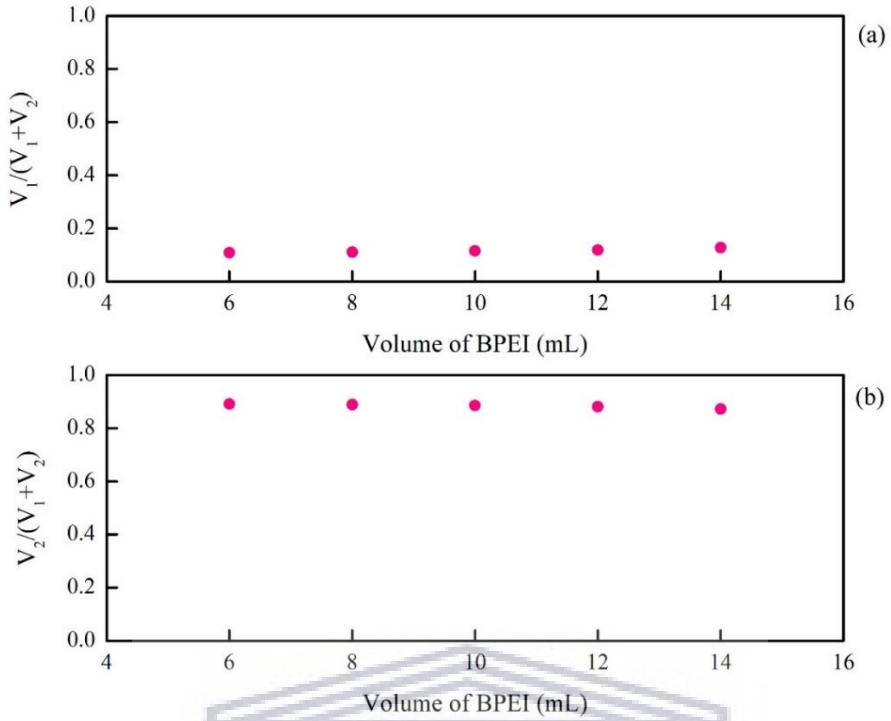

Figure 96. Illustrated above are the values for calculations pertaining to the effective dialysis of amine-capped carbon dots for the molar quantity optimisation of branched polyethylenimine; presenting the above-mentioned requirements with V_2 = 300 mL for (a) $\frac{V_1}{V_1+V_2}$, and (b) $\frac{V_2}{V_1+V_2}$.

As established in Section 4.1.1.1 and as illustrated in Figure 96 above, when V_2 = 300 mL the process of dialysis is more effective than for smaller amounts as it yields much better values for the 2nd and 3rd requirements of $\frac{V_1}{V_1+V_2} << 1$ and $\frac{V_2}{V_1+V_2} \approx 1$, with its calculated values much smaller than 1 and much closer to 1, respectively.

Table 48. Mass table for dialysis of a-CDs for the molar quantity optimisation study of BPEI.

	Day	***Time***	***BPEI _Opt_B16***	***BPEI _Opt_B17***	***BPEI _Opt_B18***	***BPEI _Opt_B19***	***BPEI _Opt_B20***
Mass (g)	***1***	***IN 15:23***	37.8838	39.1417	40.4490	42.2479	46.1988
Mass (g)		***OUT 20:38***	52.8445	58.0573	63.3155	72.2963	83.0210
		IN 20:52					
Mass (g)	***2***	***OUT 15:22***	60.5351	67.0217	73.3246	86.5489	100.2206
		IN 15:43					
Mass (g)	***3***	***OUT 16:05***	51.2230	57.0877	61.4978	72.1433	84.3440

In this section, data regarding the dialysis of the above-mentioned samples for the optimisation of the molar quantity of BPEI in the synthesis of a-CDs is presented. The samples underwent dialysis right after heating in a Si-oil bath (through a procedure described in Section 3.6) to ensure effective purification of a-CDs through the removal of unreacted reagent molecules and small molecular by-products from the solution mixture. Shown in Figure 97 below are images of a-CDs before and after dialysis.

Figure 97. The dialysis of a-CDs for the molar optimisation of BPEI, (a) before, and (b) after dialysis.

In Figure 97, the dialysis bags after dialysis were larger in size when compared to those before dialysis, and could once again be attributed to the initial osmotic flow into the bag (as described in Section 4.1.1.1). It is noticeable that diffusion occurred from the higher concentrated sample inside the dialysis bag to the surrounding solution of lower concentration. The masses of dialysis bags over the 2-day dialysis procedure for the molar quantity optimisation study of BPEI in the synthesis of a-CDs are tabulated in Table 48. In Figure 98, the mass of dialysis bag is plotted against the time elapsed throughout the dialysis procedure.

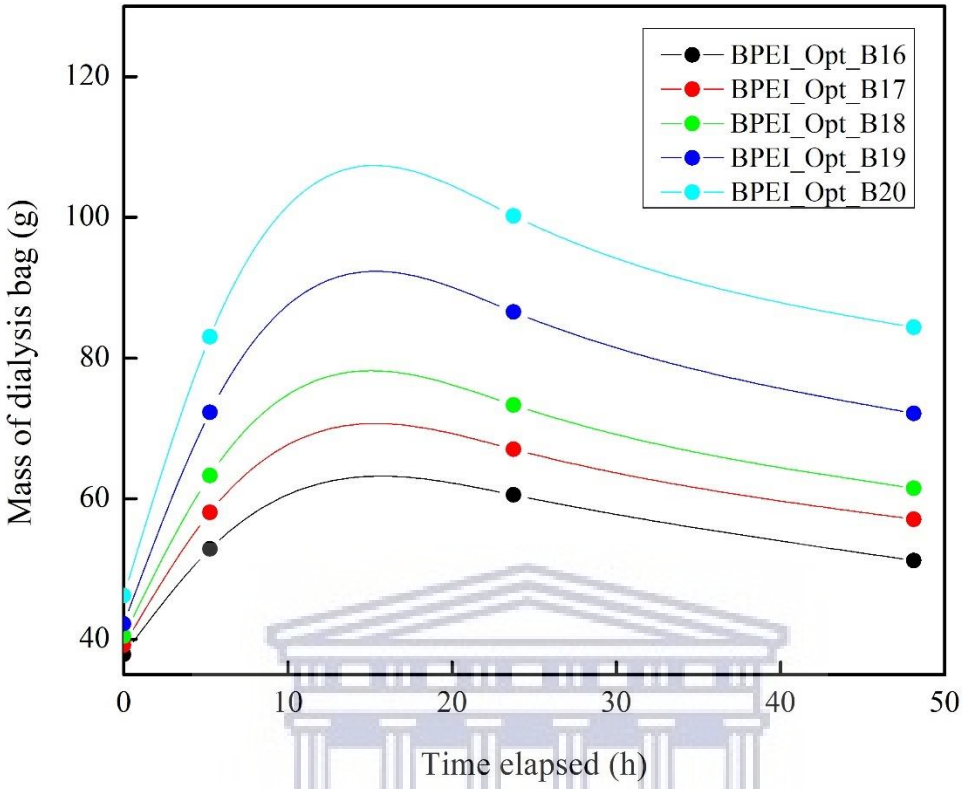

Figure 98. Dialysis of a-CDs in the molar optimisation study of BPEI.

According to the data displayed in Figure 98, the masses of the dialysis bags for each of the above-mentioned samples initially increased and then decreased. This behaviour is expected as the initial increase in mass for all samples could once again be attributed to the explanation provided in Section 4.1.1.1 in which diffusion is hindered by the occurrence of osmosis into the dialysis bags (Hunter 1987). However, the mass of each bag eventually reached a somewhat constant mass after the dialysis period.